Thèse

pour l'obtention du grade de Docteur de l'Ecole Polytechnique

Influence of Yb^{3+} and Er^{3+} ions environment on the evolution of its' luminescent properties in oxide glasses under ionizing irradiation

par

Vera Pukhkaya

Soutenue le

29 novembre 2013

Nadège Ollier	Directrice de thèse
Sylvain Girard	Rapporteur
Jean-Luc Adam	Rapporteur
Thierry Gacoin	Examinateur
André Monteil	Examinateur
Simonpietro Agnello	Examinateur
Philippe Goldner	Invité

Remerciements

Tout d'abord je tiens remercier ma directrice de thèse Nadège Ollier. C'est elle qui a apporté les plus belles choses dans mon travail scientifique et dans ce manuscrit. Merci Nadège pour accepter ma candidature à la thèse. Merci pour me supporter dans mes essais au cours de cette recherche. Merci aussi pour m'encourager apprendre français.

Je remercie mes rapporteurs Sylvain Girard et Jean-Luc Adam pour s'engager évaluer ce manuscrit. Je remercier ainsi tous les membres de jury. J'étais heureuse vous tous voir et vous parler à ma soutenance de thèse. Vos commentaires et remarques étaient intéressants et précis.

Enfin je dis grand merci à Philippe Goldner et Alban Ferrier. Votre apport dans ce travail est considérable. Merci pour votre aide dans l'étude de luminescence des terres rares. Merci pour votre accueil chaleureux dans votre labo durant mes visites.

Je remercie toute l'équipe d'accélérateur SIRIUS pour des irradiations aux électrons. Notamment Vincent Métayer, Bruno Boizot, Thierry Pouthier et Gaultier Brysbaert. Je vous tous remercie pour votre travail avec moi, pour votre sens d'humeur et pour la résolution des problèmes au SIRIUS.

Merci à Ludovic Bellot-Gurlet pour son aide à la spectroscopie Raman et Thibault Charpentier pour la Résonance Magnétique Nucléaire. J'étais heureuse apprendre des nouvelles techniques.

Pour gamma-irradiations je dis merci à Arbi Mejri et François Trompier. La collaboration avec François est une de choses surprenantes dans ma thèse. Je suis très contente de se retrouver François.

Enfin je remercie beaucoup mes collègues au laboratoire et en particulier Jéléna Sjakste pour son support aux moments durs dans mon travail.

Le dernier mais le plus important dans toute l'idée de mon travail en France. Merci Vitaly pour être d'accord venir ici. Merci pour ton aide, c'est inestimable. Il n'y a pas de mots français ni russes pour te dire ce que je sens. Merci.

Outline

I. Introduction 1

II. Sample preparation and experimental methods 7

1. Glass synthesis and glass compositions 7

1. a. Aluminosilicate glasses 7

1. b. Phosphate glasses 9

2. Irradiation conditions 10

2. a. Electron irradiation 10

2. b. Gamma irradiation 11

3. EPR spectroscopy 13

3. a. Theoretical aspects 13

3. a. 1 Zeeman effect 13

3. a. 2 Relaxation times 14

3. a. 3 g-factor 15

3. a. 4 Constants of hyperfine structure 16

3. b. Experimental aspects 17

4. b. 1 EPR spectrometer principle 17

4. b. 2 Parameters used for point defects study 18

4. b. 3 Parameters used for Yb^{3+} ions study 21

4. Optical measurements 24

4. a. IR-luminescence of Yb^{3+} 24

4. b. Cooperative luminescence of Yb^{3+} (CL) 26

4. c. Absorption 28

4. d. Photoluminescence of defects (LSI) 30

III. Yb-doped Na-aluminosilicate glasses 38

1. Glass structure 38

1. a. Bibliographic part 38

1. b. AS22-AS26 glass structure 41

1. c. Effect of irradiation at strong doses on glass structure 44

1. d. Yb environment 47
1. d. 1 IR-luminescence 47
1. d. 2 EPR spectroscopy 47
1. d. 3 Cooperative luminescence 49
1. d. 4 AS24_Ybx glasses 51
Raman spectroscopy 51
Cooperative luminescence 52
2. Point defects 53
2. a. Paramagnetic defects assignation 53
2. a. 1 E'-centers 53
2. a. 2 Peroxy radicals 54
2. a. 3 Non-Bridging Oxygen Hole Centers (NBOHC) 54
2. a. 4 HC defects 54
2. a. 5 Al-OHC defects 56
2. b. Formation of paramagnetic defects in AS22-AS26 glasses 56
2. b. 1 Influence of glass composition 56
2. b. 2 Influence of Yb-doping 58
2. c. Relaxation of paramagnetic defects 60
2. c. 1 Analysis of relaxation curves 62
2. c. 2 Recovery of individual defect type 64
2. d. Effect of irradiation dose and dose rate 65
2. d. 1 Total amounts of defects 65
2. d. 2 Relative amounts of defects 69
3. Luminescent properties of Yb^{3+} 73
3. a. Cooperative luminescence (CL) 73
3. a. 1 CL in AS glasses with high content of Yb clusters 73
3. a. 2 CL in AS glasses with less content of Yb clusters 76
3. b. Lifetime of Yb^{3+} $^2F_{5/2}$ excited state measurements 76
3. b. 1 Before irradiation 77
3. b. 2 Dose and dose rate effects 77
3. c. Analysis of the role of defects in CL and lifetime evolution under the irradiation 82
3. c. 1 Post-irradiation evolution in time 82
3. c. 2 Annealing treatments 83
AS22_10e8 glass 83

AS24_10e8 glass 86

4. Conclusions 89

IV. Phosphate glasses 98

1. Structure of phosphate glasses 98

1. a. Bibliographic part 98

1. b. Analysis by Raman spectroscopy 100

2. Structure of P-related point defects (bibliography part) 102

2. a. POHC defects 102

r-*POHC* 102

l-*POHC* 103

2. b. P1 defects (PO_3^{2-}) 103

2. c. P2 defects (PO_4^{4-}) 104

2. a. P3 defect 104

2. a. P4 defect (PO_2^{2-}) 104

3. Analysis of paramagnetic point defects formed under ionizing irradiation 105

3. a. Formation of paramagnetic defects 105

3. a. 1 Hole centers 105

3. a. 2 P centers 106

3. b. Relaxation of paramagnetic defects 108

3. b. 1 Relaxation of hole centers 108

3. b. 2 Relaxation of P centers 111

3. c. Dose and dose rate effect 113

3. c. 1 Dose effect 113

3. c. 2 Dose rate effect 118

4. Diamagnetic defect 121

4. a. Attribution of the defect 121

4. b. The diamagnetic defect in irradiated glasses 122

5. The lifetime of $^2F_{5/2}$ excited state evolution under e^--irradiation 125

5. a. Dose and dose rate effect 125

5. b. Relation with point defects 127

5. b. 1 Evolution in time 127

5. b. 2 Relation between the diamagnetic defects and the $^2F_{5/2}$ lifetime 127

6. Conclusions 131

V. Yb/ Er- and Er-doped AS glasses 137

1. Spectroscopy of Er^{3+} 137

1. a. Transitions of Er^{3+} ion in IR-region 137

1. b. Up-conversion 138

1. c. Yb → Er energy transfer 139

1. d. Experimental details 140

1. e. The samples 142

2. Link between the Er^{3+} environment and its luminescent properties 141

2. a. The samples 141

2. b. Characterization of Er^{3+} environment by EPR spectroscopy 141

2. b. 1 Er-doped glasses 141

2. b. 2 Yb/Er-codoped glasses 143

2. c. Er-doped glasses 144

2. c. 1 IR-luminescence 144

2. c. 2 Up-conversion process 145

2. d. Yb/Er-codoped glasses 146

2. d. 1 IR-luminescence 146

2. d. 2 Up-conversion 147

3. Effect of irradiation on Er3+ luminescent properties 149

3. a. Er^{3+} lifetime τ_{IR} 149

3. b. Er^{3+} luminescence in Yb/Er-codoped glasses 151

3. c. Up-conversion 152

4. Conclusions 154

VI. Conclusions and Perspectives 158

VII. Appendix 162

Appendix 1. Aluminosilicate glass compositions 162

Appendix 2. Irradiation conditions 163

Appendix 3. Annealing treatments of phosphate glasses 167

I. Introduction

The glass materials are used widely in many optical applications. The silica glass SiO_2 is an attractive matrix for producing the optical fibers, lenses (telescopes). It is used in semiconductor industry and in photolithography due to its high transparency (n_D = 1,4584) and chemical durability. Incorporation of alkali ions drives it easier to synthesize the glass because of lower melting temperature. Alkali-aluminosilicate glasses are even more rigid than alkali-silicates and they are used in various optical applications.

Phosphate glasses are based on phosphorus pentoxide (P_2O_5), usually with some added chemical components. They are used as laser gain media – both in bulk lasers and in the optical fibers. Phosphate glasses have a very low glass transition temperature (≈ 365 °C). That makes easier producing the devices based on phosphate glasses. Phosphate glasses exhibit a much lower optical damage threshold than silica glasses. Moreover, their primary advantages are the favorable transition cross sections and upper-state lifetimes of rare earth ions in phosphate glasses. The very high solubility of rare earth ions (erbium (Er^{3+}), ytterbium (Yb^{3+})) is well known. This means that higher concentrations of laser-active rare earth ions can be incorporated into phosphate glasses without harmful effects such as clustering, which could degrade the performance of the glass via quenching effects.

Yb-containing glasses are implied efficiently in fiber lasers production where Yb^{3+} ion is used as a dopant. In fiber lasers emitting at ~1.06-1.07 μm and in amplifiers (Yb/Er-codoping) the simplicity of Yb^{3+} energy levels structure is attractive. It is represented with only 2 energy levels $^2F_{5/2}$ and $^2F_{7/2}$ separated by 10000 cm^{-1} energy. This advantage is one of the reasons for achieving significant powers in IR-lasers [1].

For many optical applications of Yb^{3+}, with Yb concentration increase one should expect the increase of positive features such as Yb-laser's power. This is not the case; the doping content of Yb^{3+} ions is strongly limited by Yb-cluster formation, which is observed as concentration quenching. The doping concentration of Yb^{3+} in silica-based matrices maintains in range of 1-1000 ppm because of higher tendency of Yb clusters formation [2].

Studying the behavior of aluminosilicate (AS) or phosphate glasses doped with Yb under ionizing irradiation is attractive for different fields.

The aluminosilicate Yb-doped glasses under fibers form are exposed to ionizing irradiation while being used in space for satellite communication (doses ~10^3 Gy). Among the applications of irradiated phosphate glasses is their participation in vitrification process of radioactive waste in long-term storage [7]. Moreover, phosphate glasses are applied as dosimeters due to its sensitive response to low dose irradiation [8].

The irradiation can have a strong impact on luminescent properties of Rare-Earth Elements (REE) in oxide glasses via radiation-induced point defects whereas the REE doping brings some particular modifications into electronic structure of irradiated glass [9] [10] [11] [12]. In my Ph.D. the central question is around the role of cluster in the glass evolution under irradiation. It is thus essential to understand the way of charge trapping by well-diluted Yb^{3+} ions and those in clusters and their interactions with point defects, to predict the response of Yb^{3+} luminescent properties under ionizing irradiation treatment.

In present work, the characterization of the effect of Yb^{3+} environment under irradiation in oxide glass matrices on the evolution of luminescent properties is aimed. In order to compare role of glass chemical composition, 4 different aluminosilicate (AS) and 4 phosphate glasses were chosen. The cluster formation in those AS and phosphate glasses was carefully studied by B. Schaudel in her Ph.D. dissertation [13]. In AS glasses increasing of Al content (decreasing of Non-Bridging Oxygens number) leads to more Yb cluster formation whereas in phosphate glasses there is less Yb cluster due to structural difference between PO_4 and SiO_4 tetrahedra. In phosphate PO_4 group on Oxygen is always Non-Bridging leading to better dissolution of RE^{3+} ions in phosphate matrices.

One of the direct probes of Yb cluster can be cooperative luminescence of Yb^{3+} [3] [4]. It is observed as Yb^{3+} emission in 450-580 nm region under 970-980 nm excitation. Electronic Paramagnetic Resonance (EPR) of RE^{3+} ions is used as a probe of Yb clusters, too [5] [6]. Yb cluster exhibits its characteristic signal at higher g-values than isolated Yb^{3+} ions [5].

Our purpose is to compare these glasses in terms of irradiation effects. To follow that, irradiation with electrons of 2.5 MeV (SIRIUS facility, LSI) was carried out in vast achieved dose variation (10^5-$2{\cdot}10^9$ Gy). Moreover, the question of dose rate cannot be neglected, and thus electron irradiation was in comparison with γ-rays in possible dose range. Investigation of radiation-induced point defects in glasses, their evolution within time and temperature and their correlations with

luminescent properties of Yb^{3+} ions under the conditions mentioned above is the general approach in this work.

The work is presented in 6 chapters including Introduction (Chapter I) and Conclusions (Chapter VI). In the second chapter, experimental details can be found: the synthesis and precised chemical compositions of the samples are given. They are followed by the irradiation conditions. The basic principles and experimental details of EPR spectroscopy and optical spectroscopy, used in this work, complete the Chapter II.

The third chapter reports the results obtained for the Yb-doped AS glasses. The aluminosilicate glass structure is presented. The point defects are analyzed as a function of irradiation dose, dose rate and glass composition. Moreover, we will analyze the evolution of radiation-induced point defects and Yb^{3+} luminescence properties in time after irradiation. Finally, the particular relations between the defects and Yb^{3+} luminescence are discussed.

In the forth chapter, Yb-doped phosphate glasses are examined. A big part of the chapter concerns the attribution and characterization of point defects.

The fifth chapter is shorter and dedicated to Er- and Yb/Er-doped AS glasses.

The Er and Yb/Er glasses are associated with its wide application in the optical field. Er-doped glasses are used in telecommunications as Er-doped amplifiers, optical fibers and lasers [14] due to its 1.54 μm emission, but up-conversion process is harmful for the applications where high efficient 1.54 μm emission required [15].

This study was carried out at the end of my Ph.D. period and consists more on preliminary results. The aim was to extract more information on Yb^{3+} local environment by comparing with Er^{3+}. The main used distinction between Yb and Er is the absence of divalent state of Er contrary to Yb. Nevertheless, as we have obtained a few interesting result on the link between the glass structure and luminescent properties and the evolution under irradiation, we decided to add this small chapter.

The dissertation is completed by Conclusions and Perspectives in the last part.

[1] G. Liu et B. Jacquier, Spectroscopic Properties of Rare Earths in Optical Materials, New York: Springer Series in Materials Science, 2005.

[2] B. Schaudel, P. Goldner, M. Prassas et F. Auzel, *J. Alloys and Comp.,* vol. 300, p. 443, 2000.

[3] F. Auzel et P. Goldner, *Opt. Mater.,* vol. 16, p. 93, 2001.

[4] E. Nakazawa et S. Shionoya, *Phys. Rev. Lett.,* vol. 25, p. 1710, 1970.

[5] S. Sen, R. Rakhmatullin, R. Gubaidullin et A. Pöppl, *Phys. Rev. B,* vol. 74, p. 100201, 2006.

[6] T. Deschamps, N. Ollier, H. Vézin et C. Gonnet, *J. Chem. Phys.,* vol. 136, p. 01453, 2012.

[7] M. I. Ojovan et W. E. Lee, *Met. Mater. Transactions A,* vol. 42, p. 837, 2011.

[8] N. Z. Andreeva, N. N. Vil'chinskaya, A. V. Dmitryuk, A. S. Perminov, G. T. Petrovskii et O. C. Savvina, *Atom. Energiya,* vol. 58, p. 132, 1985.

[9] A. V. Amossov et A. O. Rybaltovsky, *J. Non-Cryst. Solids,* vol. 179, p. 75, 1994.

[10] L. Skuja, *J. Non-Cryst. Solids,* vol. 239, p. 16, 1998.

[11] E. Malchukova, B. Boizot, G. Petite et D. Ghaleb, *J. Non-Cryst. Solids,* vol. 354, p. 3592, 2008.

[12] N. Ollier, J.-L. Doulan, V. Pukhkaya, T. Charpentier, R. Moncorgé et S. Sen, *J. Non-Cryst. Solids,* vol. 357, p. 1037, 2011.

[13] B. Schaudel, Ph.D. dissertation, Paris: Université Paris VI, 2000.

[14] M. Van Uffelen, S. Girard, F. Goutaland, A. Gusarov, B. Brichard et F. Berghmans, *IEEE Trans. Nucl. Sci.,* vol. 51, p. 2763, 2004.

[15] J. F. Philipps, T. Töpfer, H. Ebendorff-Heidenpriem, D. Ehrt et R. Sauerbrey, *Appl. Phys. B: Lasers Opt.,* vol. 74, p. 233, 2002.

Chapter II

Sample preparation and experimental methods

II. Sample preparation and experimental methods 7
1. Glass synthesis and glass compositions 7
1. a. Aluminosilicate glasses 7
1. b. Phosphate glasses 9
2. Irradiation conditions 10
2. a. Electron irradiation 10
2. b. Gamma-irradiation 11
3. EPR spectroscopy 13
3. a. Theoretical aspects 13
3. a. 1 Zeeman effect 13
3. a. 2 Relaxation times and EPR line's shape 14
3. a. 3 g-factor 15
3. a. 4 Constants of hyperfine structure 16
3. b. Experimental aspects 17
3. b. 1 EPR spectrometer principle 17
3. b. 2 Parameters for point defects study 18
3. b. 3 Parameters for Yb^{3+} ions study 21
4. Optical measurements 24
4. a. IR-luminescence of Yb^{3+} 24
4. b. Cooperative luminescence of Yb^{3+} (CL) 26
4. c. Absorption 28
4. d. Photoluminescence of defects (LSI) 30

II. Sample preparation and experimental methods

Choice of Glass composition

One aim of the Ph.D. was to study the impact of Yb cluster on the defect formation and relaxation, and the evolution of Yb^{3+} luminescent properties under irradiation. So, we wanted to study glass samples with contrasted Yb cluster amount, but doped with same Yb content. Such aluminosilicate and phosphate glasses were carefully studied in B. Schaudel's Ph.D. [1]. We based our choice on the chemical compositions presented by B. Schaudel [1].

Two different kinds of oxide glasses were studied: aluminosilicate (Chapter III) and phosphate (Chapter IV). Finally, four aluminosilicate glass compositions with different Al content and four phosphate glasses with different P content were chosen. For more facility, same sample names than in [1] were used.

Concerning Er- and Yb/Er-codoped samples (Chapter V), the aim was, first, to compare the behavior of Yb and Er glasses (where no Er^{3+} reduced to Er^{2+} can be found) and, secondly, to evaluate the impact of irradiation on up-conversion and Yb→Er energy transfer. The number of studied samples in this Chapter was reduced: only 2 aluminosilicate glass compositions giving contrasted results on Yb clusters were studied.

1. Glass synthesis and glass compositions

1. a. Aluminosilicate glasses

Aluminosilicate (AS) glass samples were prepared with the appropriated amounts of preliminary dried powders of SiO_2, Al_2O_3, Na_2CO_3 and Yb_2O_3 and/or Er_2O_3. The initial chemicals were mixed and heated slowly (10 hours) in Pt-Au crucible up to 1600°C in a furnace under air oxygen. The slow heating was necessary for decarbonization (eliminate all CO_2 gas that takes place at ~800°C). Once the melting temperature 1600°C was reached, the dwell was 4 hours. Afterwards the glass was quenched rapidly at room temperature via putting the crucible into the water when the mixture's viscosity was too high (AS23-AS26

glasses). Otherwise, the glass was quenched rapidly between two copper plates (AS22 glasses). All the glasses were afterwards annealed at 580°C (below T_g) that in order to allow releasing the mechanical tensions.

The nominal glass compositions are presented in Table II-1. Glass compositions were refined with microprobe analysis giving <1 mol. % of average error (Appendix 1). For Yb the average error is ~0.05 mol. %.

Sample name	**SiO_2, mol. %**	**Al_2O_3, mol. %**	**Na_2O, mol. %**	**ASI Al/Na**	
AS22	74	6	20	0.3	+ 5 wt. % Yb_2O_3
AS23	68	12	20	0.6	
AS24	62	18	20	0.9	
AS26	58	22	20	1.1	
AS22_0	74	6	20	0.3	Yb-free
AS24_0	62	18	20	0.9	
AS24_005					+ 0.05 wt. % Yb_2O_3
AS24_02					+ 0.2 wt. % Yb_2O_3
AS24_05					+ 0.5 wt. % Yb_2O_3
AS24_1					+ 1 wt. % Yb_2O_3
AS24_2					+ 2 wt. % Yb_2O_3
AS24_8					+ 8 wt. % Yb_2O_3
AS22_Er	74	6	20	0.3	+ 0.5 wt. % Er_2O_3
AS22_YbEr	74	6	20	0.3	+ 0.5 wt. % Er_2O_3 + 5 wt. % Yb_2O_3
AS24_Er	62	18	20	0.9	+ 0.5 wt. % Er_2O_3
AS24_YbEr	62	18	20	0.9	+ 0.5 wt. % Er_2O_3 + 5 wt. % Yb_2O_3

Table II-1. Nominal compositions of aluminosilicate glasses

In Table II-1 in glass series AS22-AS23-AS24-AS26, the concentration of Yb_2O_3 oxide is fixed. The content of SiO_2 decreases with increase of Al_2O_3 content. The Na_2O content is fixed in all the glasses at 20 mol. %. Thereafter, in AS22-AS23-AS24-AS26 glass series the ASI (Aluminum Saturation Index) varies. It characterizes molar ratio Al_2O_3/Na_2O, it is the lowest in AS22 glass and the highest in AS26 glass.

AS24 glass composition is chosen for Yb concentration variation from 0.05 wt. % of Yb_2O_3 to 8 wt. % of Yb_2O_3. There are also 2 RE-free glasses: AS22_0 and AS24_0.

For Er-doping AS22 and AS24 glasses are chosen. In all four obtained glasses Er concentration is 0.5 wt. % of Er_2O_3. In Yb/Er-codoped glasses molar ratio Yb:Er is ~10:1 (9.6:1).

1. b. Phosphate glasses

Phosphate glass samples were prepared with the appropriated amounts of $NH_4H_2PO_4$, MgO, Na_2CO_3 and Yb_2O_3 (5 wt. %). To avoid the interactions between P_2O_5, forming at high temperature, with Pt-Au crucible, the initial chemicals were mixed and melted in silica crucible and then heated slowly to follow degasation processes: NH_3 is evaporated at 250°C and CO_2 at 800°C. The melting temperature of phosphate glasses is lower than for AS glasses, 900°C. The glass transition temperature T_g of such phosphate glasses is in 370-400°C range [2] [3]. The cooling temperature must be not seriously lower then T_g otherwise the glass becomes less stable [2]. The melted glass was quenched rapidly into Pt-Au crucible on an electric plate at 300°C and immediately annealed at 350°C to release mechanical tensions and to avoid high cooling rate. To revoke the interaction with silica crucible at high temperature, the glasses were analyzed by microprobe where it was demonstrated the absence of Si in all the samples.

The nominal glass compositions are presented in Table II-2.

Sample name	**P_2O_5, mol. %**	**MgO, mol. %**	**Na_2O, mol. %**	
2743	66.7	11.1	22.2	+ 5 wt. % Yb_2O_3
2742	50	16.7	33.3	
2745	45.4	18.2	36.4	
2746	40	20	40	
2743_0	66.7	11.1	22.2	Yb-free
2745_0	45.4	18 .2	36.4	

Table II-2 . Nominal compositions of phosphate glasses

Keeping fixed concentration of Yb, phosphorus content decreases from 2743 to 2746 glass. The total amount of MgO and Na_2O consequently increases. The phosphate glass structure can be described by ratio $R=(MgO+Na_2O)/P_2O_5$ which varies as a function of network type. There are also 2 non-doped glasses: 2743_0 and 2745_0 samples.

The glass compositions is checked by Raman spectroscopy in Chapter IV (see section 1)

2. Irradiation conditions

2. a. Electron irradiation

The “Laboratoire des Solides Irradiés” has a high energy electron Pelletron NEC accelerator, named SIRIUS (Figure II-1). The energy of available electron is between 200 keV and 2.5 MeV. The accelerator is equipped with 2 irradiation lines, CRYO1 cell is for low temperature irradiations (20K), and CIRANO is for 16-350°C irradiations. We used CIRANO cell.

Massive glass samples (5×5 mm) were continuously irradiated with 2.5 MeV electron beam of 20 mm beam size with dose rate close to 25 MGy/h. To obtain homogeneous integrated dose, we had to take care about the sample thickness. Slices of 500-700 μm thickness were prepared in order to consider as negligible the energy loss of 2.5 MeV electrons. The sample holder was maintained around 40°C with a water cooling system by measuring 12-14 μA current at the sample (Figure II-1).

The achieved integrated doses were 10^5Gy, 10^6 Gy, $3\cdot10^6$Gy, 10^7 Gy, 10^8 Gy and $1.5\cdot10^9$Gy (Table II-3).

Unfortunately, some current instability (±20%) faced us to use precise irradiation conditions. Moreover, few interruptions took place during long-term dose collecting – >10^9 Gy. During the interruption time some relaxation processes should occur and thus the final result may be different. Problems of current instability and lack of proper irradiated at strong doses samples drive some difficulties into results analysis.

We have also irradiated some samples under powder form to measure the cooperative luminescence. To be precise in optical measurements, the glasses were grounded into powders of 100-125 μm particle size. For powders, the achieved integrated doses were **10^5 Gy, $3\cdot10^6$ Gy and 10^8 Gy**.

Moreover, we irradiated slice samples with $3\cdot10^6$ Gy by using a 2.5 MeV electron beam of 200 nA current which gives 300 kGy/h dose rate of (2 orders of magnitude lower).

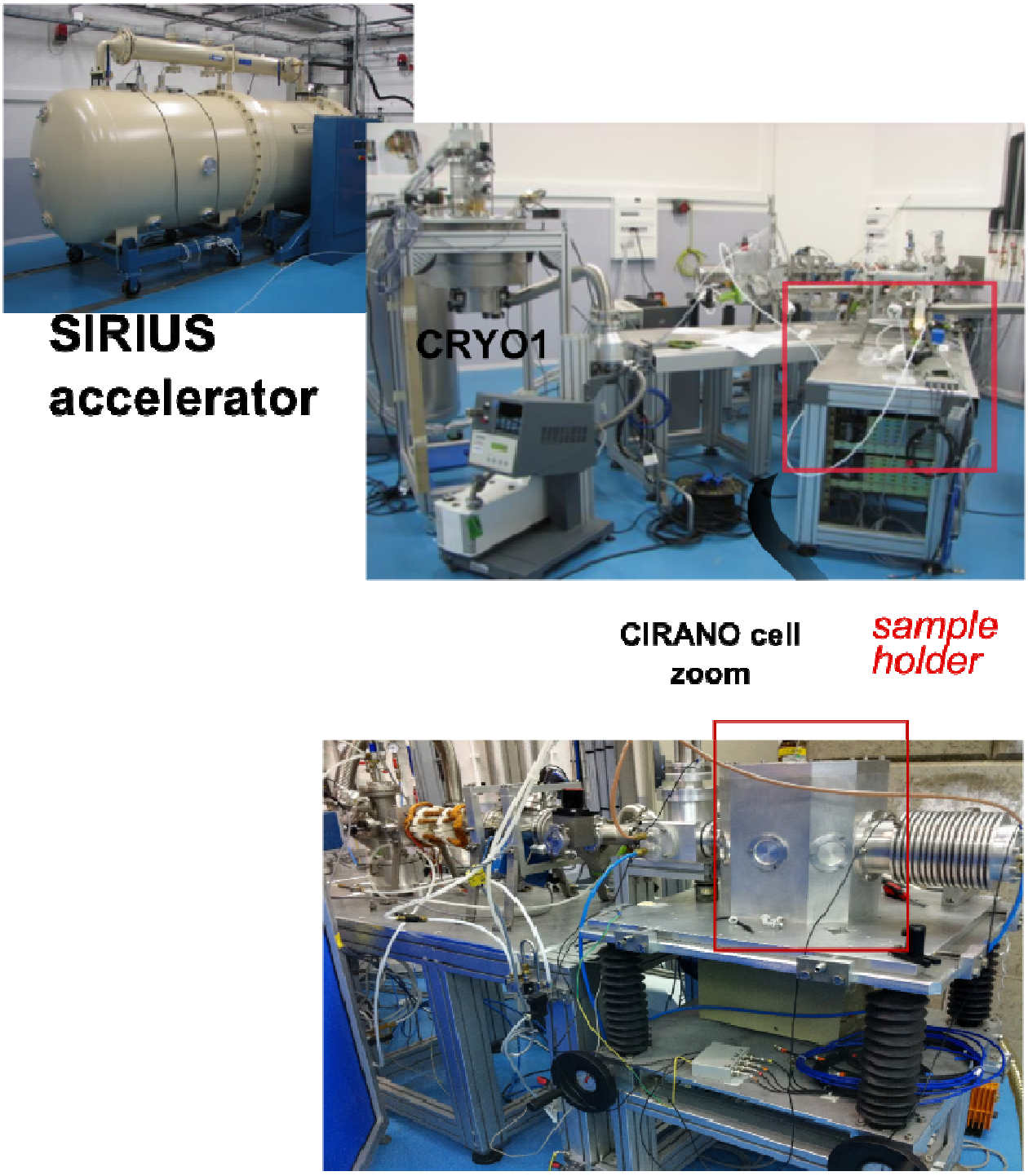


Figure II-1. SIRIUS accelerator in LSI: from top to down. Photo of irradiation source where electron beam is created, photo of two irradiation cells, zoom at CIRANO and sample holder.

2. b. Gamma-irradiation

To investigate the effect of irradiation dose rate, the samples under slices as well as powders were also irradiated with γ-rays of 1.25 MeV in "Centre National des Sciences et Technologies Nucléaires" in Tunisia (CNSTN). The dose rate in this case

was 5.64 kGy/h. The energy of γ-rays more than 1.022 MeV implies high probability of electron-positron pair induction that can result point defect creation [4]. Comparison of electron irradiation with gamma-rays can be carried out also because of low mass of electrons. Its lower mass leads to lower losses through material penetration in comparison to other particle irradiations such as protons or α particle.

The achieved doses were 10^4, 10^5, 10^6 and $3 \cdot 10^6$ Gy (Table II-3). It was possible therefore to compare **3 same irradiation doses (10^5, 10^6 and $3 \cdot 10^6$ Gy)** of 2 different dose rates.

<table>
<tr><th colspan="3">Electron</th></tr>
<tr><th>Dose rate, MGy/h</th><th>Beam energy, MeV</th><th>Dose, Gy</th></tr>
<tr><td rowspan="7">25</td><td rowspan="6">2.5</td><td>10^5</td></tr>
<tr><td>10^6</td></tr>
<tr><td>$3 \cdot 10^6$</td></tr>
<tr><td>10^7</td></tr>
<tr><td>10^8</td></tr>
<tr><td>$1.5 \cdot 10^9$</td></tr>
<tr><td>Comment: Er-serie</td><td>$2 \cdot 10^9$</td></tr>
<tr><td>0.3</td><td>2.5</td><td>$3 \cdot 10^6$</td></tr>
<tr><th colspan="3">Gamma</th></tr>
<tr><th>Dose rate, kGy/h</th><th>Beam energy, MeV</th><th>Dose, Gy</th></tr>
<tr><td>5.64</td><td>1.25</td><td>10^4</td></tr>
<tr><td></td><td></td><td>10^5</td></tr>
<tr><td></td><td></td><td>10^6</td></tr>
<tr><td></td><td></td><td>$3 \cdot 10^6$</td></tr>
</table>

Table II-3 . Irradiation conditions

More details on the irradiated series and on irradiation conditions are given in Appendix 2.

After the irradiation the samples were stored in dark at room temperature to limit the impact of photobleaching of the paramagnetic point defects [5].

3. EPR spectroscopy

3. a. Theoretical aspects

Electronic Paramagnetic Resonance (EPR) or Electronic Spin Resonance (ESR) spectroscopy is a powerful tool of analysis of atoms, ions, molecules or elements with non-zero electron's spin moment (e.g. with unpaired electron). Paramagnetic particles that are analyzed with EPR can be of various origins such as: free radicals in gas, liquid and solid state; point defects in materials; transition ions and rare earth element. In 1944 E. K. Zavoisky discovered this phenomenon [6]. Most of theoretical aspects presented in this section are consulted with A. Abragam and B. Bleaney [7]

3. a. 1 Zeeman effect

Without any magnetic field, all the magnetic momenta of unpaired electrons are of random direction, e.g. the system consists of degenerated energy states. Once the magnetic field B is applied (Figure II-2), the degeneracy of the system disappears (Zeeman effect) and the gap between electrons' energy levels is

$$\Delta E = g\mu_B B$$

where

1) g is Landé factor, g of free electron g_e=2.0023

2) μ_B (Bohr magneton) is $9.274 \cdot 10^{-24}$ J/T

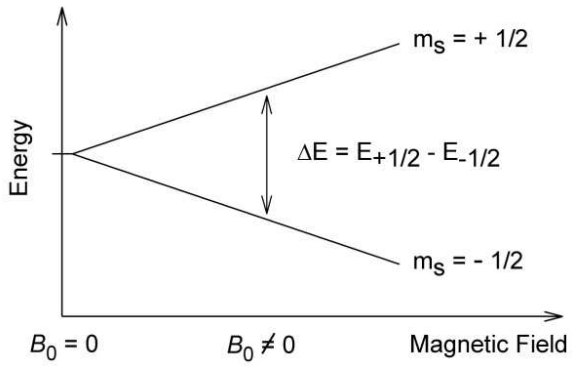


Figure II-2. Energy levels splitting under applied magnetic field

The parameter B can also be used where the permeability of free space is μ_0=1.257·10^{-6} H/m. The distribution of the electrons between the sublevels obeys to the Boltzmann law $n_1/n_2=\exp(-\Delta E/kT)$ with k is Boltzmann constant and T is the

absolute temperature. If a sample is under an alternating perpendicular magnetic field of frequency ν, it induces the transitions between the sublevels with absorption or emission of energy ΔE=hν, where

$$h\nu = g\mu_B B$$

h=6.6262·10^{-34}J·sec is Plank constant

3. a. 2 Relaxation times and EPR line's shape

To maintain the Boltzmann distribution of energy levels' populations the relaxation processes are essential. The relaxation processes are electron transitions from excited states to ground states with energy exchanges with lattice, so-called spin-lattice relaxation, and with other electrons, so-called spin-spin relaxation. The relaxation times are noted, respectively, T1 and T2. They characterize the system recovery after the magnetic field has been applied.

Intensity – the area under the absorbance curve (integral) is proportional to unpaired spin number in the sample. Therefore, the driven integrals are efficient to compare the detected paramagnetic species.

One can register usually the first, more rarely the second, derivatives of absorption that increases the sensitivity and the resolution of the spectra (Figure II-3). Sometimes, the integral S_{int} is estimated obeying the equation

$$S_{int} = I_{max}(\Delta B_{max})^2$$

where ΔB_{max} is line's full width at half max. Both the first and the second derivatives are strongly sensitive to the absorbance shape.

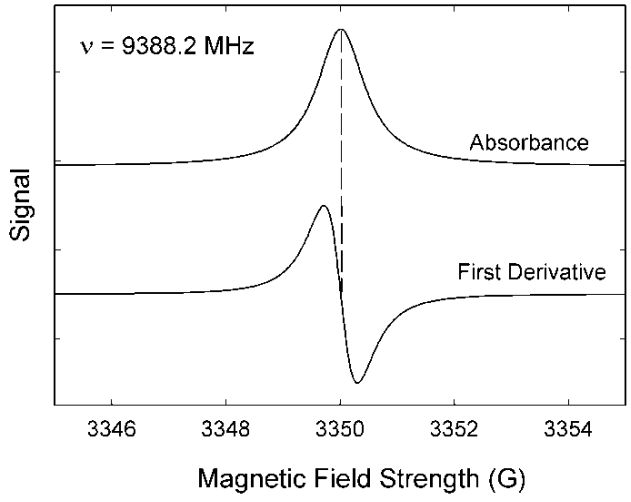


Figure II-3. Curves recorded with EPR spectroscopy

The shape of the EPR line can be fitted either with Lorenz equation $y = \frac{a}{1+bx^2}$ or with Gauss equation $y = a \times \exp(-bx^2)$. The Lorenz's lines are usually observed in materials with low concentration of unpaired spins. Once the line is a superposition of many other lines (unresolved hyperfine structure), it is of Gauss type.

Experimentally, the EPR lines are partly Lorentz partly Gauss types. Full with at half maximum ΔB_{max} is an important EPR parameter. It is in connection with both relaxation times T1 and T2

$$\Delta B_{max} \approx \frac{1}{T1} + \frac{1}{T2}$$

The value T1 is Zeeman level population relaxation time. T1 is the constant which characterizes the decay of the z component of the magnetization vector. According to uncertainty principle, EPR line broadens at low T1. T1 value of the paramagnetic ions is of 10^{-7} – 10^{-9} s order, it is the basic relaxation channel responsible for many broad lines. In some cases, helium temperatures allow carrying out EPR spectra due to higher T1 (Rare-Earth Elements). When the lifetime T1 is high(~10^{-6} s), the parameter ΔB_{max} depends mostly on T2 value.

3. a. 3 g-factor

Landé's g-factor is

$$g = 1 + \frac{J(J+1) + S(S+1) - L(L-1)}{2J(J+1)}$$

Where L, S and J are orbital, spin and full momenta numbers, consequently. In case of spin magnetism, L=0 (free electron case) and g=2.0023. Any deviation from g=2.0023 indicates additional orbital magnetism (spin-orbit coupling) leading to dispersion of resonance field. Once there is a strong spin-orbit interaction, which is an efficient sensor to the ligand surroundings, it is linked to crystal field. For ions g-factor is

$$g = 2(1 - {}^{\lambda}/_{\Delta})$$

λ – spin-orbit coupling constant

Δ – splitting in ligand's field

In case of high Δ and low negative λ, g-factor is close to that of free electron and the dispersion of g-value can be in the 0.001 order.

Generally, all the interactions in spin system are anisotropic which comes from wave functions' anisotropy except unpaired s-electrons. The value of resonance field and g-factor thus depend on relative magnetic field direction and crystal axes orientation in case of single crystal samples. In amorphous phase anisotropic interactions equalize bringing an isotropic effect on g-factor value: the signal does not depend on sample's orientation. In a crystalline phase the symmetry is either cylindrical or inferior as a function of the structure.

In a cubic symmetry of g-tensor all three components are equal $g_x=g_y=g_z$. In an axial symmetry the g-factor is represented with $g_{||}$ (parallel to *z* axe field) and $g_{\perp}$ (perpendicular to *z* axe field). In a lower symmetry (rhombic) one can detect all three g-components g_x, g_y and g_z.

Fine structure is detected when there are more than 1 unpaired electrons ($S>½$). In case for example of $S=^3/_2$, 4 equidistant M_S sublevels are created. The only resonance peak is observed at $h\nu= g\mu_B B$. In real systems the energies between the sublevels are not equal anymore because of crystal field inhomogeneity. Therefore, the absorption can be registered at various magnetic field values giving rise to 3 resonance lines.

3. a. 4 Constants of hyperfine structure

The hyperfine structure of EPR spectra comes from interactions between unpaired electron and nuclei momenta. When nuclei momentum is $I\neq0$ one can observe $2I+1$ lines instead of one. For example, 23% of natural abundance of Er is ^{167}Er isotope with $I=^7/_2$. Thus 8 supplementary lines are detected by EPR (Figure II-4).

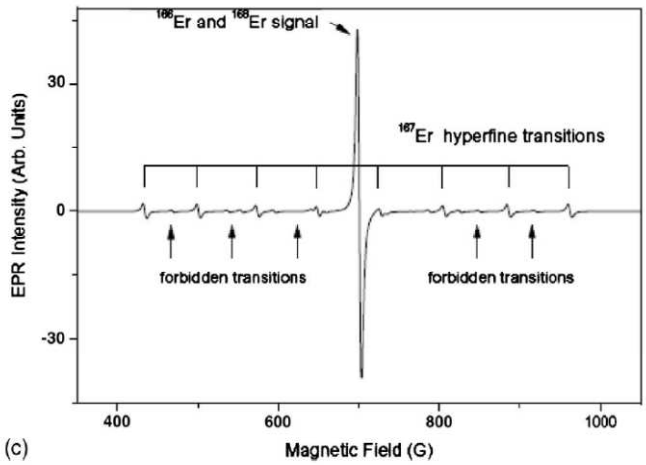


Figure II-4. ERP spectra of Er^{3+} in β-Ga_2O_3 [8]

3. b. Experimental aspects

3. b. 1 EPR spectrometer principle

Radiation source in EPR spectrometer is provided by a klystron giving a monochromatic radiation (Figure II-5). The attenuator allows controlling the power at the sample. The cuvette with the sample is of parallelepiped or cylindrical shape. The cuvette's size is enough to form a static wave. The static magnetic field is provided by an electromagnet.

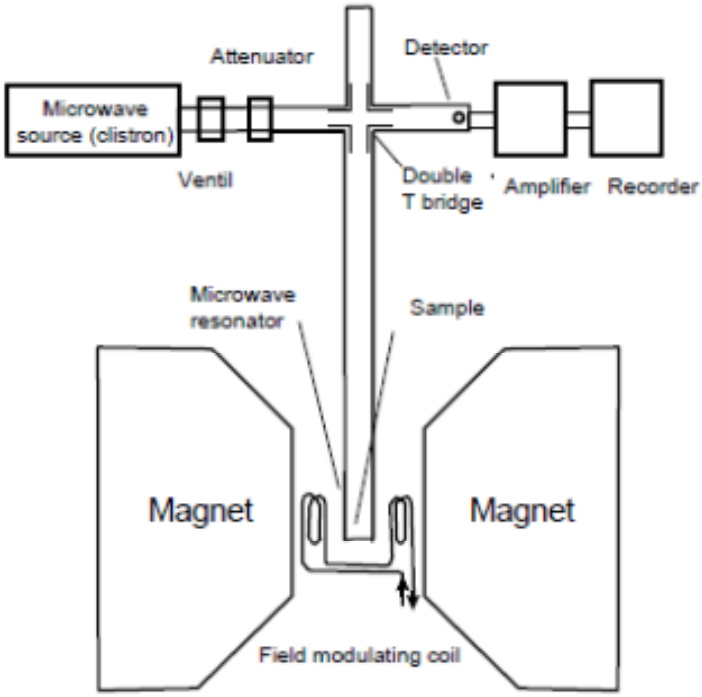


Figure II-5. The principal scheme of EPR spectrometer

After the signal of the sample comes through the detector with an amplifier, it is being registered. An important point is that they work with a fixed frequency (X band or Q band…) and a variable magnetic field. The amplification is executed with modulations of the high-frequency magnetic field. For technical reasons, the recorded common EPR signal corresponds to the absorption's derivatives.

In this work, the EPR experiments were carried out with a Bruker X-band EMX spectrometer. The frequency was 9.8 GHz. The signal was normalized afterwards by attenuator's gain and by sample's mass.

3. b. 2 Parameters for point defects study

All the paramagnetic point defects were observed at room temperature. For each type of defect in AS and phosphate glasses, we determined the microwave power by establishing the power saturation curve. In aluminosilicate glasses the analysis of hole centers gave the curve in Figure II-6.

The intensities brought from double integration were plotted versus power's square root.

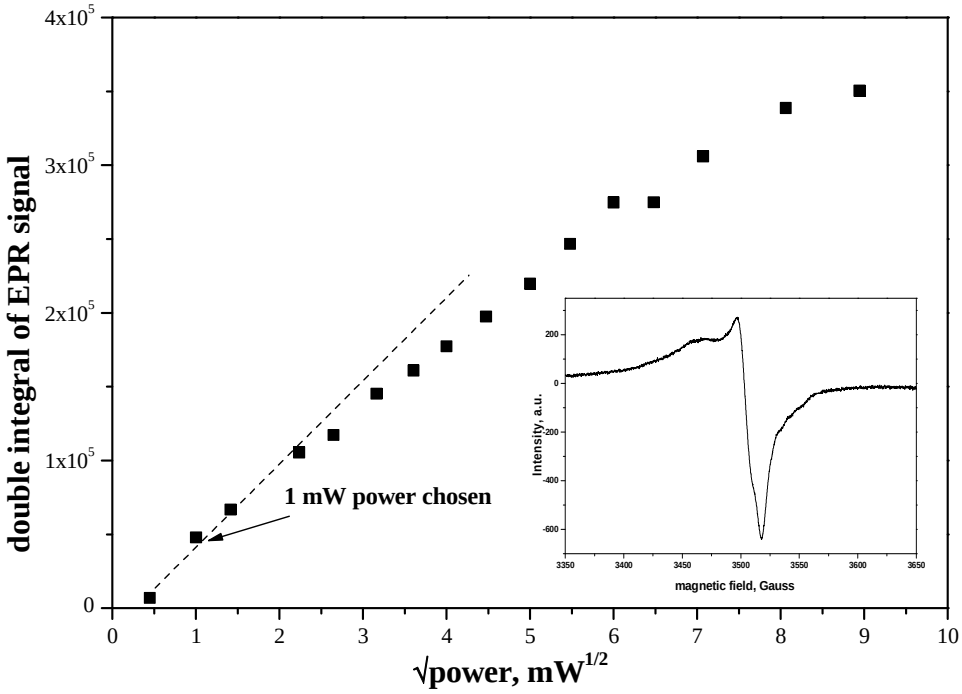


Figure II-6. Power saturation of hole centers in AS glasses

The chosen power for hole centers in aluminosilicate glasses was 1 mW which was under linear law presented above (Figure II-6), therefore, it was in proportional range and could be applied to intensity comparison.

At doses higher than $3 \cdot 10^6$ Gy, some E' centers were induced (Figure II-7). It is well-known that E' signal saturates at low powers [9] [10] [11]. Since E' centers are observed together with hole centers, the double integration technique did not promise to be as efficient as in previous case. The solution was the absolute difference between the maxima of E' signal (Figure II-7). It was proportional to the integrated value because of very narrow shape.

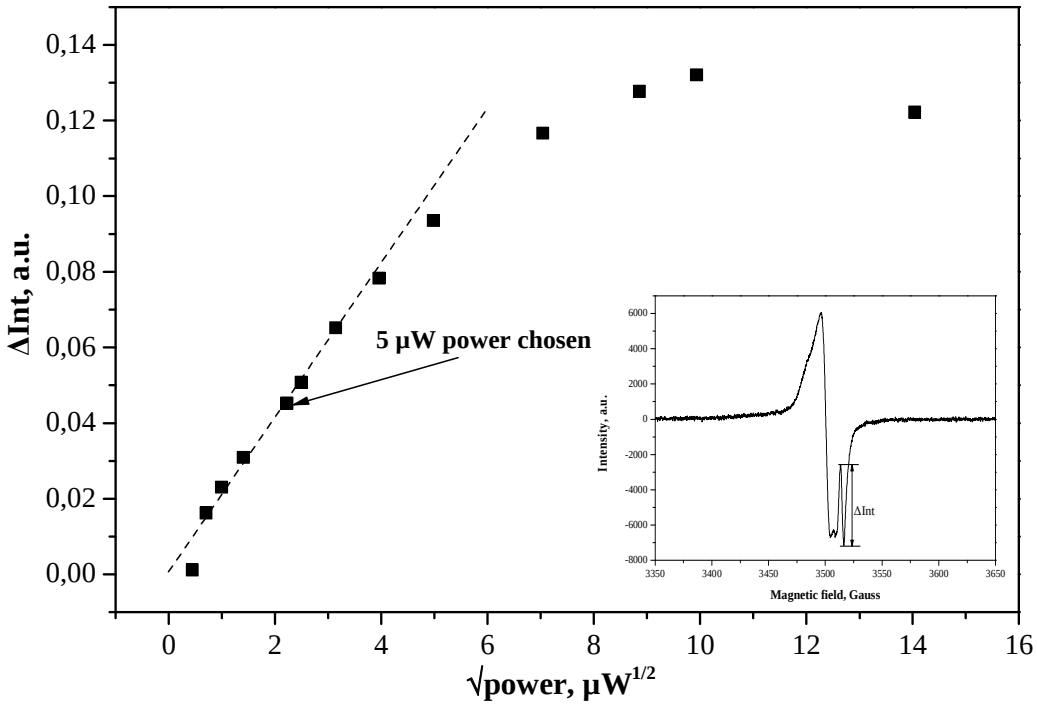


Figure II-7. Power saturation curve for E' centers in AS glasses

Point corresponding to 5 μW power was in the linear region and, consequently, was chosen for further experiments (Figure II-7).

Concerning microwave power in P-containing glasses and fibers, the information in literature is too various. The microwave power, announced in literature, varies from 0.01 to 20 mW. D. Griscom et al. [12] recorded all the defects in P-doped silica at 100K, but there is no information on saturation power. Working also with P-doped silica fibers at room temperature, G. Origlio et al. [13] used 0.19 mW and 1.9 mW powers for POHC and P defects, respectively. H. Hosono et al. [14] analyzed phosphate glasses at 77 K using 0.01 mW power to avoid signal saturation. Contrary to that, P. Ebeling et al. [15] observed paramagnetic defects in phosphate glasses at room temperature at 20 mW to have the whole signal visible. There is no principle agreement in this information neither in working temperature nor in saturation power. Therefore, it is important to attenuate carefully the microwave power to detect paramagnetic defects in our phosphate glasses.

In phosphate glasses, P centers were detected as well as POHC centers (Figure II-8). For each type, the power saturation laws were realized.

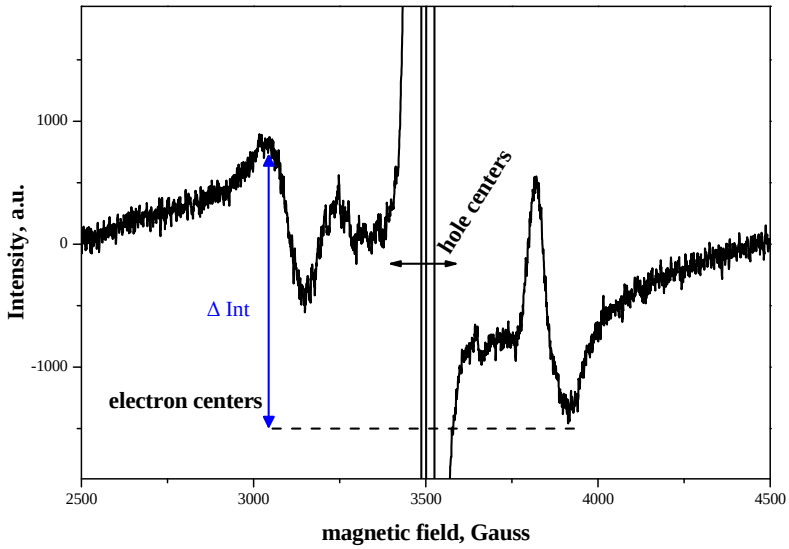


Figure II-8. EPR spectrum of P centers in phosphate glasses

The defects in phosphates were presented with double resonances due to hyperfine interaction. Its intensity was estimated as the absolute difference between 2 vertical maxima indicated in Figure II-8. The spectra were registered in vast microwave power range in 2500-4500 Gauss. The value of 1 mW was in linear region and thus chosen for P centers.

The narrow part in 3350-3650 Gauss corresponds to POHC defects (Figure II-9). Its intensity was estimated in common way as for P defects.

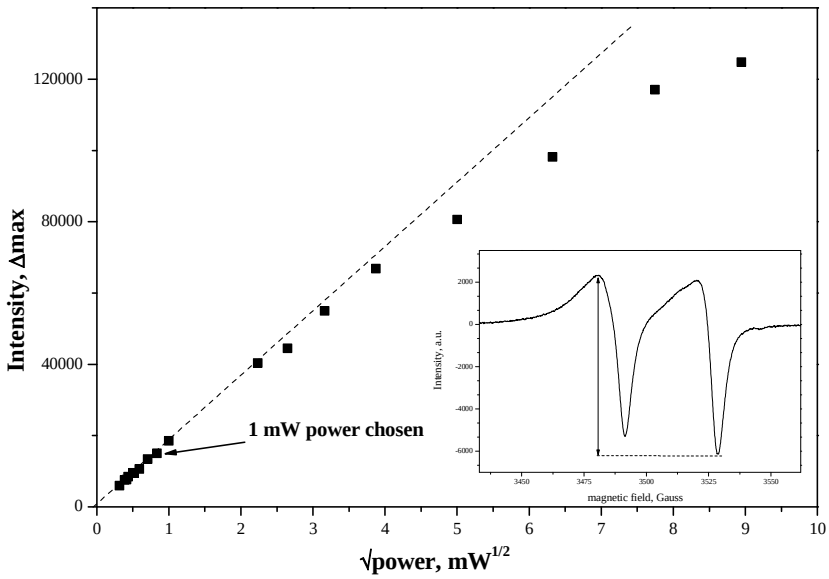


Figure II-9. EPR spectrum of POHC defects in phosphate glasses (inset) and its power saturation

At the common plot (Figure II-9) same power of 1 mW was chosen for POHC centers in phosphate glasses.

Thereafter, all the EPR spectra of paramagnetic defects in irradiated phosphate glasses were recorded at 1 mW power as it was driven from the power saturation experiment above.

3. b. 3 Parameters for Yb^{3+} ions study

Yb is a 4f-element with electronic structure $4f^{14}\ 5s^2\ 5p^6\ 6s^2$ (Figure II-10). The +3 charge can be reached by leaving out 3 electrons (Figure II-10 red spins). At first, 2 electrons leave 6s orbital. The 5s and 5p orbitals are complete and screen the internal 4f shell with 13 electrons. It is worth to point out here that $4f^{14}$ configuration is stable and it is thus possible to detect Yb^{2+} ions. Nevertheless, the ionization potential of Yb^{2+} ion (-2.8 V) is higher than that of Yb^{3+} (-2.22 V) which is formed by leaving of 1 4f electron. Yb^{3+} ions have therefore 13 f-electrons.

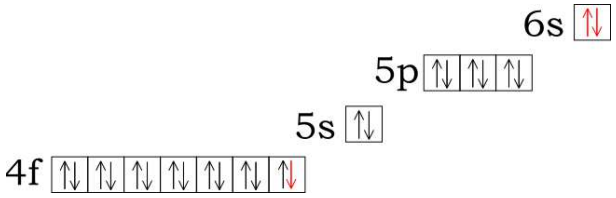


Figure II-10. The orbitals in Yb atom and Yb^{3+} ion formation

We can now calculate the term symbols of Yb^{3+} ion. The term is represented as $^{2S+1}L_J$. In our case spin angular momentum $S=\sum_1^{13} s_i$ where s_i is electron's spin +½ or -½. Consequently, S=±½ and spin multiplicity 2S+1 is 2 or 0 which means a doublet of energy levels. Orbital angular momentum $L=\sum_0^{n-1} l_i$ where l_i is the azimuthal quantum number and n is the principal quantum number, 4 in our case. L=3 (0, 1, 2, 3, 4, 5 … are S, P, D, F, G, H …) and it is written thus F. The total angular momentum quantum number values are J=|L-S|. Spin angular momentum of Yb^{3+} ion is either +½ (ground state because of positive spin projection) or -½ (excited state because of negative spin projection), and J can be $^7/_2$ and $^5/_2$, consequently. There are finally 2 energy levels of Yb^{3+} ions $^2F_{7/2}$ and $^2F_{5/2}$ (Figure II-11).

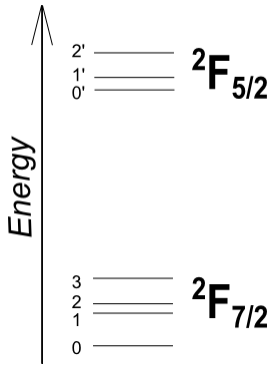


Figure II-11. Energy levels of Yb^{3+} ion

The f-electrons of lanthanides can be regarded as in weak crystal field due to 5s and 5p screen. The number of f-electrons of Yb^{3+} ion is odd. The levels described above can be thus degenerated into J+½ sublevels, 4 for $^2F_{7/2}$ and 3 for $^2F_{5/2}$ (Figure II-11). Each sublevel is a Kramers doublet. These transitions can be detected with EPR at low temperature only because of short T1 value at room temperature.

Yb is represented with 7 stable isotopes, 2 of them have non-zero nuclear momentum: ^{171}Yb (14.31% natural abundance) has I=½ and ^{173}Yb (16.31% natural abundance) has I=$^5/_2$. Thereafter, the EPR hyperfine signal of Yb^{3+} ions derives from 2 isotopes ^{171}Yb and ^{173}Yb. Yb^{3+} ions in various crystallized compounds occupy sites of various symmetry types. The parameters of g-tensors of Yb^{3+} paramagnetic ions in various compounds are given below (Table II-4).

Composition	Symmetry of Yb site	g-parameters	Source
YbB_{12}	O_h, cubic	g=2.52, slight anisotropy	[16]
β-PbF_2	cubic	g=3.434	[17]
$KMgF_3$	C_{4v}, tetragonal	$\|g_\parallel\|$=1.070, $\|g_\perp\|$=4.430	[18]
$LuVO_4$	D_{2d}, tetragonal D_2, C_{2v}, rhombic	$g_\parallel$=6.464, $\|g_\perp\|$=0.59 $\|g_\parallel\|$=2.75, $\|g_\perp\|$=0.89 $\|g_\parallel\|$=2.84, $\|g_\perp\|$=0.89 ---	[19]
BaY_2F_8	C_2, monoclinic	Isolated $g_\parallel$=4.91, $g_\perp$=5.09 Pairs $g_\parallel$=2.216, $g_\perp$=2.241	[20]
$KYb(WO_4)_2$	C_2, monoclinic	g_x=1.039, g_y=0.997, g_z=6.62	[21]
$CsCdBr_3$	D_{3d}, trigonal	$g_\parallel$=2.503 $g_\perp$=2.619	[22]

Table II-4. The symmetry of Yb sites and g-tensors parameters in various compositions

EPR was carried out quite a lot to characterize the Yb^{3+} ion symmetry and obtain some information on pairs in crystals [16] [20] [23] but less results could be found on glasses in literature [24] [25] [26] due to the broad signal. The intensity of Yb^{3+} EPR line is extremely sensitive to the temperature: it decreases crucially when T≥20 K due to the quick relaxation time T1 of rare earth element (except $4f^7$ element). The relaxation time T1, some distortion of Yb sites in glassy network and the multisite presence bring the Yb^{3+} line broadening in glass.

The EPR signal of Yb^{3+} in AS glasses at 4 K is a broad resonance at g=4.1 because it is not observed in glasses without Yb (Figure II-12). It was thus attributed to Yb^{3+} ions.

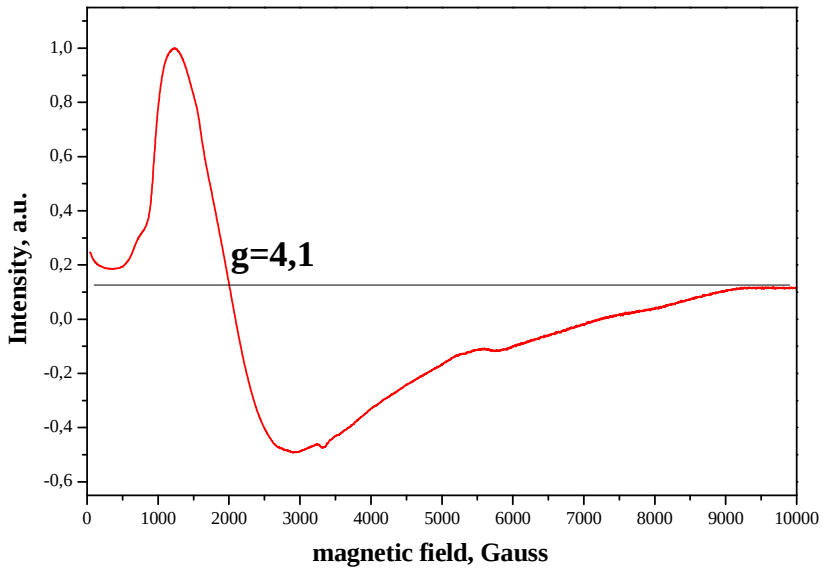


Figure II-12. EPR spectra of non-irradiated AS24 glass at 4K.

The dominant resonance position corresponds to g=4.1. It is close to the g-values in irradiated Yb-doped aluminoborosilicate (ABS) glasses [25].

For power saturation curve, the intensity estimated as Δmax and plotted is given in Figure II-13. The power optimal at 4K is 3mW (Figure II-13).

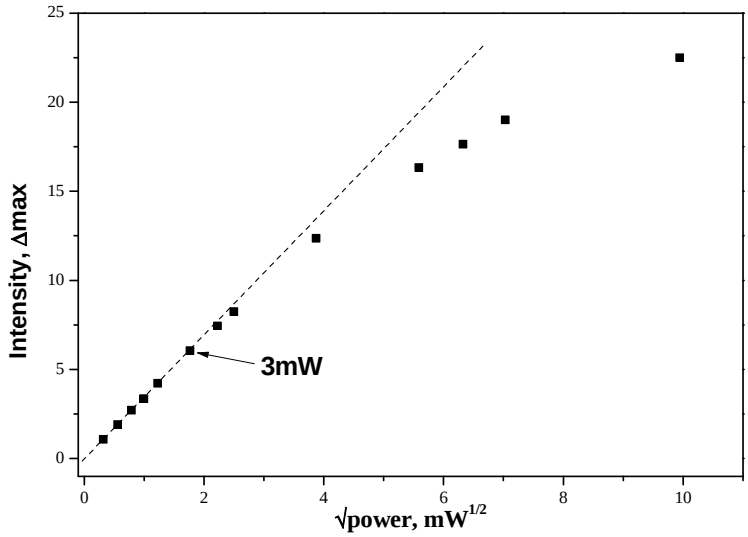


Figure II-13. Power saturation for Yb^{3+} ions in non-irradiated AS24 glass at 4K

For phosphate glasses microwave power saturation was recorded as well. The value 1mW at 4K was chosen.

4. Optical measurements

The Yb^{3+} spectroscopic properties were studied by carrying out absorption, lifetimes τ_{IR} and τ_{CL} and cooperative emission measurements. This part of work was executed in fruitful collaboration with Philippe Goldner and Alban Ferrier (ENSCP, Paris).

4. a. IR-luminescence of Yb^{3+}

Yb^{3+} emission $^2F_{5/2} \rightarrow {}^2F_{7/2}$ in the IR-region was recorded in LSI by HORIBA Jobin Yvon spectrofluorimeter under Xe lamp excitation with a 1200 gr/mm grating. The studied glasses were in powders of controlled particle size, 100-125 μm.

To follow the post-irradiation relaxation processes, the lifetimes τ_{IR} were recorded as well using the same equipment. The non-irradiated AS24_8 powder was chosen as reference. The established absolute error was estimated to 0.02 ms.

By reason of complexity and lack of time to irradiate all the samples under powders form as well as under slices form, the dose and dose rate effects were studied on slice samples only. The results from slices and powder irradiated in the same conditions were compared to exclude the serious deviation due to different physical substances. Besides, the powders were analyzed in ENSCP (with friendly

participation of P. Aschehoug) under 975 nm laser excitation in order to eliminate the error originating from equipment change (Table II-5, Table II-6). In all analyzed samples the decay curves were single-exponential indicating the absence of other processes.

Sample	My results			B. Schaudel powders [1], ms
	Spectrofluorimeter in LSI		Laser excitation in ENSCP, powder, ms	
	Slice, ms	Powder, ms		
AS22	2.45	**2.55**	**2.14**	**1.90**
AS23	1.80	**2.17**	**1.97**	**1.70**
AS24	1.41	**1.31**	**1.15**	**1.00**
AS26	1.13	**0.87**	**0.94**	**0.90**

Table II-5. Lifetimes τ_{IR} recorded in non-irradiated AS glasses

In aluminosilicate glasses the lifetimes were similar between powders and slices (Table II-5). The results obtained in LSI and in ENSCP were in good agreement, too. The lifetimes from B. Schaudel's work are shorter than in this work. This can come from small variations in synthesis methods: losses of Na at glass melting temperatures can affect the network structure and, consequently, Yb^{3+} environment.

The lifetimes τ_{IR} observed in phosphate glasses are given in Table II-6.

Sample	My results			B. Schaudel powders [1], ms
	Spectrofluorimeter in LSI		Laser excitation in ENSCP, powder, ms	
	Slice, ms	Powder, ms		
2743	0.82	**0.73**	**0.68**	**1.00**
2742	0.84	**0.84**	**0.81**	**0.95**
2745	1.16	**1.22**	**1.15**	**1.00**
2746	1.43	**1.34**	**1.40**	**1.15**

Table II-6. Lifetimes τ_{IR} recorded in non-irradiated phosphate glasses

Despite the values obtained in slices and in powder either in LSI or in ENSCP are in good correlation, the lifetimes τ_{IR} in B. Schaudel's work were different. With high probability it was generated by deviation in the phosphate glass synthesis.

4. b. Cooperative luminescence of Yb^{3+} (CL)

A weak green emission of Yb^{3+} in $YbPO_4$ was first observed by E. Nakazawa et al. in 1970 [27] where they proposed the term "cooperative luminescence".

Pairs of Yb^{3+} ions absorb simultaneously radiation of energy to excite $^2F_{5/2}$ state with consequent emitting of one photon which energy is twice higher than in case of common IR luminescence (Figure II-14). That is the mechanism leading to an emission in the visible region (480-530 nm). The lifetime value in this case is 2 times shorter than τ_{IR}. In different matrices it varies in the 300-550 μs range [27] [28] [29] [30].

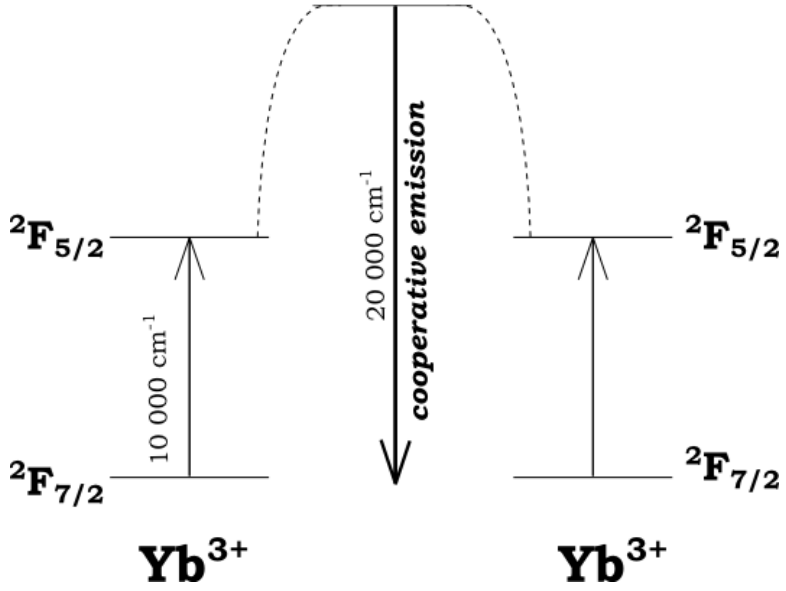


Figure II-14. Scheme of Yb^{3+} ions pairs energy levles

The quantitative theoretical interpretation of the experiments on cooperative luminescence is not yet well developed [31]. It concerns the cases of Yb cluster formation. However, in [32] the authors demonstrated the importance of cooperative emission probability in study of Yb-Yb pair interactions. After some particular calculations, the probability of cooperative luminescence X was given with formula that was applied to compare the intensities of cooperative emission probability [1]

$$X \propto \frac{I_{coop}}{P_{abs}^2 \tau^2}$$

P_{abs} was the absorbance power of the sample

Taking into account that the sample consists on equi-dimensional particles, the absorbance power was transformed into the coefficient a_D^2 that was calculated by multiplying the absorption spectrum of the sample and emission spectrum of the diode (normalized at maximum). The coefficient a_D was the area under the result curve.

$$X \propto \frac{I_{coop}}{\alpha_D^2 \tau^2}$$

One more reference was AS24_8 sample that was analyzed each time of experiments. Taking into account that its cooperative emission intensity was stable, its spectra recorded in all days of measurements were used to normalize the intensity as well.

To measure the cooperative emission, the same approach than B. Schaudel [1] was followed (Figure II-15) with the same laser diode [29]. The limited power allowed us first to study efficiently the samples with strong Yb^{3+} cooperative emission only (AS23, AS24, AS24_8, AS26). It was applied to follow the evolution in time of cooperative emission in these samples. Afterwards, we obtained the possibility to use a new laser diode to study the stabilized samples with low Yb^{3+} cooperative emission, too (AS22, AS24_05, phosphates).

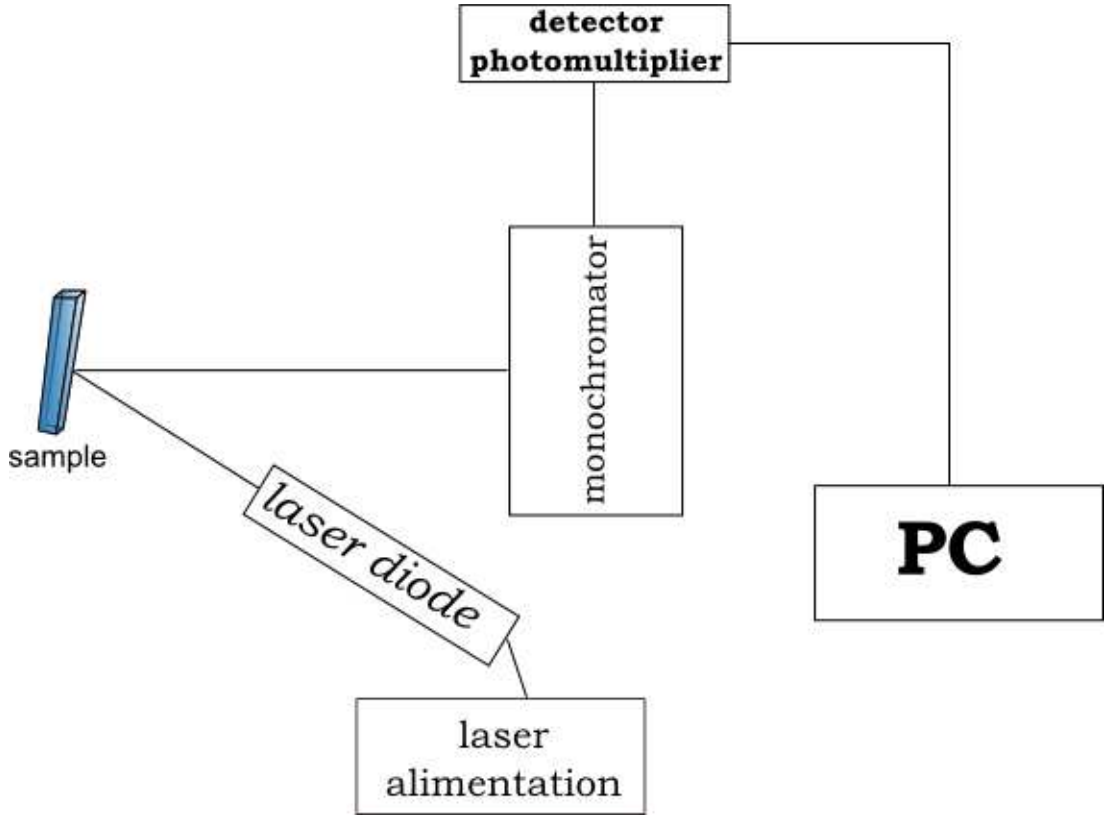


Figure II-15. The scheme of experimental setup for cooperative emission measurements

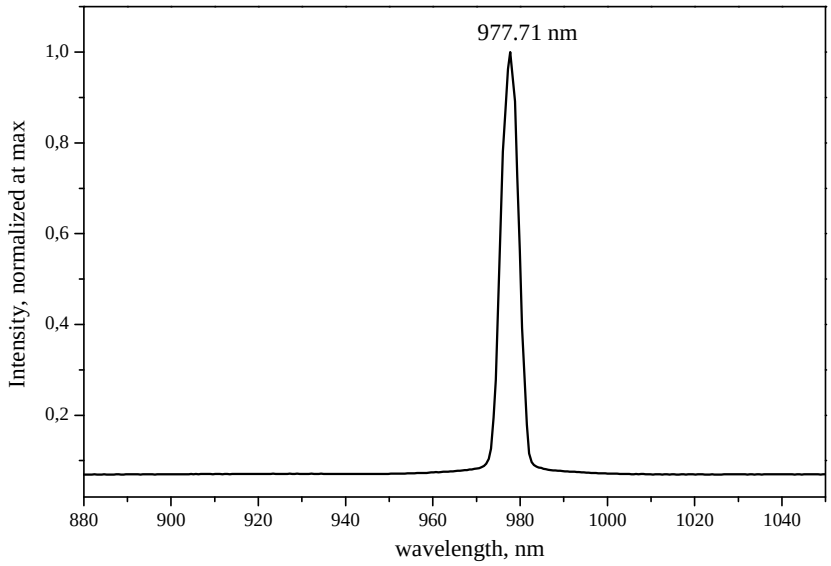


Figure II-16. Laser emission spectrum normalized at maximum

The spectrum of laser emission was implied to normalize the probability of cooperative luminescence (Figure II-16, Figure II-17). The spectrum was multiplied with absorption spectrum giving absorbance power P_{abs} in laser excitation region. It was reasonable in case of variable absorption for different Yb concentrations [1].

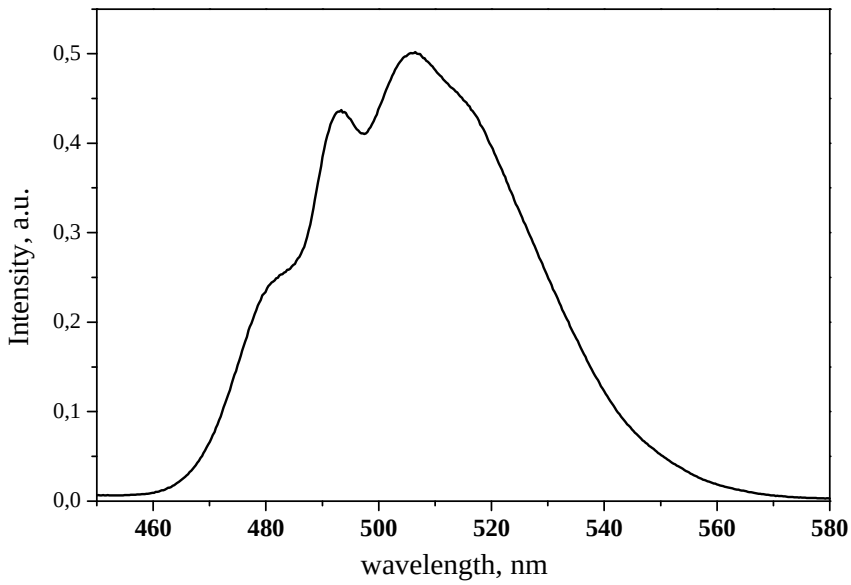


Figure II-17. Cooperative emission of Yb-Yb pairs under 975 nm excitation (aluminosilicate glass AS24_8)

4. c. Absorption

Absorption measurements were carried out with Cary 6000i UV-Vis-NIR spectrofluorimeter and InGaAs detector. The wavelength resolution was 0.5 nm. The

maximum range was 300-1200 nm. It was mainly useful for cooperative luminescence normalization.

The measurements were performed with powder sample of 100-125 μm particles. The measured parameter was Reflectance, after that it was derived into Absorbance using Kubelka-Munk formula

$$F(R) = \frac{(1-R)^2}{2R} = \frac{k}{s} = \frac{Abs \times c}{s}$$

F(R) – derived value of Kubelka-Munk function

R – reflectance

k – absorption coefficient

s – scattering coefficient

c – concentration of absorbing species

Abs – absorbance

Taking into account that the concentration of absorbing species was the same in most of the samples – 5 wt. % of Yb_2O_3, it was supposed that c/s is identical in the samples. Therefore, the comparison of derived from reflectance k/s could be used effectively.

The question of reference was of high importance. Since the interest was concentrated on Yb^{3+} absorption, the non-doped samples were used as the reference. Same principle was applied to study the irradiated samples: irradiated non-doped samples were used as the references. In Kubelka-Munk formula given above the parameter R was presented from

$$R = \frac{R_{sample}}{R_{refer}}$$

To exclude the effect of Yb-clusters on Yb^{3+} absorption, the experiment was calibrated as a function of the Yb concentration. The polished transparent non-irradiated slices were analyzed. The normalization by the thickness was implied to the results.

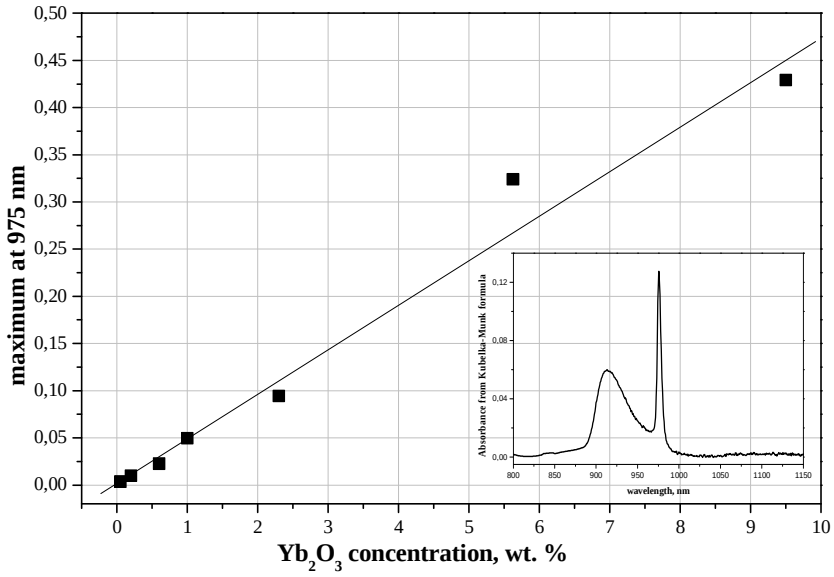


Figure II-18. Maxima of absorption in AS24_Ybx non-irradiated polished slices. Normalization by thickness. Absorption spectrum of AS24 glass is in inset

Yb^{3+} absorption obeyed to linear dependence within Yb concentration (Figure II-18) in the sample except the sample AS24_Yb5, the most used Yb concentration in this work. Stronger absorption could take place in case of cooperative effects, in particular, cooperative absorption.

4. d. Photoluminescence of defects (LSI)

In some particular cases, the radiation-induced point defects were analyzed by time-resolved photoluminescence in slices at room temperature. We used 266 nm and 532 nm laser excitations (pulsed Nd:YAG laser). For the detection Shramrock SR-303i spectrometer is associated to an ANDOR ICCD camera.

The beam energy of 266 nm excitation at the sample was 1.3 mJ. This technique was applied to investigate some diamagnetic defects in phosphate glasses which lifetime was estimated 5-6 ms. The power of the laser was optimized to detect the signal with the best signal/noise ratio without inducing photobleaching or defect creation.

The 532 nm excitation has been used to investigate NBOHC defects in aluminosilicate glasses. The delay was 500 ns and the gate width was 100 µs. The estimated lifetime of the defect was ~10 µs. The signal of Sm^{3+} emission was taken as reference to control the stability of experimental conditions (wavelength and intensity).

[1] B. Schaudel, Ph.D. dissertation, Paris: Université Paris VI, 2000.

[2] N. A. Bokov, *Glass Phys. Chem.,* vol. 31, p. 734, 2005.

[3] M. Abid, A. Shaim et M. Et-tabirou, *Materials Research Bulletin,* vol. 36, p. 2453, 2001.

[4] C. Bourgeois, Interaction particules-matière, Techniques de l'Ingénieur, traité Sciences fondamentales.

[5] N. Ollier et V. Pukhkaya, *Nucl. Instr. and Meth. in Phys. Res. B,* vol. 277, p. 121, 2012.

[6] E. K. Zavoisky, *State Register of Discoveries of the USSR, №85 Electronic Paramagnetic Resonance.*

[7] A. Abragam et B. Bleaney, Electron Paramagnetic Resonance of Transition Ions, Oxford: Clarendon Press, 1970.

[8] J. Vincent, O. Guillot-Noël, L. Binet, P. Aschehoug et Y. Le Du, *J. Appl. Phys.,* vol. 104, p. 033519, 2008.

[9] E. J. Friebele, D. L. Griscom, M. Stapelbroek et R. A. Weeks, *Phys. Rev. Lett.,* vol. 42, p. 1346, 1979.

[10] L. Nuccio, S. Agnello et R. Boscaino, *Phys. Rev. B,* vol. 79, p. 12505, 2009.

[11] H. Nishikiawa, E. Watanabe, D. Ito et Y. Ohki, *J. Non-Cryst. Solids,* vol. 179, p. 179, 1994.

[12] D. L. Griscom, E. J. Friebele, K. J. Long et J. W. Fleming, *J. Appl. Phys.,* vol. 54, p. 3743, 1983.

[13] G. Origlio, F. Messina, M. Cannas, R. Boscaino et S. Girard, *Phys. Rev. B,* vol. 80, p. 205208, 2009.

[14] H. Hosono, Y. Abe et H. Kawazoe, *J. Non-Cryst. Solids,* vol. 71, p. 261, 1985.

[15] P. Ebeling, D. Ehrt et M. Friedrich, *Opt. Mater.,* vol. 20, p. 101, 2002.

[16] T. S. Altshuler, Y. V. Goryunov, M. S. Bresler, F. Iga et T. Takabatake, *Phys. Rev. B,* vol. 68, p. 014425, 2003.

[17] K. I. Gerasimov, A. M. Leushin et M. L. Falin, *Phys. Solid State,* vol. 43, p. 1675, 2001.

[18] M. L. Falin, V. A. Latypov, B. N. Kazakov, A. M. Leushin, H. Bill et D. Lovy, *Phys. Rev. B,* vol. 61, p. 9441, 2000.

[19] O. Guillot-Noël, P. Goldner, M. Bettinelli et E. Cavalli, *J. Phys.: Condens. Matter,* vol. 17, p. 3061, 2005.

[20] S. M. Kaczmarek, G. Leniec, J. Typek, G. Boulon et A. Bensalah, *J. of Lumin.,* vol. 129, p. 1568, 2009.

[21] M. C. Pujol, M. Aguilo, F. Diaz, M. T. Borowiec, A. D. Prokhorov, V. P. Dyakonov, A. Nabialek, S. Piechota et H. Szymczak, *Physica B,* vol. 388, p. 257, 2007.

[22] V. Mehta, O. Guillot-Noël, D. Simons, D. Gourier, P. Goldner et F. Pellé, *J. All. Comp.,* vol. 323&324, p. 308, 2001.

[23] T. Bodziony, S. M. Kaczmarek et C. Rudowicz, *Physica B,* vol. 403, p. 207, 2008.

[24] D. L. Smith, H. J. Stapleton et M. B. Weissman, *Phys. Rev. B,* vol. 33, p. 7417, 1986.

[25] N. Ollier, R. Planchais et B. Boizot, *Nucl. Instr. and Meth. in Phys. Res. B,* vol. 266, p. 2854, 2008.

[26] G. Dantelle, M. Mortier, P. Goldner et D. Vivien, *J. Phys. Condens. Matter,* vol. 18, p. 7905, 2006.

[27] E. Nakazawa et S. Shionoya, *Phys. Rev. Lett.,* vol. 25, p. 1710, 1970.

[28] T. G. Ryan et S. D. Jackson, *Opt. Commun.,* vol. 273, p. 159, 2007.

[29] B. Schaudel, P. Goldner, M. Prassas et F. Auzel, *J. Alloys and Comp.,* vol. 300&301, p. 443, 2000.

[30] P. Barua, E. H. Sekiya, K. Saito et A. J. Ikushima, *J. of Non-Cryst. Solids,* vol. 354, p. 4760, 2008.

[31] F. Auzel et P. Goldner, *Opt. Mater.,* vol. 16, p. 93, 2001.

[32] P. Goldner, F. Pellé, D. Meichenin et F. Auzel, *J. Lumin.,* vol. 71, p. 137, 1997.

List of Figures

Figure II-1. SIRIUS accelerator in LSI: from top to down. Photo of irradiation source where electron beam is created, photo of two irradiation cells, zoom at CIRANO and sample holder. 11
Figure II-2. Energy levels splitting under applied magnetic field 13
Figure II-3. Curves recorded with EPR spectroscopy 14
Figure II-4. ERP spectra of Er^{3+} in β-Ga_2O_3 [7] 16
Figure II-5. The principal scheme of EPR spectrometer 17
Figure II-6. Power saturation of hole centers in AS glasses 18
Figure II-7. Power saturation curve for E' centers in AS glasses 19
Figure II-8. EPR spectrum of electron centers in phosphate glasses 20
Figure II-9. EPR spectrum of hole centers in phosphate glasses (inset) and its power saturation 20
Figure II-10. The orbitals in Yb atom and Yb^{3+} ion formation 21
Figure II-11. Energy levels of Yb^{3+} ion 22
Figure II-12. EPR spectra of non-irradiated AS24 glass at 4K and 10K. show Δmax on the picture 23
Figure II-13. Power saturation for Yb^{3+} ions in non-irradiated AS24 glass at 4K 24
Figure II-14. Scheme of Yb^{3+} ions pairs energy levles 26
Figure II-15. The scheme of experimental setup for cooperative emission measurements 27
Figure II-16. Laser emission spectrum normalized at maximum 28
Figure II-17. Cooperative emission of Yb-Yb pairs under 975 nm excitation (aluminosilicate glass AS24_8) 28
Figure II-18. Maxima of absorption in AS24_Ybx non-irradiated polished slices. Normalization by thickness 30

List of Tables

Table II-1. Nominal compositions of aluminosilicate glasses 8
Table II-2 . Nominal compositions of phosphate glasses 9
Table II-3 . Irradiation conditions 12
Table II-4. The symmetry of Yb sites and g-tensors parameters in various compositions 22
Table II-5. Lifetimes τ_{IR} recorded in non-irradiated AS glasses 25
Table II-6. Lifetimes τ_{IR} recorded in non-irradiated phosphate glasses 25

Chapter III

Yb-doped Na-aluminosilicate glasses

III. Yb-doped Na-aluminosilicate glasses 38

1. Glass structure 38

1. a. Bibliographic part 38

1. b. AS22-AS26 glass structure 41

1. c. Effect of irradiation at strong doses on glass structure..... 44

1. d. Yb environment 47

1. d. 1 IR-luminescnce..... 47

1. d. 2 EPR spectroscopy..... 47

1. d. 3 Cooperative luminescence..... 49

1. d. 4 AS24_Ybx glasses 51

Raman spectroscopy..... 51

Cooperative luminescence..... 52

2. Point defects 53

2. a. Paramagnetic defects assignation..... 53

2. a. 1 E'-centers..... 53

2. a. 2 Peroxy radicals 54

2. a. 3 Non-Bridging Oxygen Hole Centers (NBOHC)..... 54

2. a. 4 HC defects 54

2. a. 5 Al-OHC defects 56

2. b. Formation of paramagnetic defects in AS22-AS26 glasses..... 56

2. b. 1 Influence of the glass composition..... 56

2. b. 2 Influence of Yb-doping 58

2. c. Relaxation of paramagnetic defects 61

2. c. 1 Analysis of relaxation curves..... 63

2. c. 2 Recovery of individual defect type 64

2. d. Effect of irradiation dose and dose rate 65

2. d. 1 Total amounts of the defects..... 65

2. d. 2 Relative amounts of defects (dose effect) 69

3. Luminescent properties of Yb^{3+} 73

3. a. Cooperative luminescence (CL) 73

3. a. 1 CL in AS glasses with high content of Yb clusters 73

3. a. 2 CL in AS glasses with less content of Yb clusters 76

3. b. Lifetime of Yb^{3+} $^2F_{5/2}$ excited state 76

3. b. 1 Before irradiation 77

3. b. 2 Dose and dose rate effects 77

3. c. Analysis of the role of defects in CL and lifetime evolution under irradiation 82

3. c. 1 Post-irradiation evolution in time 82

3. c. 2 Thermal annealing treatments 83

AS22_10e8 glass 83

AS24_10e8 glass 86

4. Conclusions 89

III. Yb-doped Na-aluminosilicate glasses

In this Chapter III aluminosilicate glasses doped with Yb are discussed. Yb cluster content is different from one glass to another in this series AS22-AS26 [1]. Therefore, it is interesting to study in aluminosilicate glasses the role of Yb cluster on point defects formation which has an impact on the Yb^{3+} luminescent properties. After analysis of differences in glass structure and Yb^{3+} environment, we discuss the evolution of glass properties under irradiation.

The point defects are investigated as a function of irradiation dose rate, dose and time. Yb cooperative luminescence and the lifetime of excited $^2F_{5/2}$ state are studied in a vast dose range. The role of Yb cluster will be discussed.

We tried to understand the role of point defects in the decrease of the lifetimes τ_{IR} and τ_{CL}.

1. Glass structure

1. a. Bibliographic part

Glass network-forming SiO_4 polyhedra are usually corner-linked via Bridging Oxygens (BO). They form a three-dimensional extended connected network according to Continuous Random Network model of Zachariasen (CRN) (Figure III-1 a) [2]. Modifying cations, such as alkalis, destroy the connectivity of the oxide network and create Non-Bridging Oxygens (NBO) that are linked to only one network-forming cation. The structure of a modified glass can be pictured as a combination of a partly depolymerized network and an ionically packed modifying oxide according to the Modified Random Network (MNR) model (Figure III-1 b) established by Greaves [3]. When tetrahedral network-formers like Al^{3+} ions are incorporated into a modified silicate glass composition they form negatively charged $(AlO_4)^-$ units that must be compensated by the modifying cations and the concentration of NBOs is thus reduced proportionally (Figure III-1 c). The structure

of aluminosilicate glass is described in Compensated Continuous Random Network (CCRN) [3].

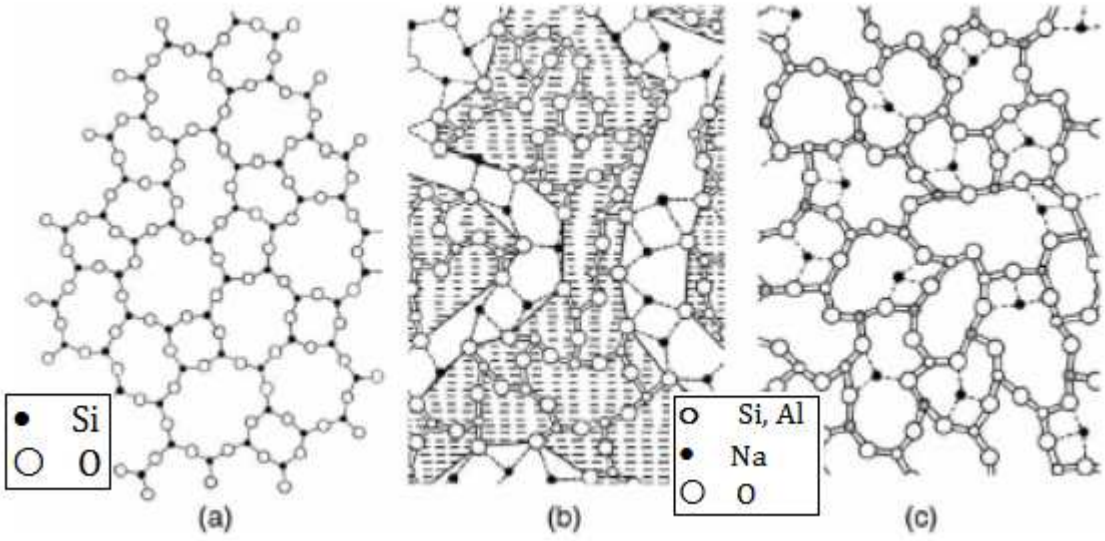


Figure III-1. Structure of silicate glasses [2]

The contents of Al and alkali ion can be characterized by Aluminum Saturation Index (ASI) which is molar ratio Al_2O_3/Na_2O in our case. Variances from ideal CCRN tetrahedral aluminosilicate network described above take place with the presence of AlO_4-AlO_4 connections. In the case of glasses modified by high field strength cations such as La^{3+} and Y^{3+}, ^{27}Al NMR studies have detected five- and six-coordinated Al species [4].

Rare-Earth elements diluted in low concentrations are regarded as network modifiers because of positive charge +3. They can stabilize $[AlO_4]^-$ tetrahedra as well. Further increase of RE^{3+} content leads to a cluster formation and their role in glass network modification evolves. When the ratio “ionic charge”/“ionic radius” is high, as it is for La^{3+} or Y^{3+} ions, these cations are believed to compete strongly for oxygen with Al^{3+}, pushing the last mentioned into higher coordination. On the other hand, AlO_5 and AlO_6 groups were also observed by ^{27}Al NMR in binary Al_2O_3–SiO_2 glasses in addition to the prevailing AlO_4 groups [5] [6]. AlO_6 groups were also detected in under-compensated CaO–Al_2O_3–SiO_2 glasses where ASI<1 [7]. In all of these cases, the lack of enough charge-balancing modifier ions or its complete absence brings the formation of higher-coordinated Al groups in order to stabilize the charge balance.

Rare-earth ions are applied as dopant agents (~1% order) in materials because of limited chemical solubility and consequent self-quenching. RE clusters degrade

strongly the luminescent properties and they are thus a troublesome feature of fabrication RE-containing materials. According to simulation works [8], in Na-modified silicate glasses Eu^{3+} ions can form clusters at 1 mol. % concentration, mostly consisting 2 ions in a cluster. In Nd-doped SiO_2 glasses the formation of Nd-O-Nd linkages was shown by Sen [9]. The EXAFS study executed by d'Acapito et al. of Er- and Yb-doped silica-titania-alumina [10] and aluminophosphate [11] glasses revealed the absence of any RE-RE correlation. The authors do not deny, however, the possibility of RE-cluster formation with longer RE-RE distances that are detectable by EXAFS (>4 Å) [11].

Yb^{3+} ions have their advantage in study of RE clusters because of cooperation effects such as luminescence or absorption that arise from Yb clusters [1]. Therefore, Yb is an attractive ion for RE cluster probe. Yb cluster formation is impacted by glass matrix composition, too. The number of Non-Bridging Oxygens plays a key role [12]. It was demonstrated by S. Sen et al. that in Yb-doped SiO_2 glass at ~1000 ppm concentration of Yb_2O_3 the second coordination shell of Yb^{3+} ions consists on both Si and Yb giving rise to Yb-O-Yb linkages [13].

1. b. AS22-AS26 glass structure

I remind here that we studied four AS glasses with 20 mol. % of Na_2O and varied SiO_2 and Al_2O_3 contents. Raman spectroscopy was executed in LADIR (Paris VI) on massive glasses. For each slice several points were recorded and homogeneous structure was confirmed in all the glasses analyzed (powders and slices). All the Raman spectra of non-irradiated Yb-doped AS22-26 glass are presented in Figure III-2.

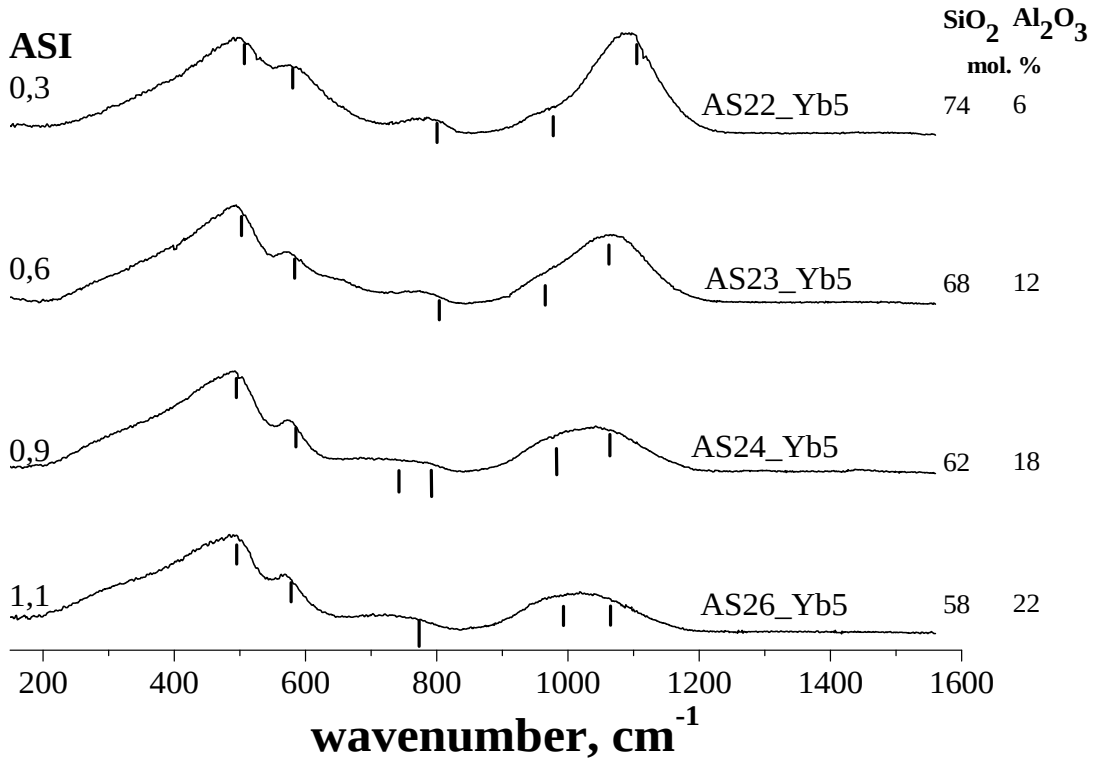


Figure III-2. Raman spectra of non-irradiated Yb-doped AS glasses

The dominant band is at 495 cm^{-1} with a quite wide shoulder at 300 cm^{-1} (Figure III-3). The shoulder becomes more and more obvious and the band becomes asymmetrically broader as Al content increases. We can observe moreover a relatively narrow peak at 570 cm^{-1} of less intensity. Its maximum moves to higher values of wavenumbers with increasing Al content.

To follow the glass network evolution within chemical composition in more details, the spectra is hereafter superposed and normalized at 495 cm^{-1} (Figure III-3).

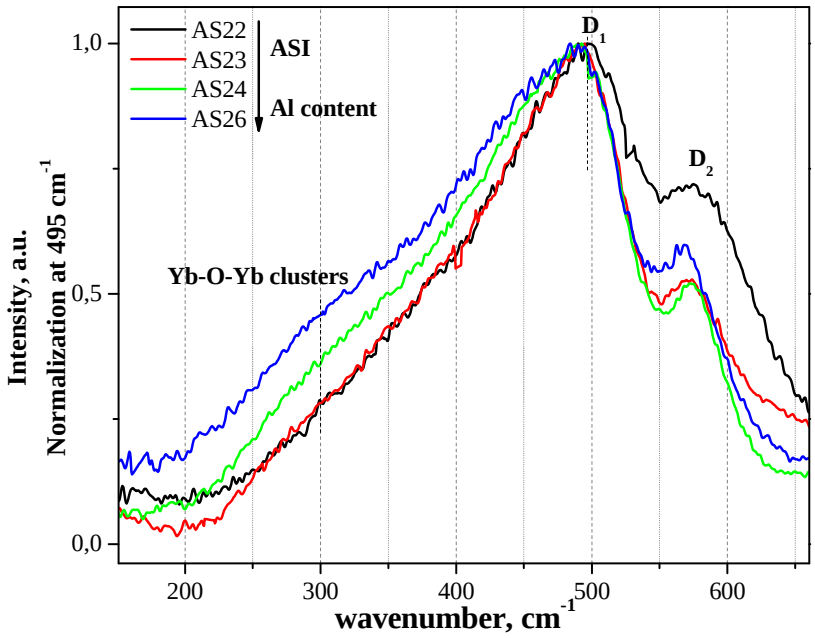


Figure III-3. Zoom on Raman spectra, normalization at 495 cm^{-1}

The bands at 495 cm^{-1} and 606 cm^{-1} are associated with D_1 (4-membered rings) and D_2 (3-membered rings), respectively [14]. The D_2 peak is visible only for the lowest Al content (AS22). Insertion of more Al in the silicate network suppresses the formation of SiO_4 3-membered rings. The band at 570 cm^{-1} is associated with the vibration modes of Al-O-Al linkages [15]. Its presence is more expressive in glasses with more Al. We conclude thus that the less intensive band in 570-600 cm^{-1} region is attributed to 3-membered rings with involved AlO_4 tetrahedra.

According to Ellison et al. [16] and Li et al. [17], at 300 cm^{-1} and 910 cm^{-1} one can see formation of Ln-O-Ln clusters. We note an increase of Yb-O-Yb clusters in AS24 and AS26 glasses. This result is in agreement with cooperative luminescence measurements.

The intensities of the bands at 600-900 cm^{-1} are low (Figure III-2). For glasses with low Al content (AS23, AS22) one can observe one band at 780 cm^{-1} due to both Al and O displacements at Al-O stretching motions [15]. As Al content increases, a new band at 720 cm^{-1} appears. At the same time maximum of first mentioned band moves to lower wavenumbers.

It is however difficult to conclude precisely from Raman spectroscopy data on the type of Al polyhedra. We realized ^{27}Al MAS NMR analysis for each glass composition; the NMR spectra are displayed in Figure III-4. The MAS NMR spectra have been acquired in collaboration with Th. Charpentier (IRAMIS CEA).

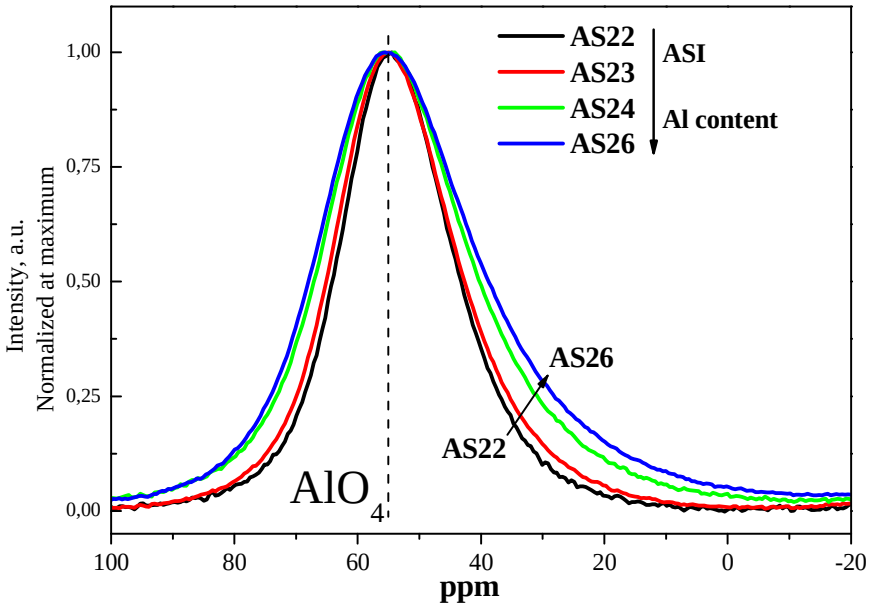


Figure III-4. ^{27}Al MAS NMR spectra of non-irradiated non-doped glasses

The isotropic chemical shift ~60 ppm corresponds to AlO_4 species (Figure III-4). We also detect a slight increase of the quadrupolar interaction from sample AS22 to AS26 (Al increasing) characterized by the broadening of the band indicating a disorder around Al(IV) with Al content increases.

Let us now discuss in details the Raman spectra in the 800-1300 cm^{-1} range. The spectra, normalized at 1000-1100 cm^{-1} are in Figure III-5.

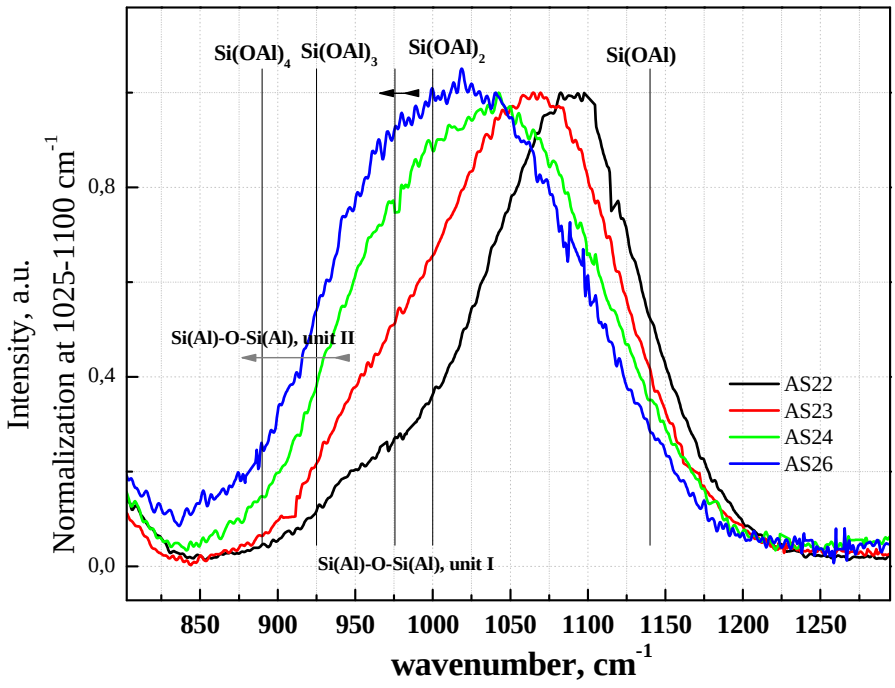


Figure III-5. Zoom of Raman spectra at 900-1300 cm^{-1} range

The broad Raman band in the 850-1200 cm^{-1} region can be attributed to SiO_4 tetrahedra connected to Si or Al and Si(Al)-O-Si(Al) linkages [15] [18].

The following linkages and their corresponding Raman modes can be found: [15]: Si(OAl) – 1140 cm^{-1}, $Si(OAl)_2$ – 1000 cm^{-1}, $Si(OAl)_3$ – 925 cm^{-1}, $Si(OAl)_4$ – 890 cm^{-1}. Movement of the broad band's maximum to lower wave-numbers when Al content increases can be assigned to an appearance of more Si ions connected to Al through O-bridges. This effect is corroborated by ^{29}Si MAS-NMR measurements: the maximum of the NMR band moves from AS22 glass to AS26 towards higher values of chemical shift indicating the presence of more Al atoms linked to Q_n species [19].

It is also possible that increasing of Yb-clustering level as mentioned above, at 910 cm^{-1} position impacts the evolution of the Raman spectra. This hypothesis is in agreement with cooperative luminescence experiment results.

1. c. Effect of irradiation at strong doses on glass structure

Since an impact of strong doses on the glass structure can occur, it was important to compare irradiated and non-irradiated samples. Irradiation conditions can be consulted to Chapter II, section 2.

Strong dose effect on glass structure has been studied by NMR and Raman spectroscopy. For NMR spectroscopy non-doped samples were irradiated to avoid the line broadening due to quadrupolar interactions with paramagnetic Yb^{3+} or Er^{3+} ions, achieved dose was $1.7 \cdot 10^9$ Gy.

The shape of 495 cm^{-1} band is modified (Figure III-6). It becomes narrower indicating less dispersion in Si-O-Si angle variation.

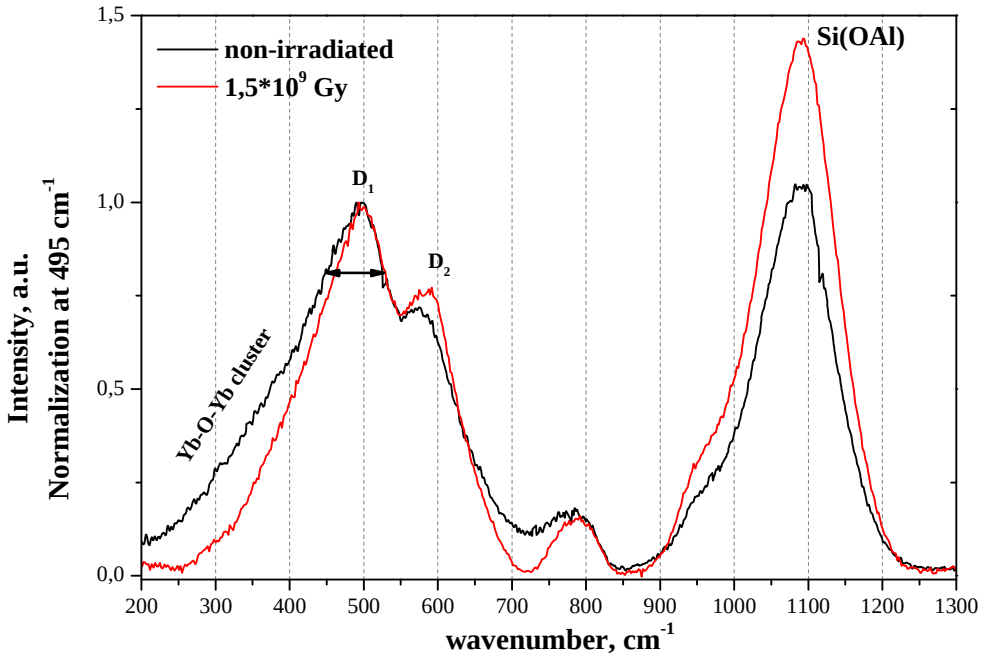


Figure III-6. Raman spectra of AS22 glasses, normalization at 495 cm^{-1}

The increase of D_2 component is associated to more 3-membered rings in glass network. In conclusion, it means the increase of glass densification under irradiation with strong doses (>1.5·10^9 Gy).

^{27}Al MAS NMR spectrum of this non-doped glass exhibits some distortion in Al^{3+} environment and a very slight shoulder at 20 ppm corresponding to Al(V) presence (Figure III-7).

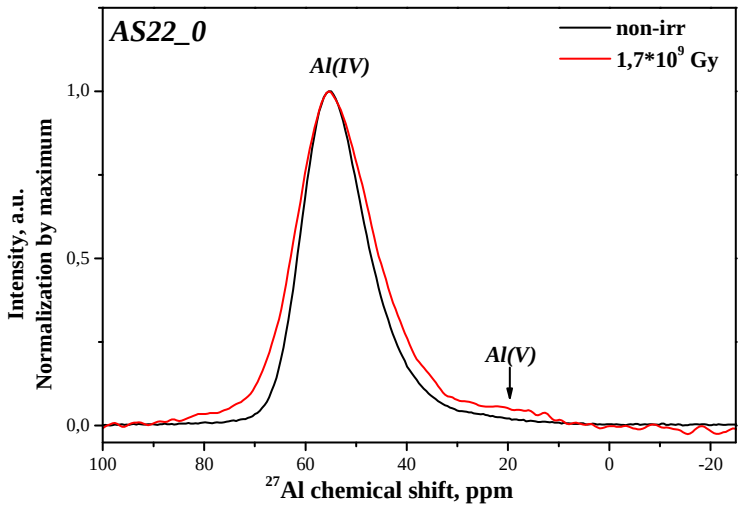


Figure III-7. 2D ^{27}Al MAS NMR spectra of AS22_0 glasses

2D ^{27}Al MAS NMR experiment confirms this attribution with presence of the small component of Al(V) in irradiated Er-doped AS22_Er glass (0.5 wt. % of Er_2O_3) (Figure III-8).

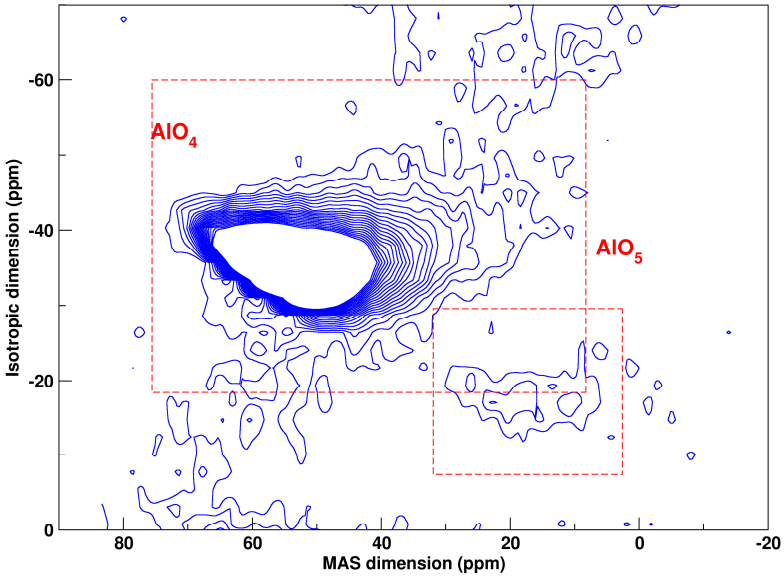


Figure III-8. 2D ^{27}Al MAS NMR spectrum of e-irradiated AS22_Er glass at $2 \cdot 10^9$ Gy

Al^{3+} in higher coordination needs more positive charge to stabilize their polyhedra of Oxygens. So, the presence of Al(V) is in according with the Na^+ ions migration occurring under irradiation in this glass.

In other 3 glass compositions AS23, AS24 and AS26 no structural modifications are observed under irradiation. No molecular oxygen is observed in irradiated glasses.

1. d. Yb environment

1. d. 1 IR-luminescnce

Yb^{3+} ions exhibit $^2F_{5/2} \rightarrow {}^2F_{7/2}$ emission in the IR-range (Figure III-9).

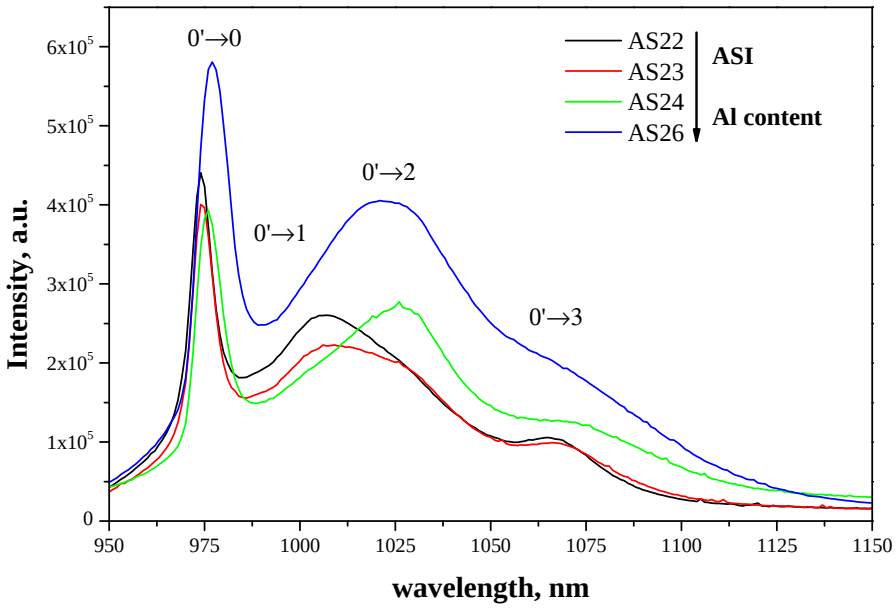


Figure III-9. Yb^{3+} luminescence in non-irradiated AS glasses

The particular transitions are marked in Figure III-9; the labels are from Figure II-11. The lifetime of $^2F_{5/2}$ excited state varies in 1-2 ms range in AS22-AS26 glasses.

The most intensive component of $^2F_{5/2} \rightarrow {}^2F_{7/2}$ emission is 0'→0 in all four glasses. One can see the principle difference between emission spectra shape of AS22-AS23 glasses and AS24-AS26 glasses. In AS22-AS23 glasses 0'→1 and 0'→3 components are more intensive. In AS24-AS26 glasses 0'→2 component is well distinguished. This result is attributed to different Yb^{3+} environment in AS22-AS23 and AS24-AS26 glasses.

1. d. 2 EPR spectroscopy

The Yb^{3+} EPR signal in glasses is represented by a broad line which is recorded in the full range of available magnetic field (Figure III-10).

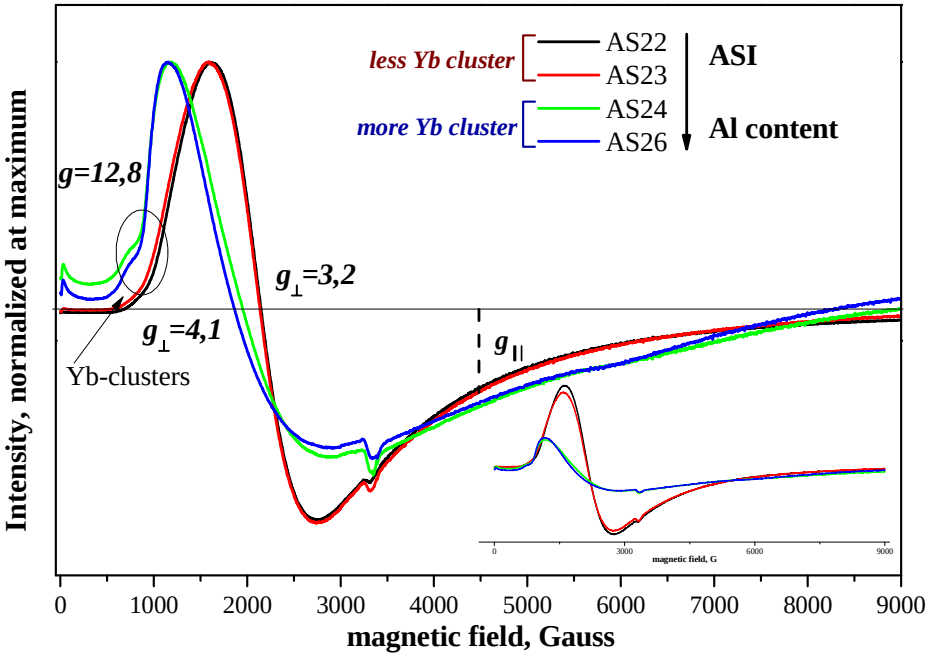


Figure III-10. EPR spectra of non-irradiated AS glasses at 4K, normalized at maximum. Normalization by mass and attenuation gain is inset

The series of 4 chemical compositions with same Yb concentrations divided into 2 types with different EPR intensities and resonance positions.

In AS24 and AS26 glasses EPR signal is much lower despite the same amount of Yb in all four glasses (Figure III-10 inset). This decrease indicates that a part of Yb^{3+} ion is not detected due to probable too short relaxation time T1. It can occur when Yb^{3+} ions form clusters. The g-factor can be described by an axial symmetry of Yb^{3+} sites in AS glasses. The value of $g_{\perp}$ is ~3.2 in AS22 and AS23 glasses and ~4.1 in AS24 and AS26 glasses. The parameter $g_{\parallel}$ is in higher magnetic field range. It is difficult without any simulation to give the precise values, but we can estimate that $g_{\parallel}$ is ~1.3-1.4 in AS22 and AS23 glasses while in AS24 and AS26 glasses $g_{\parallel}$ is ~1.1. The separation of Yb^{3+} environment in AS22-AS23 and AS24-AS26 glasses is in agreement with $^2F_{5/2} \rightarrow {}^2F_{7/2}$ emission in the IR-region.

Besides, there can be seen a shoulder at g=12.8 assigned to Yb clusters because, according to Sen [13], isolated Yb^{3+} ions give an EPR signal below g~8.

The $g_{\perp}$ parameter in AS22 and AS23 glasses is 3.2, close to Yb-doped ABS glasses [20] where g-factor varies from 3.17 to 3.32. As in AS22 and AS23 samples, in aluminoborosilicate glasses the concentration of Yb clusters is relatively lower than in AS24 and AS26 samples [20]. It corresponds to the similarity of Yb^{3+} environments in aluminoborosilicate glasses and aluminosilicate with less Yb

clusters. In consequence, the shoulder of Yb cluster at g=12.8 is absent in AS22 and AS23 glasses. It is also interesting to indicate the similarity between Yb^{3+} environment in a phosphate glass and in AS22 with the least Al content (Figure III-11).

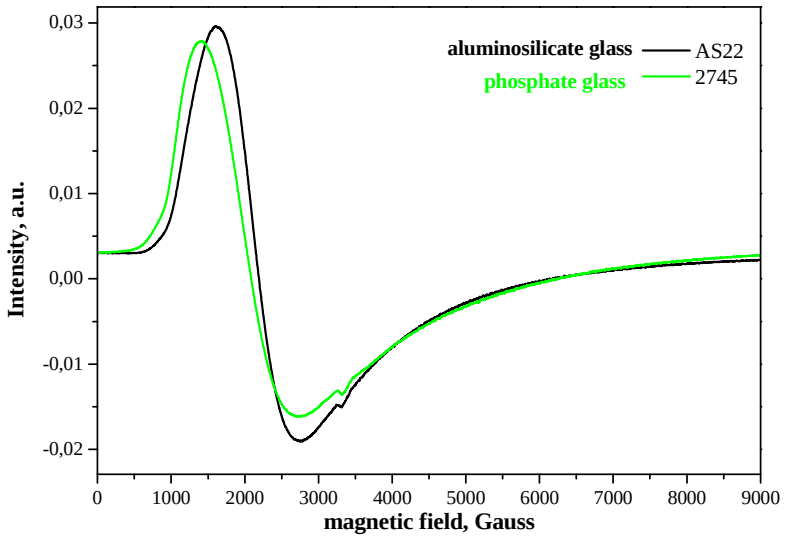


Figure III-11. EPR spectra of non-irradiated glasses, 4K

In both 2745 phosphate and AS22 glasses no Yb cluster is detected by EPR spectroscopy.

1. d. 3 Cooperative luminescence

We remind here that the theoretical aspects of cooperative luminescence phenomenon and the experimental technique are given in Chapter II, section 4.b.

Cooperative luminescence was studied in powders to avoid the effects of sample's geometry deviation. The influence of e^--irradiation was studied for 10^5 Gy, $3.2 \cdot 10^6$ Gy and 10^8 Gy doses. To compare the results with γ-irradiation, 10^5 Gy and $3.2 \cdot 10^6$ Gy doses were chosen. In order to study the link between Yb^{3+} cooperative luminescence and the point defects, the evolution of cooperative emission in time after the irradiation was followed for 10^5 Gy dose (both irradiation types) and 10^8 Gy dose in glasses with higher Yb cluster content: AS24, AS26 and AS24_8. The impact of glass composition on cooperative luminescence under irradiation was investigated after the defects stabilization.

The probabilities of cooperative luminescence in non-irradiated glasses obtained in this work are shown in Figure III-12.

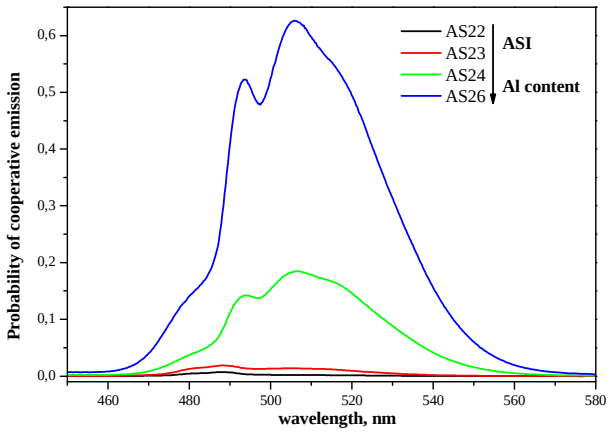


Figure III-12. Probability of cooperative luminescence in non-irradiated AS2x_Yb5 glasses. Normalization by absorption and lifetime τ_{IR}

The probability of cooperative emission is higher in AS26 and AS24 glasses whereas in AS22 and AS23 it is significantly lower. As shown before [12], in AS glasses the ASI parameter has an impact on the cooperative emission intensity, and thus on Yb cluster formation, despite the same Yb concentration. Our results are in agreement with B. Schaudel [12], Raman and EPR spectroscopy at low T. Thereafter, the studied AS glasses are confirmed to be divided into 2 series: one of high Yb cluster content (AS24 and AS26) and another one of low Yb cluster content (AS22 and AS23).

Concerning our samples, significant variation of Yb cluster was assigned in aluminosilicate glasses to Al content variation [12]. The cause is in different amount of Non-Bridging Oxygens (NBOs) in studied glasses when SiO_2 dioxide was coherently replaces with Al_2O_3 oxide with unchanged Na_2O content. Since Al^{3+} ions in contrary to Si^{4+} ions need to compensate the charge to 4+, more Na^+ ions take part in this, precluding NBO formation. Yb^{3+} ions cannot be surrounded equally with NBOs, they form thus Yb clusters in glasses with higher ASI.

1. d. 4 AS24_Ybx glasses

Raman spectroscopy

As Yb concentration increases in AS24_Ybx glasses, one can observe some changes in the Raman spectra of AS24 glass (Figure III-13).

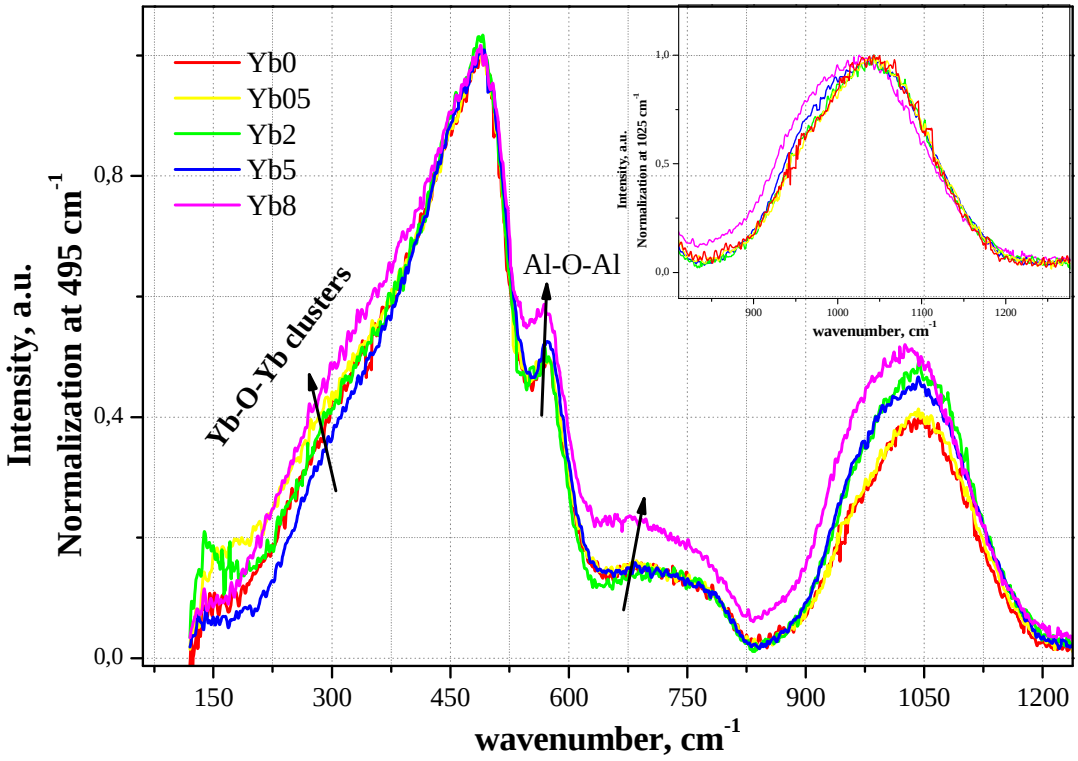


Figure III-13. Raman spectra of non-irradiated AS24_Ybx glasses, normalization at 1050 cm^{-1} is inset

Shoulder at 300 cm^{-1} becomes stronger indicating an increase of Yb-clustering in AS24_8 sample [16] [17]. The broad band at ~1050 cm^{-1} changes its shape to asymmetric with tail increasing at lower wave-numbers component (Figure III-13, inset). It indicates a lower polymerization of Yb5 and Yb8 glasses showing the role of Yb^{3+} ions as modifiers. The bands at 575 cm^{-1} and 700 cm^{-1} corresponding to Al polyhedra motions becomes more intensive. Insertion of 8 wt. % of Yb_2O_3 modifies the glass network by Al-O-Al linkages increasing as well as Yb clusters. We suppose thus the proximity between Yb^{3+} and Al^{3+} ions in aluminosilicate glasses.

Cooperative luminescence

The cooperative emission is logically more intensive in glasses with more Yb (Figure III-14).

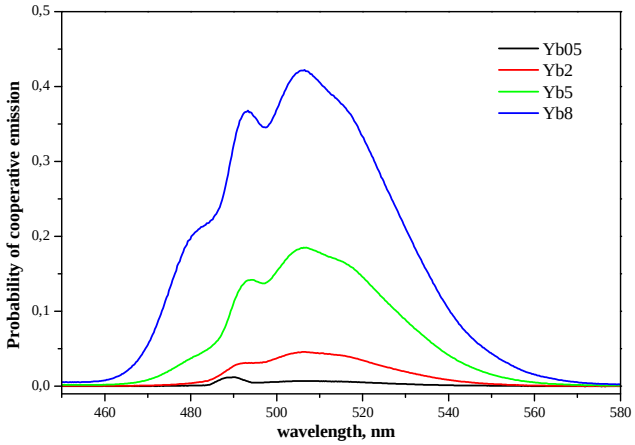


Figure III-14. Probability of cooperative luminescence in non-irradiated AS24_Ybx glasses

This increase of cooperative emission intensity is attributed to Yb cluster formation with further incorporating of Yb. We can note that Yb cluster formation is significant for ≥2 wt. % of Yb_2O_3 concentration.

- **Increasing of Al content leads to more Al-O-Al linkages. Since the Na content is the same in all four glasses (AS22-AS23-AS24-AS26), less NBOs are formed in glasses with more Al.**
- **Yb-doping leads to more Yb-O-Yb clusters and more Al-O-Al linkages.**
- **Yb^{3+} ions have different environment in AS22-AS23 and AS24-AS26 glasses. Moreover, more Yb cluster is suggested in AS24-AS26 glasses according to EPR spectroscopy, and cooperative emission probability.**
- **Under irradiation with strong doses (>1.5·1⁹ Gy), in AS22 glass Al^{3+} ions are pushed into 5-fold coordination instead of 4-fold in pristine glasses. Glass network densification due to more 3-membered rings is shown as well.**

2. Point defects

2. a. Paramagnetic defects assignation

Under ionizing irradiation (electron- , γ-irradiation) in Na-aluminosilicate glass the following paramagnetic point defects can be induced: E'-centers, Peroxy radicals, Non-Bridging Oxygen Hole Centers (NBOHC), Hole Centers (HC) and Al-Oxygen Hole Centers (Al-OHC).

2. a. 1 E'-centers

E'-center is represented by an unpaired spin delocalized on dangling sp^3 orbital of Si with three bridging oxygen atoms. This defect can be formed at an Oxygen vacancy (V_O) via trapping of one electron. The other Si atom, which is positively charged, relaxes becoming surrounded by three bridging oxygens in the same plane (Figure III-15 B).



Figure III-15. A) fragment of perfect lattice; B) the "classic" model of E'_1 center in α-quatrz or E'_γ center in silica, from L. Skuja's review [21]

Different E'-type defects were extensively investigated up to now. The E'_1 center from Figure III-15 B is formed in α-quartz whereas E'_γ center corresponds to its analogous in glassy SiO_2. This type of E' centers (E'_γ) in silica-based glasses is the best understood at the present moment [21]. The *g*-tensor of E' is of cubic symmetry with $g_1=g_2=g_3$=2.0011 [22] [23].

Contrary to many other paramagnetic defects, E'-centers are registered at low microwave power ~0.2-1 μW because of quick saturation of their EPR signal [24] [25] [26].

2. a. 2 Peroxy radicals

Peroxy radicals are detected in most irradiated silicate glasses. This is a hole center with unpaired spin delocalized on superoxide ion bonded to one or two Si atoms (Figure III-16) ≡Si-O-O• [23].

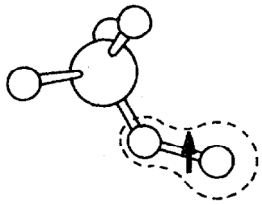


Figure III-16. Model of peroxy radical in *a*-SiO_2 [27]

EPR spectrum of Peroxy radicals is similar to that of NBOHC that always brings some discrepancy into interpretation (Table III-1). Separate both contributions is possible either with further annealing experiments or with computer simulations.

	NBOHC	**Peroxy**
g_1	2.0010	2.0018
g_2	2.0095	2.0078
$<g_3>$	2.08	2.067

Table III-1. Parameters of g-tensors of NBOHC and Peroxy radicals in amorphous SiO_2 [21]

2. a. 3 Non-Bridging Oxygen Hole Centers (NBOHC)

NBOHC is electronically neutral and corresponds to a hole center on non-bridging oxygen ≡Si-O• which EPR spectrum resembles that of Peroxy radicals due to close parameters of *g*-tensors except the g_3-components which have more broadening, so, put in $<g_3>$ [21].

2. a. 4 HC defects

HC defect is a hole center on non-bridging oxygen with close presence of alkali ion. They are registered commonly in alkali-silicate glasses. In potassium-silicate glasses two types of HC defects can be distinguished: HC_1 and HC_2 defects (Table III-2) [22].

	HC_1	HC_2
g_1	2.0026	2.0118
g_2	2.0088	2.0127
g_3	2.0213	2.0158

Table III-2. Parameters of g-tensor of HC_1 and HC_2 defects [22]

HC_1 is a hole trapped on $2p_z$ orbital of Non-Bridging Oxygen with close presence of alkali ion in xy plane which is perpendicular to $2p_z$ orbital (Figure III-17).

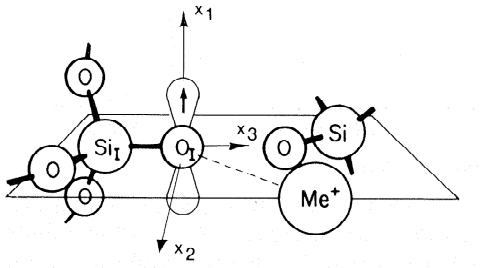


Figure III-17. Model representation of the HC_1 defect [22]

HC_2 defects were presented by Griscom [22] in two configurations that were recorded at low and at high temperatures, respectively (Figure III-18). In the first mentioned configuration, the hole is delocalized on two Non-Bridging Oxygens lying in the same plane (Figure III-18 a). The alkali-ion is along the perpendicular axe to these NBOs.

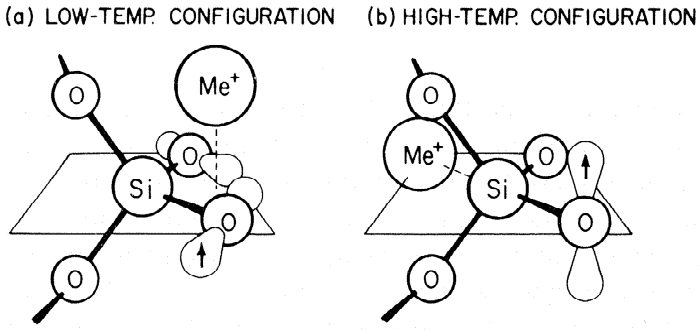


Figure III-18. Model of two HC_2 defects configurations [22]

With temperature increase, the alkali-ion is pushed into another position where the hole moves to the only NBO (Figure III-18 b). The properties of EPR signal are modified, too. This configuration is similar to HC_1 defect. Therefore, HC_2 defects can easily transform into HC_1 defect at higher temperatures.

2. a. 5 Al-OHC defects

There is relatively less information on Al-OHC defects in the literature. Griscom reported about two types of Al-OHC defects in Ca-aluminosilicate glasses [28]. According to those results, Al-OHC defects are represented by holes trapped on non-bonding oxygen *p* orbitals close to Al atoms. Nuclear spin of ^{27}Al is $I=5/2$, so, one should observe, due to hyperfine interaction, 6 lines in the EPR spectrum. In fact, these lines are not well-resolved at room temperature (RT).

Laguta et al. reported about Al-related paramagnetic defects in $YAlO_3$ single crystal of perovskite structure [29]. They presented well-resolved EPR spectra of various types of these defects. The parameters of its *g*-tensor are close to those of one of Al-OHC defects in Griscom's paper (Table III-3).

	Griscom [28]	**Laguta [29]**
g_1	2.0023	2.0028
g_2	2.0182	2.0143
g_3	2.0353	2.0440

Table III-3. Parameters of g-tensors of Al-OHC defects

In [29] it was proposed that the hole is localized on an oxygen $2p_\pi$ orbital in the plane perpendicular to the Al-O-Al direction.

2. b. Formation of paramagnetic defects in AS22-AS26 glasses

As it was announced above, the total amount of the defects was estimated from double integration of EPR spectra. The error bars are 10%. The total number of spins was estimated using Bruker references – two pitches added into KCl giving weak and strong signals to establish the bench marks. **The magnitude of spin concentration ranges between 10^{15} and $5\cdot10^{15}$ spin/cm^3 in all irradiated stabilized glasses.**

2. b. 1 Influence of the glass composition

Under electron irradiation below $3.2\cdot10^6$ Gy, only hole centers are detected in AS glasses. The shape of EPR spectra of AS22-23 samples (Figure III-19) exhibits

the main presence of hole centers on Non-Bridging Oxygens bonded to Si with g_1=2.0035, g_2=2.0095 and g_3=2.0187 which are close to those of HC_1 defects. It is worth to underline that the parameters of g-tensor from the literature are for potassium-silicate glasses. Presence of sodium at molar concentration 20% gives rise to 10 times broadening of the HC_1 EPR line according to carried out calculation works [22]. Thereafter, it is difficult to distinguish HC_1 and HC_2 defects in the current samples thus HC notation will be used for hole centers.

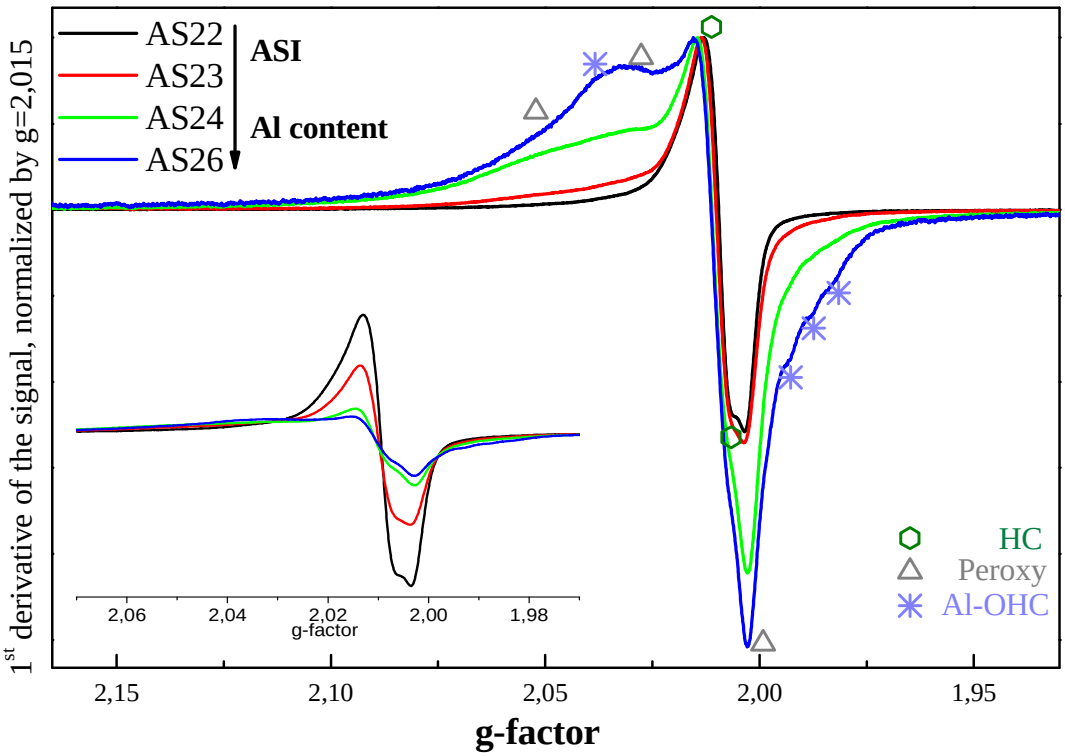


Figure III-19. EPR spectra of Yb-doped e^- -irradiated AS glasses just after the irradiation, dose 10^5 Gy, normalization at g=2.015. EPR spectra normalized only by mass and gain are in the inset.

Another signal characterized by g_1=2.0030, g_2=2.0104 and g_3=2.0381 can be also observed mostly in AS24 and AS26 glasses. It can be assigned to NBOHC or to POR (PerOxy Radical) defects. The recovery experiments, which will be discussed in part 3.c.2, rather indicate the formation of Peroxy radicals. Moreover, in the spectra of AS24 and mostly in AS26 glasses one can see the hyperfine structure arising from Al-OHC defects. This result is logically explained by the Al content increase in these glasses and Al-O-Al linkages detected by Raman spectroscopy.

When Al content increases while keeping the same quantity of Na in AS22-23-24-26 glasses, more Na^+ ions are used to compensate the charge of $[AlO_4]^-$ tetrahedra. In consequence, less Na^+ ions participate in the glass depolymerization

as modifiers. Therefore, less HC defects are created. Despite a lower silicon content in AS24 glass compared to AS22, less Na^+ ions take part in HC defects formation because of the increase of Al and thus more hole centers on oxygens bonded to Al tetrahedra are trapped leading to– more Al-OHC defects.

Despite the higher intensity of HC defects' EPR signal in glasses with less Al - AS22 and AS23 glasses (Figure III-19, inset), the glasses AS24 and AS26 contain higher value of the total defects' quantity obtained after double integration of the signal (discussion in section 2.d). It originates from Al-OHC defects which bring large tails into the spectra.

Concerning the electron centers, we observe E' centers at doses higher than 10^5 Gy only in AS22_0 and AS22 glasses, at doses higher than $3 \cdot 10^6$ Gy in AS24_0 and AS24 glasses doped with low Yb concentrations (<5 wt. % of Yb_2O_3).

In non-doped AS22_0 glasses with less Al content, more E' centers are induced than in AS24_0 glasses (Figure III-20).

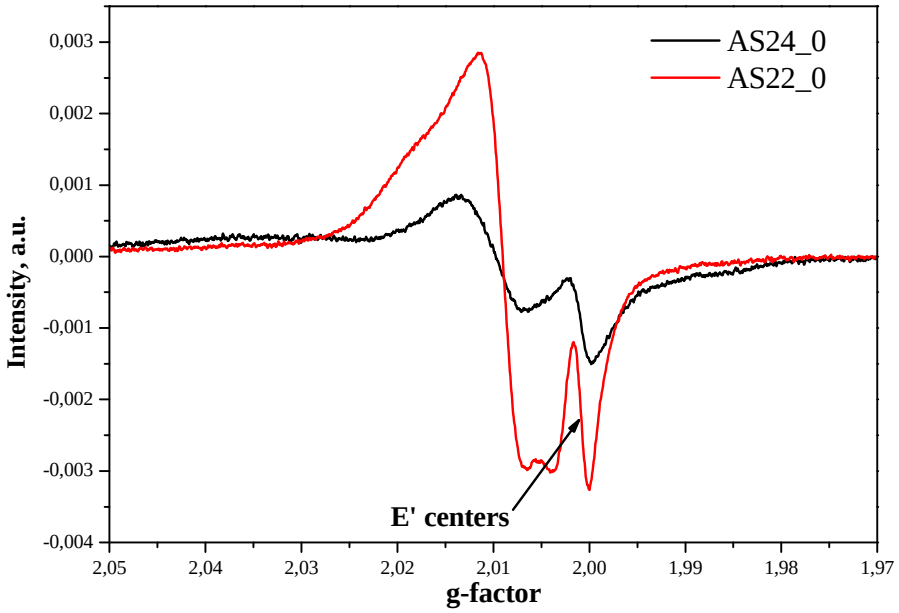


Figure III-20. EPR spectra of e^--irradiated AS24_0 and AS22_0 glasses, dose 10^7 Gy, stabilized samples.

2. b. 2 Influence of Yb-doping

Yb-doping impacts the shape and the intensity of the EPR line (Figure III-21). It thus plays a role on relative defect concentration. In AS24 glass the total defects' amount decreases (Figure III-21 inset), but we also point out that the relative

content of Al-OHC defects increases (Figure III-21) with Yb doping. This result is in agreement with Raman spectroscopy of AS24_Ybx glasses where Al-O-Al linkages signal increases with Yb doping (Figure III-13).

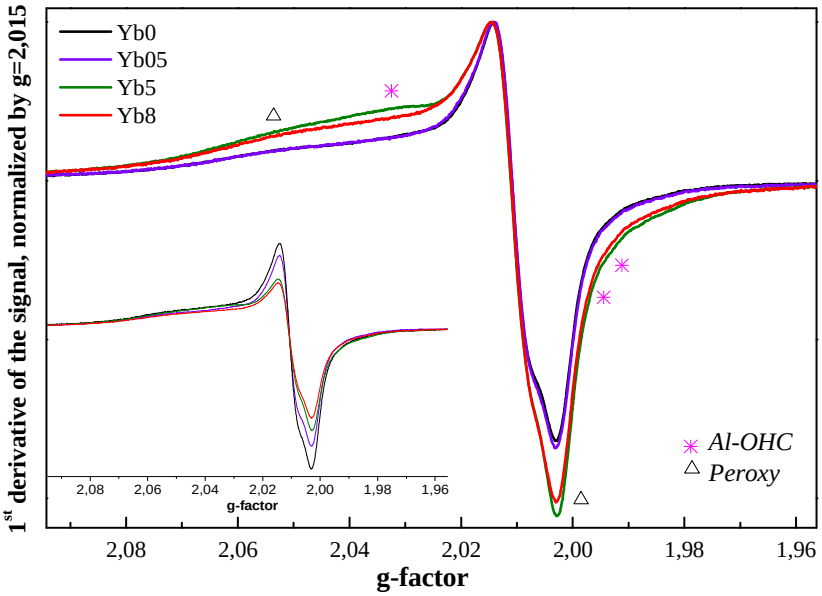


Figure III-21. EPR spectra of e^- -irradiated AS24_Ybx glasses, dose 10^5 Gy, normalization at g=2.015. EPR spectra recorded just after the irradiation and normalized only by mass and gain are in the inset

Yb incorporation leads to a decrease of E' defects (Figure III-22). When Yb concentration reaches 5 wt. % of Yb_2O_3, these defects are not observed anymore.

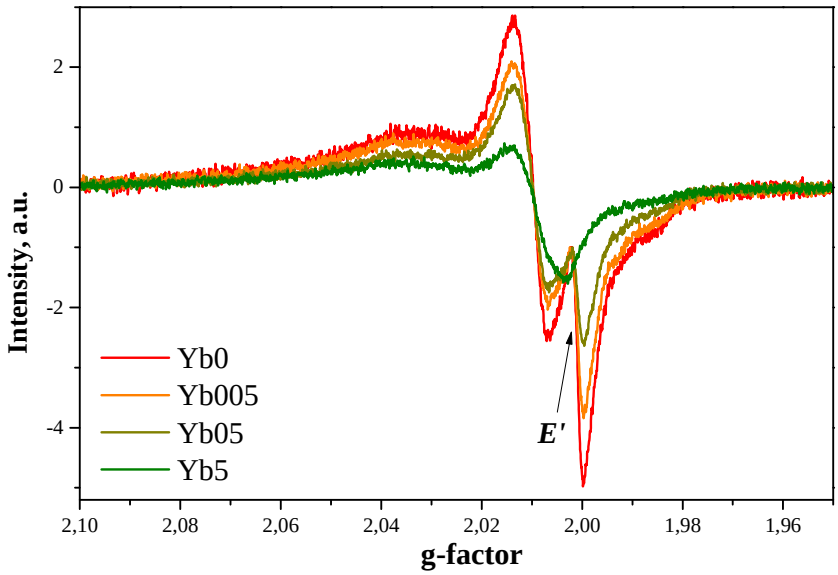


Figure III-22. EPR spectra of AS24_Ybx glasses, dose 10^7 Gy, stabilized samples.

The role of Yb-doping in E' centers formation can be also illustrated by Table III-4. One can see that E' centers are created in glasses with less Al and/or low Yb concentrations. We should remind here that in both cases the number of Yb cluster is low.

	10^5 Gy	10^6 Gy	$3.2 \cdot 10^6$ Gy	10^7 Gy	10^8 Gy
AS22_0	-	+	+	+	+
AS22	-	+	-	-	-
AS23	-	-	-	-	±
AS24_0	-	-	-	+	+
AS24_005		-	+	+	+
AS24_02		-	-	+	
AS24_05	-	-	-	±	+
AS24	-	-	-	-	-
AS24_8	-	-	-	-	-
AS26	-	-	-	-	-

Table III-4. E' centers detected in stabilized e^--irradiated AS glasses: red - no E', green - E' detected, yellow - traces of E', grey - no sample

We can see that Yb-doping leads to paramagnetic point defects saturation (Figure III-21, Figure III-22). It is in agreement with previous works performed in "Laboratoire des Solides Irradiés" [30] [31] [32] [33] where Sm- and Gd-doping of ABS glasses was studied as well. RE ions can trap some hole and electron charges and thus decreasing the number of point defects observed after irradiation [30] [31].

The saturation of total defect amount with Yb-doping in aluminoborosilicate (ABS) glasses was already reported by Ollier et al. [30]. In case of ABS glasses, this effect was associated with charge trapping by Yb^{3+} ions and consequent reduction $Yb^{3+} \rightarrow Yb^{2+}$ [30].

The E' saturation in Yb-doped aluminoborosilicate (ABS) glasses [34] is observed from 0.2 wt. % of Yb_2O_3 in the glass. Even if the reduction of Yb^{3+} ions into Yb^{2+} in our aluminosilicate glasses is not obviously demonstrated by EPR at low temperature, we assume that an effective charge trapping of Yb^{3+} ions under cluster form is responsible for the E' disappearing when the glass is 5 wt.% doped.

2. c. Relaxation of paramagnetic defects

We have studied the thermal post-irradiation behavior of the paramagnetic defects in irradiated glasses within 276 days. The double-integration of the spectra drives the value proportional to the total amount of paramagnetic defects. All the relaxation curves are normalized at its maxima on the 1st day of EPR recording performed less than 1 hour after the irradiation.

The total amount of the defects decreases in time after irradiation during the first 2 months, before remaining stable. The most rapid relaxation is observed during the first 7 days (Figure III-23, Figure III-24).

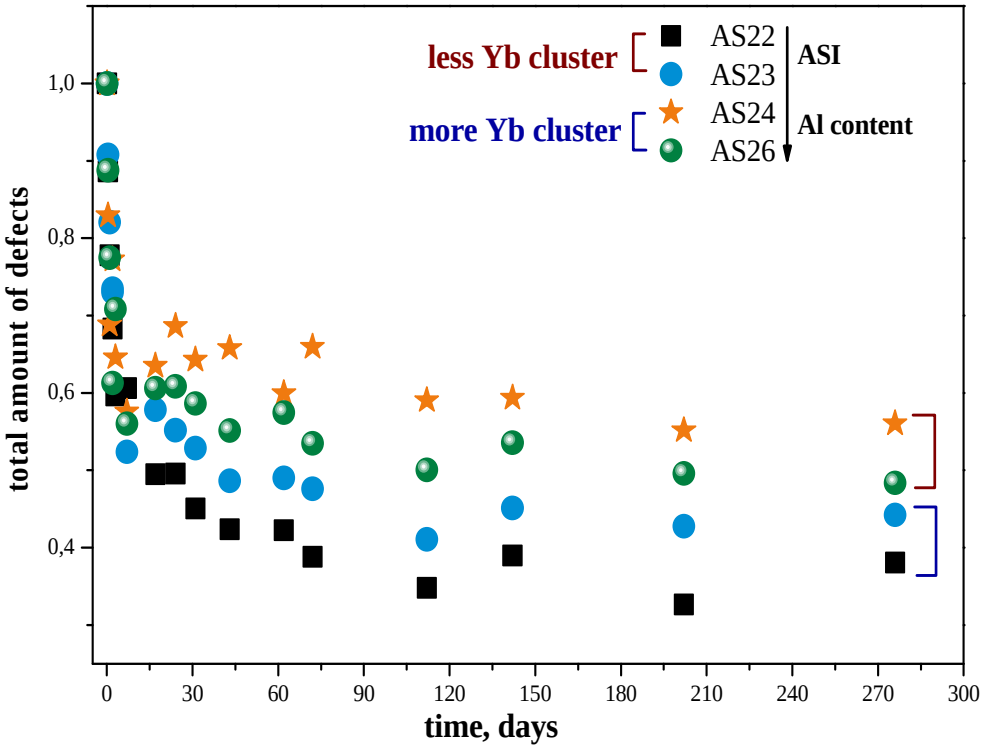


Figure III-23. Relaxation curves of Yb-doped e— -irradiated AS2x_Yb5glasses, dose 10^5 Gy

The relaxation rate is the same for all the glasses during this first period whereas after 1 week of storage it becomes slower in glasses with higher Al content – AS24 and AS26 (Figure III-23).

Finally, in AS24 glass the total bleaching of defects does not exceed 40% of the initial amount whereas in AS22 it reaches about 60%.

We observe a contrasted evolution of relaxation curve in glasses with different Yb cluster amount. It is slower in AS24 and AS26 glasses where Yb cluster content is higher. We assume that Yb cluster amount impacts on the defect recovery. We propose that e^--hole recombination leading to the defect fading is less active when a high amount of cluster is present in the glass, due to an effective charge trapping by Yb clusters.

If we compare now the relaxation of non-doped glasses with Yb-doped in Figure III-24, we observe a clear acceleration of the relaxation rate with Yb doping.

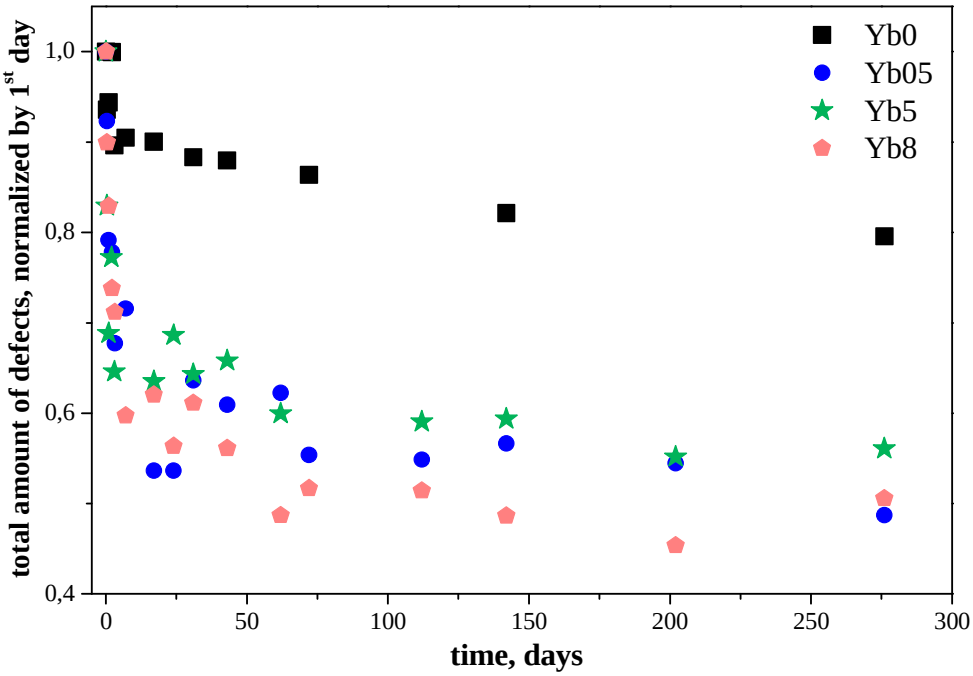


Figure III-24. Relaxation curves of Yb-doped e— -irradiated AS24_Ybx glasses, dose 10^5 Gy

The higher relaxation rate with Yb-doping can be explained by the presence of electrons trapped on Yb^{3+} ions close to the defects such as Al-OHC. We thus assume due to this proximity that defects recovery is more efficient. The vicinity of Yb and those defects is demonstrated by the influence of Yb concentration and Al-OHC defects formation (Figure III-21). This effect was already observed in borosilicate glasses [30].

When analyzing the role of Yb-doping in the defect relaxation rate, we remind here that in Yb5 and Yb8 glasses the number of Yb cluster is higher than in Yb05 glass. Therefore, with further increase of Yb concentration from 0.5 wt. % to 5 wt. %

and 8 wt. %, there is no acceleration of defect recovery. It confirms thus our hypothesis that presence of Yb cluster inhibits the defect relaxation in time.

2. c. 1 Analysis of relaxation curves

As described before, relaxation curves exhibit two regions (Figure III-25). The first region can be expanded to 20 days, the curve can be fitted with a sum of two first-order kinetics with 2 half-times

$$I = I_0 + A_1 e^{-t/a} + A_2 e^{-t/b}$$

where $\tau_1 = a \times ln2$ and $\tau_2 = b \times ln2$

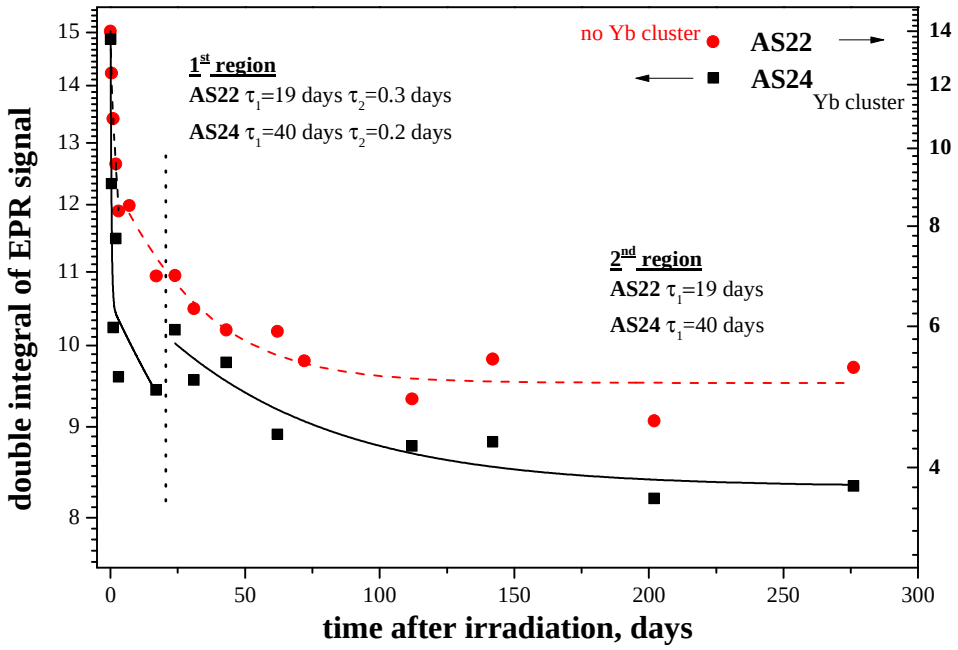


Figure III-25. Relaxation curves of Yb-doped e^- -irradiated AS22 and AS24 glasses, dose 10^5 Gy. The axes of abscissas are in logarithm

The second region can be fitted by a first-order decay. Similar relaxation curve type can be found in the literature despite the curve is obtained from optical absorption of the defects in the visible region [35] [36]. It implies a fast defects recovery in the first region and slower processes in the second one.

The 1st region is characterized with similar values of half-time τ_2 for all the glass series: ~0.3 days. The quick part of the relaxation curve up to 10-15 days could be associated to similar fast processes of defects recovery in all four glasses.

Along this period the best seen change in EPR spectra is the decrease of relative HC and Peroxy defects intensity.

The second region represents the long-term fading. It can be fitted with a first-order exponential law with longer half-time τ_1 values. Generally the second part of the relaxation curve corresponds to electron diffusion [37] and it presents different slope in our glasses according to the ASI/Yb cluster amount. Therefore it demonstrates that the Yb cluster amount is involved into e^--diffusion in irradiated glasses. More precisely, when cluster amount is high, the half time is longer implying a very efficient charge trapping by the Yb cluster. The lifetime τ_2 varies from 19 days in glass AS22 to 36 days in glass AS26.

The long-term fading half-times of the defects in soda-lime silicate glasses were obtained as 276-530 days depending on irradiation conditions [35]. These values are probably longer because the glasses are Yb-free. In our case, Yb-doping accelerates the defects recovery (Figure III-24).

2. c. 2 Recovery of individual defect type

In Figure III-26 we observe an evolution of the EPR spectra shape within time implying different recovery rate of each point defect. In e^--irradiated AS23 glass a relative increase of HC defects has been observed in parallel to an Al-OHC defects decrease (Figure III-26).

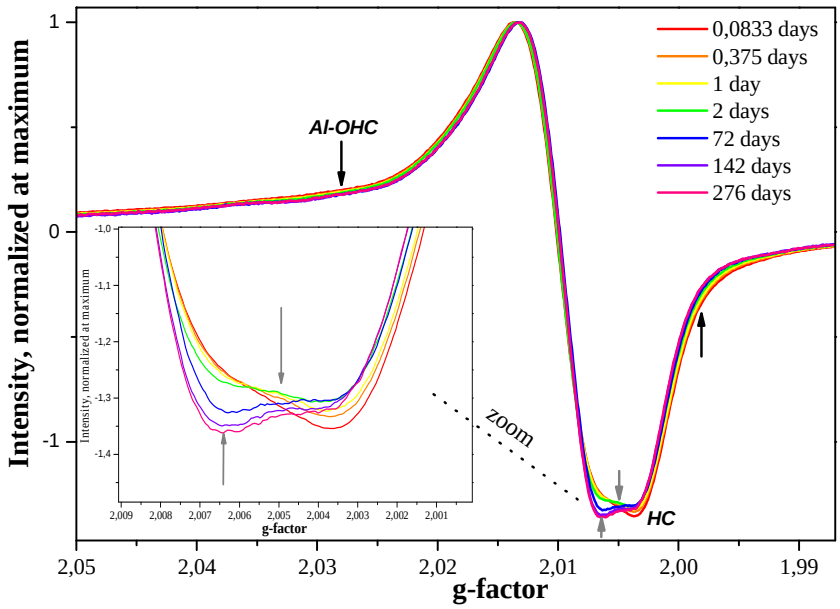


Figure III-26. Evolution in time of e^--irradiated AS23 glass,dose 10^5 Gy, normalization at g=2.013

A linear anticorrelation between Al-OHC defects and HC defects (Figure III-27) can be underlined: Al-OHC defects' concentration decreases with time while the content of HC defects increases. It implies that the relaxation of Al-OHC defects is quicker than HC.

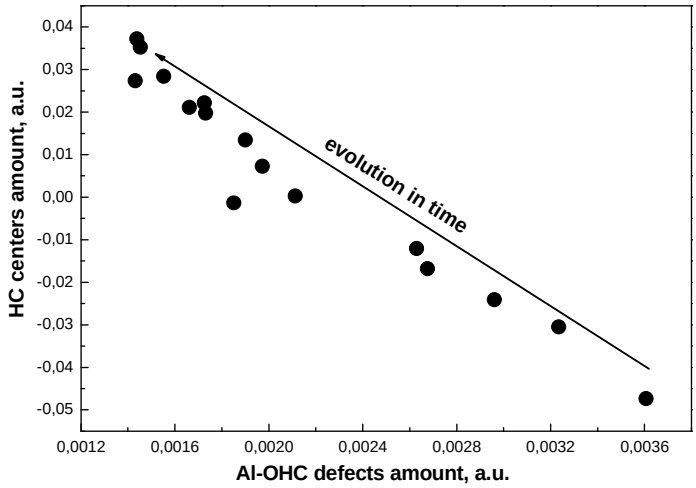


Figure III-27. Evolution in time of Al-OHC and HC defects in e^--irradiated AS23 glass, dose 10^5 Gy

Concerning the linear anti-correlation between Al-OHC and HC defects, it implies structural modifications of those point defects during post-irradiation processes. This could be due to hole migration from NBO linked to $[AlO_4]^-$ to a close NBO linked to $[SiO_4]$ in AS glasses.

2. d. Effect of irradiation dose and dose rate

2. d. 1 Total amounts of the defects

Dose effect

All the results presented below in the section 2.d have been obtained from stabilized samples (>6 months after the irradiation).

In electron-irradiated samples the effect of irradiation dose has been analyzed due to collection in a large dose range 10^5-$1.5 \cdot 10^9$ Gy.

All 4 glass compositions expose similar behavior within dose increase (Figure III-28). In the range of medium doses 10^5 – $3 \cdot 10^6$ Gy, defects concentration maintains unvaried with the dose. Thereafter, in $3 \cdot 10^6$ – 10^8 Gy dose range, the

defects concentration increases reaching its maxima at 10^8 Gy. Irradiation at strong integrated dose $1.5 \cdot 10^9$ Gy leads to a decrease of the defects content.

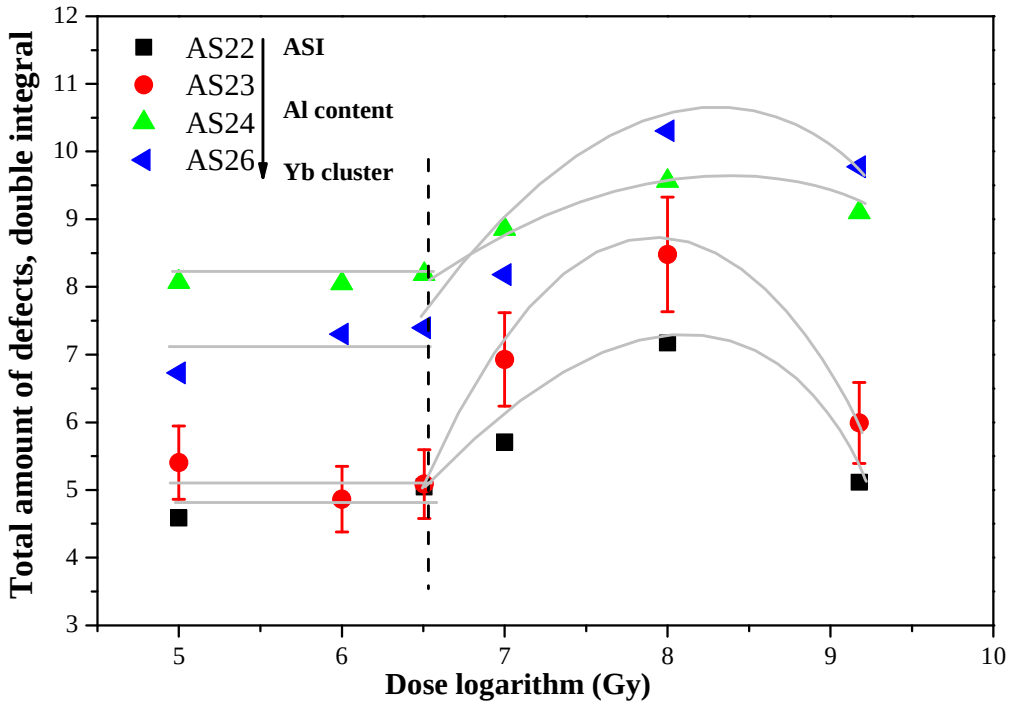


Figure III-28. Dose dependence in electron-irradiated glasses

AS22 and AS23 glasses are more sensitive to dose effect whereas AS24 glass exhibits the smallest deviation of defects amount within dose. This result is in accordance with the results of relaxation processes. Once again, we can suspect that the presence of Yb clusters drives the system into a higher stability regarding to the radiation-induced paramagnetic defects.

Same curve with 2 regimes – constant in medium doses and reaching its maximum in higher doses – was already reported for Yb-doped aluminoborosilicate glasses [30] [34]. Ollier et al. showed a non-linear increase of the defects with log(dose) in non-doped ABS glasses [30]. It is interesting because it indicates rather the influence of Yb-doping than the glass matrix and the nature of defect.

The influence of Yb-doping has been investigated in more details in AS24 glass series where the samples are doped with Yb_2O_3 in various concentrations: 0.05, 0.2, 0.5, 5 and 8 wt. % as described in Chapter II. The total amount of paramagnetic defects in these samples is plotted vs. lg(dose) in Figure III-29.

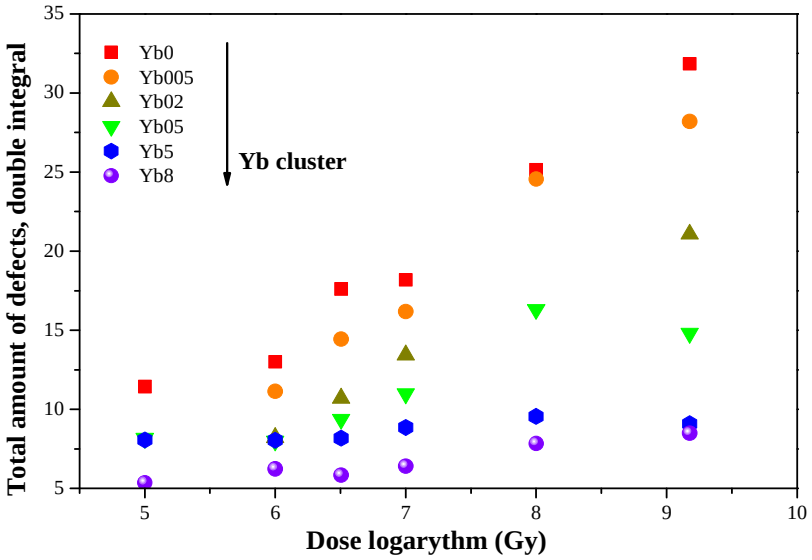


Figure III-29. Dose dependence in AS24_Ybx samples, electron irradiation

In non-doped glasses and in glasses with low Yb concentrations (up to 0.2 wt. %), the number of defects increases linearly within lg(dose) (Figure III-29). We notice that the slope is lower for 0.2 wt %. Doping with Yb_2O_3 of at least 0.5 wt. %. leads to a maximum of point defects at 10^8 Gy. This effect associated to saturation effect at high doses and can be seen more efficiently for 5 and 8 wt. % of Yb_2O_3. For these 3 glasses Yb05, Yb5 and Yb8 the cooperative emission has been detected. Therefore, even at 0.5 wt. % of Yb_2O_3 Yb clusters are formed. It is worth underlying the similarity of obtained curves between those glasses and AS22-AS26 glasses (Figure III-28).

As shown for ABS glasses [34], Yb-doping at 0.5 mol. % leads to a strong saturation of paramagnetic defects with dose. In this study one can see the similar result for 5 and 8 wt. % In AS24 and AS24_8 glasses where Yb cluster content is higher, Yb clusters trap the charge efficiently preventing further increase of radiation-induced point defects with irradiation dose.

In conclusion, AS22, AS23 and AS24_05 glasses with low Yb cluster content exhibit similar defects amount dependence vs. lg(dose). Whereas in AS24, AS26 and AS24_8 with higher Yb cluster content, the total amount of paramagnetic defects varies slowly with lg(dose). We attribute this evolution type to Yb cluster influence on paramagnetic defects creation under irradiation.

Dose rate effect

If we analyze now the dose rate effect, let's compare the results between γ-irradiated and e^--irradiated samples with 2 currents 25μA and 200nA. The dose

rate during γ-irradiation was 5.64 kGy/h; the dose rate of e^--irradiation of 25μA current was 25 MGy/h and in the case of 200nA it was 0.3 MGy/h. In both types of electron irradiation the beam energy was 2.5 MeV while the gamma rays energy was 1.25 MeV.

Figure III-30 presents the total amount of paramagnetic defects as a function of the integrated dose for each dose rate.

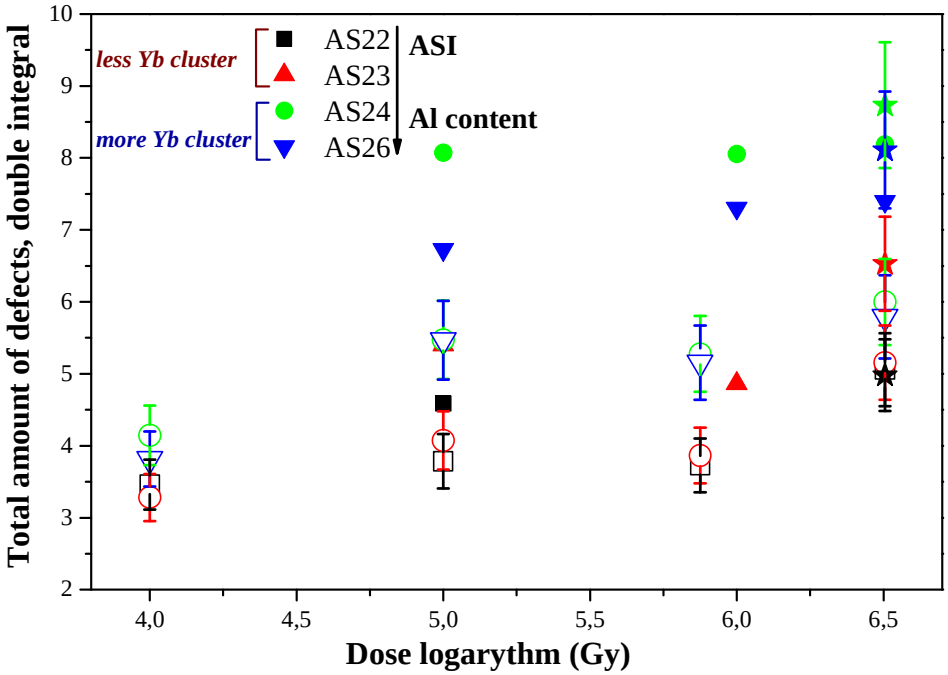


Figure III-30. Dose dependence in gamma irradiated samples. Dose rate effect. Full signs – 25 MGy/h (e^-), empty signes – 5.64 kGy/h (gamma) and stars – 0.3 MGy/h (e^-)

The first remark concerns the 10^4 Gy dose (γ-irradiation) where the point defect number is almost the same whatever the glass composition.

No difference is observed between 0.3 MGy/h or 25 MGy/h (2 orders of magnitude) dose rates on defects' intensity. However, γ-irradiated samples show a lower amount of the defects. This difference is visible for AS24 and AS26 glasses. This effect can be connected to the difference between dose rates (3 orders of magnitude) and implies that for a lower production of excitons (γ-rays), the presence of Yb cluster leads to a lower content of the defects.

2. d. 2 Relative amounts of defects (dose effect)

To study the relative defects concentrations all the spectra are normalized at their maxima at g=2.013. In all irradiated glasses the resonance position moves within dose to lower g-values (Figure III-31). The shape modification implies that the relative amount of defect is different according to the dose.

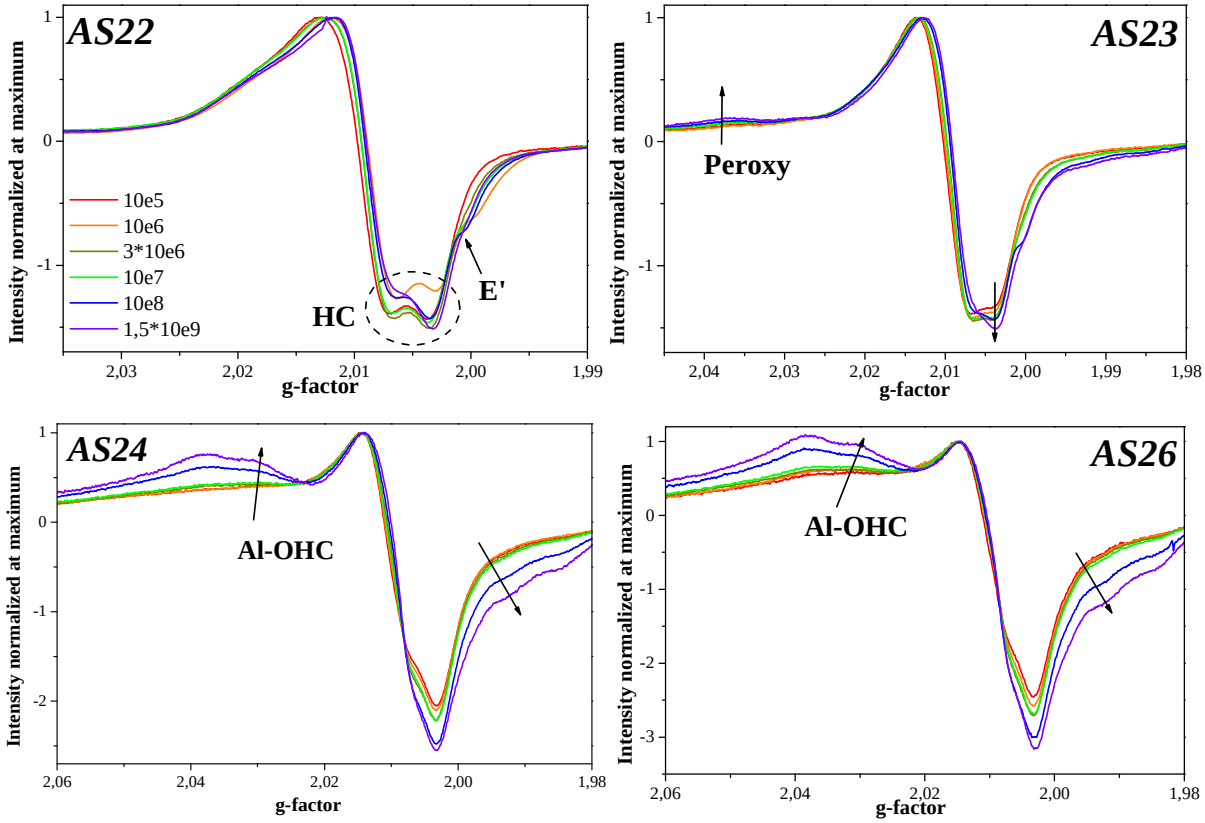


Figure III-31. Normalized EPR spectra of AS2x_Yb5 glasses, electron irradiation

With irradiation dose increase the most significant modifications take place in AS24 and AS26 glasses with more Al content. In particular, in AS24 and AS26 glasses more Peroxy radicals are induced with dose increase. Moreover, in AS24 and AS26 glasses irradiated at dose $\geq 10^8$ Gy the number of Al-OHC defects enhances significantly (Figure III-31).

The effect of strong doses $>10^9$ Gy on point defects should be discussed separately from other results because when irradiation dose is stronger than 10^9 Gy, some glass structural modifications can occur linked in particular to the alkali ions migration [38], section 1.c.

The evolution within time of EPR spectra of AS26 glass, where Al content is the highest, is shown in Figure III-32.

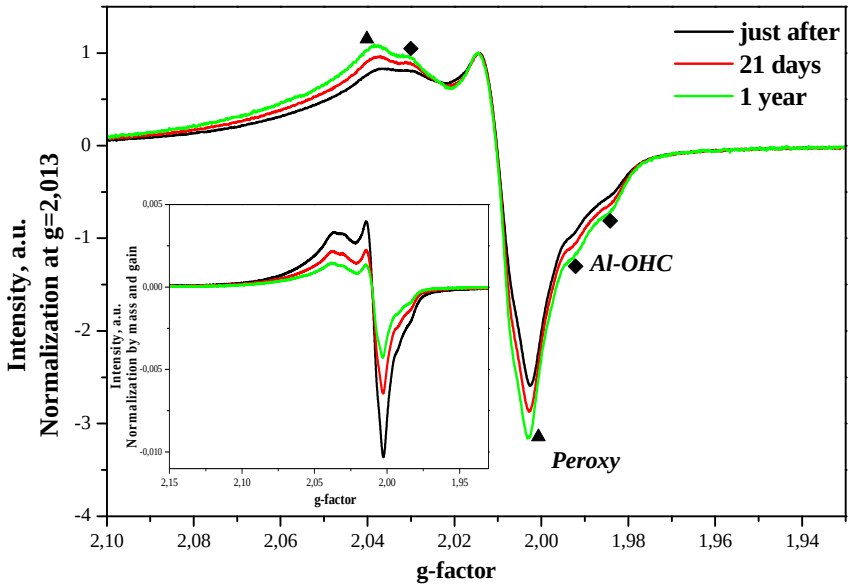


Figure III-32. EPR spectra of AS26 glass irradiated at 1.5·10⁹ Gy. Normalization by mass&gain in inset

In all the samples the total amount of the defects decreases with time (Figure III-32 inset). However, the analysis of relative concentrations of paramagnetic defects reveals some important features. In particular, relatively more Al-OHC defects are observed within time after the irradiation (Figure III-32). This effect has been detected in glasses with more Al: AS24_Ybx series and AS26. It corresponds to different relaxation rates of the paramagnetic defects. Contrary to lower doses (10^5 Gy), the relaxation of Al-OHC defects is slower than Peroxy radicals. It means that the relaxation of point defects is impacted by the irradiation dose.

In glasses with less Al (AS22 and AS23) in medium dose range (10^5 – $3.2\cdot10^6$ Gy), the number of HC defects rises up (Figure III-31). In glasses with low Al and/or low Yb clusters, at doses stronger than 10^5 Gy E' centers are observed (Table III-4). The non-doped AS22_0 sample has the largest dose range available to study E' formation in aluminosilicate glasses. Its EPR spectra are plotted in Figure III-33.

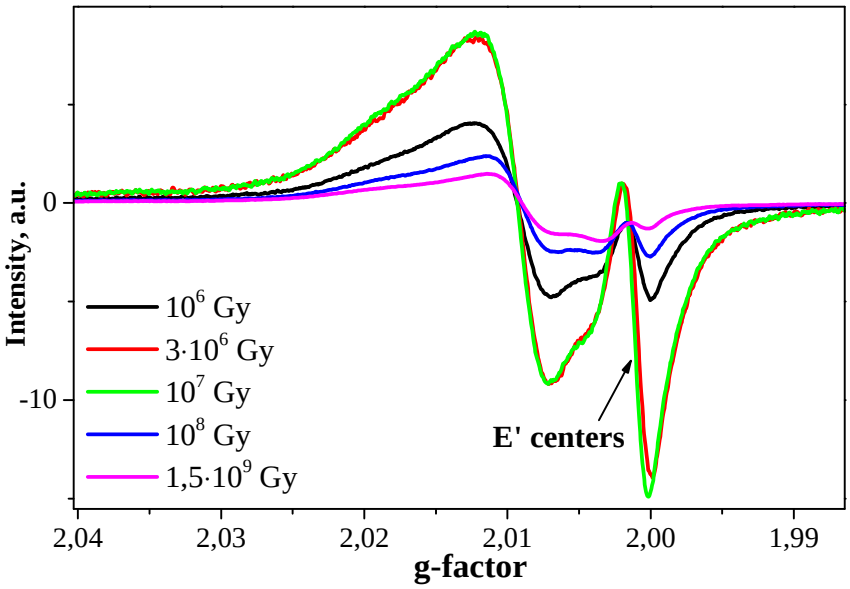


Figure III-33. EPR spectra e^- -irradiated with various doses AS22_0 glasses, stabilized samples

In e^--irradiated AS22_0 glass E' intensity increases up to the dose 10^7, and then one can see the decrease of E' signal (Figure III-33). It is assigned to additional electrons trapping by E' centers which become EPR-silent defect [23].

- **More Al-OHC and Peroxy radicals are induced in glasses with more Al (AS24-AS26) and more HC defects in others (AS22-AS23). It is in correlation with more Al-O-Al linkages in AS24-AS26 glasses. Al-OHC defects are induced in higher quantity under >10^8 Gy. Adding of Yb leads to more Al-OHC defects**

- **Point defect recovery is slow down by the presence of Yb cluster. The increase of point defects within irradiation dose in $3 \cdot 10^6$-$1.5 \cdot 10^9$ Gy is also attenuated.**

- **The defects dependence on lg(dose) exhibits 2 regimes – constant in medium doses and reaching its maximum in higher doses. The variation in high dose range is less sensitive in glasses with more Yb cluster.**

- **More paramagnetic point defects are induced under e^--irradiation of 3 order dose rate higher than under γ-irradiation in glasses with more Al (AS24-AS26).**

- **After irradiation at strong doses ($1.7 \cdot 10^9$ Gy) in AS glasses the paramagnetic defects relax with different rates. The relaxation rate of Al-OHC defect is slower than in case of 10^5 Gy dose.**

3. Luminescent properties of Yb^{3+}

3. a. Cooperative luminescence (CL)

3. a. 1 CL in AS glasses with high content of Yb clusters

All the spectra of CL might be normalized by absorption and lifetime τ_{IR} as described in Chapter II. The evolution of absorption spectra of Yb^{3+} in AS24 glass irradiated at 10^5 Gy is presented in Figure III-34.

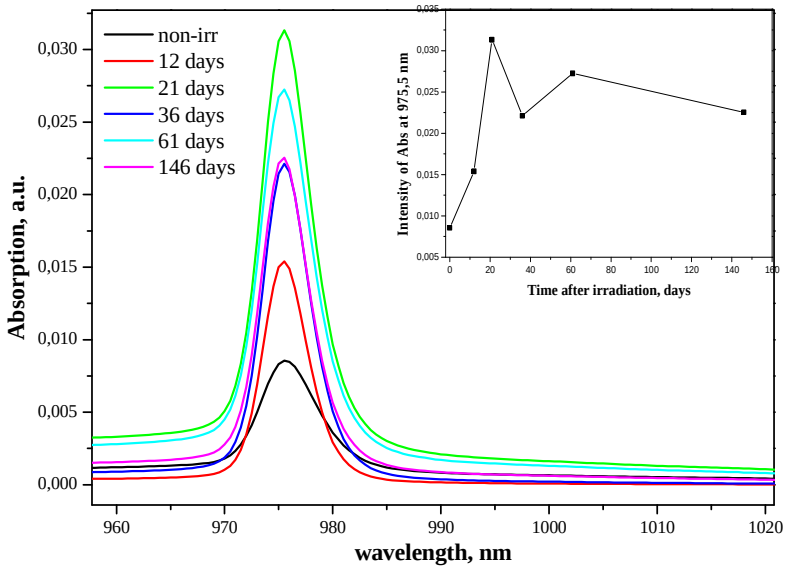


Figure III-34. Absorption of e^--irradiated AS24 glass, 10^5 Gy. Evolution in time. Maximum of absorption is in inset

It is clear to see that absorption increases seriously under irradiation. Afterwards, its intensity varies quite ambiguously in time. It is difficult to explain rationally the non-stability of absorption spectra within time. To understand the origin of this variation it is worth to remind that the plotted absorption is derived from Kubelka-Munk formula

$$F(R) = \frac{Abs \times c}{s}$$

In Figure III-34 the presented value *F(R)* is applied as a value proportional to absorption *Abs* supposing that both, concentration of absorbing species *c* and scattering coefficient *s*, are the same in different samples. This is true for the value *c* because of same Yb-doping level in AS2x_Yb5 glasses. This is true also for the

value *s* in non-irradiated samples because they were prepared as powders of similar particle size 100-125 µm. We suspect that under the irradiation and afterwards within time, the evolution of the powder surface could impact on the absorbance. Therefore, the final parameter *F(R)* cannot be used to normalize the spectra of CL of irradiated samples because of the scattering coefficient that is unknown in this series. **Hereafter, the cooperative emission spectra will be normalized without normalization with absorption; only lifetime τ_{IR} normalization will be applied.**

Yb^{3+} cooperative luminescence intensity decreases crucially in irradiated AS24 and AS26 glasses (Figure III-35). 25MGy/h dose rate (e^--irradiation) instead of 5.64 kGy/h dose rate (γ-irradiation) has no impact on the intensity decrease. So, neither dose rate, nor dose effect seem to impact on the intensity of CL decrease.

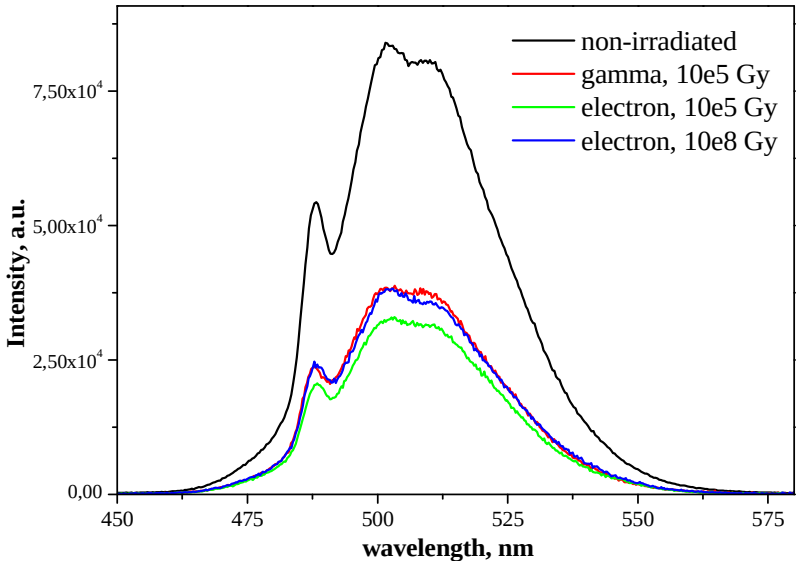


Figure III-35. The spectra of cooperative emission in e^--irradiated AS24 glasses, doses 10^5 Gy and 10^8 Gy

Among the mechanisms responsible for the CL decrease, one can suggest the formation of point defects due to re-absorption of the photons in 500 nm region.

The absorption of the defects in 450-580 nm region is the same whatever the dose or dose rate (Figure III-36).

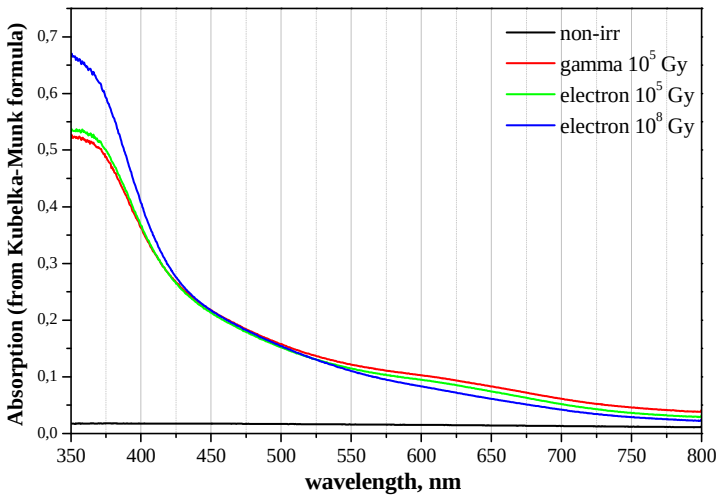


Figure III-36. Absorption spectra of irradiated AS24 glasses

Cooperative emission has been followed within time from 12 days to 146 days after the irradiation. Consequently, the CL stability presented in Figure III-37 is in the period of "slow" paramagnetic defects relaxation, see section 2. Moreover, it is important to point out higher stability of paramagnetic defects in AS24 and AS26 glasses. The observed stability is similar whatever the dose and dose rate.

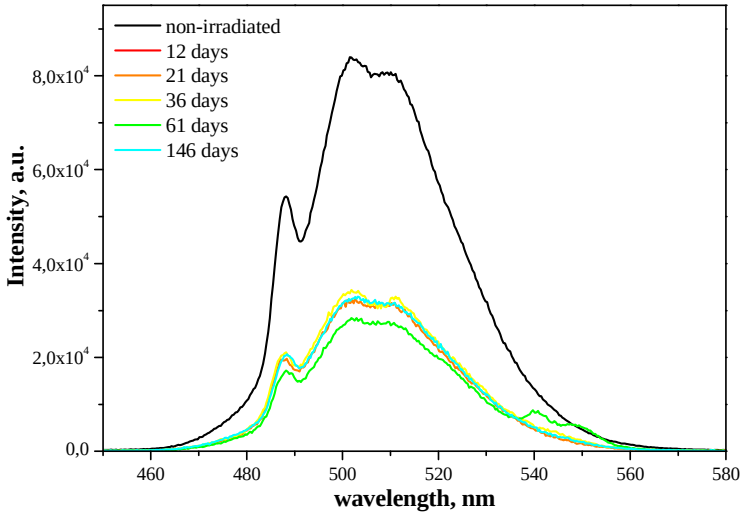


Figure III-37. Cooperative emission of e^--irradiated AS24 glass, dose 10^5 Gy

The stability of cooperative luminescence in time is observed not before than 12 days after the irradiation. The most rapid defect recovery has been already completed to that moment. Therefore, it is impossible to make any correlation of with paramagnetic defects during their most expressive evolution. However, we conclude that cooperative emission stability is in agreement with slow evolution of paramagnetic point defects after irradiation.

3. a. 2 CL in AS glasses with less content of Yb clusters

In non-irradiated AS22 and AS23 glasses with less Al content low Yb^{3+} cooperative emission is observed. So, only the powerful diode allowed us studying the stabilized AS22 irradiated samples. The CL intensity change in AS22 and AS23 glasses under irradiation is negligible (Figure III-38).

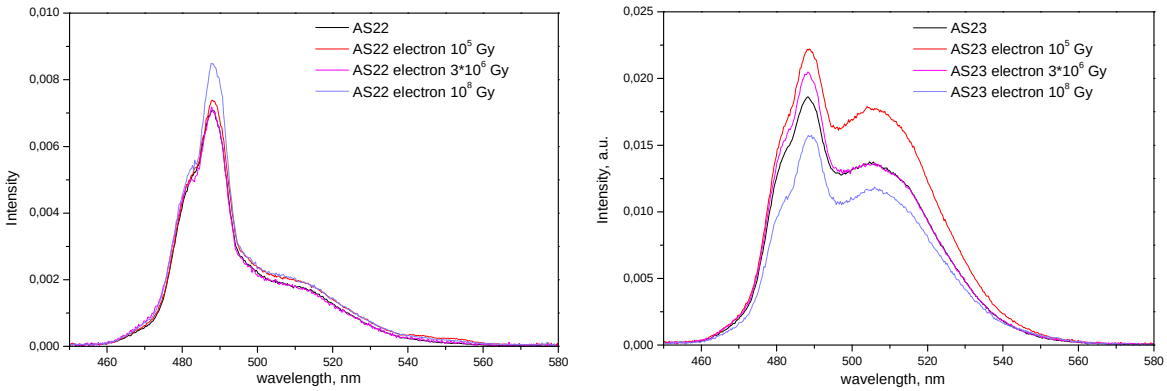


Figure III-38. The CL spectra in e^--irradiated AS22 (left) and AS23 (right) glasses

Neither effect of dose rate is detected in irradiated AS22 and AS23 glasses, the intensity of CL maintains similar. This result shows that a decrease of the Yb pair number by trapping some e^-/h is for both glasses poorly efficient.

In both AS22 and AS23 glasses, the Al-OHC defect is poorly detected. Among the defects that could affect the decrease of CL under irradiation, it is strongly suspected because at first Yb^{3+} and Al proximity and also because of Al-OHC absorption at 550 nm [39].

3. b. Lifetime of Yb^{3+} $^2F_{5/2}$ excited state

The lifetime τ_{IR} of $^2F_{5/2}$ excited state in Yb^{3+} ions was measured under 975 nm excitation; the monitored emission was at 1000 nm. The lifetimes τ_{IR} were measured in both powders and slices. The evolution in time was followed in powders, but the dose and dose rate effects were completed also by using the samples in slices.

The lifetimes τ_{CL} of "virtual $^2F_{5/2}$ state" with emission at 510 nm under 975 nm excitation were obtained for powders only.

The powders have been analyzed in ENSCP (in coll. with Ph. Goldner and A. Ferrier) under laser excitation whereas the slices have been studied in LSI under

lamp excitation. In both cases the samples were excited by λ_{ex}=975 nm and the detection was carried out at λ_{det}=1000 nm (for more details see Chapter II, section 4.a).

3. b. 1 Before irradiation

The lifetimes τ_{IR} values in non-irradiated glasses depend on the glass composition. In particular, it decreases when the number of Yb cluster increases in AS24 and AS26 glasses (Table III-5).

Sample	τ_{IR}, ms	τ_{CL}, ms
AS22	2.14	0.84
AS23	1.97	0.78
AS24	1.15	0.52
AS26	0.94	0.43
AS24_8	1.00	0.45

Table III-5. The lifetimes τ_{IR} and τ_{CL} in non-irradiated samples

Lifetime registered in the IR-region τ_{IR} originates from all Yb^{3+} ions while the lifetime registered in the visible region τ_{CL} originates from Yb-Yb pairs only. The lifetimes τ_{CL} are usually 2 times lower than τ_{IR}. We observed that in glasses with low Yb cluster content (AS22-AS23) τ_{CL} is lower than $\tau_{IR}/2$. When Yb^{3+} ions are well-diluted in the matrix, the minor presence of Yb-Yb pair interactions leads to a τ_{CL} lifetime lower than $\tau_{IR}/2$. Whereas in case of high Yb cluster content the lifetimes τ_{IR} and τ_{CL} obey to the rule $\tau_{CL} \approx \tau_{IR}/2$ more properly.

3. b. 2 Dose and dose rate effects

The effects of irradiation dose and dose rate on τ_{IR} and τ_{CL} have been analyzed on stabilized samples (after 1 year). It was impossible to irradiate all the powders with 2.5 MeV electrons because of lack of beamtime on SIRIUS accelerator. Therefore, both powders and slices of the glasses were used. The comparison of massive samples' and powders' results has not revealed any principle difference (see Chapter II, section 4.a). Nevertheless, the two series are presented below separately.

Powders

In all the glasses the lifetimes τ_{IR} decrease under irradiation (Table III-6). The reduction is higher under strong dose while no effect of dose rate is seen at 10^5 Gy.

Whatever the irradiation dose and dose rate, the lifetime decrease is stronger in glasses with more Al and/or Yb clusters. In e^--irradiated AS22 glasses (the lowest concentration of Al) the lifetimes τ_{IR} are 86% and 71% of its initial value, for 10^5 Gy and 10^8 Gy respectively. In e^--irradiated AS26 glasses (the highest concentration of Al) the lifetimes τ_{IR} are 65% and 51% of its initial value, for 10^5 Gy and 10^8 Gy respectively.

Sample	**Non-irradiated**	**Electron-irradiation**		**Gamma-irradiation**
		10^5 Gy	**10^8 Gy**	**10^5 Gy**
AS22	2.14	1.83	1.53	1.72
AS23	1.97	1.52	1.35	
AS24	1.15	0.82	0.69	0.84
AS26	0.94	0.61	0.48	0.61
AS24_Yb8	1.00	0.52	0.42	0.52

Table III-6. Lifetimes τ_{IR} in irradiated powders, ENSCP

Besides, the ionizing irradiation affects the lifetime τ_{IR} stronger when the Yb concentration is higher, see AS24_8 glasses in Table III-6. It confirms the impact of Yb clusters.

Slices

The dose effect on lifetime τ_{IR} has been studied in more details with slices (7 doses). Figure III-39 presents the lifetimes τ_{IR} plotted vs. lg(dose) in stabilized samples.

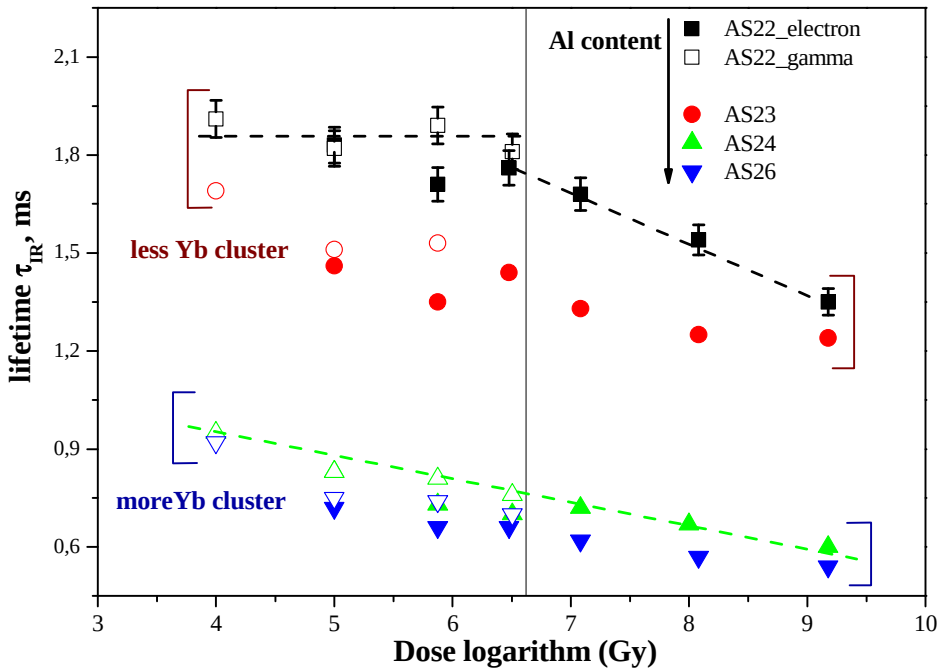


Figure III-39. Lifetimes τ_{IR} in irradiated slices, LSI. Fulled symbols - e^--irradiation, empty symbols – γ-irradiation

The first result concerns the dose rate effect. No impact on τ_{IR} lifetime is observed whatever the glass composition for 3 doses: 10^5, 10^6, $3 \cdot 10^6$ Gy.

Two regions can be distinguished separated by $3.2 \cdot 10^6$ Gy dose for AS22 and AS23 glasses.

In AS24 and AS26 glasses only one linear variation is observed (Figure III-39). The lifetime τ_{IR} decreases slowly linearly with irradiation dose. In AS22 and AS23 glasses the τ_{IR} lifetime decrease is more expressive in $3.2 \cdot 10^6$-$1.5 \cdot 10^9$ Gy dose range.

Let's observe now the variation of the lifetime τ_{IR} within the lg(dose) in AS24_Ybx glasses (Figure III-40).

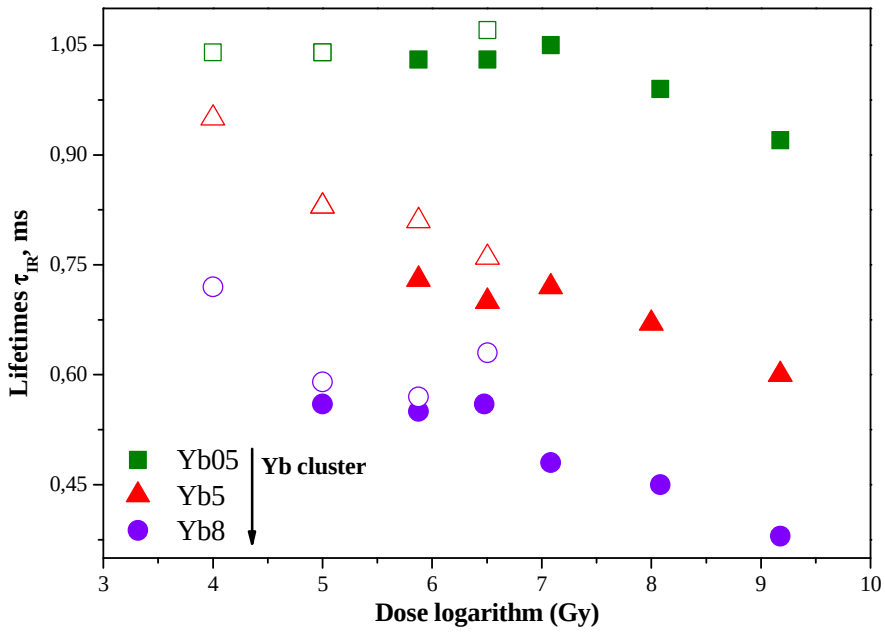


Figure III-40. Lifetimes τ_{IR} in irradiated slices. Yb-doping effect

We observe the same two steps of behavior described in Figure III-39 for Yb05 sample. In Yb8 and Yb5 glasses the lifetime τ_{IR} linear variation with lg(dose) looks like AS24 and AS26 glasses. The common point between those glasses is their high content of Yb cluster. So, we would attempt to associate this effect to the Yb repartition in the glass.

In glasses with significant amount of Yb cluster the evolution of lifetime τ_{IR} with lg(dose) decreases linearly whereas for glasses with lower amount of Yb cluster a two-step variation is observed. It is very interesting to remark that same two-step behavior was visible in ABS glasses [31] and in phosphate glasses (Chapter IV). We will discuss it is also for Er-containing AS glasses in Chapter V. Moreover, it is worth to correlate also those effects with the variation of paramagnetic point defects within irradiation dose. We observe this two-step variation of total defect amount with dose. We saw that the impact of dose on the defects' amount is lower for glasses presenting a linear variation of the τ_{IR} lifetime with lg(dose) (Figure III-28, Figure III-29).

The lifetimes τ_{CL} of Yb-Yb pairs evolution under 10^5 Gy and 10^8 Gy doses are presented in Table III-7.

Sample	Non-irradiated	Electron-irradiation		Gamma-irradiation
		10^5 Gy	10^8 Gy	10^5 Gy
AS22	0.84	0.52	0.70	0.55
AS23	0.78	0.65	0.62	
AS24	0.52	0.38	0.33	0.39
AS26	0.43	0.29	0.23	0.29
AS24_Yb8	0.45	0.25	0.26	0.21

Table III-7. Lifetimes τ_{CL} in irradiated AS glasses, powders

Under irradiation, the lifetime τ_{CL} decreases slightly. It can be noticed that no dose rate effect is visible, as for the lifetimes τ_{IR}. However, it is interesting to mention the dose effect on the lifetimes τ_{CL}. This result is important because it suggests that **the mechanisms limiting the lifetimes τ_{IR} and τ_{CL} are different. A saturation effect is visible for Yb pairs at dose 10^5 Gy.**

3. c. Analysis of the role of defects in CL and lifetime evolution under irradiation

In order to understand the role of the defects in the lifetime τ_{IR} evolution, we try now to correlate the evolution of the defects within time and under thermal annealing with the lifetime τ_{IR} evolution.

3. c. 1 Post-irradiation evolution in time

We have measured for 10^5 Gy (e^-- and γ-irradiations) and 10^8 Gy (e^--irradiation) doses the τ_{IR} lifetimes evolution in AS glasses during 120-180 days.

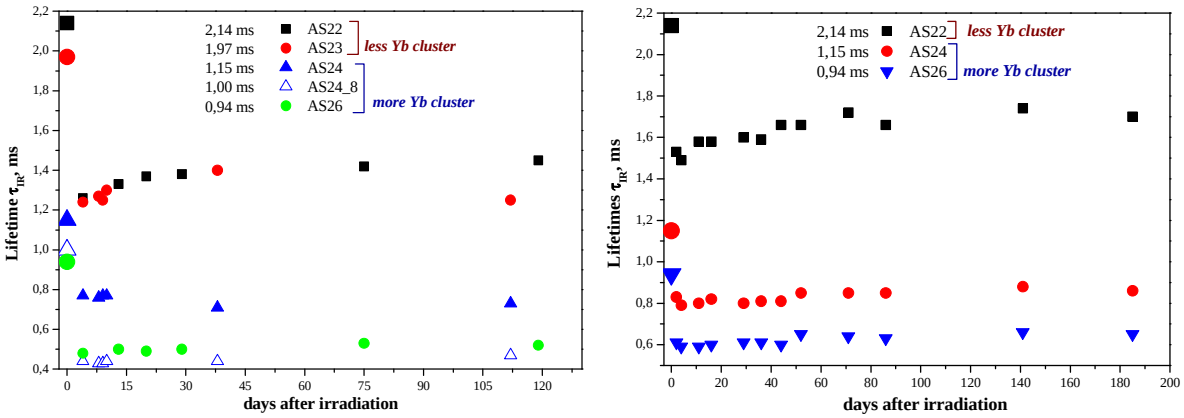


Figure III-41. Lifetime τ_{IR} evolution in time: after the e^--irradiation in AS glasses, dose 10^8 Gy (left) and after the γ-irradiation in AS glasses, dose 10^5 Gy (right). Bigger signes are initial values

The curves of Figure III-41 show that the lifetime decrease is stable in time in glasses with high content of Yb clusters (AS24, AS24_8 and AS26). This is true also for γ-irradiated samples at 10^5 Gy.

In e^--irradiated AS22 and AS23 glasses a slight recovery of τ_{IR} is detected. Same effect is noticed for γ-irradiated AS22 sample (Figure III-41, right).

More specifically, we focus now on the first week where 50% of paramagnetic defects have recovered, whereas the lifetime seems stable.

Correlation can not be done in absence of lifetime measurements each day of the first week. It is thus difficult to associate the lifetime evolution with the total amount of the paramagnetic defects. However, it corroborates the idea of stable

charge trapping by Yb clusters in AS24 and AS26 glasses implying a higher stability of τ_{IR} such glasses.

3. c. 2 Thermal annealing treatments

In order to investigate the thermal stability of induced point defects and to look for any correlation between defects formation/relaxation and Yb^{3+} lifetime τ_{IR}, some thermal annealing treatments were carried out on AS22_10e8 and AS24_10e8 glasses, both electron-irradiated. These glasses exhibit contrasted content of Yb clusters (AS22<AS24).

The bulk samples were annealed for 10 min in corundum crucibles under air atmosphere. The temperature range was 100-400°C with ~20°C step. The time necessary to stabilize the temperature after the crucible with samples had been placed into the oven was 100 sec. Each annealing step was followed by EPR and, in case of changes of spectrum, by the lifetime τ_{IR} measurements and PL under laser excitation at 532 nm as well. Finally, Yb^{3+} cooperative emission was registered once the whole annealing cycle had been completed.

AS22_10e8 glass

The lifetime τ_{IR} in AS22 decreases from 2.14 ms to 1.53 ms under 10^8 Gy irradiation dose. As it has been shown above, in AS22 irradiated glasses, mostly HC and few Peroxy defects are induced. It is worth to remind here that in Yb-free AS22 glasses E' centers are created at 10^8 Gy irradiation dose. Almost no Al-OHCs are seen.

Under annealing, the total amount of all paramagnetic defects decreases implying the thermal recovery of defects (Figure III-42). One can better see the signature of E' centers from 120°C with HC reduction, a further increase of E' signal and, finally, recovery at 224°C. At 399°C almost no paramagnetic defects are detected.

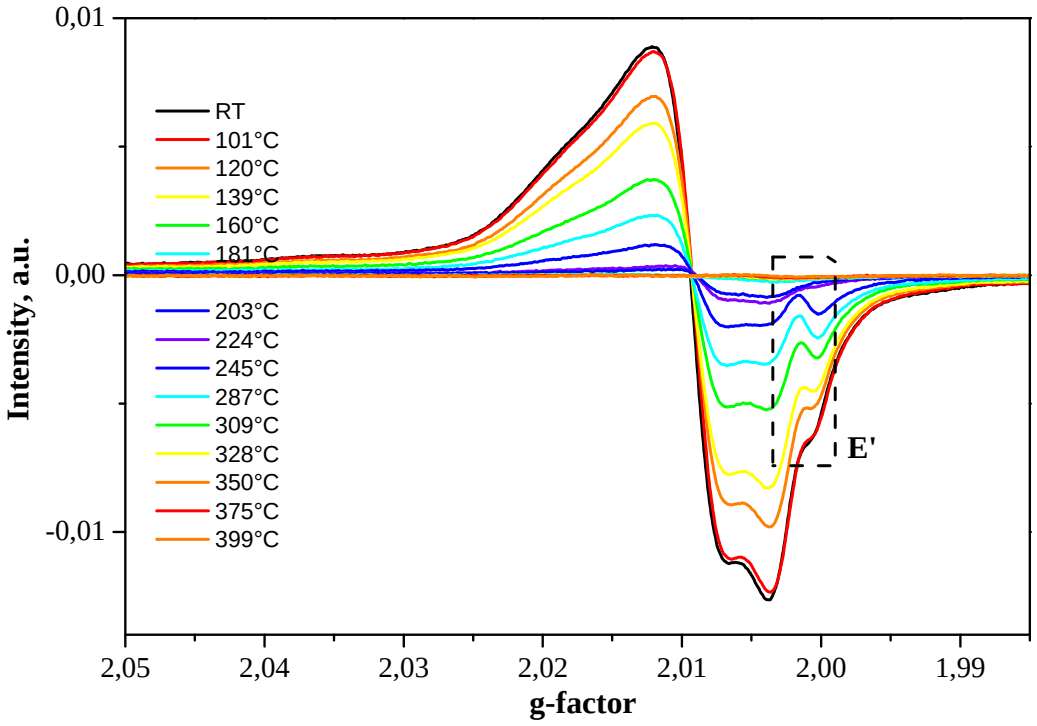


Figure III-42. EPR spectra of AS22_10e8 after annealing at high temperatures

The Figure III-43 presents the emission band under a 532 nm excitation in irradiated sample only. We assume thus that this band corresponds to a point defect created under irradiation. Even if the emission is centered at 730 nm instead of usual 650 nm for SiO_2 [21], the band was attributed to NBOHC defects because the lifetime corresponding to the band was estimated ~10µs which is close to NBOHC defects [21] [40].

After annealing at 203°C, 224°C and 309°C, the lifetime τ_{IR} and the PL of NBOHC were registered as well (Figure III-43).

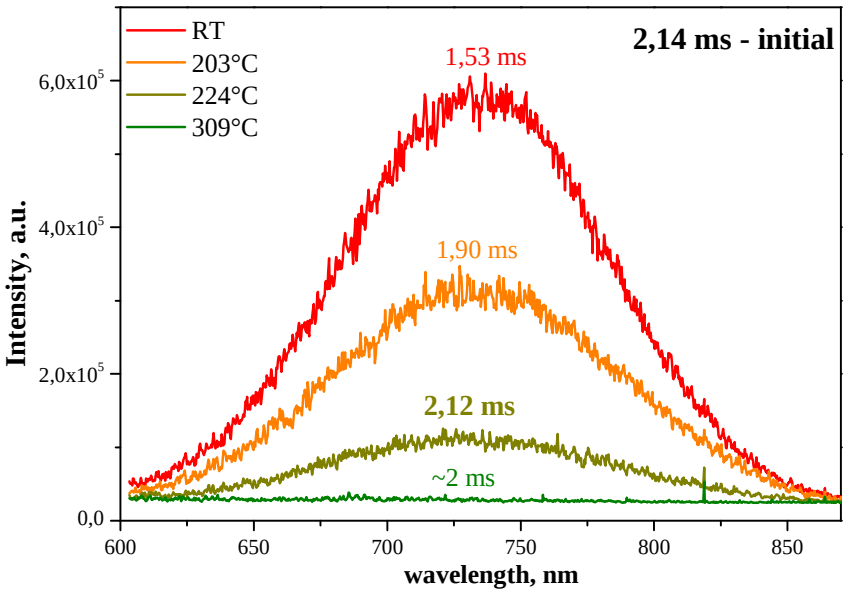


Figure III-43. Photoluminescence of NBOHC in AS22_10e8 after annealing treatments

The lifetime τ_{IR} increases with annealing up to its initial value ~2.1 ms at 224°C. After annealing at this temperature some HC defects are still observed (Figure III-44). Moreover, the luminescence band at 730 nm is still detected. It eliminates at 309°C.

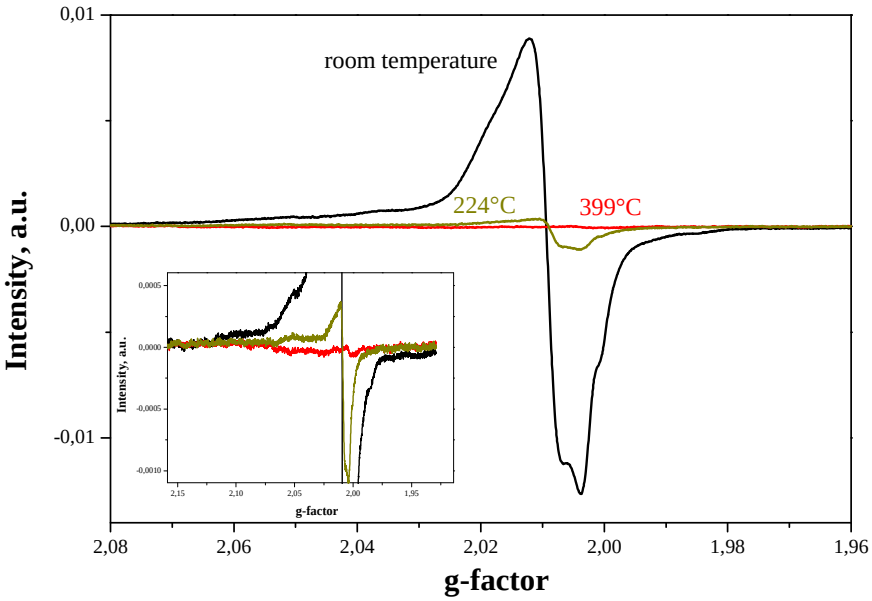


Figure III-44. EPR spectra of AS22_10e8 glass during the annealing treatments

Therefore, in AS22 glass with low Yb cluster content neither NBOHC nor HC defects can be the only responsible for the stable decrease of the lifetime τ_{IR}.

AS24_10e8 glass

In AS24 glasses the defects composition is different than in AS22 glasses. In particular, Al-OHC defects are clearly detected and mostly Peroxy radicals. The question of attribution of EPR lines either to NBOHC or to Peroxy radicals was resolved here.

The thermal annealing treatment of AS24_10e8 glass was carried out in parallel with AS22_10e8 glass with the same experimental conditions.

The total amount of defects in AS24_10e8 decreases logically when the annealing temperature increases (Figure III-45).

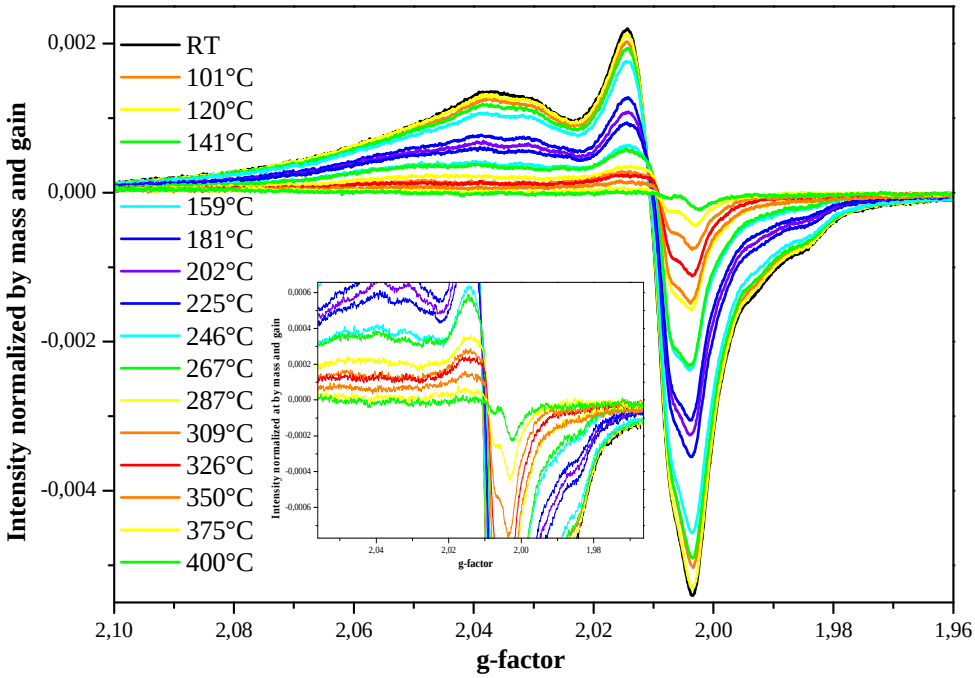


Figure III-45. EPR spectra of AS24_10e8 sample at annealing treatments

In the final EPR spectrum a signal with g_1=2.0037, g_2=2.0086, g_3=2.0502 is still visible (Figure III-45, inset). It confirms the presence of Peroxy radicals. They are more stable at higher temperatures than NBOHC [41]. The singlet at g=2.0026 can be assigned to carbon contamination [41].

One can see that Al-OHC defects are active until their recovery at 225°C (Figure III-45). The thermal stability of Al-OHC defects is in agreement with the results of annealing treatments of Yb-doped Al/P-containing glass fibers [39].

The lifetime τ_{IR} and the emission of NBOHC were carried out after annealing at 202°C, 309°C and 400°C (Figure III-46).

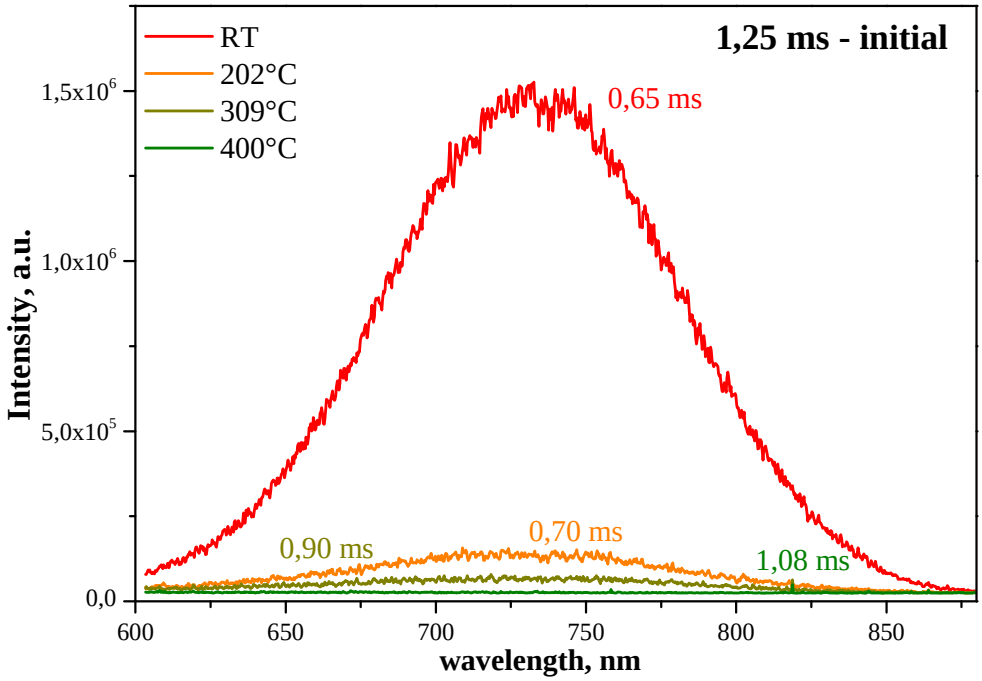


Figure III-46. Photoluminescence of NBOHC in AS24_10e8 under annealing treatment

Up to 200°C there is no evolution in the lifetime τ_{IR} while the NBOHC emission decreases crucially. The lifetime τ_{IR} is not yet back at 225°C to the pre-irradiation value. We conclude thus that Al-OHC defects cannot be the only defect responsible for the lifetime τ_{IR} decrease under the irradiation. At the last temperature the photoluminescence band at 730 nm disappears. However, the lifetime τ_{IR} is 13% lower than its pre-irradiation value. We assume thus that NBOHC defects are not responsible for the lifetime τ_{IR} decrease under irradiation.

However, some Peroxy radicals were still detected after annealing at 400°C. Its absorption band is at 1.97 eV (630 nm) [21] which tail is superposed with Yb^{3+} absorption. It implies their participation in the τ_{IR} lifetime decrease under the irradiation.

- **Cooperative emission of Yb^{3+} decreases under the irradiation in AS24 and AS26 glasses. Neither dose, nor dose rate effect is observed. This effect is stable in time (146 days).**
- **The lifetimes τ_{IR} and τ_{CL} decrease under the irradiation in all studied glasses. No dose rate effect is observed for both lifetimes τ_{IR} and τ_{CL}. The lifetime τ_{IR} stability is higher in glasses with more Yb cluster (AS24-AS26, AS24_8)**
- **In glasses with less Yb cluster (AS22-AS23, AS24_05) the lifetime τ_{IR} dependence vs. lg(dose) exhibits 2 regimes: stable in medium dose range (10^4-$3.2\cdot10^6$ Gy) and linear decrease in stronger dose range ($3.2\cdot10^6$-$1.5\cdot10^9$ Gy). With increase of Yb cluster content in glass, the lifetime τ_{IR} dependence is modified into one-regime with linear decrease in a vast dose range (10^4-$1.5\cdot10^9$ Gy).**
- **The lifetime τ_{IR} is sensitive to the dose whereas no dose effect is visible for τ_{CL}. We suppose the saturation effect for Yb pairs at low doses (10^5 Gy).**
- **In glasses with high Al content, Peroxy radicals could be partly responsible for the lifetime τ_{IR} decrease under the irradiation.**

4. Conclusions

Yb clusters are less formed in case of more Non-Bridging Oxygens (AS22-AS23) [1]. Presence of Yb clusters in Na-aluminosilicate glasses stabilizes the system regarding at point defects relaxation and lifetime τ_{IR} evolution in time. We have demonstrated thus the efficiency and stability of Yb cluster's in charge trapping impacting the recovery of point defects and, in consequence, the lifetime τ_{IR} evolution.

In addition, the Yb cluster presence attenuates also the increase of point defects with irradiation dose increase.

The decrease of cooperative luminescence under irradiation seems to be more impacted by the defect creation such as Al-OHC and Peroxy radicals than the formation of Yb^{3+}-Yb^{2+} or Yb^{2+}-Yb^{2+} pairs.

There is no dose effect in the lifetime τ_{CL} decrease contrary to the lifetime τ_{IR}. This result shows saturation in charge trapping by Yb pairs at low doses (10^5 Gy).

[1] B. Schaudel, P. Goldner, M. Prassas et F. Auzel, *J. Alloys and Comp.,* vol. 300&301, p. 443, 2000.

[2] W. H. Zachariasen, *J. Am. Cer. Soc.,* vol. 54, p. 3841, 1932.

[3] G. N. Greaves et S. Sen, Inorganic glasses, glass-forming liquids and amorphizing solids, Advances in Physic, 2007.

[4] T. Schaller et J. F. Stebbins, *J. Phys. Chem. B,* vol. 102, p. 10690, 1998.

[5] S. H. Risbud, R. J. Kirkpatrick, A. P. Taglialavore et B. Montez, *J. Amer. Ceram. Soc. C,* vol. 70, p. 12, 1987.

[6] R. K. Sato, P. F. McMillan, P. Dennison et R. Dupree, *J. Phys. Chem.,* vol. 95, p. 4483, 1991.

[7] G. Engelhardt, M. Nofz, K. Forkel, F. G. Wishmann, M. Magi, A. Samoson et E. Lippmaa, *Phys. Chem. Glasses,* vol. 26, p. 157, 1985.

[8] L. Kokou et J. Du, *J. Non-Cryst Solids,* vol. 358, p. 3408, 2012.

[9] S. Sen, *J. Non-Cryst. Solids,* vol. 261, p. 226, 2000.

[10] F. d'Acapito, S. Mobilio, L. Santos et R. M. Almeida, *Appl. Phys. Lett.,* vol. 78, p. 2676, 2001.

[11] F. d'Acapito, S. Mobilio, P. Bruno, D. Barbier et J. Philipsen, *J. Appl. Phys.,* vol. 90, p. 265, 2001.

[12] B. Schaudel, Ph.D. dissertation, Paris: Université Paris VI, 2000.

[13] S. Sen, R. Rakhmatullin, R. Gubaidullin et A. Pöppl, *Phys. Rev. B,* vol. 74, p. 100201, 2006.

[14] F. L. Galeener, *J. Non-Cryst. Solids,* vol. 49, p. 53, 1982.

[15] P. McMillan, B. Piriou et A. Navrotsky, *Geochim. Cosmochim. Acta,* vol. 46, p. 2021, 1982.

[16] A. J. G. Ellison et P. C. Hess, *J. Geophys. Res.,* vol. 95, p. 15717, 1990.

[17] H. Li, Y. Su, L. Li et D. M. Strachan, *J. of Non-Cryst. Solids,* vol. 292, p. 167, 2001.

[18] B. O. Mysen, D. Virgo et F. Seifert, *Am. Mineral.,* vol. 70, p. 88, 1985.

[19] J. Hiet, D. Massiot, M. Deschamps, F. Fayon, G. Ferru, M. Derieppe et N. Pellerin, *Phys. Chem. Chem. Phys.,* vol. 10, p. 1298, 2008.

[20] N. Ollier, R. Planchais et B. Boizot, *Nucl. Instr. and Meth. in Phys. Res. B,* vol. 266, p. 2854, 2008.

[21] L. Skuja, *J. Non-Cryst. Solids,* vol. 239, p. 16, 1998.

[22] D. L. Griscom, *Journ. of Non-Cryst. Solids,* vol. 64, p. 229, 1984.

[23] D. L. Griscom, *Journ. of Non-Cryst. Solids,* vol. 357, p. 1945, 2011.

[24] D. L. Griscom, *Phys. Rev. B,* vol. 20, p. 1823, 1979.

[25] H. Nishikiawa, E. Watanabe, D. Ito et Y. Ohki, *J. Non-Cryst. Solids,* vol. 179, p. 179, 1994.

[26] L. Nuccio, S. Agnello et R. Boscaino, *Phys. Rev. B,* vol. 79, p. 12505, 2009.

[27] E. J. Friebele, D. L. Griscom, M. Stapelbroek et R. A. Weeks, *Phys. Rev. Lett.,* vol. 42, p. 1346, 1979.

[28] D. A. Dutt, P. L. Highby et D. L. Griscom, *Journ. of Non-Cryst. Solids,* vol. 130, p. 41, 1991.

[29] V. V. Laguta, M. Nikl, A. Vedda, E. Mihokova, J. Rosa et K. Blazek, *Phys. Rev.*

B, vol. 80, p. 045114, 2009.

[30] N. Ollier, R. Planchais et B. Boizot, *Nucl. Instr. and Meth. in Phys. Res. B,* vol. 266, p. 2854, 2008.

[31] N. Ollier, J.-L. Doulan, V. Pukhkaya, T. Charpentier, R. Moncorgé et S. Sen, *J. Non-Cryst. Solids,* vol. 357, p. 1037, 2011.

[32] E. Malchukova, B. Boizot, G. Petite et D. Ghaleb, *J. Non-Cryst. Solids,* vol. 354, p. 3592, 2008.

[33] H. Ebendorff-Heidepriem et D. Ehrt, *Opt. Mater.,* vol. 18, p. 419, 2002.

[34] N. Ollier et V. Pukhkaya, *Nucl. Instr. and Meth. in Phys. Res. B,* vol. 277, p. 121, 2012.

[35] J. Sheng, K. Kadono et T. Yazawa, *Appl. Radiat. Isot.,* vol. 57, p. 813, 2002.

[36] K. Farah, A. Kovacs, A. Mejri et H. Ben Ouada, *Radiat. Phys. Chem.,* vol. 75, p. 1523, 2007.

[37] T. R. Waite, *Phys. Rev.,* vol. 107, p. 471, 1957.

[38] B. Boizot, N. Ollier, F. Olivier, G. Petite, D. Ghaleb et E. Malchulova, *Nucl. Instr. and Meth. in Phys. Res. B,* vol. 240, p. 146, 2005.

[39] T. Deschamps, H. Vézin, C. Gonnet et N. Ollier, *Opt. Express,* vol. 21, p. 8382, 2013.

[40] L. Vaccaro, M. Cannas et R. Boscaino, *Solid State Commun.,* vol. 146, p. 148, 2008.

[41] D. L. Griscom, C. I. Merzbacher, R. A. Weeks et R. A. Zuhr, *J. Non-Crust. Solids,* vol. 258, p. 34, 1999.

List of Figures

Figure III-1. Structure of silicate glasses [2] 39
Figure III-2. Raman spectra of non-irradiated Yb-doped AS glasses..... 41
Figure III-3. Zoom on Raman spectra, normalization at 495 cm^{-1} 42
Figure III-4. ^{27}Al MAS NMR spectra of non-irradiated non-doped glasses 43
Figure III-5. Zoom of Raman spectra at 900-1300 cm^{-1} range..... 43
Figure III-6. Raman spectra of AS22 glasses, normalization at 495 cm^{-1}..... 45
Figure III-7. 2D ^{27}Al MAS NMR spectra of AS22_0 glasses 45
Figure III-8. 2D ^{27}Al MAS NMR spectrum of e-irradiated AS22_Er glass at $2 \cdot 10^9$ Gy 46
Figure III-9. Yb^{3+} luminescence in non-irradiated AS glasses..... 47
Figure III-10. EPR spectra of non-irradiated AS glasses at 4K, normalized at maximum. Normalization by mass and attenuation gain is inset..... 48
Figure III-11. EPR spectra of non-irradiated glasses, 4K..... 49
Figure III-12. Probability of cooperative luminescence in non-irradiated AS2x_Yb5 glasses. Normalization by absorption and lifetime τ_{IR}..... 50
Figure III-13. Raman spectra of non-irradiated AS24_Ybx glasses, normalization at 1050 cm^{-1} is inset..... 51
Figure III-14. Probability of cooperative luminescence in non-irradiated AS24_Ybx glasses 52
Figure III-15. A) fragment of perfect lattice; B) the "classic" model of E'_1 center in α-quatrz or E'_γ center in silica, from L. Skuja's review [21] 53
Figure III-16. Model of peroxy radical in α-SiO_2 [27] 54
Figure III-17. Model representation of the HC_1 defect[2] 55
Figure III-18. Model of two HC_2 defects configurations [22]..... 55
Figure III-19. EPR spectra of Yb-doped e^- -irradiated AS glasses just after the irradiation, dose 10^5 Gy, normalization at g=2.015. EPR spectra normalized only by mass and gain are in the inset. 57
Figure III-20. EPR spectra of e^--irradiated AS24_0 and AS22_0 glasses, dose 10^7 Gy, stabilized samples..... 58
Figure III-21. EPR spectra of e^- -irradiated AS24_Ybx glasses, dose 10^5 Gy, normalization at g=2.015. EPR spectra recorded just after the irradiation and normalized only by mass and gain are in the inset..... 59
Figure III-22. EPR spectra of AS24_Ybx glasses, dose 10^7 Gy, stabilized samples.. 59

Figure III-23. Relaxation curves of Yb-doped e— -irradiated AS2x_Yb5glasses, dose 10^5 Gy 61
Figure III-24. Relaxation curves of Yb-doped e— -irradiated AS24_Ybx glasses, dose 10^5 Gy 62
Figure III-25. Relaxation curves of Yb-doped e^- -irradiated AS22 and AS24 glasses, dose 10^5 Gy. The axes of abscissas are in logarithm 63
Figure III-26. Evolution in time of e^--irradiated AS23 glass,dose 10^5 Gy, normalization at g=2.013 64
Figure III-27. Evolution in time of Al-OHC and HC defects in e^--irradiated AS23 glass, dose 10^5 Gy 65
Figure III-28. Dose dependence in electron-irradiated glasses 66
Figure III-29. Dose dependence in AS24_Ybx samples, electron irradiation 67
Figure III-30. Dose dependence in gamma irradiated samples. Dose rate effect. Full signs – 25 MGy/h (e^-), empty signes – 5.64 kGy/h (gamma) and stars – 0.3 MGy/h (e^-) 68
Figure III-31. Normalized EPR spectra of AS2x_Yb5 glasses, electron irradiation... 69
Figure III-32. EPR spectra of AS26 glass irradiated at $1.5 \cdot 10^9$ Gy. Normalization by mass&gain is inset 70
Figure III-33. EPR spectra e^- -irradiated with various doses AS22_0 glasses, stabilized samples 71
Figure III-34. Absorption of e^--irradiated AS24 glass, 10^5 Gy. Evolution in time.... 73
Figure III-35. The spectra of cooperative emission in e^--irradiated AS24 glasses, doses 10^5 Gy and 10^8 Gy 74
Figure III-36. Absorption spectra of irradiated AS24 glasses 75
Figure III-37. Cooperative emission of e^--irradiated AS24 glass, dose 10^5 Gy 75
Figure III-38. The CL spectra in e^--irradiated AS22 (left) and AS23 (right) glasses. 76
Figure III-39. Lifetimes τ_{IR} in irradiated slices, LSI. Fulled symbols - e^--irradiation, empty symbols – γ-irradiation 79
Figure III-40. Lifetimes τ_{IR} in irradiated slices. Yb-doping effect 80
Figure III-41. Lifetime τ_{IR} evolution in time: after the e^--irradiation in AS glasses, dose 10^8 Gy (left) and after the γ-irradiation in AS glasses, dose 10^5 Gy (right). Bigger signes are initial values 82
Figure III-42. EPR spectra of AS22_10e8 after annealing at high temperatures 84
Figure III-43. Photoluminescence of NBOHC in AS22_10e8 after annealing treatments 85
Figure III-44. EPR spectra of AS22_10e8 glass during the annealing treatments... 85

Figure III-45. EPR spectra of AS24_10e8 sample at annealing treatments 86
Figure III-46. Photoluminescence of NBOHC in AS24_10e8 under annealing treatment 87

List of Tables

Table III-1. Parameters of g-tensors of NBOHC and Peroxy radicals in amorphous SiO_2 [21] 54
Table III-2. Parameters of g-tensor of HC_1 and HC_2 defects [22] 55
Table III-3. Parameters of g-tensors of Al-OHC defects 56
Table III-4. E' centers detected in stabilized e^--irradiated AS glasses: red - no E', green - E' detected, yellow - traces of E', grey - no sample 60
Table III-5. The lifetimes τ_{IR} and τ_{CL} in non-irradiated samples 77
Table III-6. Lifetimes τ_{IR} in irradiated powders, ENSCP 78
Table III-7. Lifetimes τ_{CL} in irradiated AS glasses, powders 81

Chapter IV

Phosphate glasses

IV. Phosphate glasses 98
1. Structure of phosphate glasses 98
1. a. Bibliographic part 98
1. b. Analysis by Raman spectroscopy 100
2. Structure of P-related point defects (bibliography part) 102
2. a. POHC defects 102
r-POHC 102
l-POHC 103
2. b. P1 defects (PO_3^{2-}) 103
2. c. P2 defects (PO_4^{4-}) 104
2. d. P3 defect 104
2. e. P4 defect (PO_2^{2-}) 104
3. Analysis of paramagnetic point defects formed under ionizing irradiation 105
3. a. Formation of paramagnetic defects 105
3. a. 1 Hole centers 105
3. a. 2 P centers 106
3. b. Relaxation of paramagnetic defects 108
3. b. 1 Relaxation of hole centers 108
3. b. 2 Relaxation of P centers 111
3. c. Dose and dose rate effect 113
3. c. 1 Dose effect 113
3. c. 2 Dose rate effect 118
4. Diamagnetic defect 121
4. a. Attribution of the defect 121
4. b. The diamagnetic defect in irradiated phosphate glasses 122
5. The lifetime of $^2F_{5/2}$ excited state evolution under e^--irradiation 125
5. a. Dose and dose rate effect 125
5. b. Relation with point defects 127
5. b. 1 Evolution in time 127
5. b. 2 Relation between the diamagnetic defects and the $^2F_{5/2}$ lifetime .. 127

6. Conclusions 131

IV. Phosphate glasses

In this Chapter IV another glass type is studied: phosphate glasses. Many studies concerning RE^{3+} luminescent properties in phosphate glasses can be found [1], but poor information is available on radiation-induced point defects. Therefore, a big part of Chapter IV is dedicated to paramagnetic point defects. The interpretation is complicated because of too complex composition of paramagnetic point defect created under irradiation and analyzed by EPR spectroscopy. Comparison with literature is limited as well. We observe, moreover, a P-related diamagnetic defect poorly studied in literature except by Origlio et al. in 2009 [2]. Its relations with paramagnetic defects are discussed.

Despite less attention paid to the evolution of Yb^{3+} luminescence under irradiation in Chapter IV, we studied the lifetime of $^2F_{5/2}$ excited state in vast irradiation dose range as for AS glasses. We also tried to correlate the lifetime τ_{IR} evolution under irradiation with point defects.

1. Structure of phosphate glasses

1. a. Bibliographic part

The structure of phosphate glass consists on a continuous random network of phosphorus tetrahedra (Figure IV-1). Each phosphorus tetrahedron is sourrounded by four oxygen atoms: one oxygen atom shares a double bond with the phosphorus atom, while the remaining three oxygen atoms can either be bridging (bridging oxygen: BO) forming a P-O-P bond or Non-Bridging Oxygen (NBO) forming a mixed ionic-covalent bond. P-tetrahedra can be classified using Q^n terminology like for silicate glasses, where n represents the number of bridging oxygen atoms. Figure IV-1 illustrates the different forms of P-tetrahedra that can exist in phosphate glasses. The proportion of each form of P-tetrahedra is determined primarily by the stoichiometry of the glass, specifically the ratio of oxygen atoms to phosphorus atoms. Q^2, Q^1, and Q^0 P-tetrahedra are negatively charged units; charge neutrality is preserved through the presence of network modifiers, typically alkali, alkali earth or rare earth metal ions.

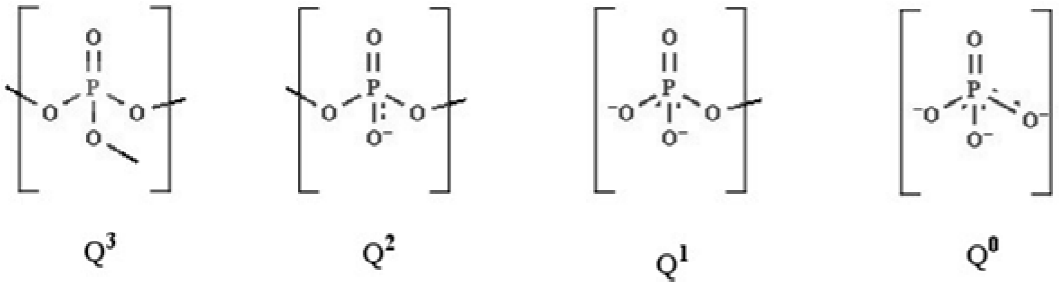


Figure IV-1 . PO^n polyhedra

For binary $xR_2O\cdot(1-x)P_2O_5$ [$xR'O\cdot(1-x)P_2O_5$] glasses, the concentrations of Q^n tetrahedra generally follow simple predictions based on the glass composition.

In the **ultra-phosphate** region ($0\le x\le 0.5$), the fractions of Q^2 and Q^3 tetrahedra are given by

$f(Q^2)=x/(1-x)$

$f(Q^3)=(1-2x)/(1-x)$

Meta-phosphate glasses (x=0.50) have network based entirely on Q^2 chains and rings.

Between the meta-phosphate (x=0.500) and **pyrophosphate** (x=0.67) boundaries, the fraction of Q^1 and Q^2 tetrahedra are given in **poly-phosphates** by

$f(Q^1)=(2x-1)/(1-x)$,

$f(Q^2)=(2-3x)/(1-x)$.

According to the glass compositions studied in this work (see Chapter II, section 1.b), we should expect the following distribution of fractions of structure groups and phosphate glass types according to the Q^i:

sample	type	mol. Na_2O and MgO	mol. P_2O_5	R	theor. fractions of Q^i
2743	Ultra-	x=0.333	1-x=0.667	0.5	$f(Q^2)=0.50$ $f(Q^3)=0.50$
2742	Meta-	x=0.50	1-x=0.50	1	$f(Q^2)=1$
2745	Poly-	x=0.546	1-x=0.454	1.2	$f(Q^1)=0.20$ $f(Q^2)=0.80$
2746	Poly-	x=0.60	1-x=0.4	1.5	$f(Q^1)=0.50$ $f(Q^2)=0.50$

Table IV-1 . Types of phosphate glasses studied in the work

The phosphate glass structure can be described by ratio $R=(MgO+Na_2O)/P_2O_5$ which varies as a function of network type. It increases with phosphorus content decrease (Table IV-1). We underline here that 2743 glass is the only composition with Q^3 species.

In phosphate glasses the RE cluster amount is lower than in aluminosilicate glasses because in PO_4 tetrahedra at least one oxygen is non-bridging $-O_3P=O$. This particularity leads to easier dissolution of RE^{3+} ions in phosphate matrices [3].

1. b. Analysis by Raman spectroscopy

The analysis of phosphate glass structure by Raman spectroscopy is important to check the theoretical structure described in Table IV-1 and to better understand the glass composition influence on the point defect formation.

The Raman spectra of non-irradiated glasses are displayed in Figure IV-2.

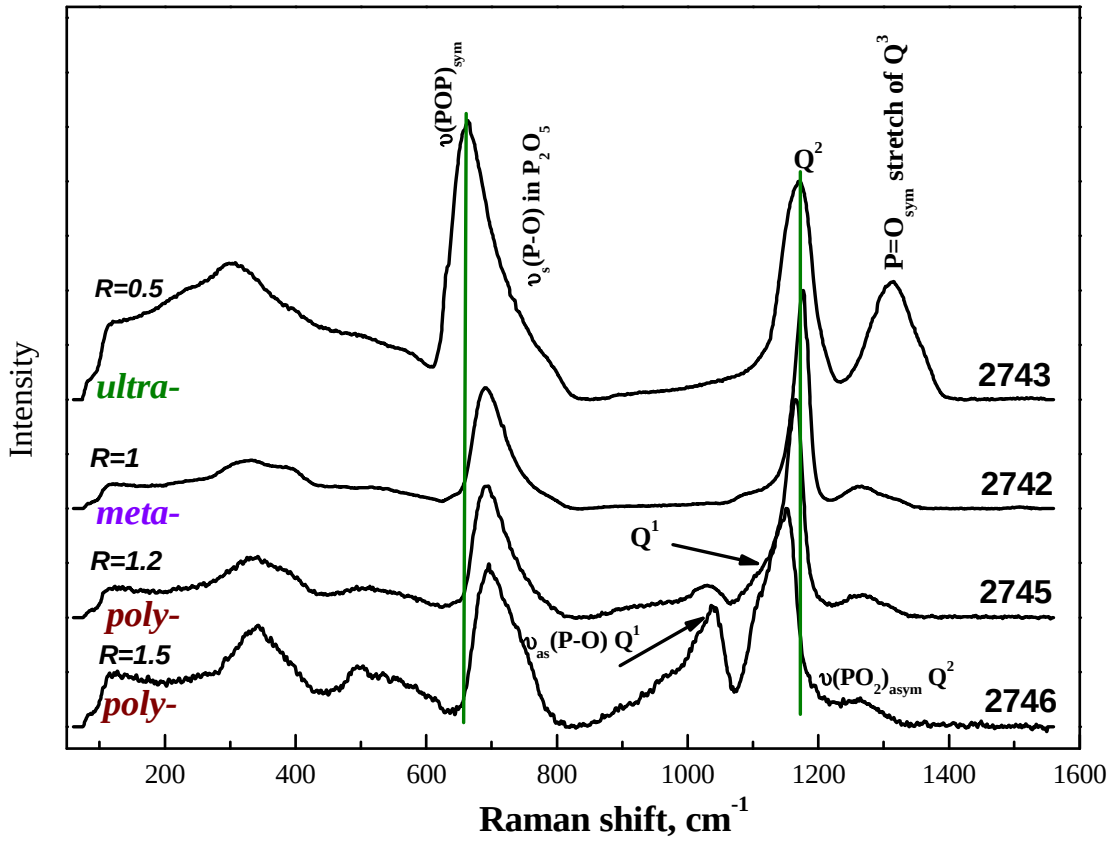


Figure IV-2. Raman spectra of non-irradiated Yb-doped phosphate glasses

According to Brow's review [4] the Raman bands in the 1000-1400 cm^{-1} range are due to the symmetric and asymmetric stretching modes of P-non-bridging bonds, whereas bands in the 620-820 cm^{-1} range are due to the symmetric and asymmetric vibrations of bridging oxygens.

With monotonic decrease of P content from 2743 glass to 2746, the Raman spectra evolve. Because of phosphate network depolymerization with decreasing of P-content (and increasing of Na_2O and MgO contents), one can see that P=O motions (due to presence of Q^3 tetrahedra) disappear in 2742-2745-2746 glasses. The shifts of the band attributed to Q^2 (1153-1177 cm^{-1}) and $\nu(POP)_{sym}$ bands (663-694 cm^{-1}) are assigned to glass network depolymerization [5]. The motions of non-bridging oxygens in Q^1 tetrahedra, as a shoulder in 2745 glass, become clearly visible in 2746 glass only (Figure IV-2). In 2742 glass, however, in agreement with the prediction (Table IV-1) only Q^2 tetrahedra are seen.

The glass 2743 is the only sample where P=O double bondings are detected. The Raman spectra confirm the Q^i fraction that should be present in each glass according to its theoretical composition.

- **In only ultra-phosphate glass (2743) P=O bondings are detected**
- **In meta-phosphate glass (2742), only Q^2 tetrahedra with 2 bridging oxygens are detected**
- **In poly-phosphate glasses (2745 and 2746) Q^2 and Q^1 tetrahedra are detected**

2. Structure of P-related point defects (bibliography part)

In Yb-doped phosphate glasses (2743-2746) under ionizing irradiation P-related point defects are created. The unpaired spins delocalized on P^{5+} ion give rise to P1, P2, P3 and P4 defects. Once an unpaired spin is delocalized on Non-Bridging Oxygens, Phosphorus Oxygen Hole Center (POHC) defects are created. There is a detailed review of Griscom et al. on P-related paramagnetic point defects in P-doped silica fibers [6]. There are also some rigorous works of D. Ehrt on RE-doped phosphate glasses [7] [8]. We will use these informations in order to attribute the defects and to interpret the results.

The nuclear momentum of ^{31}P is I=½ that leads to a hyperfine structure in EPR spectra of P-related paramagnetic defects. Thereafter, all these defects are presented with double resonances (2I+½ lines). The value between the doublet characterizing the hyperfine structure is called *A*.

2. a. POHC defects

In literature, 2 types of POHC defects are mentioned: r-POHC and l-POHC.

r-POHC

The r-POHC is stable at room temperature. In this defect, phosphorus atom is linked to 2 NBOs and one hole is delocalized on both of them (Figure IV-3).

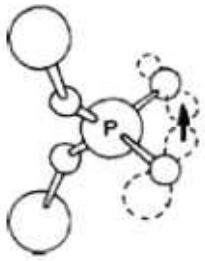


Figure IV-3. The structure of r-POHC defect [2]

In EPR spectra of r-POHC defects, the g_1 doublet strongly dominates. The g_2 doublet is hardly distinguished with X-band and g_3 doublet is observed as a broad shoulder. The recently calculated parameters of g-factor with hyperfine parameters are given in Table IV-2 [9].

l-POHC

Contrary to r-POHC defects, l-POHC was initially detected at low temperatures in P-doped silica fibers [6]. Nowadays, there is some assumption about l-POHC stability at RT [2]. In l-POHC defect there is one NBO with hole delocalized on it (Figure IV-4).

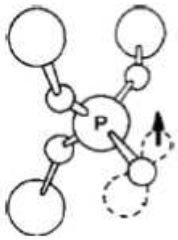


Figure IV-4. The structure of l-POHC defect [6]

The parameters of g-factor of l-POHC are close to those of r-POHC defect (Table IV-2). The simulated EPR spectra of l-POHC defects are alike as for r-POHC with g_1 doublet's domination.

	r-POHC	**l-POHC**
g_1	2.0071	2.0032
g_2	2.0097	2.0076
g_3	2.0143	2.0459
A_1 **(exp.)**	47	44
A_2 **(exp.)**	49	50
A_3 **(exp.)**	54	55

Table IV-2. The parameters of g-factor of POHC defects [9]

2. b. P1 defects (PO_3^{2-})

Phosphorus atom P^{5+}, being network former, has tetrahedral environment with four oxygen atoms, one of them is double-bonded to phosphorus whereas the other three are bonding oxygens. Once there is an oxygen vacancy V_O, $[:PO_3]^0$ can trap an electron forming P1 defect [6] (Figure IV-5). P1 defect is regarded as an analogue of E'-center in SiO_2 [6].

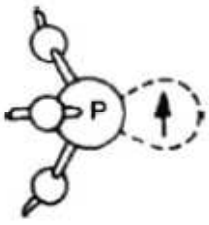


Figure IV-5. The structure of P1 defect [4]

2. c. P2 defects (PO_4^{4-})

P2 defect corresponds to one electron trapped by a 4-coordinated P atom [6]. (Figure IV-6). In phosphate glasses P2 defects are observed in case of high content of P [7] [10], enough to form PO_4 tetrahedra. It takes place in ultra-phosphate glasses where there is ≥50% of P.

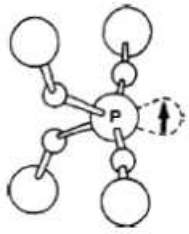


Figure IV-6. The structure of P2 defect [6]

2. d. P3 defect

There is very poor information on P3 defect in phosphate glasses. It was observed in alkali- and alkali-earth–phosphate glasses with 38-50 mol. % of phosphorus by Weeks et al. in 1968 [10]. The structure of P3 defect has not been understood yet.

2. e. P4 defect (PO_2^{2-})

The same precursor as for P1 defect $[:PO_3]^0$ can give P4 defect via electron trapping. P4 defect is formed when P^{5+} ion has 2 NBOs, 2 paired electrons and one un-paired which gives rise to an EPR signal [6].

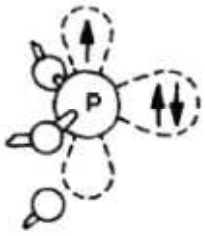


Figure IV-7. The structure of P4 defect [6]

The parameters of g-factor of P defects are summed up in Table IV-3 [6]. The g-tensors of P1, P3 and P2 defects are of isotropic signals whereas P4 defect has a g-tensor of axial symmetry.

	P1	P2	P4	P3 [10]
g_{iso}	2.005	2.0013		2.01
A_{iso}	950 Gauss	1200-140 Gauss		660 Gauss
$g_{\parallel}$			2.0014	
$g_{\perp}$			1.9989	
$A_{\parallel}$			310 Gauss	

Table IV-3. The parameters of g-factor of P-centers [6]

3. Analysis of paramagnetic point defects formed under ionizing irradiation

In irradiated Yb-doped phosphate glasses both paramagnetic and diamagnetic defects are observed and analyzed. In this section we discuss the paramagnetic defects that have been studied by EPR spectroscopy. Obtained EPR spectra are much more complex than those described in literature. Thanks to comparison between samples, following the effects of chemical composition, irradiation dose (10^4-$2\cdot10^9$ Gy), dose rate (5.64 kGy/h and 25 MGy/h) and annealing treatments, we could attribute at least 4 defects in the 3350-3650 Gauss region and 4 defects in the 2600-4200 Gauss region.

3. a. Formation of paramagnetic defects

3. a. 1 Hole centers

In all irradiated samples (2743, 2742, 2745 and 2746) r-POHC defects are detected (Figure IV-8). One can observe that g_1=2.00957 doublet with A=37 mT strongly dominates the EPR spectra. In 2742, 2745 and 2746 glasses this is the only hole center observed just after the irradiation (Figure IV-8).

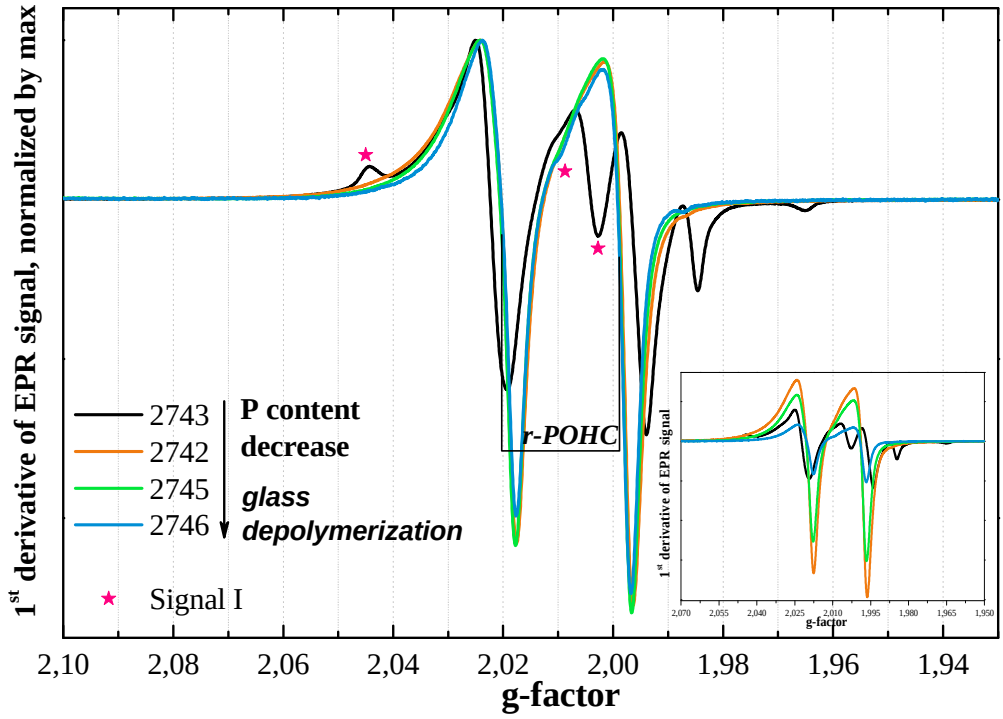


Figure IV-8. EPR spectra of just-irradiated phosphate glasses, e^--irradiation, dose 10^5 Gy. Normalization by mass&gain is in inset

The intensity of r-POHC doublet decreases from 2742 sample to 2746 sample (Figure IV-8, inset). The Q^2 molar fraction in 2742 glass is 100% followed by 2745 glass (80%), then by 2743 and 2746 glasses where it is 50% in both samples. The Q^2 species concentration in phosphate glass determines thus the number of induced r-POHC defects is in agreement with Griscom [6].

The EPR signal of 2743 glass is more complex implying the presence of other defects than r-POHC. In just-irradiated 2743 glasses a new signal is detected whatever the dose or dose rate (indicated with stars, Figure IV-8). The g-components (g_1=2.04407, g_2=2.01002, g_3=2.00451) are similar to so-called Signal I in Berger's article [11] (g_1=2.040, g_2=2.0152, g_3=2.0055). According to Berger et al. [11], its structure could be close to Peroxy radicals where two bonded Oxygens are linked to a phosphorus atom. Indeed, the shape of its EPR spectra reminds strongly the Peroxy radicals in silica and its annealing temperature is high, close to Peroxy radicals (>500°C) [12]. So, we attribute this signal to Peroxy radicals and hereafter we use the same label Signal I.

3. a. 2 P centers

P centers (P1, P2, P3 and P4) are attributed by using hyperfine coupling constants *A* that are larger than in the case of POHC defects. Moreover, P centers exhibit significantly lower intensity than POHC defects, thus the region of POHC defects is saturated in the following EPR spectra.

In only ultra-phosphate 2743 glass where P=O connections are detected by Raman spectroscopy, P2 defects (A=127 mT) are created under irradiation (Figure IV-9). This is in agreement with D. Ehrt [7] where P2 defects are seen in phosphate glasses with P=O bondings.

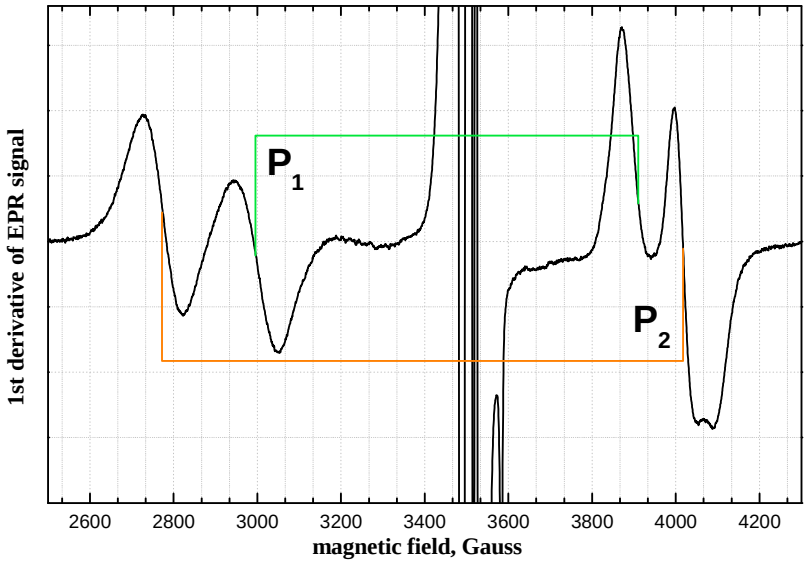


Figure IV-9. EPR spectrum of just-irradiated with electrons at 10^5 Gy 2743 glass

Its formation requires all 4 bonding-oxygen atoms; consequently, it can be formed in presence of Q^3 tetrahedra only.

Like P2 defect, in just-irradiated samples P1 defect with *A*=93 mT is detected in 2743 glasses only (Figure IV-9). Its formation requires 3 BOs which are present in the only ultra-phosphate 2743 glass with the highest P content in our series.

Another doublet is detected in other irradiated glasses than 2743 and attributed to P3 defect because the hyperfine coupling constant *A* is lower than for P1 (Figure IV-10). It is characterized by *A*=73-81 mT in different glass compositions. The *A* parameter is higher in glasses with more P.

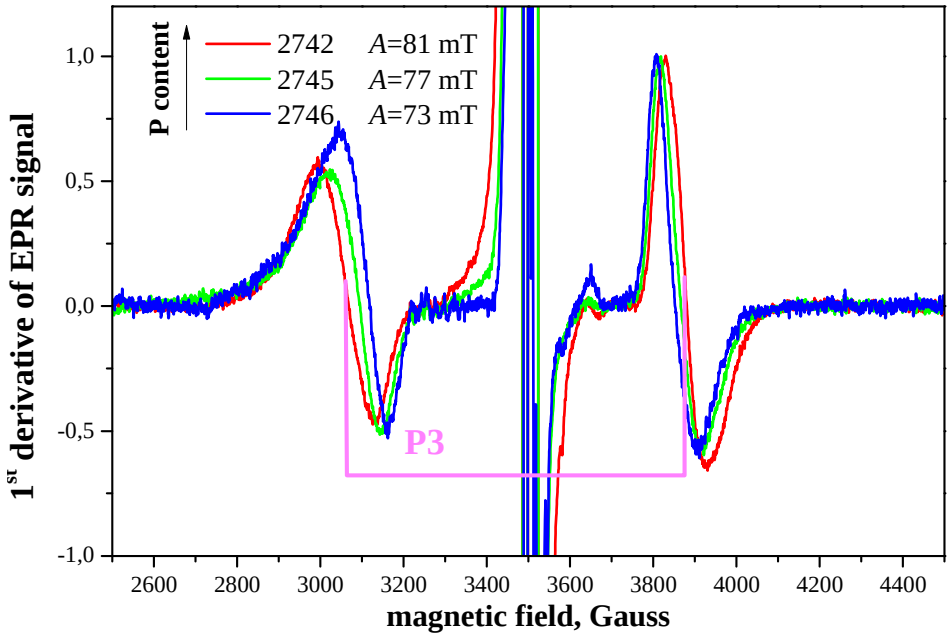


Figure IV-10. EPR spectra of e^--irradiated at 10^7 Gy phosphate glasses, stabilized samples

The information about P3 observation is poor. Weeks et al. in 1968 analyzed paramagnetic defects in phosphate glasses as a function of glass composition [10]. They showed the P3 formation in glasses with 38-50 mol. % of phosphorus. It is in agreement with our result because 2742, 2745 and 2746 glasses contain 40-50 mol. % of phosphorus.

D. Ehrt et al. [7] showed the EPR spectra of paramagnetic point defects in X-ray irradiated Tb-doped fluoride phosphate (10 mol. % of $Sr(PO_3)_2$ and 90 mol. % of fluorides), strontium-metaphosphate (SMP) and ultraphosphate (UP) glasses. In all three glasses the observed doublet was assigned to P1 defect. We suppose that in the only fluoride phosphate glass the resonance with *A*=68 mT could be attributed to P3 defect. In this work, however, we assign the doublet of *A*=73-81 mT in our glasses to P3 defect.

3. b. Relaxation of paramagnetic defects

3. b. 1 Relaxation of hole centers

The number of r-POHC defect decreases in time after irradiation. Moreover, it seems that the relaxation rate of r-POHC defect is quicker than other defects from this region because its relative intensity decreases (Figure IV-11).

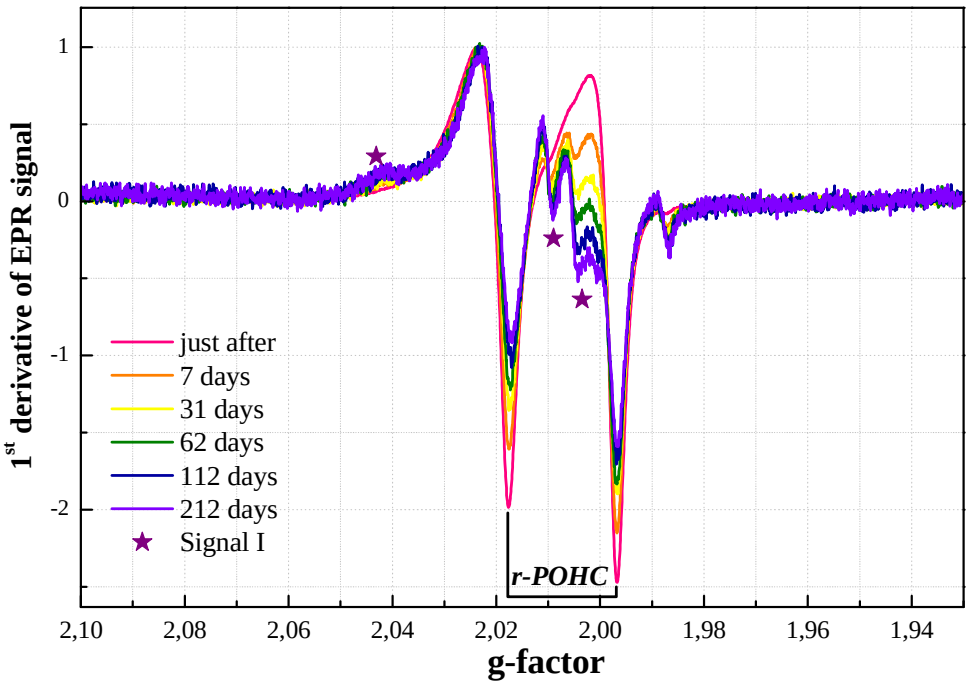


Figure IV-11. EPR spectra of e-irradiated at 10^5 Gy 2746 glass, Signal I marked with stars

A signal is more clearly visible within time (marked with stars) (Figure IV-11). It is attributed to Signal I. Its relative intensity increases within time after irradiation in all the phosphate glasses, but is the highest in 2746 glass with the lowest P content (Figure IV-11, stars).

One more signal is detected with EPR in irradiated phosphate glasses (Figure IV-12). Its g-parameters (g_1=2.02612, g_2=2.01592, g_3=2.00154) are similar to those of Signal II described by Berger's et al. [11] (g_1=2.0245, g_2=2.0124, g_3=2.0027). Its structure is associated with Peroxy radicals bonded to a phosphorus atom. The differences between Signal I and Signal II originate from different local environments of these defects [11]. Hereafter, we also use the label Signal II for it.

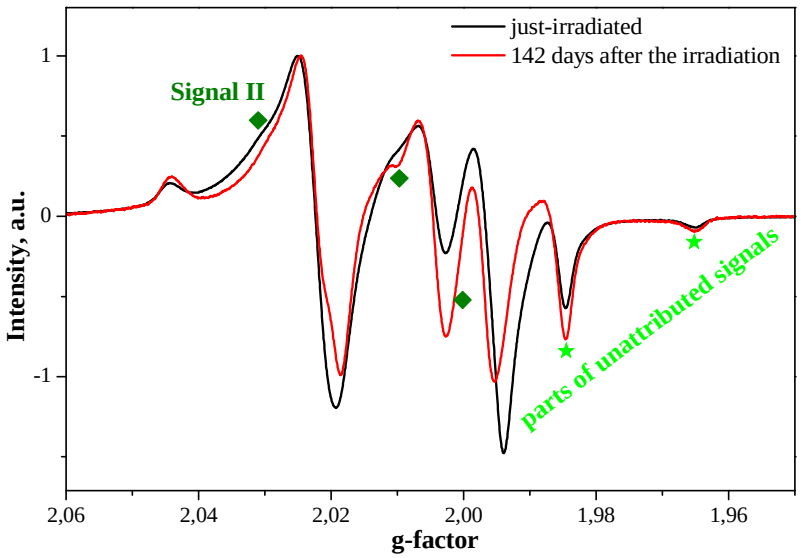


Figure IV-12. EPR spectra of e^--irradiated at 10^5 Gy 2743 glass, recorded in different dates

The Signal II marked with green rhombs in Figure IV-12 in just-irradiated samples is hardly visible, but can be easier observed after 142 days in ultra-phosphate 2743 glasses with the highest P content (Figure IV-12). In other glasses, the Signal II is even less intensive, but it can be seen during the annealing treatments (Appendix 3).

The signals observed in all our glasses and marked with green stars in Figure IV-12 are difficult to attribute. One attribution was proposed thanks to Q-band EPR analysis executed in collaboration with F. Trompier (IRSN, Fontenay-aux-Roses) (Figure IV-13). We suggest that one component of these signals at g=1.96-1.99 (Figure IV-12) corresponds to ^{55}Mn (II) impurity in the glasses.

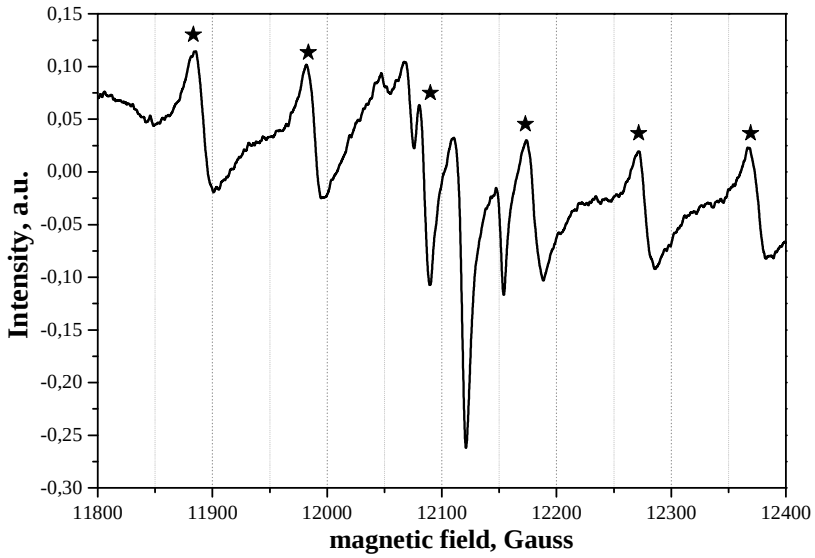


Figure IV-13. Q-band EPR spectrum of γ-irradiated at 150 Gy 2743 glass

We observe a signal including a hyperfine structure. Since the nuclear spin of ^{55}Mn is I=$^{5}/_{2}$, one should expect 6 transitions. Five of them with *A*=98 mT are clearly seen, the last one is superposed with POHC defect signal. The g-value (g=2.0075) that is close to g=2.0000 could correspond to ^{55}Mn (II) impurity.

The total number of hole centers can be estimated via double integration of EPR signal (see Chapter II, section 3.b.2 and Chapter III, section 2.c). In 2742-2745-2746 glasses it concerns essentially r-POHC defects. In 2743 glass the result is impacted by Signal I presence. That is why we compare the relaxation rates of r-POHC defects in 2742-2745-2746 glasses without 2743 sample (Figure IV-14).

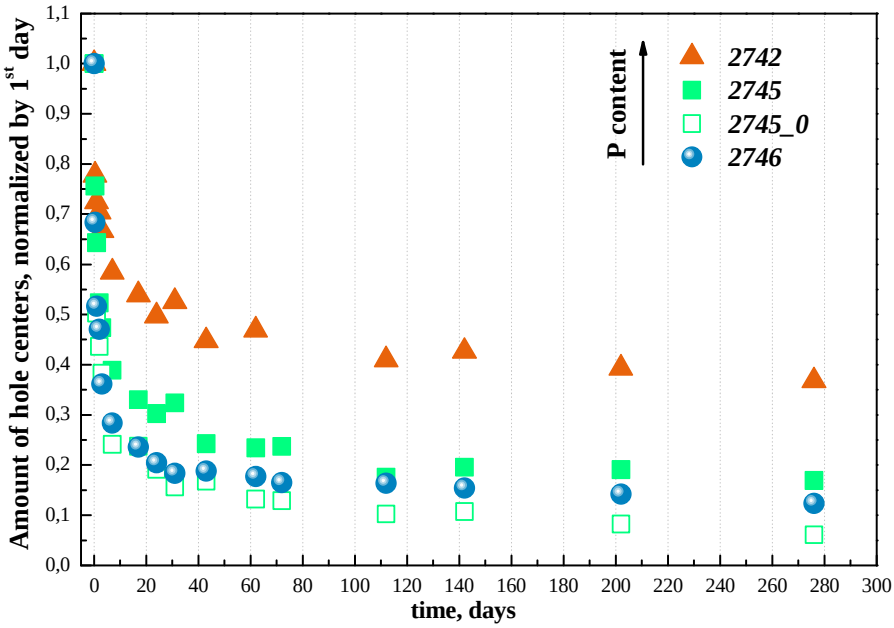


Figure IV-14. Relaxation curves of hole centers in e^{-}-irradiated with 10^5 Gy phosphate glasses, normalization at the 1st day

The relaxation of r-POHC defects is strong the first week, same result was observed for the hole centers in AS glasses (Chapter III, section 2.c.1).

One can see that the relaxation rate is the quickest in glass with less P content (2746). We assume that in more depolymerized glasses the r-POHC recovery is quicker.

Concerning Yb-free 2745 glass, presence of Yb inhibits the relaxation of hole centers. This effect could be assigned to Yb cluster presence because no difference in relaxation rates is observed between 2743 and 2743_0 glasses where there is no Yb cluster (Figure IV-15).

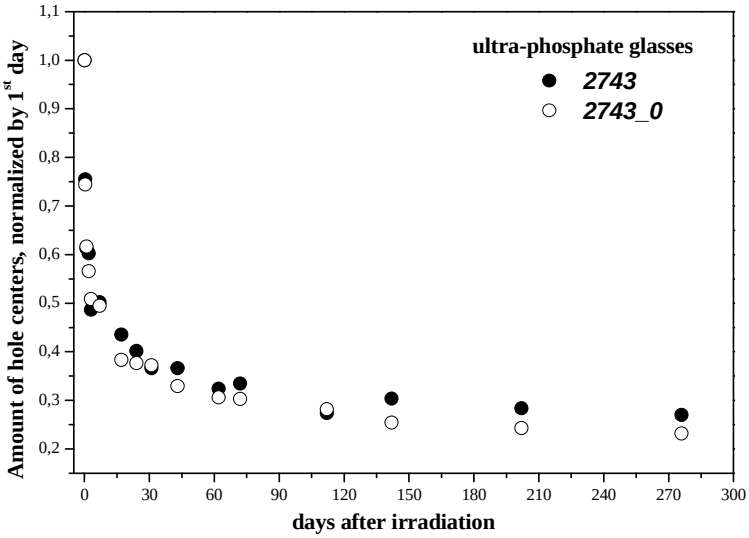


Figure IV-15. Relaxation curves of hole centers in e^--irradiated with 10^5 Gy 2743 glasses, normalization at the 1st day

Similar influence of Yb cluster on paramagnetic defects recovery within time has been already demonstrated for Yb-doped aluminosilicate glasses in Chapter III.

3. b. 2 Relaxation of P centers

In the only ultra-phosphate 2743 glass the content of P2 defects decreases crucially with time after irradiation (Figure IV-16). 1 month after irradiation only ~35% of initial amount of P2 defects is detected in Yb-free glass and ~25% in Yb-doped glasses irradiated at 10^5 Gy by 2.5 MeV electrons.

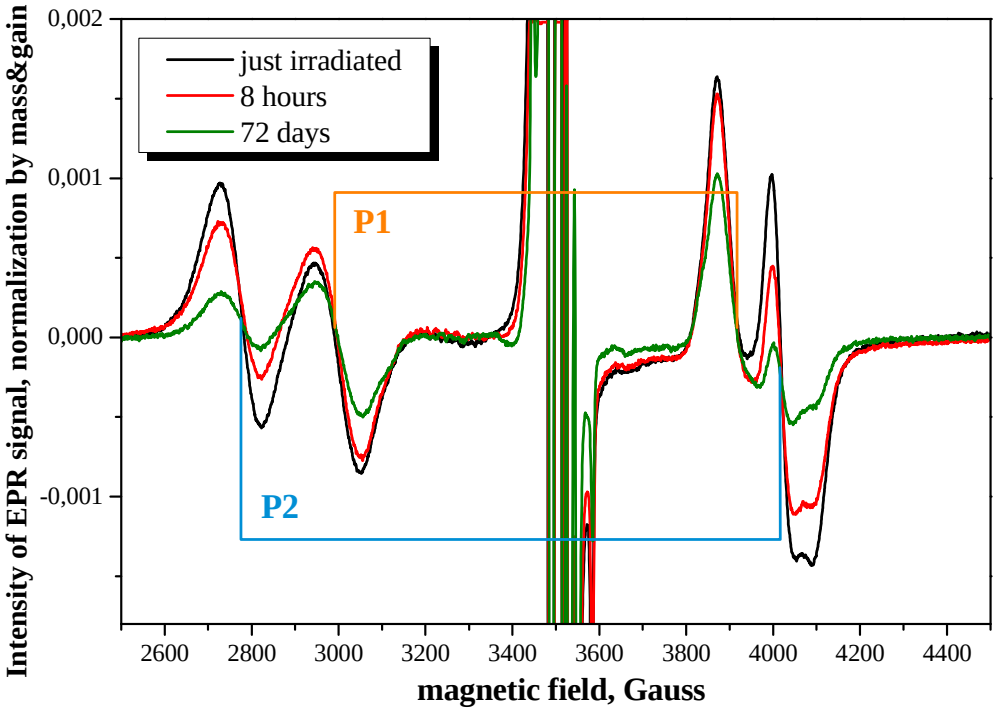


Figure IV-16. EPR spectra of e-irradiated at 10^5 Gy 2743 glasses

The recovery of P1 defects is slower than P2 defects.

3. c. Dose and dose rate effect

3. c. 1 Dose effect

r-POHC

The effect of irradiation dose on r-POHC together with Signal I and Signal II is the best seen in 2743 glasses (with the highest P content) (Figure IV-17), but similar tendency is observed for the other glasses, too.

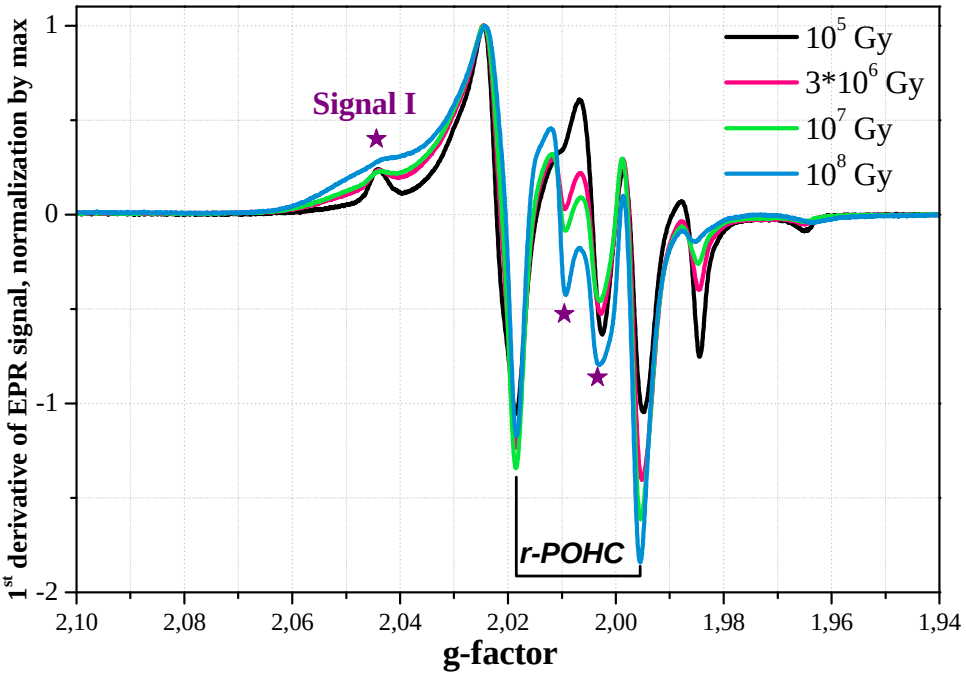


Figure IV-17. EPR spectra of e^--irradiated 2743 glasses, 1 month after the irradiation

The intensity of Signal I (Peroxy I) increases efficiently at 10^8 Gy (Figure IV-17). In parallel with that, we observe the slight decrease of r-POHC defects formation Figure IV-18. It can be associated with saturation of r-POHC defects with further formation of Peroxy I. This situation can be illustrated by r-POHC dependence vs. lg(dose) (Figure IV-18).

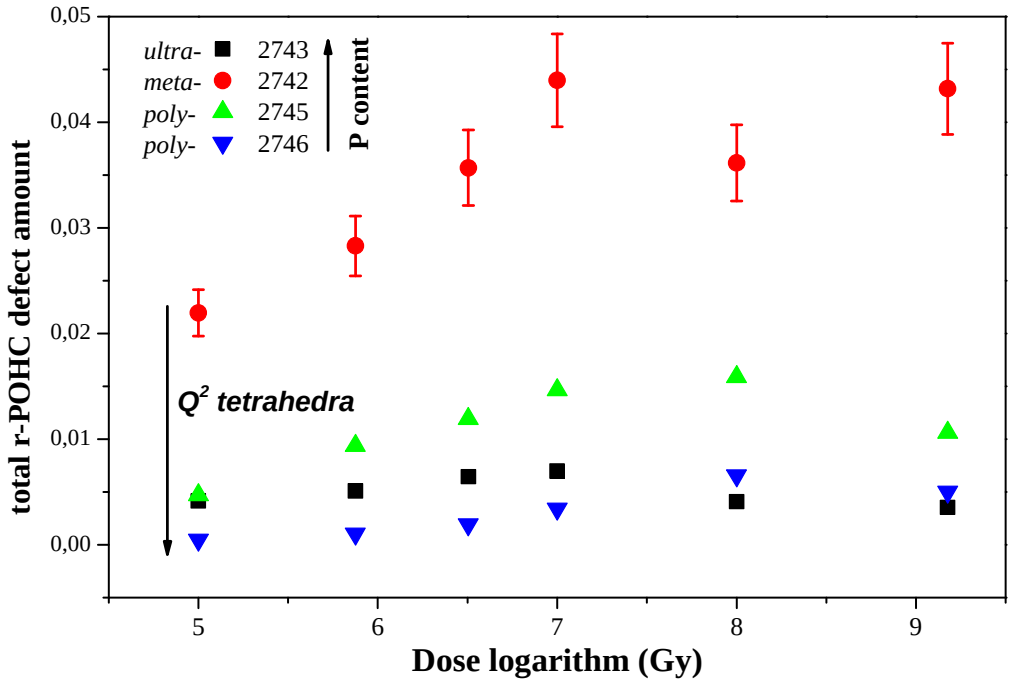


Figure IV-18. Total amount of r-POHC defects in e^--irradiated phosphate glasses

Within irradiation lg(dose) increase the number of induced r-POHC defects increases linearly up to 10^7 Gy (Figure IV-18), the most intensively in meta-phosphate 2742 glass. In 2743 and 2746 glasses the defects' amount variation is lower. We remind here that in 2742 glass the molar fraction of Q^2 tetrahedra is the highest. The slope of r-POHC amount vs. lg(dose) is in correlation with Q^2 tetrahedra content. At strong doses (>10^7 Gy) one can observe a saturation of r-POHC. The saturation is observed together with an enhancement of Peroxy I defect.

Our results are in agreement with Griscom [6] where in 10^5-10^7 Gy dose range the POHC defect amount increased. There is no information in literature up to now on P-related defects behavior under irradiation doses ≥10^8 Gy.

The EPR spectra of stabilized 2743 glasses irradiated in vast dose range are given in Figure IV-19. The EPR spectra are different from those in Figure IV-17 which are recorded 1 month after irradiation.

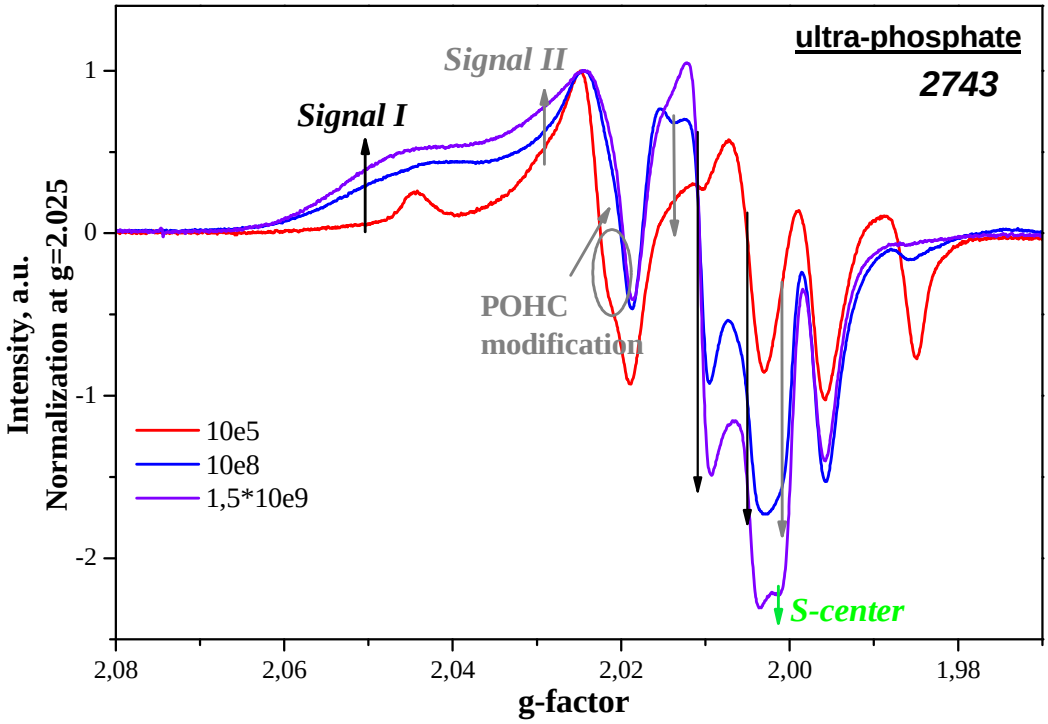


Figure IV-19. EPR spectra of e^--irradiated stabilized 2743 glasses

One can see some modifications of r-POHC signal within irradiation dose (Figure IV-19). They are more expressive at $1.5 \cdot 10^9$ Gy. It implies some symmetry modifications of r-POHC under irradiation with strong doses linked to the motions of alkaline ions in glasses.

The evolution of Signal II within irradiation dose is too complex due to the weak intensity and superposition of other defects. Its precise investigation requires thus the simulation study.

In ultra-phosphate 2743 glass with the highest P content an isotropic resonance at g=2.00389 called "S center" appears under irradiation at strong doses such as $1.5 \cdot 10^9$ Gy (Figure IV-19). It is best seen via annealing treatments (see Appendix 3). It appears once the recovery of all the other defects has been already completed.

Griscom et al. associated the S center with silicon rather than with phosphorus [6] because of isotropic character and absence of any superhyperfine structure. However, according to microprobe analysis, there is no silicon in our studied Yb-doped phosphate glasses. We assume thus that this S center cannot be related to silicon in our case. This signature is not assigned at this stage of the study.

P centers

The EPR spectra of P defects recorded in vast irradiation dose range of e^--irradiated ultra-phosphate 2743 glasses are presented in Figure IV-20.

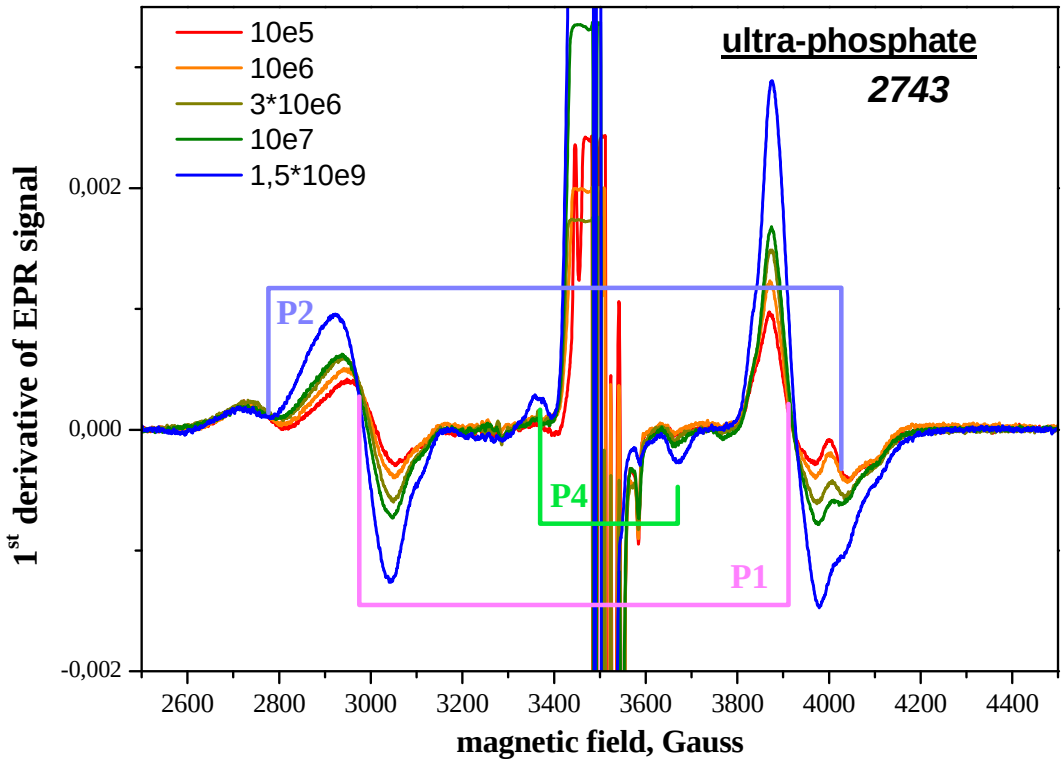


Figure IV-20. EPR spectra of e^--irradiated 2743 glasses

With irradiation dose increasing, we see that the intensity of EPR signal corresponding to each P defects evolves separately (Figure IV-20). We observe first a decrease of P2 defects' content from $3 \cdot 10^6$ Gy. It is in agreement with Griscom who rather mentioned a saturation effect for P2 defect [6].

The intensities of P1 doublet do not vary seriously in 10^5-10^8 Gy dose range (Figure IV-20), but at strong dose $1.5 \cdot 10^9$ Gy its intensity enhances 2 times.

One can see the presence of P4 defect (A=30.5 mT) in 2743 glass irradiated with strong dose $1{,}5 \cdot 10^9$ Gy (Figure IV-20).

It is remarkable that P4 defects are seen together with P1 and P2 defects in 2743 glass (with the highest P content). Griscom et al. supposed some structural linkages between these three types of defects [6]. In particular, P1 and P4 defects have the same precursor $[:PO_3]^0$ which is transformed into P1 via hole trapping or into P4 via electron trapping [6]. This interpretation seems to be confirmed by the high dose behavior. We assume that, via breaking of P=O bondings in four-fold PO4 tetrahedra, more PO3 structural elements are created leading to the formation of P1 and P4 defects. As it has been already demonstrated in section 1.b, double bondings P=O are present in only ultra-phosphate glass 2743.

For meta-phosphate 2742 glass, we observe an increase of P3 defects within irradiation dose. However, the shape of EPR spectra evolves, too. These spectra normalized at g=1.884 are displayed in Figure IV-21.

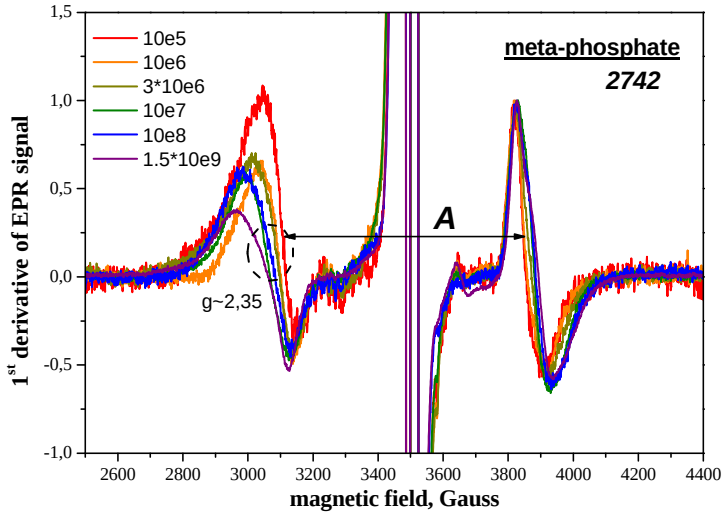


Figure IV-21. EPR spectra of e⁻-irradiated 2742 glasses, normalization at g=1.844

We observe an increase of the hyperfine structure parameter *A* from 74 mT in 10^5 Gy to 84 mT in $1.5 \cdot 10^9$ Gy (Figure IV-21). It can be noticed that the shape is asymmetrically modified with dose around g=2.35. This asymmetric variation indicates the presence of another defect. It could correspond to a modification of P3 defect or to P1 defect which exhibits close positions of its doublet to P3 defect. It is difficult now to give the right answer without proper simulations.

It is worth to notice here that further decrease of P content in poly-phosphate 2745 and 2746 glasses decreases asymmetrical modifications of P3 signal (Figure IV-22). No other defects are supposed to be formed with irradiation dose variation. The dose effect in poly-phosphate glasses is displayed in Figure IV-22.

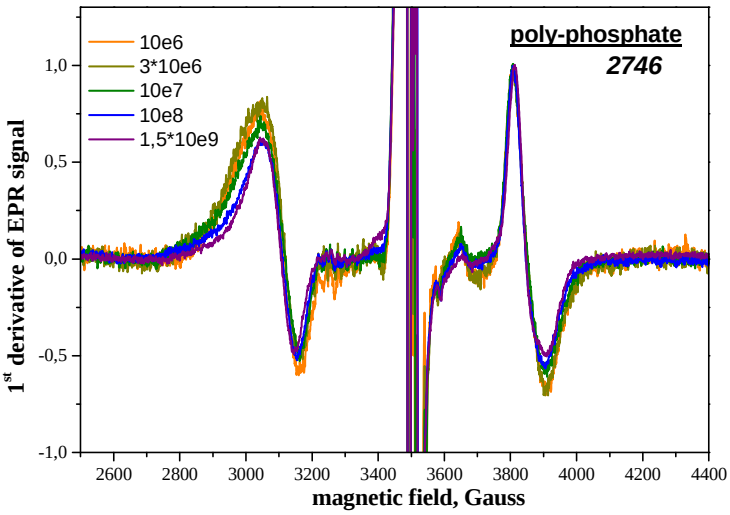


Figure IV-22. EPR spectra of e⁻-irradiated 2746 glasses, normalization at g=1.884

3. c. 2 *Dose rate effect*

The comparison between electron- and gamma-irradiations recorded at two different dates is presented on ultra-phosphate 2743 glass in Figure IV-23.

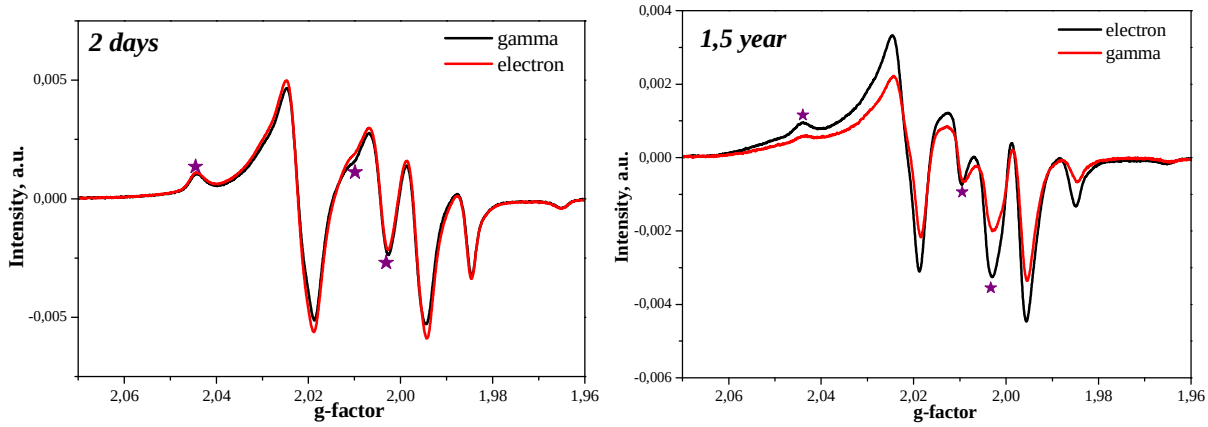


Figure IV-23. EPR spectra of irradiated at 3·10⁶ Gy 2743 glasses, 2 days and 1.5 year after the irradiation

One can see no dose rate effect 2 days after irradiation (Figure IV-23, left). In stabilized samples (Figure IV-23, right) the amount of Signal I is higher in electron-irradiated sample. Such a difference indicates rather different relaxation rates in these samples; in case of e^--irradiation this defect is more stable. The similar tendency is seen for all the other phosphate glasses.

Concerning P centers, the situation is identical whatever P-center and glass. No difference is seen 2 days after irradiation. Whereas in stabilized γ-irradiated glasses the signal is less intensive. It indicates a slower relaxation of all paramagnetic defects in e^--irradiated Yb-doped phosphate glasses.

So, the dose rate impacts more the relaxation rate of the defects than its formation.

Finally, the information on POHC defects and P centers is summarized in Table IV-4 and Table IV-5, respectively.

The g-parameters of all the defects in 3350-3650 Gauss region discussed in this Chapter IV, their attribution are sum up in Table IV-4.

defect	g-values		glass	dose, Gy
r-POHC	g_1	2.0096	all	
Signal I – Peroxy I	g_1	2.0441	2743 – just after irradiation 2742-2745-2746 – in time	
	g_2	2.0100		
	g_3	2.0045		
S center	g_{iso}	2.0039	with T	10^8 - $1{,}5 \cdot 10^9$; 2743
Signal II – Peroxy II	g_1	2.0261	2743 – with T and dose 2745 – with T	
	g_2	2.0159		
	g_3	2.0015		
^{55}Mn, unattributed	g	1.9845	all	
	g	1.9647		$<10^8$; 2743

Table IV-4. The summary of paramagnetic defects recorded in 3450-3550 Gauss in irradiated phosphate glasses

Precise determination of Peroxy I and Peroxy II structures requires a rigorous simulation study. To attribute properly S center, the simulations are essential, too.

The basic characteristics of discussed above P -centers are sum up in Table IV-5.

defect	structure	glass	*A*, Gauss	annealing T	doses, Gy
P1	PO_3^{2-}	2743-2742/ less in 2745-2746	910	323°C	10^5-$1.5*10^9$
P2	PO_4^{4-}	2743	1257	224°C	10^5-$1.5*10^9$
P3	?	2742-2745-2746	740	>425°C	10^5-$1.5*10^9$
P4	PO_2^{2-}	2743	305	394°C	$>10^8$

Table IV-5. The characteristics of P centers in Yb-doped phosphate glasses

- **r-POHC defects formation is controlled by Q^2 tetrahedra quantity. Its influence is followed in r-POHC relaxation in time and its variation with dose.**
- **Due to Yb cluster presence the relaxation of r-POHC is inhibited as well.**
- **Two types of P-related Peroxy radicals are observed in phosphate glasses: Peroxy I and Peroxy II. Their relaxation is slower than for r-POHC. In consequence, its signal becomes better seen within time.**
- **The saturation of r-POHC defects is observed at strong doses. However, with an increase of the intensity of Signal I at doses $>10^8$ Gy, we suggest a competitive character between r-POHC and Peroxy I formation.**
- **P1, P2 and P4 defects are observed in ultra-phosphate 2743 glass with presence of PO_4 tetrahedra. Its formation requires 4-coordinated P atom for P2 and 3-coordinated P atom for P1 and P4 defects.**
- **At strong doses, enhancement of P1 and P4 signals is linked with possible breaking of P=O bondings in ultra-phosphate glass leading to the common precursor.**
- **P3 defect is observed in 2742-2745-2746 glasses with P content less than 50 mol. %.**
- **A new isotropic signal of S-center is detected at g=2.0039. Contrary to Griscom, we cannot assign it to silicon presence.**
- **No dose rate effect is detected on any defect formation in any glass. However, in e^--irradiated glasses paramagnetic defects relax slower than in γ-irradiated.**

4. Diamagnetic defect

A diamagnetic defect has been registered in phosphate glasses. Contrary to paramagnetic defects, this one is detected also in non-irradiated glasses.

4. a. Attribution of the defect

This defect gives an emission band at 425 nm under 266 nm laser excitation at room temperature. Its lifetime is estimated at 5-6 ms.

The emission spectra of non-irradiated samples are displayed in Figure IV-24.

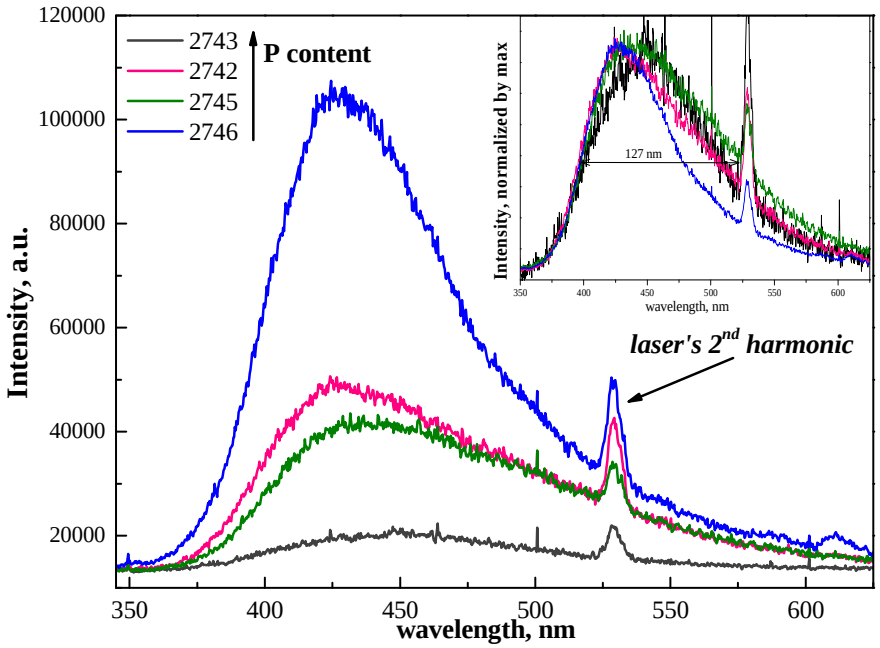


Figure IV-24. Emission spectra of diamagnetic defect in non-irradiated phosphate glasses, λ_{ex}=266 nm; normalization at the maximum in inset

The emission intensity increases in 2743-2742-2745-2746 glasses raw where the glass depolymerization increases (Figure IV-24). The content of this diamagnetic defect is higher for less polymerized glasses. Together with increasing of the emission intensity, the FWHM decreases from 127 nm in 2743 glass to 78 nm in 2746 (Figure IV-24). It is associated with a shift of the maximum position from 450 nm in 2743 to 425 nm in 2746 glasses.

The emission band position and the associated lifetime allow us to attribute this defect to four-folded $[PO_4]^+$ defect reported by Origlio et al. [2] in P-doped silica.

One can suspect the presence of another emission at 500 nm (Figure IV-24, inset). Its lifetime is estimated ~0.5 ms. This band is not seen in irradiated glasses. Hereafter, our attention will be concentrated on the first mentioned P-related diamagnetic defect.

4. b. The diamagnetic defect in irradiated phosphate glasses

The emission spectra of irradiated 2745 glasses at the same 10^6 Gy dose are shown in Figure IV-25.

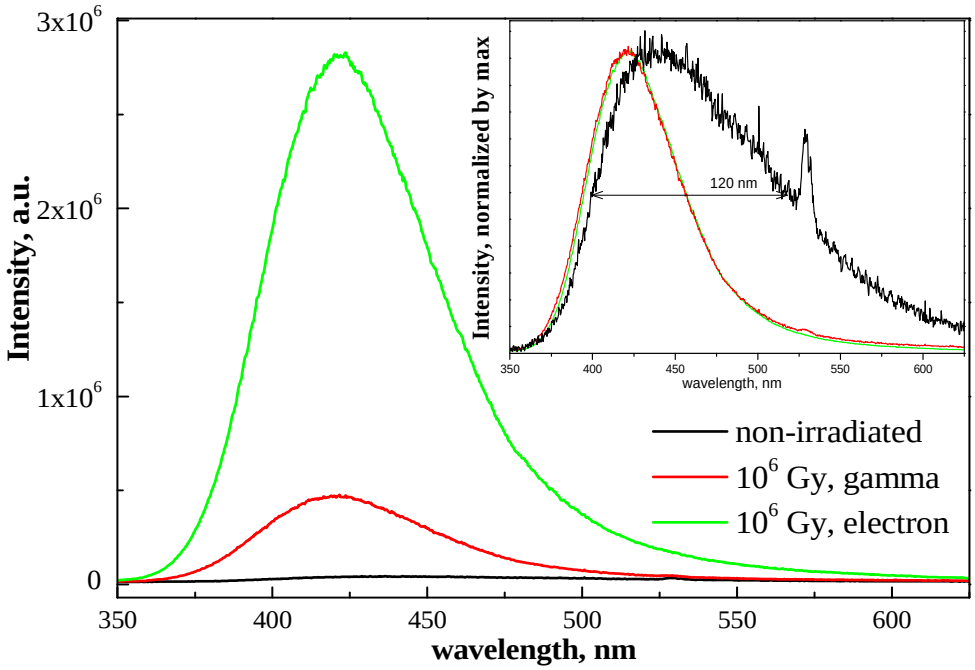


Figure IV-25. The emission spectra of irradiated at 10^6 Gy 2745 glasses, normalization at the maximum in inset

The comparison with non-irradiated sample reveals the strong enhancement of diamagnetic defect's content under ionizing irradiation (Figure IV-25). The lifetime decreases under irradiation to 4-5 ms.

Moreover, one can see the serious impact of dose rate: under e^--irradiation more diamagnetic defects are induced. The FWHM decreases twice under irradiation, without dose rate effect on it (Figure IV-25, inset). It can be attributed to the absence of the emission at 500 nm in irradiated samples.

Comparison of e^--irradiated glasses at the same 10^6 Gy dose is shown in Figure IV-26. The enhancement of emission is the most expressive in poly-phosphate 2746 glass.

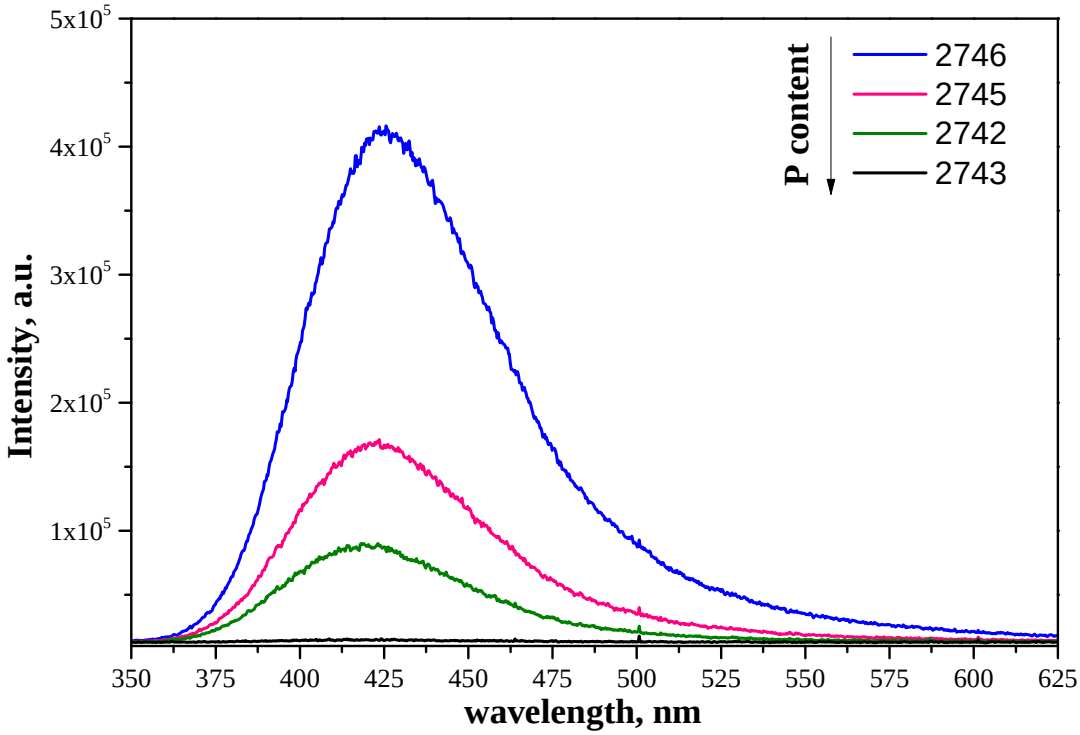


Figure IV-26. The emission spectra of e^--irradiated phosphate glasses compared with pristine glasses, dose 10^6 Gy

The increase of 425 nm emission is higher in irradiated glasses with less phosphorus content. It follows the same variation with P content that in non-irradiated samples (Figure IV-24).

In [2] the authors proposed the following scenario of structural transformations under the irradiation (Figure IV-27): the diamagnetic defect would be formed from the P=O ionization giving rise to $(PO_4)^+$ defect that leads to POHC and P2 defects.

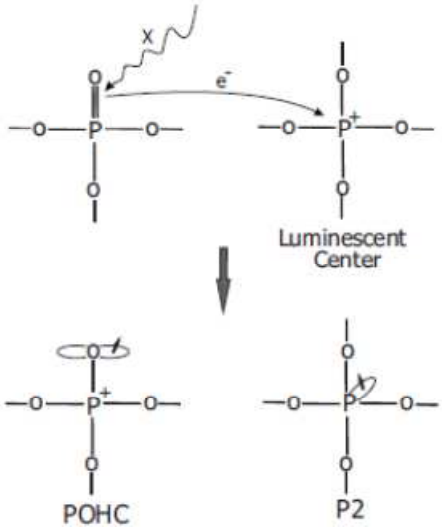


Figure IV-27. The scheme of diamagnetic center formation and its consequent transformation [2]

In the case of our phosphate glasses, the diamagnetic center is detected even in glasses without P=O bonding (2742, 2745, 2746). Moreover, this defect created under irradiation, is in higher quantity in glasses with less P, when there are no P=O bonding. We assume thus the possibility of other precursor type for this diamagnetic defect in phosphate glasses.

Moreover, r-POHC defect is observed in all the glasses contrary to P2 defect which is seen in 2743 glass only, with P=O bondings. So, Origlio's model is not fully reproduced in our phosphate glasses. Another structure than $P(-O)_4$ exists as a possible link between diamagnetic and r-POHC defects.

- **The diamagnetic defect formation does not require the presence of P=O bondings. Moreover, its formation is favored under irradiation in glasses with less P content.**

5. The lifetime of $^2F_{5/2}$ excited state evolution under e^--irradiation

As in case of irradiated Yb-doped aluminosilicate glasses, the lifetime of $^2F_{5/2}$ excited state measurements have been carried out for different doses. The experimental details can be consulted in Chapter III, section 3.b. In non-irradiated glasses the values are the following: 0.73 ms (2743 glass), 0.84 ms (2742 glass), 1.22 ms (2745 glass) and 1.34 ms (2746 glass). It decreases with glass polymerization. One of the reasons can be a higher hygroscopic character of the glasses with more P. The absorption of water from the air leads to non-radiative energy transfer via OH^- groups resulting in shorter lifetimes τ_{IR}.

5. a. Dose and dose rate effect

The lifetimes τ_{IR} decrease slightly in all the phosphate glasses under the irradiation. The obtained values for stabilized samples are displayed as a function of lg(dose) in Figure IV-28.

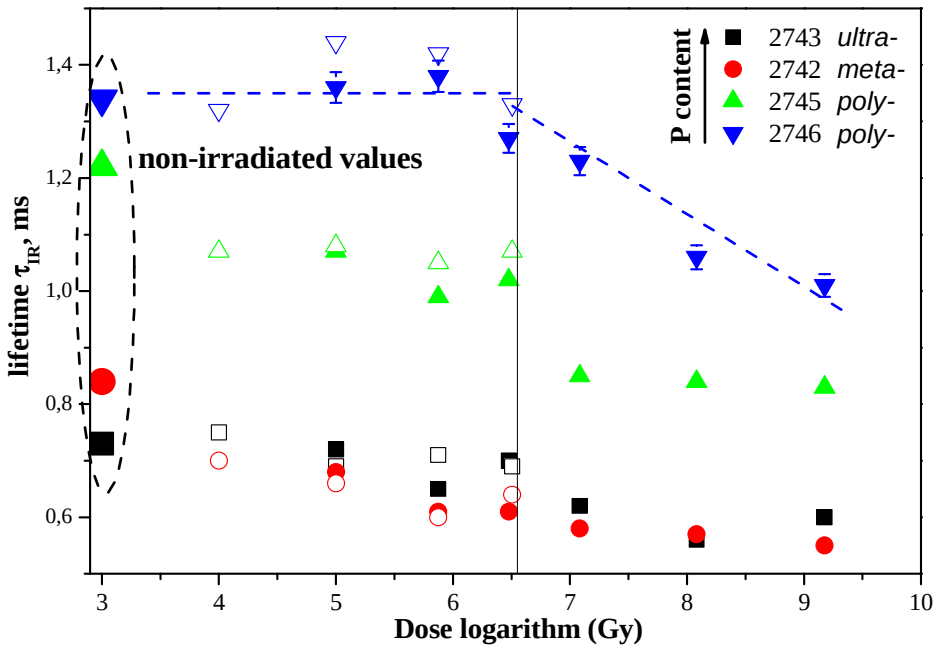


Figure IV-28. The lifetimes τ_{IR} in e^--irradiated phosphate glasses, empty symbols – γ-irradiation, full symbols - e^--irradiation

In 2746 and almost 2745 glass series two regimes are observed: below and above $3.2 \cdot 10^6$ Gy irradiation dose. In 2742 and 2743 glass series there is only one linear regime with slight decrease of the lifetime.

In aluminosilicate glasses 2-regime lifetime dependence vs. lg(dose) is observed in glasses with less Yb clusters. This is not the case for the phosphate glasses. The Yb pairs content in phosphate glasses can be characterized by cooperative luminescence of Yb^{3+}, (Figure IV-29).

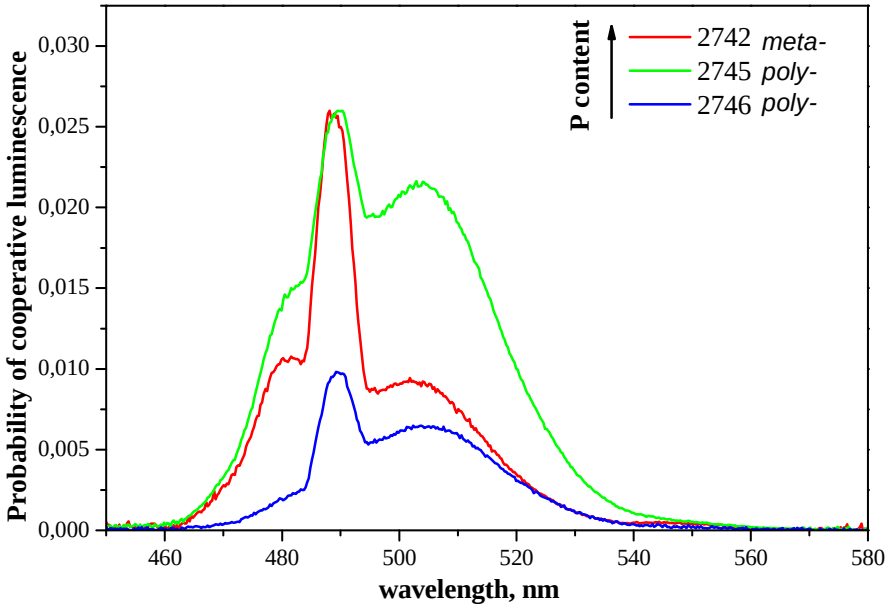


Figure IV-29. The probability of cooperative emission in non-irradiated phosphate glasses

The lowest cooperative emission probability is seen in 2746 glass where 2-regime lifetime curve is detected. The second glass series with 2-regime curve are 2745 glasses. The cooperative emission probability in this glass is the highest but is still low (probability <0.030). Its probability is close to AS23 (0.020) glass with low amount of Yb cluster.

Taking into account that in all phosphate glasses the probability of cooperative emission is low, one should expect a 2-step curve of the lifetime τ_{IR} vs. lg(dose). Such behavior is the most expressive in 2746 glass with the lowest probability of cooperative emission. The decrease of the lifetime τ_{IR} begins at $3 \cdot 10^6$ Gy that could correspond to a particular defect presence. However, in aluminosilicate (Chapter III, section 3.b.2) and in ABS glasses [13] the decrease begins at the same dose. Therefore, this effect cannot be attributed to point defects because of different chemical compositions of glasses. We assign this effect to Yb cluster influence. Indeed, the 2-step curve is observed for glasses with low Yb cluster content.

In phosphate glasses Yb cluster content is significantly lower in all 4 compositions than in AS glasses. Nevertheless, only 2 of them (poly-phosphates 2745 and 2746) exhibit 2-regime curve. Another 2 glasses (2743 and 2742) with linear decrease of the lifetime τ_{IR} have higher content of phosphorus. It implies that 2743

glasses are more hygroscopic than the others as it has been noticed at the beginning of this section. In particular, it leads to a shortening of the lifetime τ_{IR} values. This effect makes difficult the analysis of the lifetime τ_{IR} behavior within irradiation dose in phosphate glasses.

5. b. Relation with point defects

5. b. 1 Evolution in time

The only phosphate glass composition, for which the lifetime evolution within time has been followed for 2 doses, is 2745 glass. The lifetime τ_{IR} of excited $^2F_{5/2}$ energy state of Yb^{3+} ion increases in time after the irradiation (Figure IV-30).

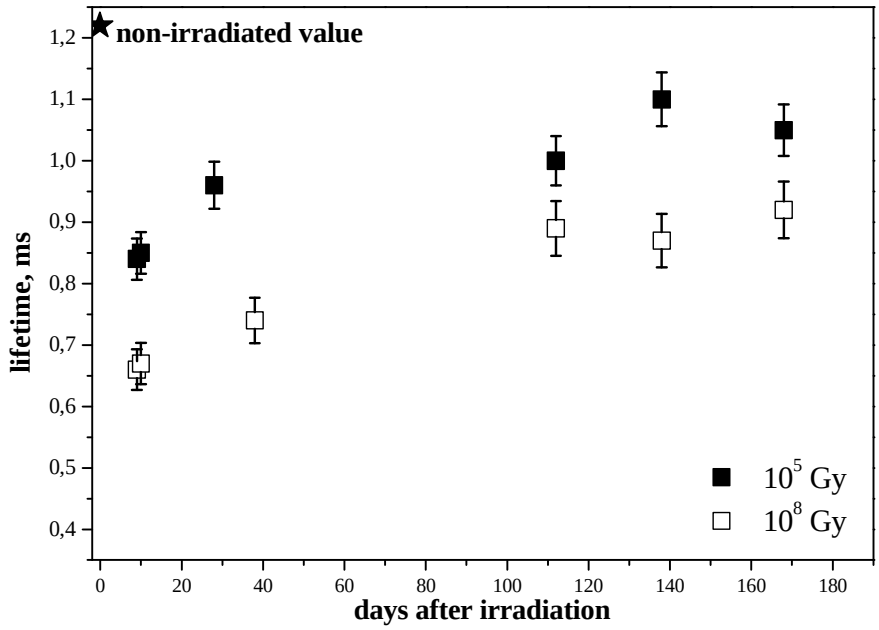


Figure IV-30. The lifetime τ_{IR} evolution in time in e^--irradiated 2745 glasses

In 2745 glass irradiated at 10^5 Gy, the lifetime τ_{IR} is close (1.09 ms) to its pre-irradiation value after 140 days followed the irradiation. In 2745 glass irradiated with 10^8 Gy the lifetime τ_{IR} is not recovered. We should remind here the enhancement of Peroxy I in phosphate glasses at 10^8 Gy. So, Peroxy radicals could be responsible for the non-reversibility of the lifetime τ_{IR}.

5. b. 2 Relation between the diamagnetic defects and the $^2F_{5/2}$ lifetime

The diamagnetic defect number decreases logically, as for paramagnetic defects, within time after the irradiation (Figure IV-31).

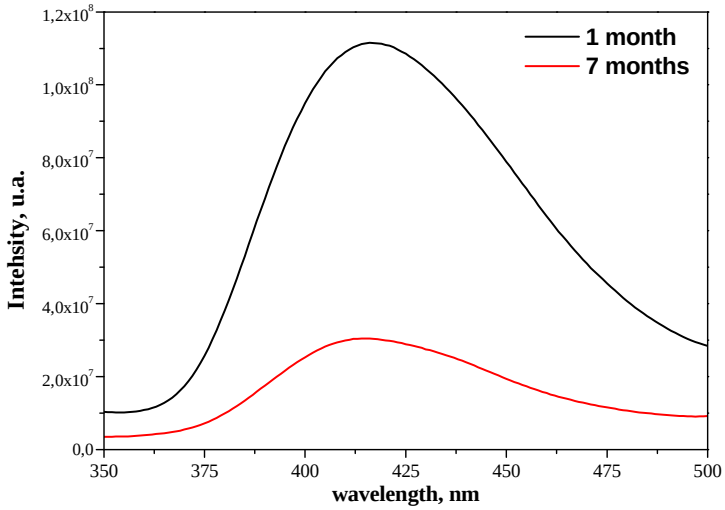


Figure IV-31. The emission band of diamagnetic defect in e^--irradiated at 10^5 Gy 2745 glass, lamp excitation at 266 nm

It is interesting that in parallel with defects amount decrease, the lifetime τ_{IR} increases slowly after the irradiation. It illustrates the influence of point defects on the lifetime τ_{IR} evolution.

We performed some thermal annealing treatments on 2743_10e8 and 2745_10e8 glasses in order to make easier the attribution of paramagnetic point defects, to investigate its thermal stability and to look for any correlation between defects formation/relaxation and Yb^{3+} lifetime τ_{IR}. The detailed description of these annealing treatments can be consulted in Appendix 3.

During the annealing treatments of 2745_10e8 glass, the emission at 400 nm has been registered as well. The corresponding spectra are presented in Figure IV-32.

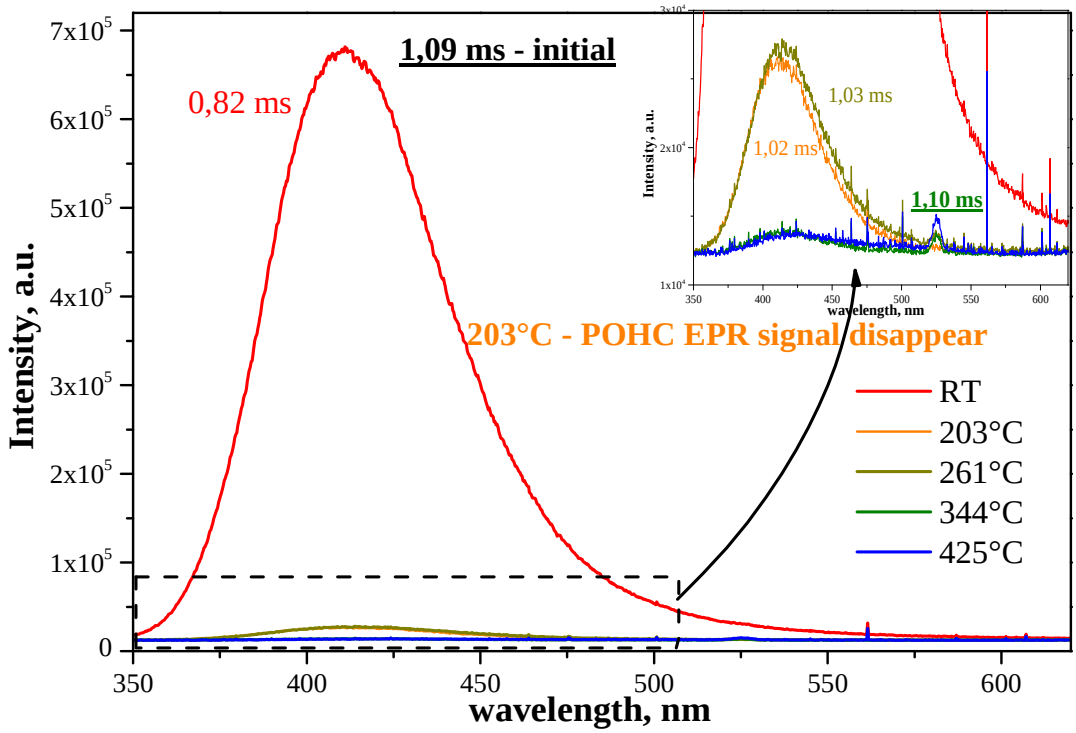


Figure IV-32. The emission of the diamagnetic defect under 266 nm laser excitation in 2745_10e8 glass during the isochronal annealing treatments, zoom on low intensities is inset

The crucial decrease of emission intensity at 400 nm is observed after 203°C annealing (Figure IV-32). In parallel, the r-POHC defects have been recovered and the lifetime τ_{IR} is closely back to its pre-irradiation value. From this result one can confirm the structural links between the diamagnetic defect and r-POHC defects. The structural link between the diamagnetic defect and r-POHC is in agreement with Origlio's report [2]. Moreover, this defect or r-POHC participation in the lifetime τ_{IR} decrease under ionizing irradiation can be suspected. However, POHC defect displays 3 absorption bands at 325, 430 and 540 nm [7]. The last one could overlap with the Yb^{3+} absorption band (~900 nm). So, r-POHC defect is more credible than the diamagnetic defect to play a role in the τ_{IR} lifetime decrease.

- **The 2-regime curves of the lifetime τ_{IR} vs. lg(dose) are observed for phosphate glasses containing the lowest amount of Yb cluster.**
- **Structural link between r-POHC and the diamagnetic defect is confirmed.**
- **Peroxy radicals are supposed to play a role in the decreasing of the lifetime τ_{IR} within time and in particular in the non-reversibility at high dose**
- **POHC defects are supposed to have an impact on the lifetime τ_{IR} decrease under irradiation.**

6. Conclusions

In this Chapter IV we have characterized P-related point defects induced under e^-- and γ-irradiation in Yb-doped phosphate glasses. Our experimental results are quite in agreement with literature. However, some new results have been obtained.

We confirm the formation of 2 hole centers in phosphate glasses under ionizing irradiation labeled Signal I and Signal II (Peroxy I and Peroxy II) which structure is supposed to be close to Peroxy radicals. We report also P3 defect formation in less polymerized glasses.

Structural relations between the diamagnetic defects and r-POHC are confirmed. However, it has been demonstrated that P=O bondings are not necessary to form the diamagnetic defect in phosphate glasses.

We report also 2-regime curves of the lifetimes τ_{IR} vs. lg(dose) in phosphate glasses. The crucial influence of Yb cluster on this behavior is corroborated by poly-phosphate 2745 and 2746 glasses.

Concerning the influence of point defects on the lifetime τ_{IR} of $^2F_{5/2}$ excited state of Yb^{3+} ion, we suppose the impact of r-POHC defect.

[1] G. Liu et B. Jacquier, Spectroscopic Properties of Rare Earths in Optical Materials, New York: Springer Series in Materials Science, 2005.

[2] G. Origlio, F. Messina, M. Cannas, R. Boscaino, S. Girard, A. Boukenter et Y. Ouerdane, *Phys. Rev. B,* vol. 80, p. 205208, 2009.

[3] B. Schaudel, P. Goldner, M. Prassas et F. Auzel, *J. Alloys and Comp.,* vol. 300&301, p. 443, 2000.

[4] R. K. Brow, *J. Non-Cryst. Solids,* vol. 263&264, p. 1, 2000.

[5] C. Roiland, Ph.D. dissertation, Orléans: l'Université d'Orléans, 2007.

[6] D. L. Griscom, E. J. Friebele, K. J. Long et J. W. Fleming, *J. Appl. Phys.,* vol. 54, p. 3743, 1983.

[7] H. Ebendorff-Heidepriem et D. Ehrt, *Opt. Mater.,* vol. 18, p. 419, 2002.

[8] D. Möncke et D. Ehrt, *Opt. Mater.,* vol. 25, p. 425, 2004.

[9] M. Fanciulli, E. Bonera, S. Nokhrin et G. Pacchioni, *Phys. Rev. B,* vol. 74, p. 134102, 2006.

[10] R. A. Weeks et P. J. Bray, *Journ. Chem. Phys.,* vol. 48, p. 5, 1968.

[11] M. E. Archidi, M. Haddad, A. Nadiri, F. Benyaïch et R. Berger, *Nucl. Instr. and Meth. in Phys. Res. B,* vol. 116, p. 145, 1996.

[12] D. L. Griscom, C. I. Merzbacher, R. A. Weeks et R. A. Zuhr, *J. Non-Crust. Solids,* vol. 258, p. 34, 1999.

[13] N. Ollier, J.-L. Doulan, V. Pukhkaya, T. Charpentier, R. Moncorgé et S. Sen, *J. Non-Cryst. Solids,* vol. 357, p. 1037, 2011.

List of Figures

Figure IV-1 . PO^n polyhedra..... 99
Figure IV-2. Raman spectra of non-irradiated Yb-doped phosphate glasses 100
Figure IV-3. The structure of r-POHC defect [2]..... 102
Figure IV-4. The structure of l-POHC defect [6] 103
Figure IV-5. The structure of P1 defect [4]..... 103
Figure IV-6. The structure of P2 defect [6]..... 104
Figure IV-7. The structure of P4 defect [6]..... 104
Figure IV-8. EPR spectra of just-irradiated phosphate glasses, e^--irradiation, dose 10^5 Gy. Normalization by mass&gain is in inset 105
Figure IV-9. EPR spectrum of just-irradiated with electrons at 10^5 Gy 2743 glass... 107
Figure IV-10. EPR spectra of e^--irradiated at 10^7 Gy phosphate glasses, stabilized samples 107
Figure IV-11. EPR spectra of e-irradiated at 10^5 Gy 2746 glass, Signal I marked with stars 108
Figure IV-12. EPR spectra of e^--irradiated at 10^5 Gy 2743 glass, recorded in different dates..... 109
Figure IV-13. Q-band EPR spectrum of γ-irradiated at 150 Gy 2743 glass..... 110
Figure IV-14. Relaxation curves of hole centers in e^--irradiated with 10^5 Gy phosphate glasses, normalization at the 1st day 110
Figure IV-15. Relaxation curves of hole centers in e^--irradated with 10^5 Gy 2743 glasses, normalization at the 1st day 111
Figure IV-16. EPR spectra of e-irradiated at 10^5 Gy 2743 glasses..... 112
Figure IV-17. EPR spectra of e^--irradiated 2743 glasses, 1 month after the irradiation 113
Figure IV-18. Total amount of r-POHC defects in e^--irradiated phosphate glasses .. 114
Figure IV-19. EPR spectra of e^--irradiated stabilized 2743 glasses..... 115
Figure IV-20. EPR spectra of e^--irradiated 2743 glasses..... 116
Figure IV-21. EPR spectra of e^--irradiated 2742 glasses, normalization at g=1.844. 117
Figure IV-22. EPR spectra of e^--irradiated 2746 glasses, normalization at g=1.884. 117
Figure IV-23. EPR spectra of irradiated at $3 \cdot 10^6$ Gy 2743 glasses, 2 days and 1.5 year after the irradiation..... 118
Figure IV-24. Emission spectra of diamagnetic defect in non-irradiated phosphate glasses, λ_{ex}=266 nm; normalization at the maximum is inset 121
Figure IV-25. The emission spectra of irradiated at 10^6 Gy 2745 glasses, normalization at the maximum is inset 122

Figure IV-26. The emission spectra of e^--irradiated phosphate glasses compared with pristine glasses, dose 10^6 Gy 123
Figure IV-27. The scheme of diamagnetic center formation and its consequent transformation [1] 123
Figure IV-28. The lifetimes τ_{IR} in e^--irradiated phosphate glasses, empty symbols – γ-irradiation, full symbols - e^--irradiation 125
Figure IV-29. The probability of cooperative emission in non-irradiated phosphate glasses 126
Figure IV-30. The lifetime τ_{IR} evolution in time in e^--irradiated 2745 glasses 127
Figure IV-31. The emission band of diamagnetic defect in e^--irradiated at 10^5 Gy 2745 glass, lamp excitation at 266 nm 128
Figure IV-32. The emission of the diamagnetic defect under 266 nm laser excitation in 2745_10e8 glass during the isochronal annealing treatments, zoom on low intensities is inset 129

List of Tables

Table IV-1 . Types of phosphate glasses studied in the work 99
Table IV-2. The parameters of g-factor of POHC defects [9] 103
Table IV-3. The parameters of g-factor of P-centers [6] 104
Table IV-4. The summary of paramagnetic defects recorded in 3450-3550 Gauss in irradiated phosphate glasses 119
Table IV-5. The characteristics of P centers in Yb-doped phosphate glasses 119

Chapter V

Yb/Er- and Er-doped AS glasses

V. Yb/ Er- and Er-doped AS glasses..... 137

1. Spectroscopy of Er^{3+} 137

1. a. Transitions of Er^{3+} ion in IR-region 137

1. b. Up-conversion..... 138

1. c. Yb → Er energy transfer..... 139

1. d. Experimental details 140

2. Link between the Er^{3+} environment and its luminescent properties 141

2. a. The samples..... 141

2. b. Characterization of Er^{3+} and Yb^{3+} environment by EPR spectroscopy 141

2. b. 1 Er-doped glasses..... 141

2. b. 2 Yb/Er-codoped glasses 143

2. c. Er-doped glasses..... 144

2. c. 1 IR-luminescence..... 144

2. c. 2 Up-conversion process 145

2. d. Yb/Er-codoped glasses 146

2. d. 1 IR-luminescence 146

2. d. 2 Up-conversion..... 147

3. Effect of irradiation on Er^{3+} luminescent properties..... 149

3. a. Er^{3+} lifetime τ_{IR} 149

3. b. Er^{3+} luminescence in Yb/Er-codoped glasses 151

3. c. Up-conversion..... 152

4. Conclusions 154

V. Yb/ Er- and Er-doped AS glasses

It was interesting to compare Er-doped glasses with Yb-doped under irradiation. The principle difference between these 2 Rare-Earth elements is the absence of stable divalent state for Er, so, it can change the mechanism of point defects formation (relaxation and thus the impact on luminescent properties). However, we expect that the same glasses AS24 and AS22 contain the same contrasted number of Er cluster as for Yb doped AS glasses. We will study in the same way the impact of RE cluster on glass properties.

Moreover, the aim in this part of the Ph.D. is to study the irradiation effect on Er^{3+} luminescent properties. We expect that some mechanisms (up-conversion, Yb→Er energy transfer) can be modified under ionizing irradiation. The results obtained in this Chapter can be interesting for the active fiber-radiation hardening. In modern use of Internet and in telecommunication field, the satellites in space are required to be of smaller size and processing higher energies. Er- and Yb/Er-containing glasses under fibers form are thus attractive materials for space and nuclear industry.

The part dedicated to irradiation in this Chapter is rather small. In particular, Er^{3+} emission is studied only for one dose 10^8 Gy. This study was carried out at the end of my Ph.D. program, so, irradiation possibilities were strongly limited. Therefore, this Chapter can be more considered as preliminary result that will be useful for the following studies.

1. Spectroscopy of Er^{3+}

Before presenting the results of Er-containing samples, it is necessary to remind here the structure of energy levels in Er^{3+} ions.

1. a. Transitions of Er^{3+} ion in IR-region

Er^{3+} is a $4f^{11}$-element with completed 5s and 5p orbitals and 11 electrons on 4f orbital. One can see in Figure V-1 that under 0.98 μm excitation in the $^4I_{11/2}$ state after a non-radiative transition $^4I_{11/2} \rightarrow {}^4I_{13/2}$ the well-known near-IR region

$^4I_{13/2} \rightarrow {}^4I_{15/2}$ emission at 1.54 μm is observed (Figure V-1) used in EDFA (Er-Doped Fiber Amplifier).

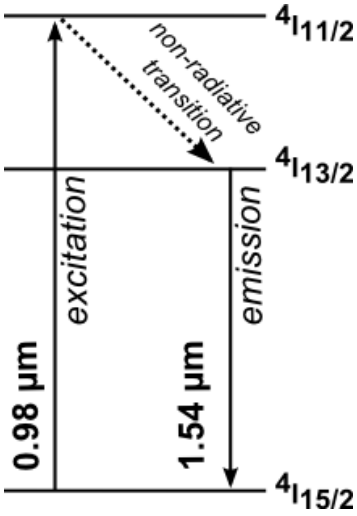


Figure V-1. Transitions of Er^{3+} ion in the IR range [1]

1. b. Up-conversion

Besides, the up-conversion process can be observed in Er-doped materials. Under excitation at 0.98 μm some radiative transitions in the visible range can be seen. Two mechanisms of up-conversion in Er^{3+} ions are distinguished [1]: Excited State Absorption (ESA) and Addition de Photon par Transferts d'Énergie (APTE) (Figure V-2).

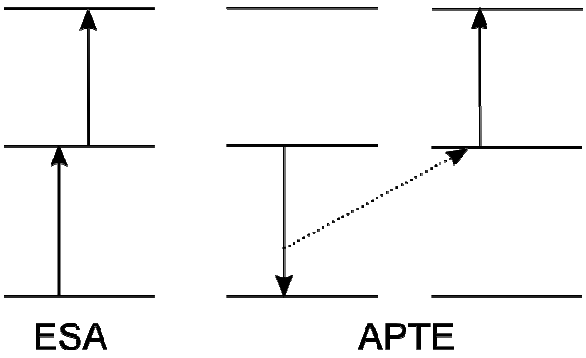


Figure V-2. Two proposed mechanisms of up-conversion process

The ESA mechanism is observed when a second photon is absorbed in Er^{3+} ion by an excited state, for example $^4I_{11/2}$. The efficiency of ESA in different materials is of $\approx 10^{-5}$ $(cm^2/W)^{n-1}$ order according to Auzel's review [2]. The APTE mechanism is observed when two Er^{3+} ions with excited $^4I_{11/2}$ level are displaced close enough. One of the photons via emitting can excite another one driving the last mentioned to

the level $^4F_{7/2}$. The probability of this mechanism is much higher than ESA ($\approx 10^{-3}$ $(cm^2/W)^{n-1}$ [2]).

The consequent emission is observed from $^2H_{11/2}$ and $^4S_{3/2}$ states to $^4I_{15/2}$ state in the green part and from $^4F_{9/2} \rightarrow {}^4I_{15/2}$ transition in the red part (Figure V-3). The other possible consequent transitions from $^2H_{11/2}$ and $^4S_{3/2}$ states to $^4I_{13/2}$ are observed at 750 nm. This emission cannot be observed in our case due to instrumental limitation.

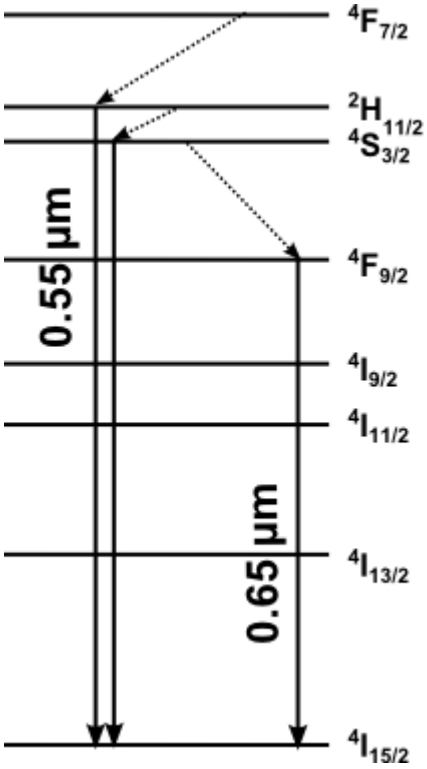


Figure V-3. Transitions in Er^{3+} ion, dicussed in the Chapter V. Solid lines – radiative transitions, dotted lines – non-radiative transitions

1. c. Yb → Er energy transfer

Yb^{3+} ions are implied efficiently to transfer the absorbed energy from $^2F_{5/2}$ state to $^4I_{11/2}$ state of Er^{3+}, increasing the $^4I_{11/2}$ population. The photons from $^4I_{11/2}$ state can move through non-radiative de-excitation to the state $^4I_{13/2}$ populating the state $^4I_{13/2}$ (Figure V-4).

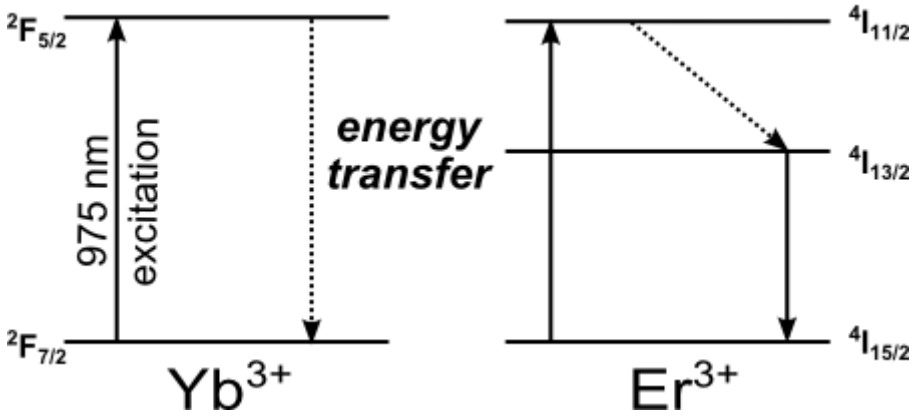


Figure V-4. Energy transfer from Yb^{3+} ion to Er^{3+} ion

1. d. Experimental details

Er^{3+} luminescence in the IR-region (1450-1650 nm) has been studied in Er- and Yb/Er-doped powders at room temperature in ENSCP.

To obtain more general results on the influence of Yb/Er-codoping and irradiation on Er^{3+}-luminescence properties, the lifetimes τ_{IR} of excited $^4I_{13/2}$ state have been measured. The experiment has been performed in ENSCP under laser excitation at 975 nm with 1.53 μm detection on slices because we did not have irradiated powders in vast dose range.

The study of up-conversion has been carried out on powders at room temperature using the same device as for cooperative luminescent measurements in ENSCP. The excitation line was 975 nm, the spectra have been registered in 400-700 nm range using afterwards lamp correction.

2. Link between the Er^{3+} environment and its luminescent properties

2. a. The samples

Two glass compositions with contrasted effect on Er cluster amounts have been chosen. They correspond to the same aluminosilicate glass compositions studied in Chapter III (cluster in AS22 < cluster in AS24). Both have been Er-doped and Yb/Er-codoped. Relative Er concentration is 10 times lower (0.5 wt. % of Er_2O_3) than Yb (5 wt. % Yb_2O_3) giving Yb:Er molar ratio 10:1 (9.6:1). This ratio drives some positive effects on Yb→Er energy tranfer process in the samples [3]. So, finally, there are 4 pristine glasses (Table V-1).

Sample name	**SiO_2, mol. %**	**Al_2O_3, mol. %**	**Na_2O, mol. %**	**ASI Al/Na**	**Er_2O_3/Yb_2O_3**
AS22_Er	74	6	20	0.3	+ 0.5 wt. % Er_2O_3
AS22_YbEr					+ 0.5 wt. % Er_2O_3 + 5 wt. % Yb_2O_3
AS24_Er	62	18	20	0.9	+ 0.5 wt. % Er_2O_3
AS24_YbEr					+ 0.5 wt. % Er_2O_3 + 5 wt. % Yb_2O_3

Table V-1. Nominal compositions of Er-doped aluminosilicate glasses

2. b. Characterization of Er^{3+} and Yb^{3+} environment by EPR spectroscopy

2. b. 1 Er-doped glasses

Both Yb^{3+} and Er^{3+} are paramagnetic ions. EPR spectroscopy is a powerful technique to study the environment of these ions not only in crystals [4], but also in glasses [5] [6]. Even if more important information can be found in crystals, for instance, on RE pair formation [7] [8], due to a more resolved signal, we will show that despite a broad signal and poor literature, some information on Er^{3+} environment can be extracted from EPR spectra.

Er^{3+} ions give their paramagnetic signal at low temperatures (4K) as most of REE, because of short spin-lattice relaxation times T1 at room temperature. The

EPR spectra of Er^{3+} at 4 K in AS22_Er and AS24_Er glasses are displayed in Figure V-5.

The signal of Er^{3+} can be seen with a very broad asymmetric negative part (Figure V-5).

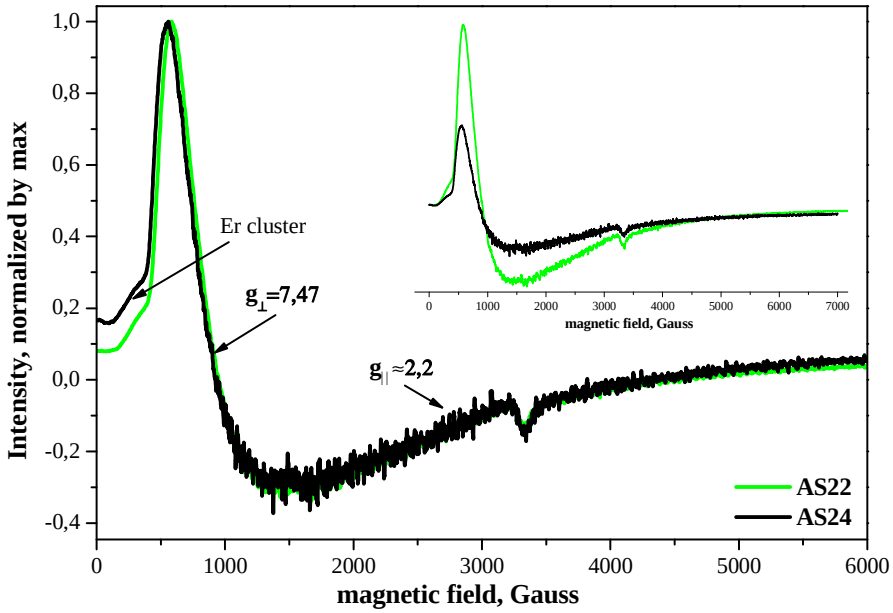


Figure V-5. EPR spectra of non-irradiated AS22_Er and AS24_Er glasses at 4 K. Normalization by mass&gain is in inset

The EPR line shape corresponds to an axial symmetry of Er^{3+} ions in both AS22 and AS24 glasses (Figure V-5). The $g_{\perp}$ is estimated at 7.47 whereas the $g_{\parallel}$ could correspond to ~2.2. The resonance position at 848 Gauss and its shape are identical in both glasses AS22 and AS24. The conclusion thus drives to identical Er^{3+} environment symmetry in AS22_Er and AS24_Er glasses.

Despite the same amount of Er in glasses, the signal is strongly lower in AS24_Er glass than in AS22_Er (Figure V-5, inset). This can be interpreted by the presence of Er-Er pairs. It is corroborated by the shoulder at g=21.5. Indeed, the g-value for Er^{3+} ion cannot exceed $2 \cdot \Lambda \cdot M$, where Λ is Landé factor g and M is the maximum value of the projection of the full angular momentum [9]. Besides, no zero field splitting is expected due to $S={}^{1}/_{2}$. Since $\Lambda={}^{6}/_{5}$ and $M={}^{15}/_{2}$, $g_{max}=18$ for isolated Er^{3+} ions.

It is worth to underline the formation of Er cluster at 0.5 wt. % of Er_2O_3. This situation is similar for AS24_Yb05 glass. However, Yb site symmetry is different in AS24 and AS22 glasses (see Chapter III). Usually, we extrapolate from one research

to another the results concerning REE properties. This is not the case for Yb- and Er-doped aluminosilicate glasses.

One reason to explain such difference can be the difference in doping concentrations (0.5 wt. % of Er_2O_3) instead of 5 wt. % of Yb_2O_3. It would be interesting to compare Er and Yb glasses doped with the same amount of REE.

2. b. 2 Yb/Er-codoped glasses

The influence of Yb-incorporating on Er^{3+} environment can be seen in Figure V-6 where EPR spectra of non-irradiated AS24 glasses are shown.

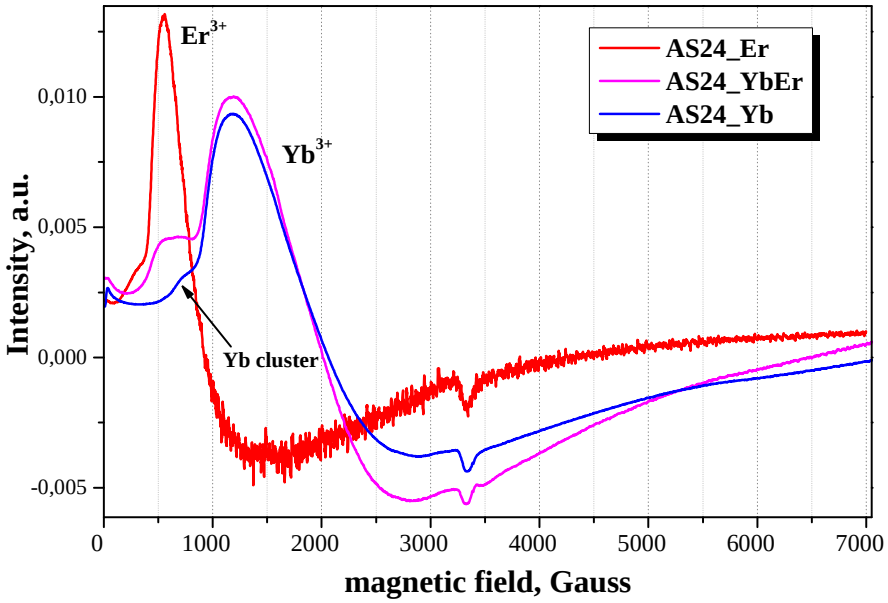


Figure V-6. EPR spectra of non-irradiated AS24 glasses recorded at 4K

One can note that in Yb/Er-codoped glass the Er^{3+} EPR signal decreases strongly (Figure V-6). The Er^{3+} signal becomes of the same order of intensity than Yb cluster in AS24_YbEr glass. This result is associated with possible Yb^{3+}-Er^{3+} pair formation. Once Er^{3+} ions involved into pairs, the EPR signal of isolated Er^{3+} ions decreases.

In AS22 glasses, there is no so important change in EPR spectra suggesting that the incorporation of Yb and Er into the glass leads to less Yb-Er pairs. This result is in agreement with lower tendency to form Yb cluster in AS22 composition linked to the glass structure (more NBO).

2. c. Er-doped glasses

2. c. 1 IR-luminescence

In 1450-1650 nm range the only $^4I_{13/2} \rightarrow {}^4I_{15/2}$ transition in Er^{3+} ions is observed (Figure V-7).

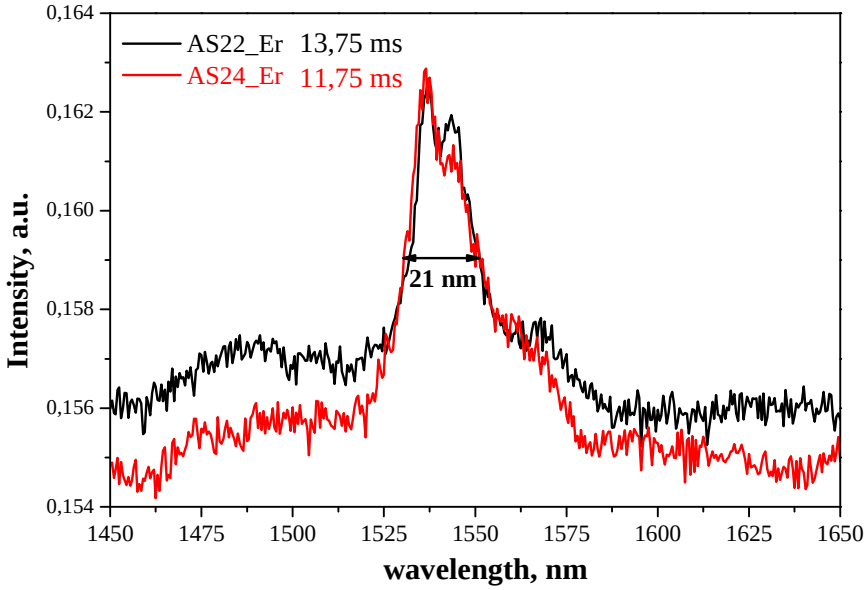


Figure V-7. IR-luminescence spectra of non-irradiated Er-doped AS glasses, corresponding to $^4I_{13/2} \rightarrow {}^4I_{15/2}$ emission under a 975 nm excitation

In both AS22_Er and AS24_Er glasses the intensities are of the same order. The shape of the spectra, its' FWHM do not change indicating similar crystal fields of Er^{3+} ions in each glass. This result is in agreement with the similarity of Er^{3+} EPR line shape in both glasses.

2. c. 2 *Up-conversion process*

The up-conversion spectra in Er-doped non-irradiated glasses are presented in Figure V-8.

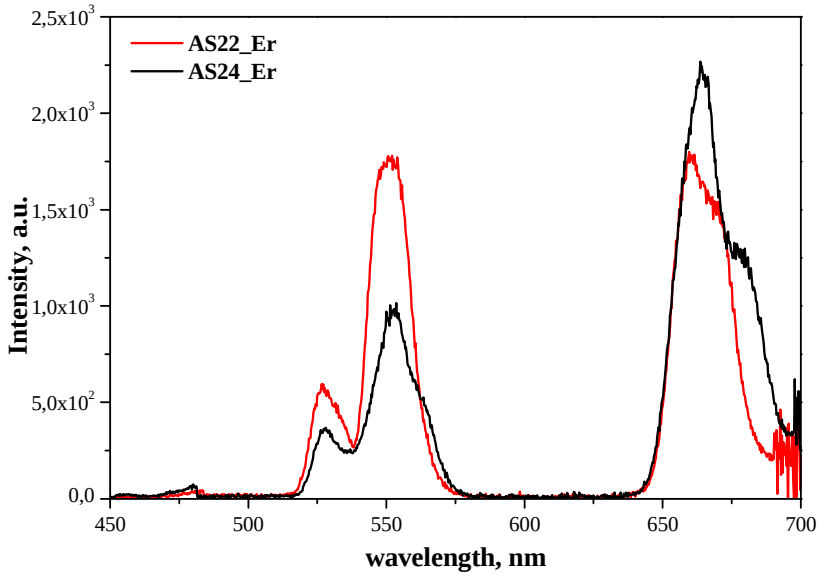


Figure V-8. Up-conversion spectra in non-irradiated Er-doped AS glasses under a 975 nm excitation

Since the experimental conditions are strictly the same for all glasses, we can assume our results as semi-quantitative.

The intensities of up-conversion emission (green and red) are of same magnitude in AS22_Er glass. The higher intensity of the red emission in AS24_Er could be assigned to a depopulation of $^4S_{3/2}$ level due to cross-relaxation process ($^4S_{3/2}$, $^4I_{15/2}$)→($^4F_{9/2}$, $^4I_{13/2}$). As a result, $^4F_{9/2}$ is more populated; the red emission is thus more intensive. Such difference in the ration red/green emission can originate from different Er-Er distances in AS22_Er and AS24_Er glasses. More effective $^4S_{3/2}$ depopulation requires closer displacements of Er^{3+} ions that take place in AS24_Er glass.

The up-conversion process illustrates shorter Er-Er distances in AS24_Er glass than in AS22_Er.

2. d. Yb/Er-codoped glasses

2. d. 1 IR-luminescence

Yb^{3+} incorporating into Er-containing glasses increases 2,5 times the intensity of the 1.54 µm emission band of Er^{3+}. As in case of Er-doping only, the 1.54 µm emission intensities do not differ a lot in AS22_YbEr and AS24_YbEr glasses (Figure V-9).

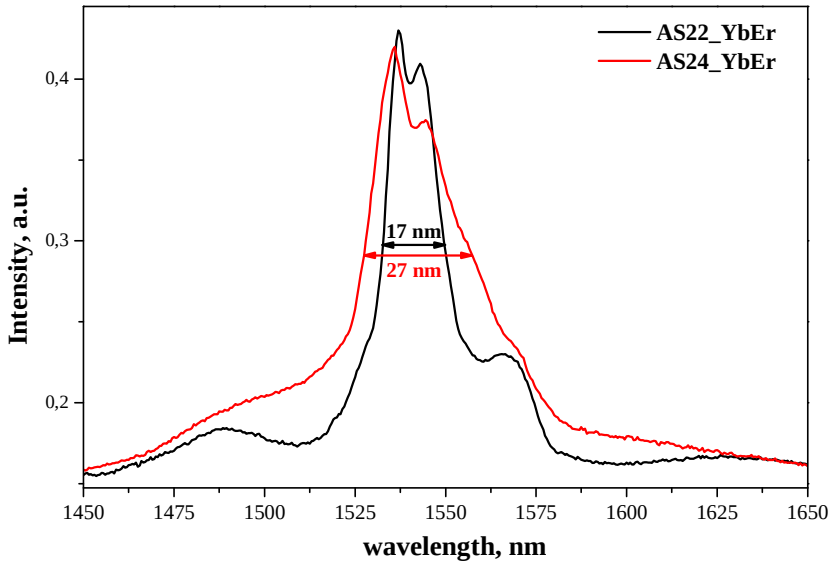


Figure V-9. Emission spectra of non-irradiated Yb/Er-codoped AS glasses, 975 nm excitation

However, the Stark components are better resolved in AS22_YbEr sample due to narrower lines; FWHM is 27 nm instead of 17 nm. The width of the emission band is a sensitive parameter for telecom applications where this particular feature is required.

We can suspect in AS24 glass that the adding of Yb leads to a wider distribution of environment for Er^{3+} ions. In particular, by EPR we have shown Yb^{3+}-Er^{3+} pair formation. The vicinity of Yb^{3+} and Er^{3+} ions could lead to a larger distribution of Er^{3+} environment and can be the reason for broadening of the Stark components.

The values of lifetimes τ_{IR} in non-irradiated samples are presented in Table V-2.

No RE cluster		**RE cluster**	
sample	lifetime τ_{IR}, ms	sample	lifetime τ_{IR}, ms
AS22_Er	13.7	AS24_Er	11.7
AS22_YbEr	14.8	AS24_YbEr	10.5

Table V-2. The lifetimes τ_{IR} of excited $^4I_{13/2}$ state in non-irradiated glasses

The shorter lifetimes of $^4I_{13/2}$ state in AS24 glasses can be associated with higher probability of $^4I_{13/2} \rightarrow {}^4I_{15/2}$ transition [10]. Yb incorporating does not bring any significant τ_{IR} variation. The lifetime of $^4I_{13/2}$ state is in error bar which is 10% (1.0-1.3 ms). The lifetime variation in non-irradiated AS glasses is in agreement with literature data where the lifetime τ_{IR} in silicates varies in 9.5-14.7 ms range [11].

2. d. 2 Up-conversion

In both glass compositions AS22_YbEr and AS24_YbEr, Yb/Er–codoping drives to higher up-conversion intensity 200 and 600 times, respectively, in comparison with Er-doped glasses. Comparison of up-conversion enhancement in AS22 and AS24 glasses reveals that in AS24_YbEr sample this process exhibits ~3 times stronger emission (Figure V-10) than in AS22_YbEr glass. One can see in the spectra of up-conversion (Figure V-10) in both glasses AS22_YbEr and AS24_YbEr the ratios between the intensities of green and red emissions are the same with a red emission ~3 times more intensive.

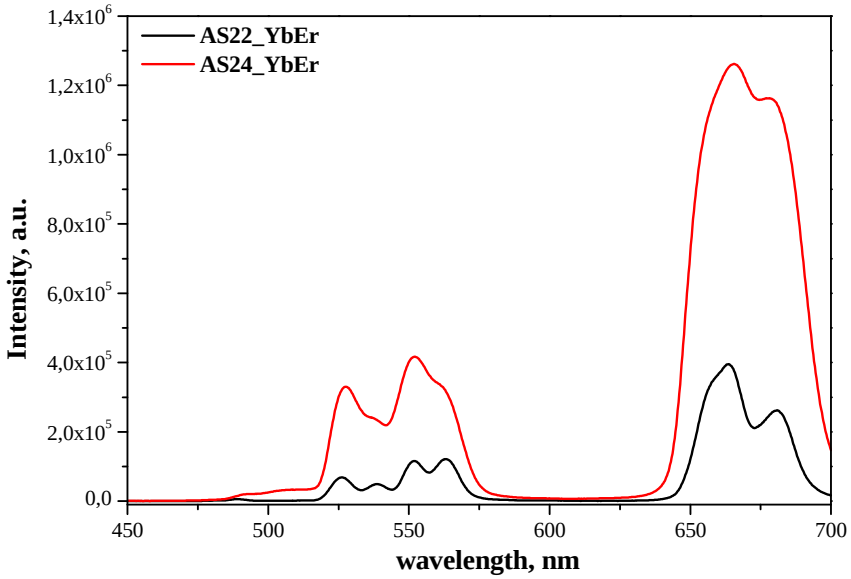


Figure V-10. Up-conversion spectra of non-irradiated Yb/Er-codoped AS glasses

By adding Yb into the glass the red/green emission ratio is enhanced in both glasses. Thus the processes of up-conversion emission are strongly influenced by doping with Yb. We can suspect that the up-conversion from $^4I_{13/2}$ state is more efficient when Yb is added. A more detailed spectroscopic study would be necessary to interpret properly those results.

- **In AS22_Er and AS24_Er glasses Er^{3+} has the same environment (0.5 wt. %) and, consequently, the same IR emission.**
- **The adding of Yb leads to the formation of more Yb-Er pairs in AS24_YbEr glass than in AS22_YbEr glass.**
- **The 1.54 μm emission is broader in AS24_YbEr than in AS22_YbEr glass due to a probable higher environment dispersion of Er^{3+} site symmetry in AS24_YbEr glass.**
- **The adding of Yb enhances the red and green up-conversion lines. The red one dominates strongly in both AS24_YbEr and AS22_YbEr glasses.**

3. Effect of irradiation on Er^{3+} luminescent properties

3. a. Er^{3+} lifetime τ_{IR}

Er-containing samples were irradiated with 2.5 MeV electrons in large dose range (Chapter II, section 2). The effect of irradiation dose on excited state $^4I_{13/2}$ lifetime τ_{IR} in aluminosilicate glasses can be observed in Figure V-11. All the decays are single-exponential indicating the absence of short component with energy transfer presence.

The lifetimes τ_{IR} in irradiated samples are plotted vs. dose logarithm.

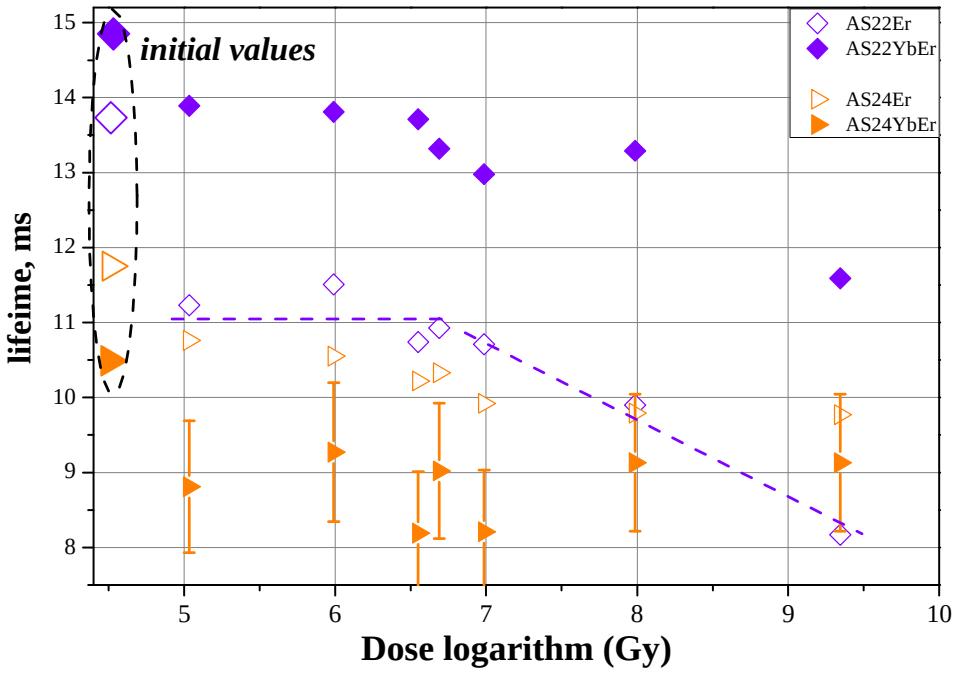


Figure V-11. The lifetimes τ_{IR} of $^4I_{13/2}$ in irradiated Er-containing AS glasses

The example of error bars is given for AS24_YbEr glasses only, to avoid too much complexity of the Figure. The lifetime τ_{IR} decreases under irradiation. The values of lifetime are comparable in medium dose range (10^5 –10^7 Gy) in all four AS glasses (Figure V-11). Then it decreases with further dose increasing more significantly (10^7-$2\cdot10^9$ Gy) in AS22_Er glasses whereas in other glasses the response is less sensitive to the dose. Once again, as for Yb-doped AS glasses, we obtain two types of curves. It is interesting to remark that Er^{3+} and Yb^{3+} display

same behavior. It should be underlined, however, that the absolute decrease of the lifetime τ_{IR} is lower for Er^{3+} ions than for Yb^{3+} ions. So, the two-step behavior observed in AS22_Yb glasses is reproduced in AS22_Er whereas in AS glasses a linear variation with lg(dose) takes place due to formation of Er cluster. Codoping with Yb seems to attenuate the dose-dependence behavior of AS24 samples. This could be linked to Yb-Er pairs formation. The lifetime stability is associated with the presence of RE clusters in Er/Yb-codoped glasses and in AS24_Er glasses. Similar behavior has been observed in irradiated Yb-doped AS glasses (Chapter III, section 3.b.2).

The decrease of the lifetime τ_{IR} in Er-doped fibers under γ-irradiation was already observed by B. Tortech in her Ph. D. [11]. She obtained a 10% decrease of the lifetime τ_{IR} recorded at different wavelengths of detection, the most significant at longer wavelengths. The lifetime τ_{IR} decrease under irradiation was linked to other channels of non-radiative de-excitation from $^4I_{13/2}$ level, in particular, to radiation-induced point defects [11]. Indeed, Al-related point defects play a role in the response of Er-doped fibers [3].

We cannot attribute the lifetime τ_{IR} decrease to the presence of P-related defects in aluminosilicate glasses. Nevertheless, we also suppose the influence of color centers in the lifetime τ_{IR} decrease.

3. b. Er^{3+} luminescence in Yb/Er-codoped glasses

The effect of e-irradiation at 10^8 Gy on $^4I_{13/2} \rightarrow {}^4I_{15/2}$ emission can be seen in Figure V-12.

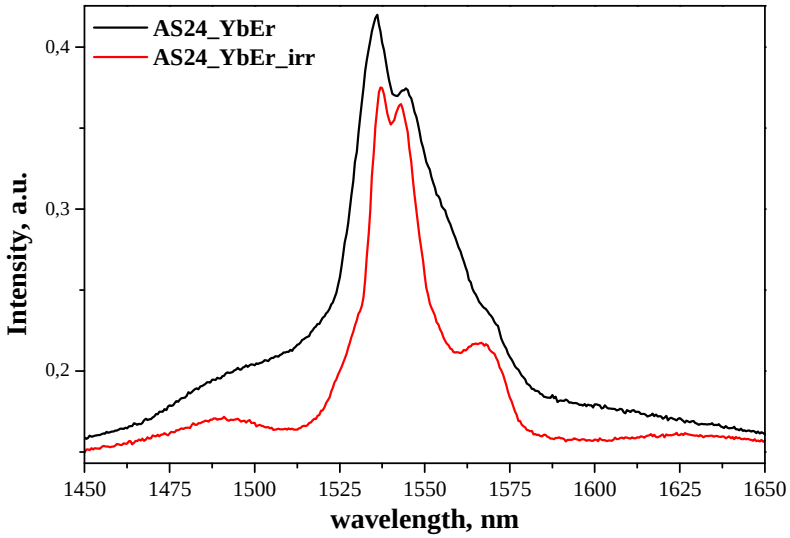


Figure V-12. Er^{3+} emission under 975 nm excitation in non-irradiated AS24_YbEr glasses and irradiated with 2.5 MeV electrons, dose 10^8 Gy

The emission band at 1.5 μm becomes narrower and less intensive (Figure V-12). The decrease of intensity could be assigned to partial $Yb^{3+} \rightarrow Yb^{2+}$ reduction in Yb-Er pairs which decreases the efficient Yb→Er energy transfer and thus IR-emission.

Concerning the shape evolution, we can suspect that reduction of Yb^{3+} into Yb^{2+} operates in the glass reducing thus the $Yb^{3+} \rightarrow Er^{3+}$ energy transfer for one part of the Er^{3+} ion. This mechanism could lead to an emission resulting from a more homogeneous group of Er^{3+} ions.

The second hypothesis consisting in a modification of the site symmetry of Er^{3+} is less probable at this dose (10^8 Gy) because no big change in the glass network is expected. It is corroborated by EPR spectroscopy at low T of irradiated at $2 \cdot 10^9$ Gy AS24_YbEr glass. No changes in Yb^{3+} or Er^{3+} environment are seen. It is thus hardly possible to obtain any modification of Er^{3+} environment at the dose lower than $2 \cdot 10^9$ Gy.

3. c. Up-conversion

In Figure V-13 the up-conversion spectra of Er^{3+} in non-irradiated and e^--irradiated AS24_Er and AS24_YbEr glasses (10^8 Gy) are compared.

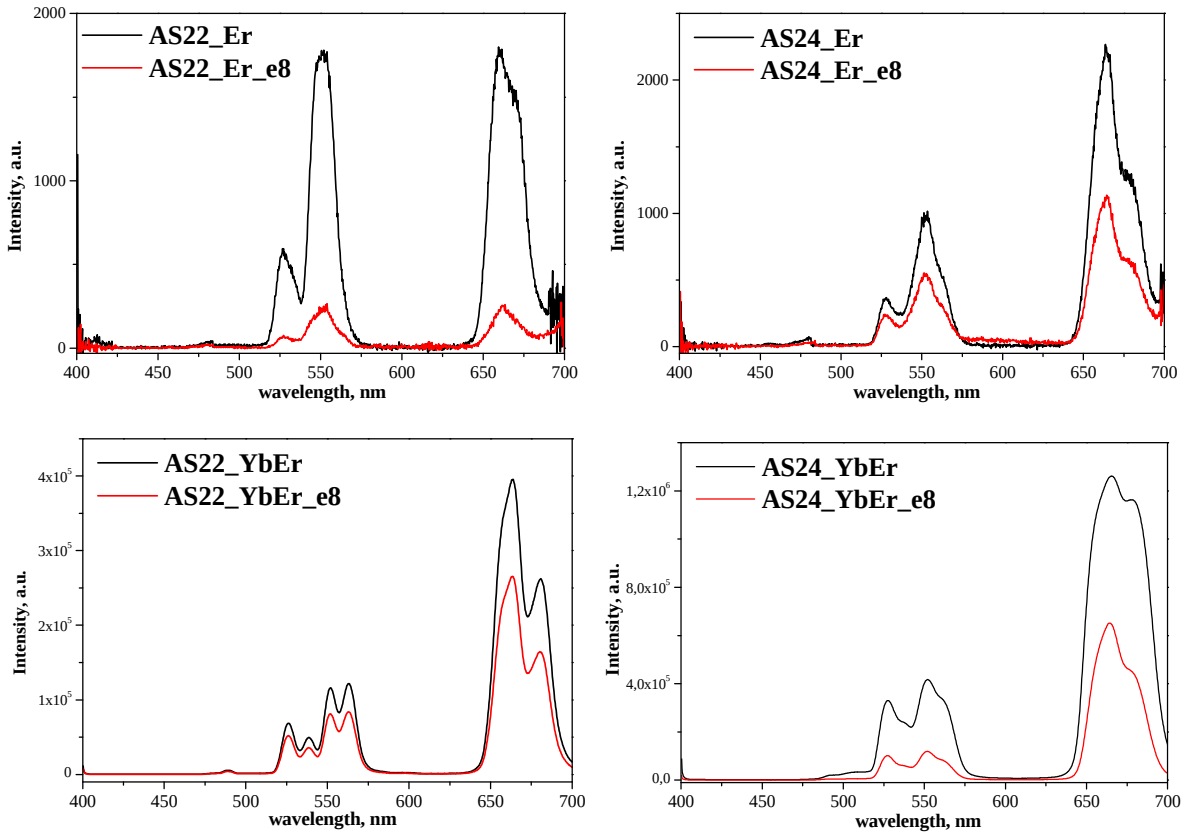


Figure V-13. Up-conversion spectra of glasses, comparison with e^--irradiated at 10^8 Gy

Under irradiation the intensity of green and red emissions in AS glasses decreases (Figure V-13). The decrease is variable according to the glass composition. However, the red/green emission ratio is maintained. On the other side, no shape evolution in up-conversion spectra is observed (Figure V-13), which is associated with no variation in Er^{3+} symmetry sites.

The main credit is of radiation-induced defects which have their absorption band in 500-700 nm range. Their absorption spectra are presented in Figure V-14.

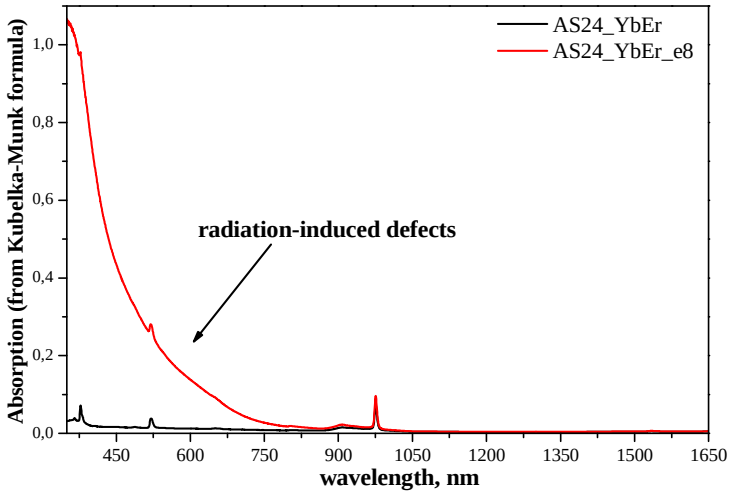


Figure V-14. Absorption spectra of AS24_YbEr glass, comparison with e^--irradiated at 10^8 Gy

- **Under irradiation the lifetime decreases, no dose effect between 10^5 and $2 \cdot 10^9$ Gy doses is seen except for AS22_Er glasses. The role of Er cluster is suspected as it was for Yb-doped AS glasses.**
- **The 1.54 μm emission broadness decreases in AS24_YbEr glass under irradiation.**
- **The up-conversion emission decreases under irradiation. It is assigned to radiation-induced point defects absorption in the visible range.**

4. Conclusions

In this short Chapter we show some interesting structure/properties results as the impact of Yb adding into Er-doped glasses leading to a broadening of the 1.54 μm emission. This effect is impacted by irradiation. In addition, we have shown a slight decrease of Er^{3+} excited state $^4I_{13/2}$ lifetime under irradiation as well as the decrease of up-conversion emission.

[1] G. Liu et B. Jacquier, Spectroscopic Properties of Rare Earths in Optical Materials, New York: Springer Series in Materials Science, 2005.

[2] F. Auzel, *Chem. Rev.,* vol. 104, p. 139, 2004.

[3] B. Tortech, Y. Ouerdane, S. Girard, J.-P. Meunier, A. Boukenter, T. Robin, B. Cadier et P. Crochet, *J. Non-Cryst. Solids,* vol. 355, p. 1085, 2009.

[4] T. Bodziony, S. M. Kaczmarek et C. Rudowicz, *Physica B,* vol. 403, p. 207, 2008.

[5] G. Dantelle, M. Mortier, P. Goldner et D. Vivien, *J. Phys. Condens. Matter,* vol. 18, p. 7905, 2006.

[6] N. Ollier, R. Planchais et B. Boizot, *Nucl. Instr. and Meth. in Phys. Res. B,* vol. 266, p. 2854, 2008.

[7] T. Bodziony, S. M. Kaczmarek et C. Rudowicz, *Physica B,* vol. 403, p. 207, 2008.

[8] T. S. Altshuler, Y. V. Goryunov, M. S. Bresler, F. Iga et T. Takabatake, *Phys. Rev. B,* vol. 68, p. 014425, 2003.

[9] N. Ollier, J.-L. Doulan, V. Pukhkaya, T. Charpentier, R. Moncorgé et S. Sen, *J. Non-Cryst. Solids,* vol. 357, p. 1037, 2011.

[10] L. Petit, Ph.D. dissertation, Bordeaux: l'Université Bordeaux I, 2003.

[11] B. Tortech, Ph. D. dissertation, Saint-Etienne, 2008.

List of Figures

Figure V-1. Transitions of Er^{3+} ion in the IR range [1]..... 138
Figure V-2. Two proposed mechanisms of up-conversion process..... 138
Figure V-3. Transitions in Er^{3+} ion, dicussed in the Chapter V. Solid lines – radiative transitions, dotted lines – non-radiative transitions 139
Figure V-4. Energy transfer from Yb^{3+} ion to Er^{3+} ion 140
Figure V-5. EPR spectra of non-irradiated AS22_Er and AS24_Er glasses at 4 K. Normalization by mass&gain is in inset..... 142
Figure V-6. EPR spectra of non-irradiated AS24 glasses recorded at 4K..... 143
Figure V-7. IR-luminescence spectra of non-irradiated Er-doped AS glasses, corresponding to $^4I_{13/2} \rightarrow {}^4I_{15/2}$ emission under a 975 nm excitation..... 144
Figure V-8. Up-conversion spectra in non-irradiated Er-doped AS glasses under a 975 nm excitation 145
Figure V-9. Emission spectra of non-irradiated Yb/Er-codoped AS glasses, 975 nm excitation 146
Figure V-10. Up-conversion spectra of non-irradiated Yb/Er-codoped AS glasses 148
Figure V-11. The lifetimes τ_{IR} of $^4I_{13/2}$ in irradiated Er-containing AS glasses..... 149
Figure V-12. Er^{3+} emission under 975 nm excitation in non-irradiated AS24_YbEr glasses and irradiated with 2.5 MeV electrons, dose 10^8 Gy 151
Figure V-13. Up-conversion spectra of glasses, comparison with..... 152
Figure V-14. Absorption spectra of AS24_YbEr glass, comparison with e^--irradiated at 10^8 Gy..... 153

List of Tables

Table V-1. Nominal compositions of Er-doped aluminosilicate glasses 141
Table V-2. The lifetimes τ_{IR} of excited $^4I_{13/2}$ state in non-irradiated glasses 147

Conclusions and Perspectives

VI. Conclusions and Perspectives

In terms of the present Ph. D. work, we have investigated the effects of ionizing irradiation on the Yb^{3+} luminescent properties in aluminosilicate and phosphate glasses by trying to understand the impact of initial Yb environment and mostly the role of Yb cluster.

We have tried to understand the particular links between the luminescence of Yb^{3+} and the radiation-induced point defects. The study has been carried out looking for the impact of some principle factors such as glass chemical composition, irradiation conditions (dose, dose rate).

The main result concerns the demonstration of the role of Yb cluster on point defect relaxation and the evolution of $^2F_{5/2}$ lifetime with irradiation.

We demonstrate that Yb clusters trap the holes and electrons efficiently produced by irradiation limiting thus the charge recombination and defect recovery. The consequence has been followed in higher stability of both paramagnetic defects and the lifetime decrease of $^2F_{5/2}$ excited state in time after the irradiation.

This result is in agreement with phosphate glasses with less Yb cluster. In Yb-doped phosphate glasses paramagnetic point defects relax quicker than in aluminosilicates. Moreover, the lifetimes τ_{IR} increase, in some cases to its pre-irradiation value, as it is shown for AS glasses almost without Yb cluster (AS22 and AS23). Finally, the lifetimes τ_{IR} are reversible in phosphate glasses under annealing treatments as in AS22_10e8 glass with neglectable Yb cluster content.

The cooperative emission of Yb^{3+} in AS glasses decreases under the irradiation. It maintains stable within time in glasses with more Yb cluster. The decreases of the lifetimes τ_{IR} and of the cooperative luminescence are associated with different radiation-induced point defects. In particular, Peroxy radicals are also responsible for the lifetime τ_{IR} decrease. Al-OHC defects are supposed to participate in the decrease of Yb^{3+} cooperative emission. For the phosphate glasses, the link between POHC defects and the lifetime τ_{IR} evolution has been shown.

Concerning dose effect on point defects, we have observed almost no variation of total amount of paramagnetic defects in medium dose range (10^5-$3.2\cdot10^6$ Gy), increase of it in stronger doses (10^7-10^8 Gy) and the decrease at strong doses (>$1.5\cdot10^9$ Gy) when some glass network modifications are seen. Such behavior had been already reported for Yb-doped ABS glasses [1]. Moreover, the

same evolution as irradiation dose function has been observed in this work in Yb-doped phosphate glasses for r-POHC defects. The similarities obtained for three different glasses (aluminoborosilicates, aluminosilicates and phosphates) can be assumed as a general result for paramagnetic point defect evolution in glasses under irradiation.

Moreover, the lifetime τ_{IR} dependence vs. lg(dose) in Er-containing glasses is in agreement with RE cluster effect obtained for Yb-doped AS glasses (Chapter III), phosphate glasses (Chapter IV) and ABS glasses [2]. In Chapter V we have demonstrated such type of behavior for another REE than Yb. We conclude thus the role of RE cluster in glasses in the lifetime τ_{IR} evolution under irradiation.

We have demonstrated in this work than number of radiation-induced paramagnetic point defects in phosphate glasses is more complex that it was considered to be. In particular, together with r-POHC defects we observe the signals of P-related Peroxy radicals. We report also S-center presence in Si-free glasses. Moreover, the evolution of so-called P3 defect as a function of dose, dose rate, time and temperature has been followed. The obtained results will be useful for the future studies to determine P3 defect's structure. In addition, a diamagnetic defect is observed even in non-irradiated phosphate glasses. This defect exhibits under UV excitation strong emission at 420 nm with long lifetime ~5-6 ms. Our data revisits the conclusions from Origlio et al. [3].

Even if the last Chapter is less developed, we have obtained interesting results inferring the role of Er and Yb environment on 1.54 μm width and up-conversion process. We have shown clearly Er^{3+} luminescent properties (emission) and the lifetime τ_{IR} are affected under irradiation as well as Yb→Er energy transfer.

However, this study should be followed by some others because there are still some ambiguous points.

We have shown that in AS glasses irradiated at strong doses (>10^8 Gy) the relaxation of paramagnetic point defects is different that with medium dose (10^5 Gy). Unfortunately, we had no possibility to investigate this relaxation in more details in order to find any correlations with lifetime τ_{IR} variation under strong doses.

Among the different ways to be go on we can cite:

- The results obtained in study of irradiated phosphate glasses cannot be interpreted clearly without rigorous simulation experiments. Our experimental results will help simulations to propose a model for high-

temperature singlet in phosphate glasses and for the evolution of P1 or P3 defect line under irradiation.

- In Yb/Er-codoped AS glasses, Yb^{3+} ions have an impact on Er^{3+} environment via creating of Yb^{3+}-Er^{3+} pairs. The consequences are seen in up-conversion process and in $^4I_{13/2} \rightarrow {}^4I_{15/2}$ emission at 1.54 μm. Moreover, ionizing irradiation has an impact on both of these properties, which cannot be neglected.
- A more detailed study of REE environment would help to understand the spectroscopic features. Among the different study, pulsed EPR spectroscopy that has been already initiated on AS24_Ybx glasses would help to characterize Yb-Er interactions as well as analysis of decay time of $^2F_{5/2}$ excited state of Yb^{3+} ions.
- Yb clusters were not detected by Transmission Electron Microscopy that indicates the size of Yb cluster less than 3 nm. Concerning Yb cluster characterization and Yb environment, it will be interesting to correlate the original EPR results that we have obtained with further EXAFS and XANES experiments in order to characterize better the site symmetry (coordination number obtained by EXAFS) and information on Yb-Yb distance.

[1] N. Ollier et V. Pukhkaya, *Nucl. Instr. and Meth. in Phys. Res. B,* vol. 277, p. 121, 2012.

[2] N. Ollier, J.-L. Doulan, V. Pukhkaya, T. Charpentier, R. Moncorgé et S. Sen, *J. Non-Cryst. Solids,* vol. 357, p. 1037, 2011.

[3] G. Origlio, F. Messina, M. Cannas, R. Boscaino et S. Girard, *Phys. Rev. B,* vol. 80, p. 205208, 2009.

Appendix

Appendix 1 : Aluminosilicate glass compositions

Appendix 2 : Irradiation conditions

Appendix 3 : Annealing treatments of phosphate glasses

VII. Appendix

Appendix 1. Aluminosilicate glass compositions

Table VII-1. Aluminosilicate glass compositions (molar fractions), microprobe analysis

		theory	experiment	difference
AS22	***O***	62,1	60,54	1,56
	Na	11,88	11,64	0,24
	Al	3,56	3,78	0,22
	Si	21,98	23,55	1,57
	Yb	0,47	0,52	0,05
AS23	***O***	61,77	60,04	1,73
	Na	11,44	11,31	0,13
	Al	6,86	7,25	0,39
	Si	19,45	20,86	1,41
	Yb	0,48	0,53	0,05
AS24	***O***	61,47	59,65	1,82
	Na	11,03	11,03	0
	Al	9,93	10,61	0,68
	Si	17,1	18,15	1,05
	Yb	0,48	0,54	0,06
AS26	***O***	61,28	60,4	0,88
	Na	10,77	10,23	0,54
	Al	11,85	12,09	0,24
	Si	15,62	16,73	1,11
	Yb	0,48	0,55	0,07
AS24_0	***O***	58,53	61,14	2,61
	Na	12,49	10,87	1,62
	Al	10,64	10,35	0,29
	Si	18,33	17,63	0,7
	Yb	0	0,01	0,01
AS24_05	***O***	59,19	60,22	1,03
	Na	11,82	11,25	0,57
	Al	10,63	10,67	0,04
	Si	18,31	17,77	0,54
	Yb	0,05	0,06	0,01
AS24_2	***O***	59,96	59,36	0,6
	Na	11,55	11,39	0,16
	Al	10,39	10,82	0,43
	Si	17,9	18,2	0,3
	Yb	0,2	0,23	0,03
AS24_8	***O***	62,92	60,72	2,2
	Na	10,54	10,43	0,11

	Al	9,48	9,91	0,43
	Si	16,33	18,02	1,69
	Yb	0,73	0,87	0,14

Appendix 2. Irradiation conditions

Table VII-2. Electron-irradiated samples: chemical compositions and doses required. In yellow - May 2011, in blue November - December 2011, in green both periods.

100 kGy	1 MGy	3,2 MGy	10 MGy	100 MGy	1,5 GGy	2 GGy
ALUMINOSILICATE GLASSES						
slices						
AS22	AS22	AS22	AS22	AS22	AS22	AS22_0
AS23	AS23	AS23	AS23	AS23	AS23	AS24_0
AS24	AS24	AS24	AS24	AS24	AS24	AS24_0
AS26	AS26	AS26	AS26	AS26	AS26	AS26_0
AS24_0	AS24_0	AS24_0	AS24_0	AS24_0	AS24_0	
AS24_05	AS24_05	AS24_05	AS24_05	AS24_05	AS24_05	
AS24_8	AS24_8	AS24_8	AS24_8	AS24_8	AS24_8	
	AS24_005	AS24_005	AS24_005	AS24_005	AS24_005	
	AS24_02	AS24_02	AS24_02		AS24_02	
AS22_0	AS22_0	AS22_0	AS22_0	AS22_0	AS22_0	
powders						
AS22		AS22		AS22		
AS23		AS23		AS23		
AS24		AS24		AS24		
AS26		AS26		AS26		
AS24_0		AS24_0		AS24_0		
AS24_05		AS24_05		AS24_05		
AS24_8		AS24_8		AS24_8		
PHOSPHATE GLASSES						
slices						
2743	2743	2743	2743	2743	2743	
2742	2742	2742	2742	2742	2742	
2745	2745	2745	2745	2745	2745	
2746	2746	2746	2746	2746	2746	
2743_0	2743_0	2743_0	2743_0	2743_0	2743_0	
2745_0	2745_0	2745_0	2745_0	2745_0	2745_0	
powders						
2743		2743		2743		
2742		2742		2742		
2745		2745		2745		
2746		2746		2746		

2745_0		2745_0		2745_0		

Table VII-3. Gamma-irradiated samples.

10 kGy	100 kGy	1 MGy	3,2 MGy
ALUMINOSILICATE GLASSES			
slices			
AS22	AS22	AS22	AS22
AS23	AS23	AS23	AS23
AS24	AS24	AS24	AS24
AS26	AS26	AS26	AS26
AS24_0	AS24_0	AS24_0	AS24_0
AS24_05	AS24_05	AS24_05	AS24_05
AS24_8	AS24_8	AS24_8	AS24_8
powders			
	AS22		AS22
	AS23		AS23
	AS24		AS24
	AS26		AS26
	AS24_0		AS24_0
	AS24_05		AS24_05
	AS24_8		AS24_8
PHOSPHATE GLASSES			
slices			
2743	2743	2743	2743
2742	2742	2742	2742
2745	2745	2745	2745
2746	2746	2746	2746
2745_0	2745_0	2745_0	2745_0
powders			
	2743		2743
	2742		2742
	2745		2745
	2746		2746
	2745_0		2745_0

Table VII-4. Electron-irraidiation conditions in November - December 2011.

samples	T, °C	I_{sample}, µA	dose rate, MGy/h	irradiation date	Dose exp. , µC	Diff. , µC	Diff. , %
10e5 Gy 181.81 µC							
2743	32,6			16 Nov 2011	204	-22,19	12,205
2742	29				197	-15,19	8,3549
2746	29				195	-13,19	7,2548
10e6 Gy 1363,575 µC							
AS24_0 AS24_005 AS24_05 AS24_02 AS22_0 AS23	33	14	2,76	16 Nov 2011	1436	-72,425	5,3114
AS22 AS24 AS24_8 AS26	38	14,4	2,84		1420	-56,425	4,138
3*10e6 Gy 5454,3 µC							
AS24_005 AS24_05 AS24_02 AS22_0	33	15,0-16,0	2,95-3,15	17 Nov 2011	5621	-166,7	3,0563
AS22 AS23 AS24 AS24_05 AS24_0 AS26 2743 2743_0	36	14,0-16,3	2,76-3,21		5610	-155,7	2,8546
10e7 Gy 18181,81 µC							
AS22_0 AS24_0 AS24_005 AS24_05 AS24 AS24_8 AS22 AS23 AS26	35	13,7-15,6 (14,6)	2,70-3,07 (2,88)	24 Nov 2011	18216	-34,19	0,188
AS24_02 2743 2743_0 2745	34	14,2-15,5	2,80-3,05		18236	-54,19	0,298

2745_0 2746 2742							
AS23 AS24_8 AS24_02 2745_0 AS24 2742 AS22 AS24_005 AS24_05	37	14,6-15,6	2,87-3,07		18218	-36,19	0,199
10e8 Gy 181818,1 μC							
AS22_0 AS23 AS24_005 AS24_0 AS24_8 2743_0 2746 AS24	36-39	14,2	2,8	5 Dec 2011	182119	-300,9	0,1655
AS24	32-34	15,0-16,6	2,95-3,27		182183	-364,9	0,2007
AS22	40-42	15,2-17,2	2,99-3,39		182169	-350,9	0,193
AS26	45-46	15,2-16,4	2,99-3,23		182197	-378,9	0,2084
AS22 AS24_05 AS26 2743 2742 2745 2745_0 2746	35-37	13,6-15,6	2,68-3,07		182176	-357,9	0,1968
2742	32-36	14,7-16,1	2,89-3,17	29 Nov 2011	183041	-1222,9	0,6726
2743	43-45	15,4-16,4	3,03-3,23		183045	-1226,9	0,6748
2746	34	14,6-15,4	2,87-3,03		183021	-1202,9	0,6616
>10e9 Gy							

AS22 AS23 AS24 AS24_0 AS24_005 AS24_8 AS26 2745 2745_0	30-35	13,6-15,0	2,68-2,95	30 Nov 2011	2633121		

Appendix 3. Annealing treatments of phosphate glasses

The bulk samples were annealed in corundum crucibles under air atmosphere. The temperature range was 100-430°C with ~20°C for 10 min step. The time necessary to stabilize the temperature after the crucible with samples had been placed into the oven was 100 sec. Each annealing step was followed by EPR and, in case of changes of spectrum, by the lifetime τ_{IR} measurements and PL under laser excitation at 266 nm as well.

2743_10e8 glass

During the annealing treatments a new isotropic signal is revealed (Figure VII-1). The position of this defect, its shape and its behavior under annealing treatments are close to S centers in P-doped silica [1] where it appears at T>477°C.

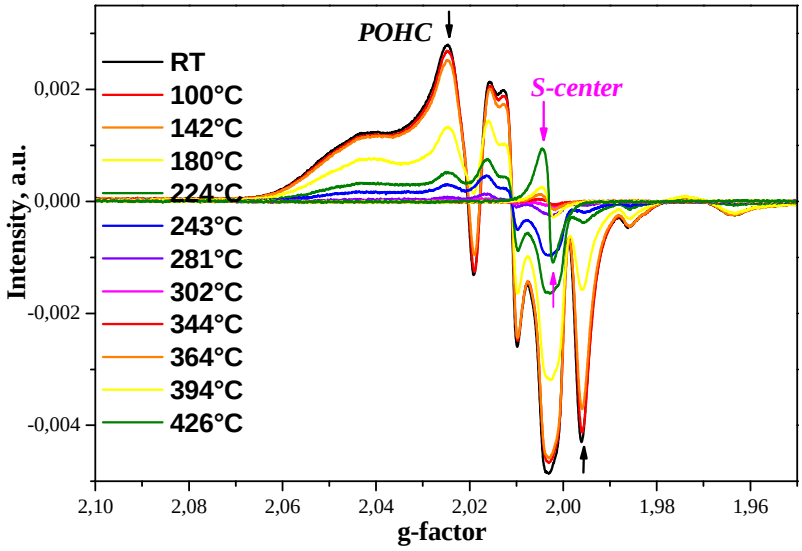


Figure VII-1. EPR spectra of e^--irradiated at 10^8 Gy 2743 glass, isochronal annealing treatments

This isotropic signal at g=2.00389 appears once the recovery of all the other defects has been already completed.

Griscom et al. associated the S center with silica rather than with phosphorus [1] because of isotropic character and absence of any hyperfine structure. However, according to microprobe analysis, there is no Si in our studied Yb-doped phosphate glasses. We assume thus that this S center cannot be related to silica in our case.

Under annealing treatments the intensities of Signal I and Signal II increase until its recovery at 365°C (Figure VII-2).

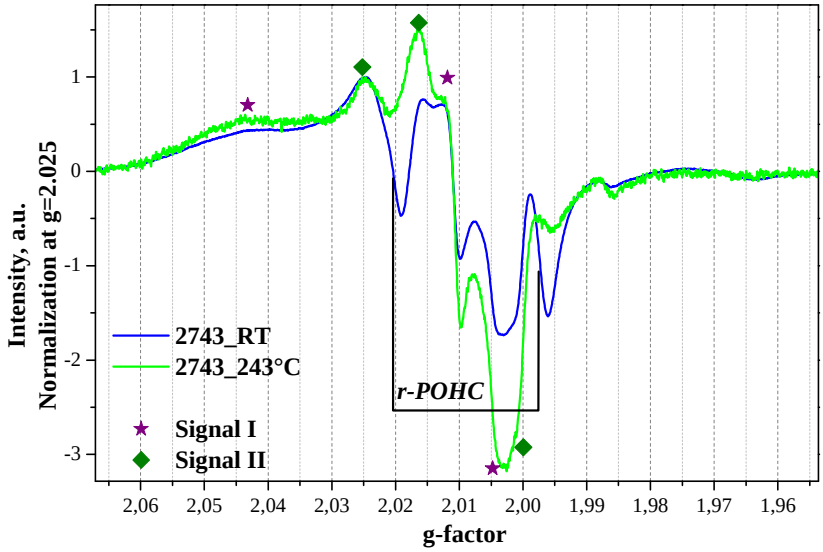


Figure VII-2. EPR spectra of e^--irradiated at 10^8 Gy 2743 glass

In alkali-tungsten-phosphate glasses both Signal I and Signal II were detected even after annealing at 420°C [2]. It can be associated with higher thermal stability of A_2WO_4-containing phosphate glasses [2].

The P2 defect's recovery is observed at 224°C. It is lower than in P-doped silica where the P2 recovery was observed at 352°C [3].

P1 defect is detected until 302°C and after annealing at 323°C it has been no more seen. Instead, P3 defect is observed (Figure VII-3). Its resonance at higher g-value is still observed after 426°C. In P-doped silica P1 defect is one of the most thermally stable, its recovery was detected in 400-450°C range [3].

P4 defect becomes easier visible during the annealing treatments until its recovery at 394°C (Figure VII-3).

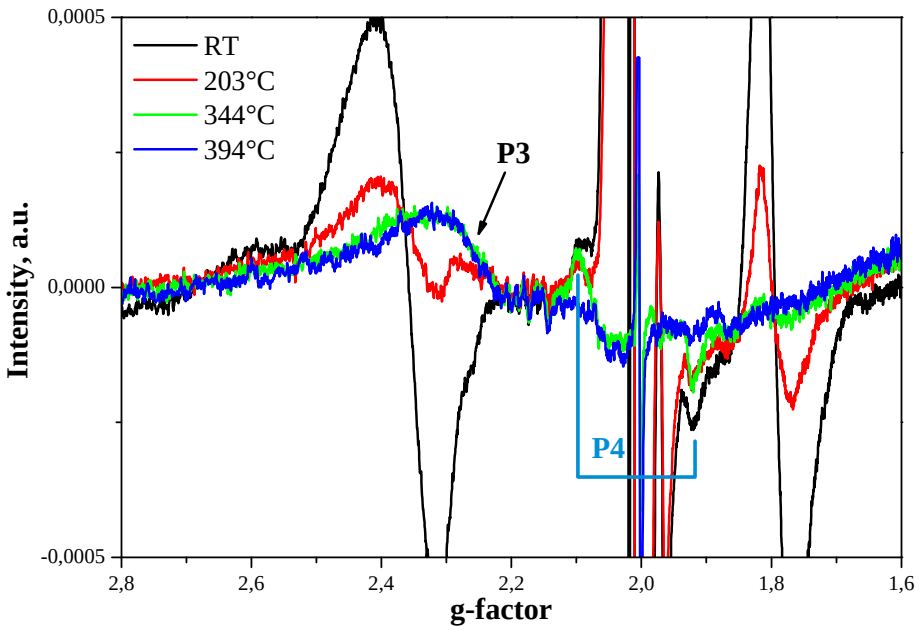


Figure VII-3. EPR spectra of 2743_10e8 glass during the annealing treatments

As in case of P-doped silica fibers, P4 defects are more stable at high temperatures than POHC [3]. It is important because once there is high content of POHC defects, its signal can overlap P4 defects which is observed in close range of magnetic field. So, it is difficult to know if P4 are formed just after the irradiation or via structural transformations during the annealing treatment.

The concentration of r-POHC and P1 defects is estimated as reported in Chapter II, section 3.b.2. The obtained values are plotted in Figure VII-4.

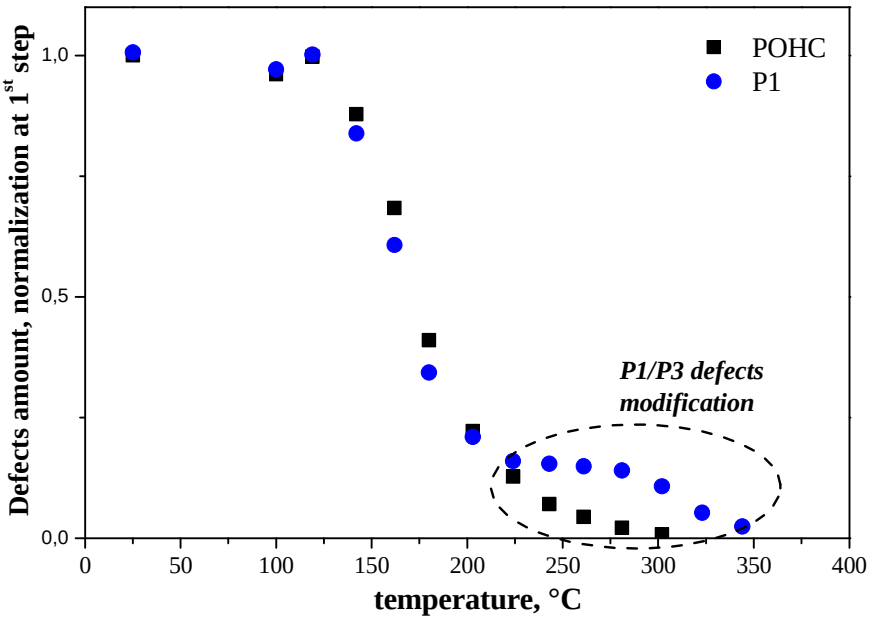


Figure VII-4. The defects recovery in 2743 glass under annealing treatments

The recovery of P1 defects takes place in parallel with r-POHC defects illustrating its structural relations.

2745_10e8 glass

In e^--irradiated glasses at 10^8 Gy, r-POHC defects recovery temperature is 224°C in 2745 glass and 302°C in 2743 glass. In both glasses, the annealing temperature is lower than in P-doped silica where r-POHC defects were eliminated at ~352°C [3]. We would attempt this effect as a fundamental consequence of more complex chemical composition of our Yb-doped Na-Mg-phosphate glasses than P-doped silica.

As it is mentioned above, the lifetime τ_{IR} is back to its pre-irradiation value once all the r-POHC defects have been recovered.

Peroxy I exhibits higher stability under isochronal annealing treatments than r-POHC defects (Figure VII-5).

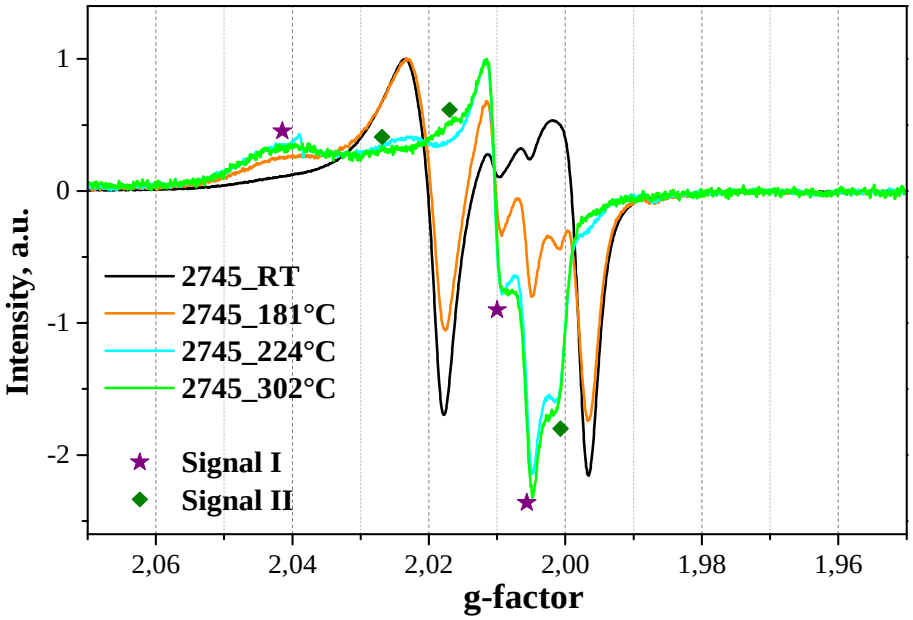


Figure VII-5. EPR spectra of annealed at various temperatures of e^--irradiated at 10^8 Gy 2745 glass, normalization at maximum

The Signal I intensity increases under annealing until its rapid recovery at 365°C.

In 2745 glass less Signal II is seen with annealing. However, the thermal stability of paramagnetic defects is higher in this sample. It can be attributed either to the impact of glass network or to Yb cluster presence in 2745 glass.

[1] G. Origlio, F. Messina, M. Cannas, R. Boscaino et S. Girard, *Phys. Rev. B,* vol. 80, p. 205208, 2009.

[2] M. E. Archidi, M. Haddad, A. Nadiri, F. Benyaïch et R. Berger, *Nucl. Instr. and Meth. in Phys. Res. B,* vol. 116, p. 145, 1996.

[3] D. L. Griscom, E. J. Friebele, K. J. Long et J. W. Fleming, *J. Appl. Phys.,* vol. 54, p. 3743, 1983.

N. Ollier, J.-L. Doualan, V. Pukhkaya,
T. Charpentier, R. Moncorgé, S. Sen

Evolution of Yb^{3+} environment and luminescence properties under ionizing irradiation in aluminoborosilicate glasses

Journal of Non-Crystalline Solides, 2011
vol. 357, p. 1037-1043

Author's personal copy

Journal of Non-Crystalline Solids 357 (2011) 1037–1043

Contents lists available at ScienceDirect

Journal of Non-Crystalline Solids

journal homepage: www.elsevier.com/locate/jnoncrysol

Evolution of Yb^{3+} environment and luminescence properties under ionizing irradiation in aluminoborosilicate glasses

N. Ollier [a,*], J.-L. Doualan [b], V. Pukhkaya [a], T. Charpentier [c], R. Moncorgé [b], S. Sen [d]

[a] CEA, IRAMIS, Laboratoire des Solides Irradiés Ecole Polytechnique CNRS 91128 Palaiseau, France
[b] CIMAP – Centre de Recherche sur les Ions, les Matériaux et la Photonique UMR 6252 CEA-CNRS-ENSICAEN, Université de Caen, 6 Boulevard Maréchal Juin, 14050 Caen, France
[c] CEA, IRAMIS, SI2M, Laboratoire de Structure et Dynamique par Résonance Magnétique, F-91191 Gif-sur-Yvette cedex, France
[d] Department of Chemical Engineering and Materials Science, University of California at Davis, Davis, California 95616, USA

ARTICLE INFO

Article history:
Received 1 March 2010
Received in revised form 4 November 2010
Available online 8 December 2010

Keywords:
Glasses;
Yb^{3+};
Photoluminescence;
Irradiation;
Defects;
EPR;
Cluster;
Cooperative luminescence

ABSTRACT

Yb-doped aluminoborosilicate glasses were irradiated with 2.3 MeV electron and gamma rays at different doses ranging between 10^4 and 2.6×10^9 Gy and the local structure around the Yb^{3+} ions has been studied using a combination of NMR, EPR and photoluminescence spectroscopic techniques. The spectroscopic results indicate the presence of two distinct Yb^{3+} sites in these glasses and their relative fractions depend on both the Yb concentration and the irradiation dose. These two sites can be attributed to Yb^{3+} ions with and without Yb next-nearest neighbors. The evolution of the shape of the $^7F_{5/2}\rightarrow{}^7F_{7/2}$ infrared emission band under irradiation is explained by a preferential reduction of the Yb^{3+} ions with Yb next-nearest neighbors at high integrated doses ($>10^8$ Gy). This interpretation is supported by a strong decrease of the visible cooperative luminescence under irradiation due to the reduction into the Yb pairs. In other terms, it shows an interesting effect of ionizing irradiation on the Yb clusters. A low intensity emission band appears in irradiated samples at 390 nm that can be attributed to Yb^{2+}. Finally, the decrease of the Yb^{3+} fluorescence lifetime observed under irradiation appears to be primarily due to electronic interaction of these ions with Non-Bridging Oxygen Hole Centre defects created by the ionizing radiation.

© 2010 Elsevier B.V. All rights reserved.

1. Introduction

Among the rare earth ions Yb^{3+}, owing to its unusual energy level scheme with only two manifolds separated by about 10,000 cm^{-1}, offers interesting spectroscopic properties for optical applications such as absence of excited state absorption and relatively long emission lifetime. A wide range of oxide glasses including phosphates, borates and silicates doped with Yb^{3+} has been explored for high power laser or amplifier applications [1–4]. Thus, the spectroscopic properties of Yb^{3+} ions in glasses are well documented in the literature and concern the $^7F_{5/2}\rightarrow{}^7F_{7/2}$ transition as well as the visible cooperative luminescence due to the simultaneous de-excitation of two interacting Yb^{3+} ions [3–5].

Many effects on the oxide glass structure under ionizing irradiation were evidenced at high doses close to 1 GGy. These structural changes including increase in glass polymerization and formation of dissolved molecular oxygen formation are linked to the alkaline motion initiated by the HC_1 (≡Si–O° Na^+) defect accumulation [6,7]. Doping glasses with rare earth or transition metal ions tends to lower the extent of such structural modification under irradiation that can be related to an efficient exciton (hole–electron pair) consumption process that involve the reduction of some trivalent rare earth element (REE) or transition metal ions [8–11]. This reduction process under ionizing radiation has been commented on in the literature [8–11] but few studies have been dedicated to track the evolution of the atomic environment around the doping ion under irradiation and to investigate the links between the REE environment in the glass and the stability of the divalent reduced REE. Here, a combination of Nuclear Magnetic Resonance (NMR), Electron Paramagnetic Resonance (EPR) and Photoluminescence (PL) spectroscopic techniques is used to obtain information on the Yb^{3+} environment in Yb-doped aluminoborosilicate glasses. The choice of this matrix type is prompted by a good knowledge of the undoped host aluminoborosilicate glass structure (French nuclear glass) and the fact that structural evolution of this host glass under ionizing irradiation has been reported in the literature [6,7].

Another aim of this study is to understand the relationship between evolution of the structure and the luminescence properties of Yb^{3+} ions under irradiation. Indeed, a lot of glass optical properties can be modified under ionizing irradiation (refractive index, laser efficiency...) [12,13] and it can be important to understand the behavior of the luminescence properties of rare earth element doped optical fiber in a radiative environment (space...).

* Corresponding author. Tel.: +33 1 69 33 45 18; fax: +33 1 69 33 45 54.
E-mail address: nadege.ollier@polytechnique.edu (N. Ollier).

0022-3093/$ – see front matter © 2010 Elsevier B.V. All rights reserved.
doi:10.1016/j.jnoncrysol.2010.11.041

Author's personal copy

2. Experimental details

The synthesis of the aluminoborosilicate glasses studied here was detailed in a previous paper [14]. Concerning the glass composition, the SiO_2 content is about 65 mol%, B_2O_3 17 mol%, Al_2O_3 4.1 mol%, Na_2O 13.6 mol% and the Yb-doping concentration ranges between 0.05 and 1 mol% of Yb_2O_3 (Yb is substituted for part of all the host glass constituents). The glass samples are designated according to their Yb content as Yb005, Yb01, Yb02, Yb05 and Yb1 corresponding to 0.05, 0.1, 0.2, 0.5 and 1 mol% Yb_2O_3, respectively. The glasses were analyzed by Raman spectroscopy and all showed an amorphous character.

All glasses were irradiated with 2.3 MeV electrons produced by a Van de Graaff accelerator (LSI, Laboratoire des Solides Irradiés, France) at different doses between 6×10^5 and 2.6×10^9 Gy. The glasses obtained by splat quenching were then cut to obtain a thickness less than 700 μm to allow a homogeneous irradiation in the glass volume; the sample temperature did not exceed 50 °C. Gamma irradiations were performed with a ^{60}Co source at room temperature with a dose rate of 87 Gy/min (CNSTN, Centre National des Sciences et Technologies Nucléaires, Sidi-Thabet, Tunisia). Three doses were reached: 10, 100 and 1000 KGy.

The cw-EPR spectra were collected with an EMX Bruker spectrometer operating in the X-band (9.420 GHz) using 100 kHz field modulation, 3 Gauss of amplitude modulation and an applied microwave power of 1 mW. All spectra were collected at 10 K using a He flow Oxford cryostat and were normalized to the same receiver gain and to 1 mg sample weight.

Two-dimensional pulsed EPR hyperfine shift correlation (HYSCORE) spectroscopy was carried out to investigate in further detail the atomic makeup of the local coordination environment of the Yb^{3+} ions in Yb05 and Yb1 glasses. HYSCORE is a four-pulse version of the familiar electron spin echo envelope modulation technique (ESEEM) which has been used successfully to study the hyperfine interactions between electrons and nearby nuclides with non-zero spin in rare earth doped glasses [14,15]. The pulse sequence $\pi/2$–τ–$\pi/2$–t_1–π–t_2–$\pi/2$-*echo* is typically used for HYSCORE measurements. The preparation interval τ between the first two $\pi/2$ pulses creates the nuclear coherence between the sublevels of the electron–nuclear spin manifolds. The populations of these manifolds are exchanged by the π pulse after the evolution period t_1. The resulting correlation between the corresponding nuclear transitions is detected with a $\pi/2$ pulse after a time t_2 in the form of an echo [17,18].

The HYSCORE measurements on the Yb05 and Yb1 glasses were carried out at 5.5 K with a commercial Bruker ELEXSYS pulsed EPR spectrometer operating in the Q-band equipped with a liquid He Oxford cryostat. Measurements were made at a magnetic field of 0.9 T. A π-pulse length of 24 ns and a $\pi/2$-pulse length of 12 ns were used. An eight-step phase cycle was applied in order to avoid any unwanted echo. Starting values of t_1 and t_2 in the pulse sequence were 96 ns. The time increment in both dimensions was chosen to be 16 ns at various τ values. Two-dimensional fast Fourier transformation was used to obtain the HYSCORE spectra from the time-domain data.

^{29}Si magic-angle-spinning (MAS) NMR spectra were collected at a magnetic field of 11.7 T (resonance frequency of 99.16 MHz) using a Bruker Avance II 500WB spectrometer and a 4 mm Bruker MAS probe. Samples were spun at 12.5 kHz in ZrO_2 rotors. Rotor-synchronized Carr–Purcell–Meiboom–Gill (CPMG) train of refocusing pulses has been used in order to increase the ^{29}Si NMR signal to noise ratio [19]. The acquired spin echoes (20 echoes) were averaged and Fourier transformed to obtain each spectrum. ^{29}Si MAS NMR spectra were collected with variable recycle delays of 0.2 s, 2 s, 20 s and 200 s to investigate the existence of any differential relaxation in the ^{29}Si NMR spectra [20].

PL spectra were acquired with the aid of a Jobin Yvon HRS2 monochromator, a photomultiplier and a lock-in amplifier. Photo-excitation was provided by an argon pumped CW Ti:Sapphire laser. All the emission spectra were corrected for the monochromator and the detector response, the calibration was done with a blackbody source. The Yb^{2+} emission was measured under a 325 nm He–Cd laser excitation at 20 K. The fluorescence decay measurements were performed by exciting the samples with a Q-switched Nd:YAG pumped OPO (optical parametric oscillator) laser and by collecting and analyzing the signals with an Oriel monochromator, a photomultiplier and a digital oscilloscope. Complementary PL experiments were also performed by exciting the samples at room temperature with the 532 and 266 nm radiations of another frequency-doubled and frequency-quadrupled Nd:YAG laser, respectively. In this case, the luminescence was analysed by a SHAMROCK spectrograph (F = 303 mm) combined with an ANDOR Istar Intensified Charge-Coupled Device (ICCD).

3. Results

3.1. Pristine glasses

The Yb^{3+} cw-EPR spectra of Yb005 and Yb1 glasses are reported in Fig. 1a. The line shapes are clearly different, showing a g parameter equalling to 3.30 and 3.17 for the Yb005 and Yb1 glasses, respectively. In addition a resonance at g≈9 (denoted as g1 in the subsequent discussion) is observed in the spectra of both glasses. The cw-EPR spectrum of the YB005 glass also shows a resonance at g≈4 corresponding to Fe^{3+} impurities in this sample. A possible explanation for the resonance at g≈9 is that it is related to the presence of Fe^{3+}

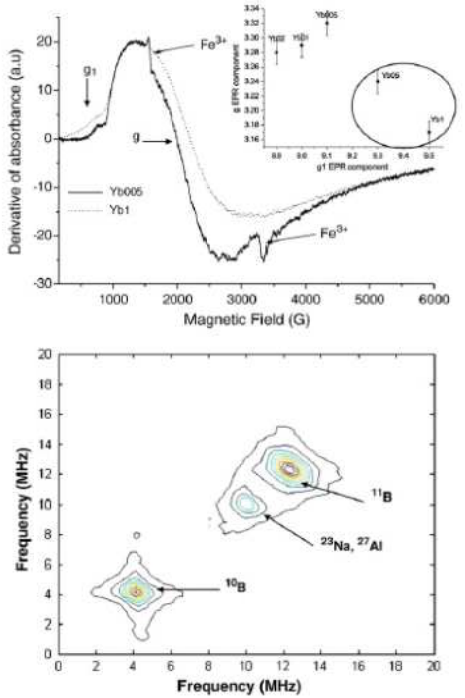


Fig. 1. (a) cw-EPR spectra of Yb005 and Yb1 glasses. Inset: evolution of the g parameter as a function of the g1 parameter in glasses with different Yb concentration. (b) Contour plot of the 2D-HYSCORE spectrum for Yb05 glass (see text for details).

Author's personal copy

impurities in the sample for which the main resonance is located at $g \approx 4$. In this scenario, the resonance at $g \approx 9$ can be attributed to Fe^{3+} in a low symmetry environment, where the zero field splitting parameters D and E are such that E/D~1/3 and D>>hν, the microwave quantum energy. In these situations the $g \approx 4$ resonance is always associated with resonances around $g \approx 9$, arising from the other Kramers doublets of the $S = 5/2$ spin system of Fe^{3+} [21]. However, such a hypothesis is not tenable for the EPR spectrum of the Yb1 sample where the $g \approx 9$ resonance is quite strong while the $g \approx 4$ resonance is not apparent in the EPR spectrum (Fig. 1). Moreover, we have often observed the $g \approx 9$ resonance in Yb-doped glass samples made with ultra high purity ingredients where no Fe^{3+} is detectable in chemical analyses and neither is the $g \approx 4$ resonance.

An alternative and more plausible explanation for the $g \approx 9$ resonance is related to the fact that Yb^{3+} is a Kramers ion with $S = 1/2$ and is therefore not expected to have any zero field splitting [22]. Theoretically the g value for Yb^{3+} cannot exceed $2\Lambda * M$, where M is the maximum value of the projection of the full angular momentum, and Λ is the Lande factor for Yb^{3+} [22]. The main term for Yb^{3+} is $^2F_{7/2}$, which yields values for $\Lambda = 8/7$ and hence for $g_{max} \approx 8$. This statement is valid for even isotopes of Yb (Yb^{168}, Yb^{170}, Yb^{172}, Yb^{174} and Yb^{176}) that have ~70% of the total natural abundance [23]. Therefore, the only reasonable explanation for the observation of EPR signal at $g \approx 9$ in these glasses is the existence of pairs or more complex clusters of Yb^{3+} ions that can behave like non-Kramers systems with $S > 1 = 2$ [24]. This resonance is denoted as g1 in the subsequent discussion. It is interesting to note that Yb1 and Yb005 glasses can be distinguished from other glass compositions according to their g and g1 values (Fig. 1, inset). The non-linear dependence of the g and g1 parameters on the Yb-doping level can be attributed to an abrupt change in the Yb^{3+} site symmetry as a function of Yb-doping level or to the presence of multiple sites with a variable proportion between sites as a function of the Yb concentration.

The HYSCORE spectra for the glass samples Yb05 and Yb1 collected at a magnetic field of 0.9 T are practically identical and only the spectrum of the Yb05 sample is shown in Fig. 1b. There are no off-diagonal cross peaks that are visible in the spectrum. The three diagonal peaks correspond well with the nuclear Larmor frequencies ν_L of the nuclides ^{10}B (natural abundance ~20%, $\nu_L = 4.1$ MHz), ^{11}B (natural abundance ~80%, $\nu_L = 12.3$ MHz), ^{27}Al (natural abundance 100%, $\nu_L = 10$ MHz) and ^{23}Na (natural abundance 100%, $\nu_L = 10.1$ MHz) at the experimental magnetic field of 0.9 T. The absence of any diagonal peak in the HYSCORE spectrum corresponding to the Larmor frequency of the ^{29}Si nuclides (~7.6 MHz) is not surprising considering the low natural abundance (~4.7%) of this nuclide. Moreover, short relaxation time of Yb is expected to preclude direct observation of neighboring ^{171}Yb and ^{173}Yb nuclides, if any, in the HYSCORE spectrum. Sole presence of diagonal peaks in the HYSCORE spectrum implies that the hyperfine interaction between the Yb^{3+} electrons and the X (X = B, Al and Na) nuclides satisfies the weak-coupling conditions and suggests the presence of X nuclides in the next-nearest neighbor coordination shell of Yb [15,16].

Differential spin-lattice relaxation analysis of the ^{29}Si MAS spectra has been carried out in order to probe the different silicon environments with respect to the Yb neighborhood. This method is based on the fact that the main mechanism of spin-lattice relaxation of ^{29}Si, a dilute spin ½ with low natural abundance, is due to dipolar coupling between the ^{29}Si nuclear spin and the electronic spins of the paramagnetic species i.e. Yb^{3+}. The closer the silicon atom is to the Yb^{3+} ion, the faster is the spin-lattice relaxation. Here, ^{29}Si NMR MAS spectra have been acquired with recycle delays ranging between 0.2 and 200 s. Spectra acquired with 0.2 s delay are dominated by silicon species close to Yb^{3+} ions whereas those acquired with a delay of 200 s allow signal from all Si sites to be detected. Difference (if any) in the two spectra will be indicative of heterogeneity of the spatial distribution of Yb^{3+} in the glass structure. For each sample the 0.2 s spectrum was fitted to a single Gaussian with Lorentzian broadening, as expected from strong dipolar coupling with paramagnetic Yb^{3+}, yielding the Si(Yb) sub-spectra (Fig. 2). Then 2 s, 20 s and 200 s spectra were fitted using two components including the Si(Yb) component with unchanged line shape parameters, as displayed in Fig. 2 (inset). Only a small chemical shift difference was observed between the Si and Si(Yb) sites whereas the Full Width at Half Maximum were about 20 and 40 ppm for Si and Si(Yb), respectively. Fig. 2 shows the portion of the Si(Yb) component that corresponds to the fast-relaxing Si component as a function of the Yb-doping concentration. The Si(Yb) fraction increases nearly linearly with increasing Yb concentration of up to 0.5 mol% Yb_2O_3, as would be expected from a random distribution of Yb^{3+} ions. However, the concentration of the Si(Yb) fraction saturates in the Yb05 and Yb1 glasses implying clustering of a fraction of Yb^{3+} ions at the highest Yb_2O_3 concentrations.

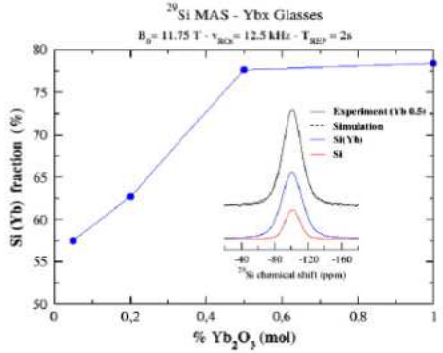


Fig. 2. Variation of the fast-relaxing Si component (denoted Si(Yb)) with respect to the glass composition. Inset: deconvolution of the ^{29}Si MAS NMR spectrum of Yb05 glass with a long (denoted Si) and a short relaxation time component (denoted Si(Yb)).

Fig. 3 displays the $^7F_{5/2} \rightarrow {}^7F_{7/2}$ infrared emission spectra of Yb^{3+} for different Yb concentrations ranging between 0.05 and 1 Yb_2O_3 mol%. Four bands at approximately 970, 1000, 1017 and 1060 nm can be assigned to the transitions from the first level of the $^7F_{5/2}$ manifold to the $^7F_{7/2}$ ground state. A systematic evolution of the emission band

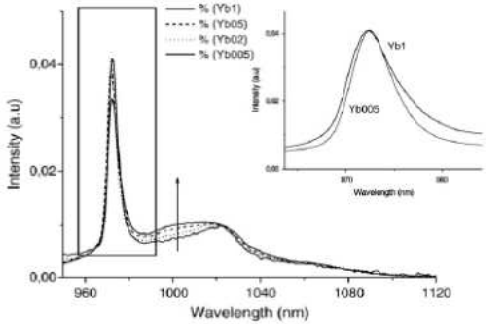


Fig. 3. $^7F_{5/2} \rightarrow {}^7F_{7/2}$ emission band of Yb^{3+} as a function of Yb concentration (spectra normalized to the 1020 nm band).

Table 1
$^7F5/2$ lifetime values (ms) for emission monitored at 1020 nm as a function of the Yb concentration.

Samples	Lifetime (ms) (1020 nm)
Yb005	1.20 ± 0.06
Yb01	1.28 ± 0.06
Yb02	1.29 ± 0.06
Yb05	0.55 ± 0.03 and 1.34 ± 0.06
Yb1	1 ± 0.05 and 1.31 ± 0.06

shape can be noticed as a function of Yb content. More precisely, the relative intensity of the 0→1 (1000 nm) transition increases and that of the 0→2 (1020 nm) transition decreases with increasing Yb concentration (Fig. 3). Moreover, a zoom of the 0→0 transition (see inset) evidences an obvious band broadening for the highest Yb concentration (Yb1) compared to the lowest (Yb005). These effects of Yb concentration on the emission band shape can be connected with an Yb^{3+} ligand field modification. The lifetimes of $^7F_{5/2}$ state are given in Table 1. Up to 0.2 mol%, the values are directly extracted from the single-exponential decay curves. The lifetime (~1.2 ms) does not vary significantly with the Yb concentration suggesting the absence of radiative energy transfer (due to the dopant increasing concentration) or non-radiative energy transfer (due to interaction with defects or impurity) [25]. The decay for the emission monitored at 1020 nm for the two samples with the highest Yb_2O_3 concentrations of 0.5 and 1 mol% is non-exponential that can be simulated with two exponentials, one with a significantly shorter lifetime compared to the other (Table 1).

A sensitive analysis for detecting the presence of Yb cluster in the glass is the cooperative luminescence. The cooperative luminescence is resulting from the simultaneous de-excitation of two interacting Yb^{3+} ions giving rise to the emission of one single visible photon around 500 nm. This emission efficiency is very low. This process relies on Coulombian interaction and thus shows a strong dependence on Yb^{3+}–Yb^{3+} distances [26,27]. Fig. 4 displays the visible emission of Yb-doped glasses under a 975 nm excitation. A broad and visible emission band centred around 510 nm is observed only for Yb concentration higher than 0.2 mol% (Fig. 4). Due to the shape and the position of this visible emission, it is attributed to a cooperative effect. Moreover, its intensity increases with the Yb concentration. Our interpretation is supported by a lifetime measurement on Yb1 glass, the visible emission lifetime is half the IR one (0.50 ms) [28].

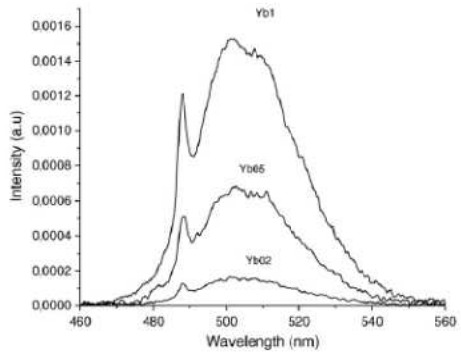


Fig. 4. The visible cooperative emission obtained under a 980 nm excitation in three Yb-doped glass compositions: Yb02, Yb05 and Yb1.

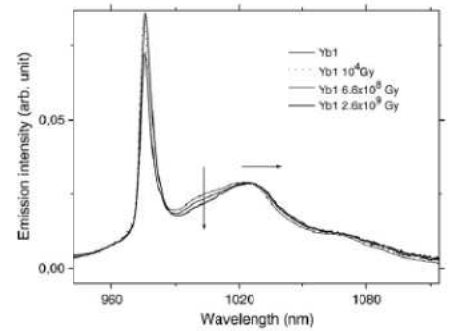


Fig. 5. $^7F5/2 \rightarrow {}^7F7/2$ emission band of Yb^{3+} in Yb1 glasses irradiated at different doses (spectra normalized to the 1020 nm band).

3.2. Irradiated glasses

A systematic evolution in the infrared emission band shape is observed with irradiation at high integrated doses in Yb05 and Yb1 glasses. Such an evolution is displayed in Fig. 5 for Yb1 where the relative intensity of the 1000 nm component decreases with irradiation for doses higher than 10^8 Gy only. The area of this emission band is found to decrease with the decrease in lifetime for the Yb1 glass sample as shown in Table 2. Even though self-absorption effects can make a quantitative estimation of the IR emission intensity difficult, a good correlation is observed between the luminescence intensity and the lifetime. The $^2F_{5/2}$ lifetime values as a function of the logarithm of irradiation dose are reported for three glass compositions in Fig. 6. The decay curves of the irradiated samples remain single exponential for low Yb-concentrations and *become* single exponential for higher doping levels under radiation. We can observe in Fig. 6 a decrease of the lifetime with the irradiation dose without any saturation effect. All glasses doped with less than 0.5 mol% Yb_2O_3 exhibit similar lifetime values (except for the highest dose) and similar variations in lifetime with increasing irradiation dose. On the other hand, compared to these glasses with low Yb concentration the Yb1 glass can be distinguished with much lower lifetimes (Fig. 6). For both categories, we can notice a two-step variation: for doses lower than 10^7 Gy (gamma irradiation), irradiation causes a slight decrease of the lifetime without any significant dose effect and for higher values (electron irradiation) a linear decrease of the lifetime is observed. This dose effect can either be connected to the dose range values or to the dose rate. Indeed, doses lower than 10^7 Gy are dominantly obtained by gamma irradiation and the dose rate operating during gamma irradiation is several orders of magnitude lower than the one used with electron irradiation.

Table 2
Comparison of the area of the $^7F5/2 \rightarrow {}^7F7/2$ emission band and lifetime evolutions under irradiation for the Yb1 glass sample. The columns on the left show the ratio between the non-irradiated Yb1 glass and the irradiated glasses at different doses.

Sample	Area	Lifetime (ms)	Area ratio irradiated/ non-irradiated	Lifetime ratio irradiated/ non-irradiated
Yb1	6.00	1.08 ± 0.05	1	1
Yb1 10 kGy	4.08	0.95 ± 0.05	0.68	0.88
Yb1 6×10^4 Gy	3.39	0.73 ± 0.04	0.57	0.67
Yb1 3.3×10^8 Gy	3.44	0.73 ± 0.04	0.57	0.67
Yb1 6.6×10^8 Gy	3.73	0.61 ± 0.03	0.62	0.56
Yb1 2.6×10^9 Gy	3.06	0.43 ± 0.02	0.51	0.40

Author's personal copy

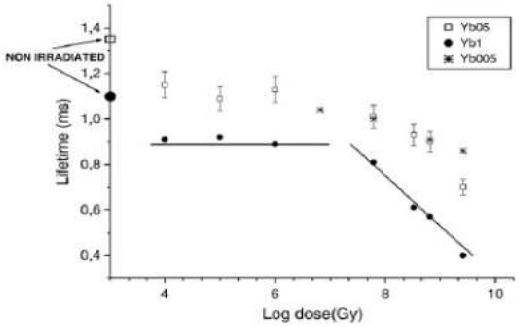


Fig. 6. $^7F5/2$ lifetimes of Yb^{3+} in Yb005 (stars), Yb05 (open squares) and Yb1 (filled circles) glasses as a function of the dose logarithm.

Luminescence spectra in the 350–450 nm region obtained under 325 nm excitation at 20 K are presented in Fig. 7. A narrow band of low intensity is observed at 390 nm. This band is detected only at low temperature in Yb-doped irradiated glasses. This band is assigned to the $4f^{13}5d \rightarrow 4f^{14}$ emission of Yb^{2+}. This assumption is supported by the fact that this band is not observed in the undoped irradiated glass. Usually, Yb^{2+} ions give rise to an emission band situated between 350 and 480 nm in crystals, depending on the nature of the host lattice [29,30].

3.3. Thermal annealing treatments

Three irradiated glass samples (Yb02 and Yb1 10^7 Gy; Yb1 $1.8 10^9$ Gy) were thermally annealed at successive temperatures ranging between 100 °C and 463 °C for 600 s.

Fluorescence lifetimes of the three annealed samples are presented in Table 3. It is important to mention that after annealing at 433 °C or 463 °C, the EPR spectra in the region corresponding to $g = 2$ becomes flat, indicating the recovery of the paramagnetic point defects (Fig. 8). It is interesting to note that the lifetime of the annealed glasses increases compared to the irradiated ones and reaches values close to that found with the non-irradiated glasses, except for the Yb1 glass irradiated at 1.8×10^9 Gy. For this sample, the Yb^{3+} lifetime obtained after annealing increases from 0.46 to 0.77 ms; this value is lower, however, than 1.1 ms

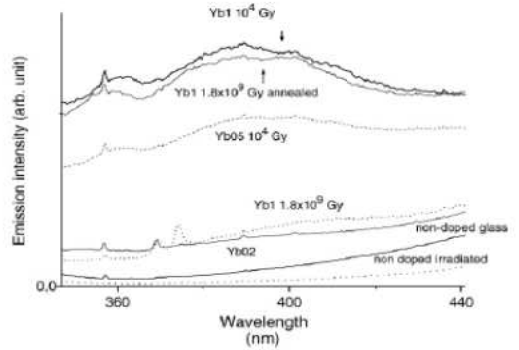


Fig. 7. Photoluminescence spectra of Yb-doped and Yb-free (undoped) glasses irradiated at different doses, obtained using 325 nm excitation at 20 K.

Table 3
$^7F5/2$ lifetimes (ms) of irradiated glasses and of the corresponding annealed glass samples. The number into brackets corresponds to the annealing temperature.

	Yb1 1.8×10^9 Gy	Yb1 10^7 Gy	Yb02 10^7 Gy
Glass	0.46 ± 0.02	0.86 ± 0.04	1 ± 0.05
Annealed glass	0.77 (463 °C) ± 0.04	0.98 (433 °C) ± 0.05	1.2 (433 °C) ± 0.06
Non-irradiated glass	1.1 ± 0.05	1.1 ± 0.05	1.28 ± 0.06

(corresponding to the non-irradiated glass). In order to better understand the lifetime evolution under irradiation, complementary PL experiments were performed. Emission spectra of different glasses excited at 532 nm are displayed in Fig. 9. It shows a broad band centred at 645 nm (1.92 eV). This band appears only in irradiated glasses and for integrated doses higher than 5×10^7 Gy suggesting an obvious link to an irradiation defect. The attribution of this band to Yb^{2+} can be rejected because it appears also in non-doped aluminoborosilicate irradiated glasses. According to its position and shape, we assume that this band can be associated with Non-Bridging Oxygen Hole Centre (NBOHC) defects [31,32]. This common defect in silica glass corresponds to an oxygen dangling bond (≡Si–O°); it is generated by a bond cleavage under ionizing radiation from a Si–O site (intrinsic process) or O–H of O–O bonds (extrinsic process) [32]. Fig. 9 also shows that the NBOHC defects in the Yb1 sample irradiated at 1.8×10^9 Gy are only partially removed via annealing at 460 °C.

4. Discussion

4.1. Yb environment in pristine glasses

The systematic dependence of the EPR spectra and of the $^7F_{5/2} \rightarrow {}^7F_{7/2}$ infrared emission bands of Yb^{3+} on Yb-dopant concentration (Figs. 1 and 3) is consistent with the presence of two different types of Yb^{3+} sites in this glass, especially at high Yb concentration. It is well known that the nature of the next-nearest neighbors surrounding the Yb^{3+} ions (B, Si or Al or other Yb) can influence the Yb–O bond characteristics and the crystal field strength. According to the Yb^{3+} ligand field and the nature of the glass, the 1 and 2 Stark levels of the $^7F_{7/2}$ ground state can be more or less distant. As a consequence, 3 or 4 components can be observed in the emission band [26]. The emission spectrum of Yb05 and Yb1 samples could result from the sum of one 4-component emission spectrum and one 3-component emission spectrum corresponding to the two Yb^{3+} sites.

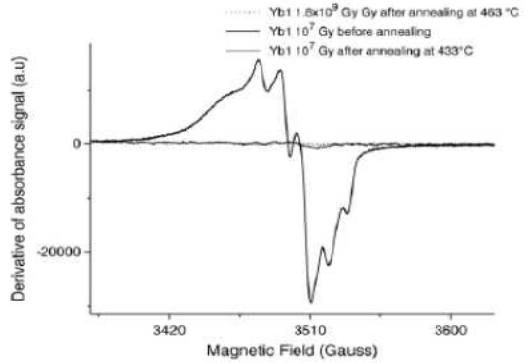


Fig. 8. EPR spectra in the region corresponding to $g = 2$ (defects) of the Yb1 irradiated at 10^7 Gy before and after annealing at 433 °C and irradiated at 1.8×10^9 Gy after annealing at 463 °C showing the recovery of the paramagnetic defects.

Author's personal copy

Cooperative luminescence measurements indicate clearly the presence of Yb cluster in Yb05 and Yb1 glasses. The presence of Yb as next-nearest neighbors would imply formation of Yb–O–Yb linkages i.e. clustering of Yb^{3+} ions. Clustering would increase the dipolar coupling between Yb^{3+} ions and consequently the line width in the EPR spectra is expected to increase with increasing Yb concentration. Indeed such an increase in the EPR line width with increasing Yb concentration is clearly observed in Fig. 1. The clustering scenario is also supported by the lifetime measurements. Bi-exponential decay curves are observed around 1020 nm for the Yb05 and Yb1 glasses with a fast decaying component that possibly corresponds to non-radiative energy transfer between the Yb next-nearest neighbors. Moreover, the saturation of the concentration of the Si sites with neighboring Yb^{3+} ions in the ^{29}Si MAS NMR spectra of Yb05 and Yb1 glasses implies clustering of a fraction of Yb^{3+} ions at the highest Yb_2O_3 concentrations. Such clustering of the doping rare earth ions even at doping levels of a few hundred to a few thousand parts per million (ppm) by weight is well documented in the literature and is believed to result from their low solubility in SiO_2-rich glasses [15,16,27,33].

4.2. Evolution under irradiation

At high irradiation doses (more than 10^8 Gy), the shape of the $^7F_{5/2} \rightarrow {}^7F_{7/2}$ infrared emission band evolves with a diminishing contribution of the 1000 nm component with increasing dose (Fig. 4). This effect is more pronounced in glasses doped with the highest Yb concentration where this component is stronger and according to the discussion in the previous section, this component can be attributed to Yb sites with Yb next-nearest neighbors.

This result is totally in agreement with the evolution of the cooperative luminescence under irradiation. Fig. 10 displays a strong decrease of the cooperative luminescence with the irradiation, without any clear correlation between the integrated dose and the decrease intensity.

Therefore the decreasing contribution from the luminescence bands (IR and visible) implies the breaking up of the Yb clusters and re-homogenization of the spatial distribution of Yb^{3+} ions upon increasing radiation dose. Another possible explanation of this phenomenon can be provided in terms of different reduction efficiency of isolated and clustered Yb^{3+} sites. In this scenario the Yb^{3+} ions in a clustered environment tend to be reduced more efficiently than isolated Yb^{3+} sites. This hypothesis seems to be more relevant because of the cooperative luminescence behavior; the important decrease at low irradiation dose indicates an efficient reduction

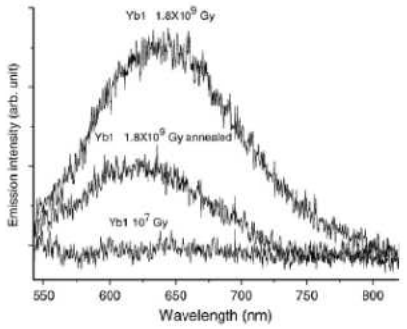


Fig. 9. Photoluminescence spectra of Yb1 glass irradiated at 1.8×10^9 Gy (unannealed and annealed) and at 10^7 Gy. These spectra were obtained using 532 nm excitation at room temperature.

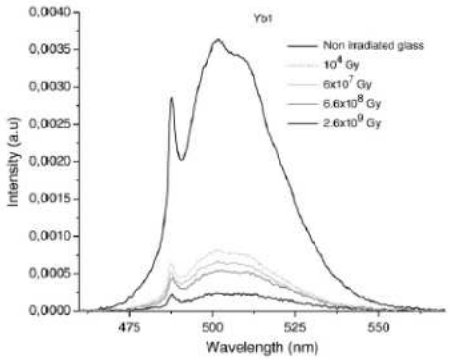


Fig. 10. Evolution of the cooperative emission of Yb1 glass under irradiation.

process into the clustered sites. This interpretation is supported by Kaczmarek et al. [34] who evidenced the formation of Yb^{3+}–Yb^{2+} pairs in CaF_2 single crystals under gamma irradiation.

Concerning the detection of Yb^{2+} centres Yb05 and Yb1 glass samples do not seem to give rise to a more intense emission band of Yb^{2+} than other glasses. However, the intensity of the emission cannot be directly associated to the amount of Yb^{2+}. Thermal quenching can occur even at 4 K and the quenching of the Yb^{2+} emission has been reported in different materials such as silicate, by Lizzo et al. [30], due to the proximity of the 5d levels to the conduction band. Moreover, the stability of the divalent Yb formed under radiation is suspected to be limited, all these parameters complicate the Yb^{2+} quantitative estimation and future XANES experiments are planned to quantify the Yb^{3+} reduction.

Besides the emission band shape variation, irradiation also results in an efficient decrease of the Yb^{3+} $^7F_{5/2}$ lifetime irrespective of the Yb concentration. This effect is more pronounced in the Yb1 glass that presents the lowest lifetime values. The lifetime decrease may result from an energy transfer from excited Yb^{3+} ions to acceptors in the irradiated host matrix. Among the species formed under irradiation that could play the role of acceptors, we can suspect Yb^{2+} ions resulting from the electron trapping on Yb^{3+} [14] and point defects. The divalent Yb^{2+} ion shows $4f \rightarrow 4f5d$ absorption bands in the UV part of the spectrum [30]. Hence, there is no spectral overlap between the emission of the donor and the absorption of the acceptor, thus reducing the energy transfer probability. Point defects created under irradiation are therefore the best candidates to explain the lifetime modification. The decay curves of the irradiated glasses are purely exponential; this result indicates that the non-radiative interaction term does not depend on the distance between donors and acceptors [35]. Polman and Poate studied the Er^{3+} lifetime change caused by ion irradiation damage in silica glasses [35]. They analysed the lifetime changes in terms of non-radiative energy transfers caused by defect creation and proposed a model assuming an inverse relation between the non-radiative lifetime and the defect density.

Paramagnetic point defects created by high-energy electron in our aluminoborosilicate glasses are mainly holes trapped at oxygen [36]. In Yb-doped glasses a strong anticorrelation between the Yb concentration and the defect concentration was pointed out in [14]. Moreover, for low Yb-doping levels (under 0.2 mol%), the defect number versus the dose logarithm shows a quasi-linear increase [16]. This trend is not reproducible for the highest irradiation doses and Yb concentrations (Yb05 and Yb1 glasses) for which the slope is rather low.

Author's personal copy

To explain the lifetime decrease of Yb^{3+} caused by the defect creation, different hypotheses can be advanced. First, the defect repartition inside the irradiated matrix may be not homogeneous generating possible multi-interaction between the Yb^{3+} ions with defects. Secondly, the increase of paramagnetic defects described in Ref. [14] concerns the whole paramagnetic signal around $g=2$ that contains all defect species. However, each species can show a different trend as a function of the Yb concentration. For example, the Oxy/BOHC (Boron Oxygen Hole Centre) ratio is increasing with the Yb concentration [16], so that a preferential interaction between the Oxy defects and the Yb^{3+} ions could be suspected. Finally, an interaction with diamagnetic defects such as Oxygen Deficient Centres (ODCs) cannot be excluded [31].

Finally, the annealing experiments bring an interesting result that must be taken into account to explain the lifetime evolution under irradiation. The original lifetime of the pristine glasses is nearly reached after annealing except for the sample irradiated at the highest dose. For this dose, some NBOHC defects were detected by photoluminescence measurements. Those measurements confirm also the presence of NBOHC in the sample annealed at 453 °C. The persistence of the Yb^{3+} lifetime quenching in the annealed sample could thus be explained by the presence of these NBOHC defects. A dose threshold around 5×10^7 Gy was evidenced for the NBOHC emission band detection. This result can be also correlated to the lifetime evolution under irradiation. The lifetime decrease observed under 5×10^7 Gy is quite low compared to that at higher doses, indicating that NBOHC defects among all irradiation defects could play a predominant role in the lifetime quenching in Yb-doped glasses under irradiation.

5. Conclusion

The Yb^{3+} ion environment in irradiated glasses has been probed by using PL, EPR and NMR spectroscopic techniques. The results, when taken together, indicate the presence of two distinct types of Yb^{3+} sites in the glasses doped with 0.5 and 1 mol% of Yb_2O_3 that correspond to isolated and clustered Yb. The isolated sites are characterized by the absence of any Yb–O–Yb linkages while their presence results in clustered sites. At high irradiation dose, the evolution of the $^7F_{7/2}\rightarrow{}^7F_{5/2}$ IR emission band and visible emission band due to the Yb pairs were interpreted as a preferential reduction of the clustered Yb^{3+} ions in Yb–O–Yb linkages. A strong lifetime quenching effect on Yb^{3+} ions is observed in irradiated glasses that can be interpreted to be due to the interaction between defects (particularly NBOHC) and the Yb^{3+} ions.

Acknowledgments

The authors are grateful to Khaled Farah for gamma irradiations and Vincent Métayer for his contribution during electron irradiation.

References

[1] J. Kirchhof, S. Unger, A. Schwuchow, S. Grimm, V. Reichel, J. Non-Cryst. Solids 352 (2006) 2399.
[2] X. Zou, H. Toratani, Phys. Rev. B 52 (1995) 15889.
[3] M.J.V. Bell, W.G. Quirino, S.L. Oliveira, D.F. de Sousa, L.A.O. Nunes, J. Phys. Cond. Matter 15 (2003) 4877.
[4] Y. Chen, Y. Huang, Z. Luo, Chem. Phys. Lett. 382 (2003) 481.
[5] B. Schaudel, P. Goldner, M. Prassas, F. Auzel, J. Alloy. Comp. 300–301 (2000) 443.
[6] B. Boizot, N. Ollier, F. Olivier, D. Ghaleb, G. Petite, E. Malchukova, Nucl. Instrum. Meth. Phys. Res. B 240 (2005) 146.
[7] N. Ollier, T. Charpentier, B. Boizot, G. Petite, J. Phys. Cond. Matter 16 (2004) 7625.
[8] E. Malchukova, B. Boizot, G. Petite, D. Ghaleb, J. Non-Cryst. Solids 353 (2007) 2397.
[9] F.Y. Olivier, B. Boizot, D. Ghaleb, G. Petite, J. Non-Cryst. Solids 351 (2005) 1061.
[10] H. Ebendorff-Heidepriem, D. Ehrt, Opt. Mater. 19 (2002) 351.
[11] M. Nogami, K. Suzuki, J. Phys. Chem. B 106 (2002) 5395.
[12] A.-S. Jacqueline, B. Ploumellec, J. Non-Cryst. Solids 351 (2005) 1196.
[13] M. Engholm, L. Norin, Opt. Express 16 (2008) 1260.
[14] N. Ollier, R. Planchais, B. Boizot, Nucl. Instrum. Meth. Phys. Res. B 266 (2008) 2854.
[15] S. Sen, R. Rakhmatullin, R. Gubaydullin, A. Poppl, Phys. Rev. B 74 (2006) 100201.
[16] S. Sen, S.B. Orlinskii, R.M. Rakhmatullin, J. Appl. Phys. 89 (2001) 2304.
[17] P. Höfer, A. Grupp, H. Nebenfür, M. Mehring, Chem. Phys. Lett. 132 (1986) 279.
[18] L. Astrakas, Y. Deligiannakis, G. Mitrikas, G. Kordas, J. Chem. Phys. 109 (1998) 8612.
[19] F.H. Larsen, I. Farnan, Chem. Phys. Lett. 357 (2002) 403.
[20] J.F. Stebbins, N. Kim, M.J. Andreajcak, P.M. Boymel, B.K. Zoitos, J. Am. Ceram. 92 (2009) 68.
[21] J.R. Pilbrow, Transition Ion Electron Paramagnetic Resonance, Clarendon Press, Oxford, 1990.
[22] A. Abragam, B. Bleaney, Electron Paramagnetic Resonance of Transition Ions, Clarendon, Oxford, 1970, p. 911.
[23] B.M. Kozyrev, S.A. Al'tshuler, Electron Paramagnetic Resonance in Compounds of Transition Elements, Wiley, New York, 1974, p. 589.
[24] S. Sen, R. Rakhmatullin, R. Gubaydullin, A. Silakov, J. Non-Cryst. Solids 333 (2004) 22.
[25] G. Boulon, L. Laversenne, C. Goutaudier, Y. Guyot, M.T. Cohen-Adad, J. Lumin. 102-103 (2003) 417.
[26] B. Schaudel, PhD thesis (Paris 6 University, 2000).
[27] P. Goldner, B. Schaudel, M. Prassas, Phys. Rev. B 65 (2002) 054103.
[28] E. Nakazawa, E. Shionoya, Phys. Rev. Lett. 25 (1970) 1710.
[29] A. Bensalah, M. Nikl, E. Mihokova, N. Solovieva, A. Vedda, H. Sato, T. Fukuda, G. Boulon, Radiat. Meas. 38 (2004) 545.
[30] S. Lizzo, E.P. Klein Nagelvoort, R. Erens, A. Meijerink, G. Blasse, J. Phys. Chem. Solids 58 (1997) 963.
[31] P.D. Dragic, C.G. Carison, A. Croteau, Opt. Express 16 (2008) 4688.
[32] L. Vaccaro, M. Camas, B. Boizot, A. Parlato, J. Non-Cryst. Solids 353 (2007) 586.
[33] K. Arai, H. Namikawa, K. Kumata, T. Honda, Y. Ishii, T. Handa, J. Appl. Phys. 59 (1986) 3430.
[34] S.M. Kaczmarek, G. Leniec, G. Boulon, J. Alloy. Comp. 451 (2008) 116.
[35] A. Polman, J.M. Poate, J. Appl. Phys. 73 (1993) 1669.
[36] B. Boizot, G. Petite, D. Ghaleb, G. Calas, Nucl. Instrum. Meth. Phys. Res. B 141 (1998) 580.

N. Ollier, V. Pukhkaya

Point defect stability in gamma irradiated aluminoborosilicate glasses: Influence of Yb^{3+} doping ions

Nuclear Instruments and Methods in Physics Research B, 2012 vol. 227, p. 121-125

Author's personal copy

Nuclear Instruments and Methods in Physics Research B 277 (2012) 121–125

Contents lists available at SciVerse ScienceDirect

Nuclear Instruments and Methods in Physics Research B

journal homepage: www.elsevier.com/locate/nimb

Point defect stability in gamma irradiated aluminoborosilicate glasses: Influence of Yb^{3+} doping ions

N. Ollier *, V. Pukhkaya

CEA, IRAMIS, Laboratoire des Solides Irradiés, Ecole Polytechnique, CNRS, 91128 Palaiseau, France

ARTICLE INFO

Article history:
Received 25 October 2011
23 December 2011
Available online 30 December 2011

Keywords:
Irradiation
Glasses
Defects
Relaxation
EPR
Yb

ABSTRACT

Yb-doped aluminoborosilicate were irradiated with gamma rays at 10^4, 10^5, 10^6 and 10^7 Gy. The thermal stability as well as the recovery at room temperature of paramagnetic point defects such as Boron Oxygen Hole Center (BOHC), peroxy radicals and E' center were studied. At first, doping with Yb induced a saturation of the E' defect production and more importantly, the E' center recovering temperature was decreased by 50 °C. E' and BOHC defects both showed a limited stability at room temperature. By doping with Yb the glasses, the fading time of defects and in particular the BOHC defect recovery was modified. The BOHC defect showed moreover a larger sensitivity to photobleaching compared to the E' centers.

Crown Copyright © 2012 Published by Elsevier B.V. All rights reserved.

1. Introduction

Irradiation effect in glasses is an active research field in different domains such as nuclear or optics industry. In particular, a lot of studies have been performed on amorphous silica glass ($aSiO_2$) or phosphate glasses due to many applications requiring a good degree of transparency [1,2]. A large amount of studies using mainly Electron Paramagnetic Resonance (EPR) and optical absorption have been performed over more than 50 years, very recently Griscom published a complete review on point defects in doped $aSiO_2$ and quartz [3].

Doping oxide glasses with transition ions or rare earth element modifies the nature and the content of the different defects produced during ionizing radiation [4,5]. In the case of Sm [6], or Yb [7] doped borosilicate glasses, the doping leads to a decrease of the total paramagnetic defect content produced by high energy electron during irradiation. Associated with this decrease, an attenuation of the different structural changes under irradiation (polymerisation increase, and decrease of Si–O–Si average angle [8], molecular oxygen production [9]) is also observed for integrated doses higher than 10^9 Gy [4,6].

In this paper, we are interested in the defect recovery processes in gamma-irradiated aluminoborosilicate glasses. These recovering aspects are of primary importance in different fields such as dosimetry and, for example, in a more recent activity around recyclable colored glasses [5,10]. The color center decay at room temperature is generally described as a first order or second order kinetics process [11–13]. However, very little data is available on other types of defect than NBOHC (Non-Bridging Oxygen Hole Center) recovery at room temperature, especially in more complex glasses than amorphous silicon dioxide where the influence of doping is poorly considered.

Most of the times, the annealing of defects is studied by applying on the irradiated sample a thermal treatment. For example, the thermal recovery of E' defect in a-SiO_2 has been attributed to the diffusion mechanisms and reactions with molecular diffusing species such as O_2, H_2O or H_2 molecules [14–16]. While the one for one growth of the peroxy radicals in low-OH silica for temperature higher than 150 °C was attributed to the combination of E' center with O_2 ($\equiv Si^{\cdot} + O_2 \rightarrow \equiv Si\text{–}O\text{–}O^{\cdot}$) [14,15], some authors rather infer the role of H_2O in the annealing process of E'_γ defect in amorphous silicon dioxide [16].

The present work is focused on the influence of Yb^{3+} ions on the paramagnetic defect recovery. Yb-doped glasses are matrix of interest in the optical field, used as high power laser fiber. Even if a great deal of work has been done in terms of dose rate and dose influence on defect formation in SiO_2 optical fiber [13], more limited knowledge is available on rare earth element doped SiO_2 and, in particular, in terms of defect stability. However, Er or Yb doped SiO_2 fiber (amplifier or laser materials) can be used in a radiative environment, for spatial application typically and we showed in [17] that the creation of paramagnetic defect can strongly modify luminescent properties such as Yb^{3+} excited state lifetime and cooperative luminescence (assigned to Yb^{3+} pairs). Therefore, these questions of defect stability can be important for doped optical materials properties like Er or Yb doped optical fibers placed in a radiative environment (e.g. space).

* Corresponding author. Tel.: +33 1 69 33 45 18; fax: +33 1 69 33 45 54.
E-mail address: nadege.ollier@polytechnique.edu (N. Ollier).

0168-583X/$ - see front matter Crown Copyright © 2012 Published by Elsevier B.V. All rights reserved.
doi:10.1016/j.nimb.2011.12.053

Author's personal copy

2. Experiments

The synthesis and preparation of the Yb-doped aluminoborosilicate glasses are reported in [17]. The concentration of Yb doping in glasses is ranging between 0.05 mol.% and 1 mol.%. The glasses are designed according to their Yb content as Yb02 for a 0.2 mol.% Yb_2O_3 doped glass. The nominal glass composition is presented in Table 1.

The glass-samples were irradiated at 10^4–10^5–10^6 and 10^7 Gy with a ^{60}Co irradiation facility based in the CNSTN (Sidi-Thabet, Tunisia). All the glass samples were stored in the dark, two samples Yb02 × 10^7 Gy and Yb1 × 10^7 Gy were also exposed to natural light to study the photobleaching.

Table 1
Nominal glass compositions expressed in mol.%

mol.%	Yb005	Yb01	Yb02	Yb05	Yb1
SiO_2	64.97	64.93	64.87	64.67	64.35
Al_2O_3	4.13	4.13	4.12	4.11	4.09
B_2O_3	17.20	17.19	17.17	17.12	17.04
Na_2O	13.66	13.65	13.64	13.59	13.53
Yb_2O_3	0.05	0.10	0.20	0.50	1.00

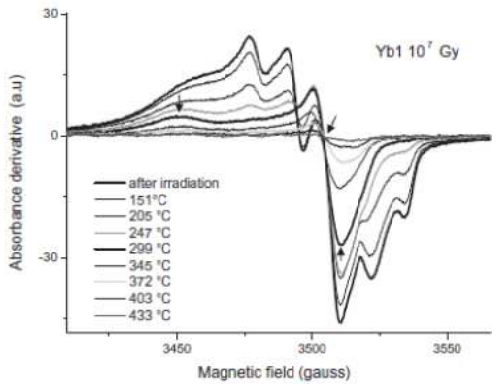


Fig. 1. EPR spectra of the Yb1 glass irradiated at 10^7 y (2 months after irradiation and successive isochronal annealing treatments of 10 mn).

Isochronal thermal treatment of 10 mn in 20 °C increments between 100 and 460 °C were performed on Yb02 and Yb1 glass samples irradiated at 10^7 Gy.

X-band (ν = 9.490 GHz) EPR spectra were recorded at room temperature and 10 K using an EMX Bruker spectrometer. The microwave power 1 mW was used with a 100 kHz modulation of 1G or 3G amplitude. The different EPR spectra presented in this paper have been normalized to the same receiver gain (1.10^4) and sample weight (100 mg) in order to get quantitative comparison of the EPR lines intensities between the different samples. The defect intensity is obtained after a double integration of the normalized derivative of the absorbance signal. We estimate the error on data obtained at room temperature is around 10% and a bit more for low temperature 15%.

3. Results

3.1. Thermal stability

Fig. 1 displays the successive EPR spectra of the Yb1 glass sample irradiated at 10^7 Gy after successive isochronal annealing treatments in the region corresponding to the point defects around $g = 2$, the g value is defined by the relation $h\nu = g\beta H$ (where h is the Plank's constant, ν the spectrometer frequency, β the Borh magneton and H is the applied magnetic field value at resonance). The more intense bold line corresponding to the spectrum before annealing is the signature of different kind of defects [18]. The main component of this EPR spectra is due to the hyperfine interaction with ^{11}B ($I = 3/2$) and corresponds to the Boron Oxygen Hole Center (BOHC) which arises from a hole trapped on one oxygen atom bonded to a boron atom [18,19]. The EPR line of low intensity around 3519G is attributed to the E' center [20]. We can suspect from [18], the presence of another hole center corresponding to Non Bridging Oxygen Hole Center (NBOHC) or peroxy radical (POR) ($Si\text{–}O\text{–}O^{\cdot}$) [21]. As a matter of fact, the spectrum after annealing at 299 °C shows a more simple signal characterized by $g_1 = 2.0030$, $g_2 = 2.0073$ and $g_3 = 2.037$ (indicated by the arrows). NBOHC and POR defects present very similar g parameter [3] but the g_3 value as well as the high recovering temperature higher 350 °C rather indicates a POR defect [21]. The E' center annealing rises to a temperature ranging between 205 and 216 °C while for BOHC the recovering temperature is reached between 263 and 299 °C.

The Fig. 2A displays the E' center concentration evolution as a function of the annealing temperature while the 2B represents

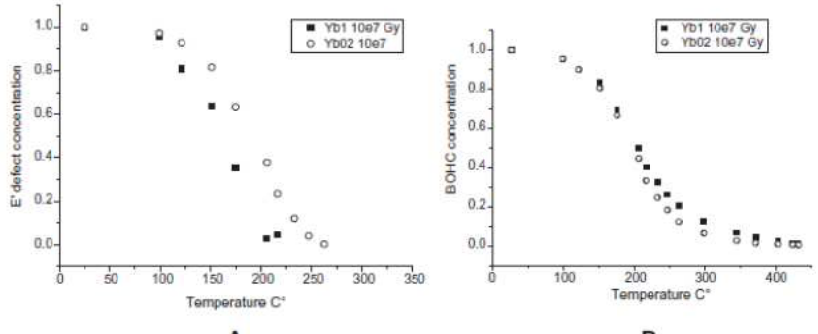


Fig. 2. E' defect concentration normalized to 1 as a function of the annealing temperature in Yb02 and Yb1 glasses both irradiated at 10^7 Gy (A). BOHC defect concentration as a function of the annealing temperature for comparison (B).

Author's personal copy

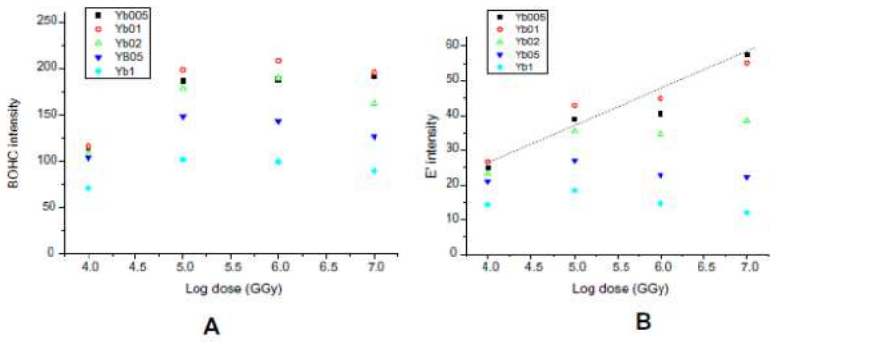


Fig. 3. BOHC defect intensity (A) as a function of the dose logarithm (GGy) and E' center intensity (B) as a function of the dose logarithm (GGy).

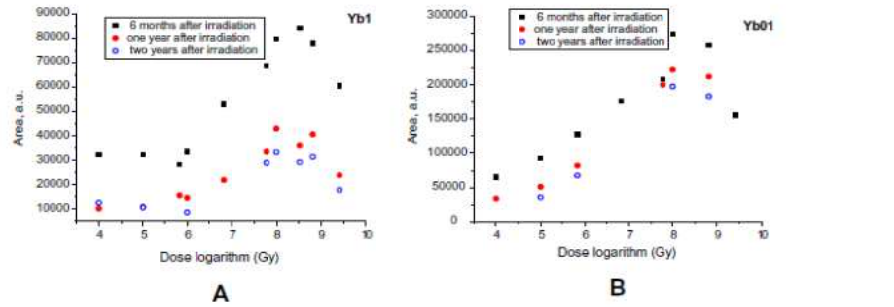


Fig. 4. Paramagnetic defect area as a function of the dose logarithm (GGy) for Yb1 glass (A) and Yb01 glass (B) for different time periods after irradiation.

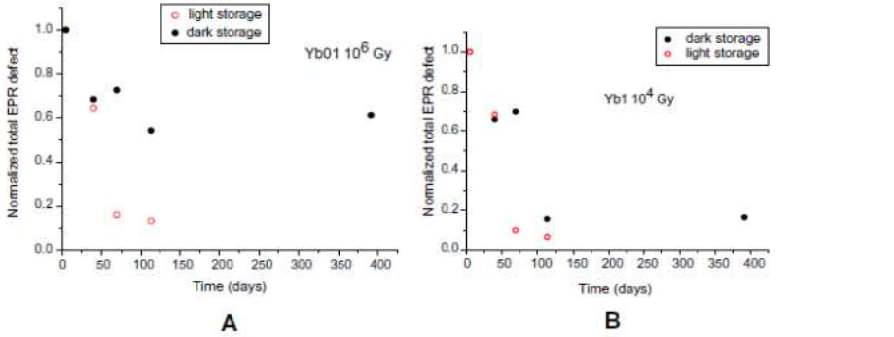


Fig. 5. Paramagnetic defect area normalized to 1 as a function of the time (days) for Yb01 glass irradiated at 10^6 Gy stored in the dark or exposed to the light (A) and paramagnetic defect area normalized to 1 as a function of the time (days) for Yb1 glass irradiated at 10^4 Gy stored in the dark or exposed to the light (A).

the BOHC concentration evolution. The intensity of both defect types has been normalized to 1 for an easier comparison between the samples doped with 0.2 and 1 mol% of Yb_2O_3, respectively. It is interesting to notice that the Yb content influences the E' recovery temperature. For the highest Yb concentration, the temperature is 50 °C lower (~200 °C instead of ~250 °C). The BOHC thermal recovery does not show any dependence on Yb concentration.

Author's personal copy

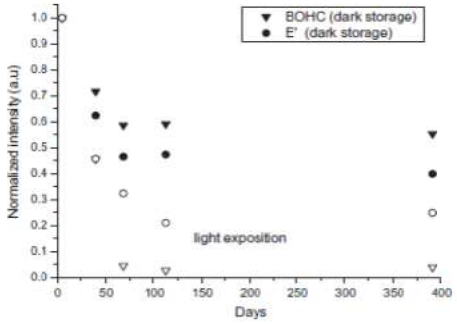


Fig. 6. BOHC and E' defects normalized to 1 as a function of the time (days) for Yb1 glass irradiated at 10^7 Gy stored in the dark or exposed to the light (A).

3.2. Influence of the Yb doping on the paramagnetic defect nature

The Fig. 3 shows respectively the BOHC (Fig. 3A) and the E' (Fig. 3B) concentration as a function of the dose logarithm for different Yb doping concentration. In both cases, doping with Yb obviously leads to a decrease of the total amount of post mortem defect concentration. Moreover, it is interesting to underline that doping with Yb leads to a strong saturation of the E' defects showing a linear increase as a function of the dose logarithm for the low Yb-doping concentration and a saturation when the Yb_2O_3 doping level reaches 0.5 mol.%. For BOHC, the saturation effect with the dose is visible since the lowest Yb concentration (0.05 mol.%).

3.3. Influence of Yb on the defect recovery

The total amount of defects in ABS glasses irradiated over a wide range of doses is plotted in Fig. 4A and B as a function the dose logarithm for Yb1 and Yb01 glasses respectively for different periods of time after irradiation. Both figures include the results obtained from 2.5 MeV electron irradiation at high doses (more than 10^8 Gy), see [7,17]. From these figures, it is obvious that doping the glasses with Yb leads to a lower defect stability.

3.4. Photobleaching

For Yb01 glass composition whatever the integrated dose, the photons from the natural light accelerate the defect recovery (see the example of 10^6 Gy in Fig. 5A). For Yb1 glass, same effect can be noticed excepted for the lowest irradiation dose 10^4 Gy where no difference appears between unlighted and lighted irradiated glasses (Fig. 5B). To analyze in further detail if one type of defect was particularly sensitive to the photobleaching, we plotted the BOHC and E' defect concentration normalized to 1 as a function of time (Fig. 6). We can observe in Fig. 6 (Yb1 glass sample, 10^7 Gy) that photobleaching is more efficient on BOHC defect than on the E' defects. The same result is obtained for a lower Yb concentration (0.1 mol.%).

4. Discussion

The main object of the paper was to analyze the influence of Yb doping on the point defects stability produced under gamma irradiation. We focused our attention on paramagnetic defects such as BOHC, E' and peroxy radicals.

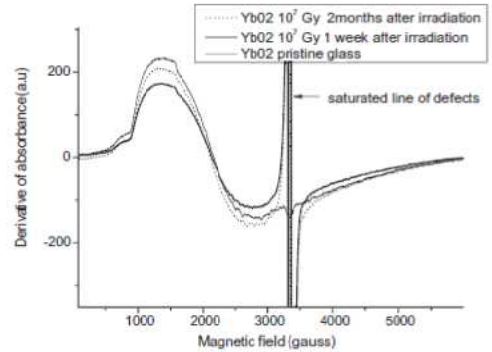


Fig. 7. Comparison of EPR spectra of Yb^{3+} performed at 10 K of Yb02 glass and Yb02 glass irradiated at 10^6 Gy (1 week after irradiation in bold line and 2 months after in dotted line).

The data suggest that doping with Yb limits the defect production, the saturation of the E' production with Yb increase is visible from 0.2 mol.%. This effect has already been observed for other rare earth element (Sm, Eu, Tb) [6,22,23] and can be attributed to a consummation of electron–hole pair during irradiation. It seems in our case that Yb^{3+} ions compete successively with E' centers in trapping electrons. Indeed, EPR measurements performed at 10 K on the gamma-irradiated aluminoborosilicate glasses doped with Yb revealed the presence of reduced Yb^{2+} species. As a matter of fact, the broad EPR line intensity corresponding to Yb^{3+} ions slightly decreases after irradiation (Fig. 7). The reduction is limited and its efficiency depends on the dose and on the Yb doping content. The stability of the Yb^{2+} ions appears to be limited as well, as it can be observed in Fig. 7 by the variation of the Yb^{3+} EPR line intensity with time and also depends on the two parameters. To explain the low content of divalent Yb^{2+} species formed under gamma irradiation compared to same glasses irradiated with 2.3 MeV electrons shown in [7], we assume that in gamma-irradiated glasses an efficient hole trapping on Yb^{2+} occurs during irradiation and/or the divalent Yb^{2+} formed under gamma irradiation shows a very limited stability. The other mechanism that can also be suggested to explain the saturation behavior of E' defects with the dose was proposed by Griscom and concerns the formation of the ESR-silent trapped-electron centers by the trapping of a second electron on oxygen pseudo vacancies [13].

In terms of thermal stability, the data suggest a difference in temperature recovery between E' and BOHC defect related to Yb. To the best of our knowledge, this result has not been mentioned elsewhere in the literature. Different hypotheses can be advanced to explain the lower temperature exhibited by the Yb1 glass. At first, we can suppose based on Edward and Fowler results [15] that a higher O_2 concentration could lead to a lower annealing temperature of the E'. This assumption is consistent with a larger peroxy radicals content that has been evidenced in [7] for the large Yb contents. A second assumption implies the Yb^{3+} ions environment in the glass. We showed in [17] that some Yb clusters were present mainly in Yb05 and Yb1 glass compositions. The presence of these paired Yb^{3+} ions (close to the Si atoms) could modify the distance between the defects and also the diffusion and recombination of released holes and electrons.

Concerning the long term stability of BOHC and E' in aluminoborosilicate glasses doped with Yb, it is important to underline the result obtained in this study showing the decay of both defect types at room temperature and more particularly the accelerated

Author's personal copy

recovery of BOHC defect when the glass is exposed to the light. The fading at room temperature of BOHC defect is obviously affected by the Yb doping even for glasses stored in the dark. This result is consistent with the study of Kadono et al. [5] that report same behavior of another trapped carrier defect (NBOHC). The defect stability is affected by dopants such as Fe, Sn, Ce and the author suggest a gradual recombination of the thermally activated electron (even at room temperature) that is trapped on the additive ions. However, contrasted results were reported by Sheng et al. who suggest an improvement of the NBOHC stability by a silver doping [24]. In phosphate glasses, even if the doping with Tb was shown to modify the defect nature by suppressing the POHC formation, Ebendorff et al.[22], reported that the stability of the $(Tb^{3+})^+$ at room temperature depends on the glass nature but the Tb^{3+} has no significant influence on the annealing behavior of the intrinsic defect at room temperature. Similar results on the defect nature and stability have been obtained in Eu-doped phosphate glasses by same authors [23]. The data from literature reveal that the link between the defect stability and the reduced or oxidized ion stability is not trivial. To go further, some studies with other Yb-doped glass-types (phosphate and aluminosilicate) are undertaken to study the role of the glass structure on the Yb^{2+} and defect stability.

Conclusion

To sum up, we were interested in the annealing process of paramagnetic defects in aluminoborosilicate glasses doped with Yb under gamma-irradiation. And more particularly, we focalized our attention on the influence of Yb doping on the BOHC and E' defect stability at room temperature or after a thermal treatment. The study demonstrates the instability of both defects types at room temperature. These data suggest an influence of Yb on BOHC and E' instability. The BOHC fading at room temperature appears to be affected by the Yb content doping and more sensitive than E' to the photobleaching.

Acknowledgments

We are grateful to Khaled Farah and Arbi Mejri (CNSTN, Tunisia) for gamma irradiation.

References

[1] D.L. Griscom, in: G. Pacchioni et al. (Eds.), Defects in SiO_2 and Related Dielectrics, Kluwer, 2000, p. 117.
[2] P. Ebeling, D. Ehrt, M. Friedrich, Optical Materials 20 (2002) 101.
[3] D. Griscom, Journal of Non-Crystalline Solids 357 (2011) 1945.
[4] F.Y. Olivier, B. Boizot, D. Ghaleb, G. Petite, Journal of Non-Crystalline Solids 351 (2005) 1061.
[5] K. Kadono, N. Itakura, T. Akai, M. Yamashita, T. Yazawa, Nuclear Instruments & Methods in Physics Research, Section B 267 (2009) 2411.
[6] E. Malchukova, Journal of Non-Crystalline Solids 353 (2007) 2397.
[7] N. Ollier, R. Planchais, B. Boizot, Nucl, Nuclear Instruments & Methods in Physics Research, Section B 266 (2008) 2854–2858.
[8] B. Boizot, N. Ollier, F. Olivier, G. Petite, D. Ghaleb, E. Malchukova, Nuclear Instruments & Methods in Physics Research, Section B 240 (2005) 146.
[9] N. Ollier, B. Boizot, B. Reynard, D. Ghaleb, G. Petite, Journal of Nuclear Materials 340 (2005) 209.
[10] Q. Wang, H. Geng, C. Sun, Z. Zhang, S. HE, Nuclear Instruments & Methods in Physics Research, Section B 268 (2010) 1478.
[11] J. Sheng, K. Kadono, T. Yazawa, Applied Radiation and Isotopes 57 (2002) 813.
[12] K. Farah, A. Kovacs, A. Mejri, H. Ben Ouada, Radiation Physics and Chemistry 76 (2007) 1523.
[13] D. Griscom, Physical Review B 64 (2001) 174201.
[14] M. Stapelbroek, D.L. Griscom, E.J. Friebele, G.H. Sigel Jr., Journal of Non-Crystalline Solids 32 (1979) 313.
[15] A.H. Edwards, W.B. Fowler, Physical Review B 26 (1982) 6649.
[16] L. Nuccio, S. Agnello, R. Boscaino, Physical Review B 79 (2009) 125205.
[17] N. Ollier, J.-L. Doualan, V. Pukhkaya, T. Charpentier, R. Moncorgé, S. Sen, Journal of Non-Crystalline Solids 357 (2011) 1037.
[18] B. Boizot, G. Petite, D. Ghaleb, G. Calas, Nuclear Instruments & Methods in Physics Research, Section B 141 (1998) 580.
[19] G. Kordas, Journal of Non-Crystalline Solids 351 (2005) 2348.
[20] R.A. Weeks, Journal of Non-Crystalline Solids 179 (1994) 1.
[21] D.L. Griscom, E.J. Friebele, Physical Review B 24 (1981) 4896.
[22] H. Ebendorff-Heidepriem, D. Ehrt, Optical Materials 18 (2002) 419.
[23] H. Ebendorff-Heidepriem, D. Ehrt, Optical Materials 19 (2002) 351.
[24] J. Sheng, J. Zhang, L. Qiao, Journal of Non-Crystalline Solids 352 (2006) 2914.

V. Pukhkaya, T. Charpentier, N. Ollier

Study of formation and sequential relaxation of paramagnetic point defects in electron-irradiated Na-aluminosilicate glasses: influence of Yb

***Journal of Non-Crystalline Solides*, 2013**
vol. 364, p. 1-8

Author's personal copy

Journal of Non-Crystalline Solids 364 (2013) 1–8

Contents lists available at SciVerse ScienceDirect

Journal of Non-Crystalline Solids

journal homepage: www.elsevier.com/locate/jnoncrysol

Study of formation and sequential relaxation of paramagnetic point defects in electron-irradiated Na-aluminosilicate glasses: Influence of Yb

V. Pukhkaya [a,*], T. Charpentier [b], N. Ollier [a]

[a] CEA, IRAMIS, Laboratoire des Solides Irradiés Ecole Polytechnique CNRS, 91128 Palaiseau, France
[b] CEA, IRAMIS, Service Interdisciplinaire sur les Systèmes Moléculaires et les Matériaux, UMR CEA-CNRS 3299, 91191 Gif-sur-Yvette, France

ARTICLE INFO

Article history:
Received 11 October 2012
Received in revised form 28 December 2012
Available online 31 January 2013

Keywords:
EPR;
Defects;
Aluminosilicate glass;
Irradiation

ABSTRACT

Paramagnetic defects in electron irradiated Yb-doped Na-aluminosilicate glasses were studied. In particular, we paid more attention to characterize the defects with Electron Paramagnetic Resonance in links with the glass structure which was analyzed by Raman spectroscopy and Magic Angle Spinning Nuclear Magnetic Resonance. Under e^--irradiation hole centers on non-bridging oxygens bonded to Si with close presence of Na^+, peroxy radicals, hole centers on oxygens bonded to Al (Al-OHC) and E′ centers were detected. Doping glasses with Yb gives rise to more Al-OHC defects. Formations of hole centers and Al-OHC defects as well as their sequential relaxation are linearly anticorrelated. After the end of irradiation, the total amount of paramagnetic defects decreases in 2 months and then remains stable. The relaxation curve presents 2 regions with different rates of defect recovery. We showed in particular that the presence of Yb-clusters in the glasses acts on the relaxation of paramagnetic point defects by decreasing significantly the recovery of defects.

© 2013 Elsevier B.V. All rights reserved.

1. Introduction

Understanding the behavior of glasses under irradiation is important in many fields: nuclear (high level waste storage, dosimetry) and optical applications. Yb doped glasses can be used for laser application in the infrared range. Operating at ~1 μm, Yb-doped laser fibers can achieve significant power due to two energy level structure of Yb^{3+} ions limiting non-radiative energy transfer leading to emission quenching. The main limit of rare earth element (REE) doped glass application is the formation of clusters even with low content of REE especially in SiO_2 [1]. Even if incorporating high-field ions such as Al^{3+} and P^{5+} in SiO_2 fiber can improve the cluster solubility [2], it is very important to study the influence of cluster on the glass aging under radiation.

Under ionizing radiation, many point defects can be formed in oxide glasses, that corresponds mainly to hole trapped on non-bridging oxygen. The structure of many paramagnetic defects in silicate type glasses was well described by D.L. Griscom in several papers: one dedicated to peroxy radicals (POR) with presence of E′ centers [4], another concerns hole centers HC_1 and HC_2 [5], the study of non-bridging oxygen hole centers (NBOHC) with $[Al]^0$ centers [6] and recent detailed review available in [7]. JA. Weil had reported some rigorous research on $[Al]^0$ centers [8,9]. Later, $[Al]^0$ centers were named Al-OHC defects [10,11].

Doping glasses with REE can modify the point defect characteristics. In particular, the REE (Yb, Gd, Eu) presence in glasses leads to less amount of paramagnetic defects under different types of irradiation (beta, gamma) [12,14,15]. Moreover, we showed an effect of Yb doping on the point defect relaxation in borosilicate glasses [12]. We also reported that luminescent properties such as Yb^{3+} ions in borosilicate glasses can be modified under ionizing irradiation [3].

The general aim of the present study is to understand the impact of initial glass structure on both point defect and Yb luminescent properties. This paper is more particularly devoted to investigate the influence of Yb clusters on the nature and relaxation of point defects formed under radiation. So the aluminosilicate glass compositions were carefully chosen to obtain glasses with various content of Yb cluster when Yb doping concentrations are the same [13].

Table 1
Nominal glass compositions.

Sample name	SiO_2, mol%	Al_2O_3, mol%	Na_2O, mol%	ASI Al/Na	
AS22	74	6	20	0.3	+5 wt.% Yb_2O_3
AS23	68	12	20	0.6	
AS24	62	18	20	0.9	
AS26	58	22	20	1.1	
AS24_0	62	18	20	0.9	
AS24_005					+0.05 wt.% Yb_2O_3
AS24_02					+0.2 wt.% Yb_2O_3
AS24_05					+0.5 wt.% Yb_2O_3
AS24_1					+1 wt.% Yb_2O_3
AS24_8					+8 wt.% Yb_2O_3

* Corresponding author at: Laboratoire des Solides Irradiés, Ecole Polytechnique, Bâtiment 5, Ecole Polytechnique, 91128 Palaiseau cedex, France. Tel.: +33 1 69 33 45 02; fax: +33 1 69 33 45 54.
E-mail address: vera.pukhkaya@polytechnique.edu (V. Pukhkaya).

0022-3093/$ – see front matter © 2013 Elsevier B.V. All rights reserved.
http://dx.doi.org/10.1016/j.jnoncrysol.2013.01.021

Author's personal copy

2. Experimental setup

Glass samples were prepared with the appropriated amounts of SiO_2, Al_2O_3, Na_2CO_3 and Yb_2O_3 (5 wt.%). The initial chemicals were mixed and melted in Pt–Au crucible at 1400 °C and then quenched rapidly at room temperature. All glasses were afterwards annealed at 580 °C to release mechanical tensions. The nominal glass compositions are presented in Table 1. Glass compositions were refined with microprobe analysis giving ~1 mol% of error.

Micro-Raman spectra were performed with a Bruker Senterra spectrometer in wavenumbers ranging 100–1500 cm^{-1} under a 532 nm laser line excitation (20 mW power) in a confocal geometry. The ×50 objective was used.

Glass samples were irradiated with 2.5 MeV electrons (LSI, SIRIUS) at 40 °C with dose rate close to 25 MGy/h. The achieved integrated doses were 10^5 Gy, 10^6 Gy, $3 \cdot 10^6$ Gy, 10^8 Gy and $1.5 \cdot 10^9$ Gy.

Paramagnetic defects were characterized at room temperature with an X-band EMX Bruker spectrometer (9.8 GHz). The modulation of the field was 20 mT for 1 mW and 20 μW microwave power. Final spectra were normalized by sample mass and receiver gain. The value proportional to the total amount of defects was extracted by double integration of initial spectra. The result of integration is defined with 10% of error bars.

^{27}Al and ^{29}Si MAS NMR spectra have been collected on a 500 Wide Bore Bruker Solid State NMR spectrometer (magnetic field 11.72 T) with a 4 mm o.d. Bruker Magic Angle Spinning (MAS) probe at a sample spinning frequency of 12.5 kHz.

For ^{27}Al, a recycle delay of 0.5 s was used and a short pulse length (1 μs, tip angle around 10°) to ensure quantitative MAS spectra (homogeneous excitation of all sites with respect to their NMR quadrupolar parameters). Chemical shift are referenced to an external sample of 1 M $AlCl_3$ aqueous solution (0 ppm).

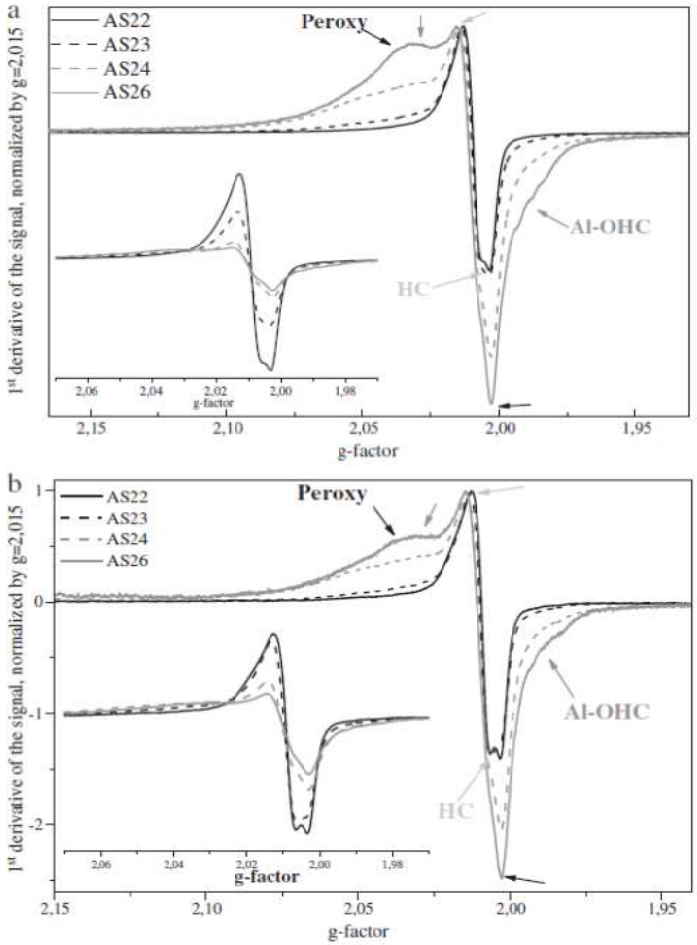


Fig. 1. EPR spectra of Yb-doped e^--irradiated AS glasses, at a dose of 10^5 Gy, and normalization at g = 2.013. EPR spectra normalized only by mass and gain are in the inset. Just after the irradiation (a) and 276 days after the irradiation (b).

Author's personal copy

For ^{29}Si, a CPMG sequence was used [18] by accumulating about 32 echoes with a delay of 6 ms between consecutive 180° pulses. The echoes were then summed up to obtain the spectrum shown. Variable recycle delays of 2 s, 20 s, 200 s and 1200 s and no spectral deformation was observed for recycle delay longer than 20 s. Chemical shifts are referenced to an external sample of TKS for which the highest-intensity peak is situated at −9.9 ppm from that of TMS.

3. Results

3.1. Nature of point defects produced under e^--irradiation

Under electron irradiation below 3.2 MGy only hole centers were detected in AS glasses. The shape of EPR spectra of the samples AS22–26 (Fig. 1a) exhibits the main presence of hole centers on non-bridging oxygens bonded to Si with $g_1 = 2.0035$, $g_2 = 2.0095$ and $g_3 = 2.0187$ which are similar to those of HC_1 defects whereas g-parameters of HC_2 defects are $g_1 = 2.0118$, $g_2 = 2.0127$, and $g_3 = 2.0158$ [5]. It is worth to underline that the reported parameters of g-tensor are from potassium-silicate glasses. The presence of sodium at molar concentration of 20% gives rise to 10 times broadening of the HC_1 EPR line according to carried out calculation works [5]. Thereafter, it is difficult to distinguish HC_1 and HC_2 defects in current samples thus HC notation will be used for hole centers.

Another signal characterized by $g_1 = 2.0030$, $g_2 = 2.0104$ and $g_3 = 2.0381$ can also be observed. It can be assigned to NBOHC or to POR (PerOxy Radical) defects. However, its g_3 parameter and high recovery temperature higher than 405 °C rather indicate POR defects [12]. Moreover, in the spectra of AS24 and AS26 glasses one can see the hyperfine structure arising from Al-OHC defects (hole centers trapped on NBO, bonded to Al ions). The nuclear spin of ^{27}Al is $I = 5/2$, giving 6 resolved lines with $g_1 = 2.0025$, $g_2 = 2.0106$, and $g_3 = 2.0186$ for Al-OHC defects observed in Al-doped silica glass [11].

In Yb-doped irradiated glasses, the HC defect amount increases with Aluminum Saturation Index decrease (ASI) that is defined in Table 1. With further ASI increasing, relatively more peroxy radicals and Al-OHC defects were created.

Yb-doping in AS24 glass leads to common effect compared to other RE-doping of silica-based glasses: total defects' amount decreases, but we also pointed out that the relative content of Al-OHC defects increases (Fig. 2).

In non-doped samples irradiated at doses stronger than 10^5 Gy E′ defects have also been detected (Fig. 3). The E′ center is the well-known electron-type center ($g = 2.0008$ [5]) corresponding to the oxygen vacancies close to Si^{4+} ions bonded to other three oxygen atoms ($O_3{\equiv}Si\bullet$) [4]. They can be observed in non-doped glasses irradiated at 10^6–$1.5 \cdot 10^9$ Gy. Its relative intensity is higher in glasses with less Al such as AS22_0, it increases up to the dose 10^7, and then it decreases significantly (Fig. 3a). Yb incorporating leads to the intensity decrease of E′ defects (Fig. 3b, inset). When Yb concentration reaches 5 wt.% of Yb_2O_3, these defects are not observed anymore.

3.2. Relaxation of defects

The total amount of defects decreases in time after irradiation during the first 2 months, before remaining stable. The most rapid relaxation is observed during the first 7 days. The relaxation rate is the same in all glasses during this first period and then becomes slower in glasses with higher Al content – AS24 and AS26 (Fig. 4). Relaxation curves exhibit two regions (Fig. 8). In the first region, the curve was fitted with an exponential law as sum of two first-order kinetics with 2 half-times ($I = I_0 + A_1 e^{-t/a} + A_2 e^{-t/b}$, $\tau_1 = a \cdot \ln 2$, $\tau_2 = b \cdot \ln 2$). The shorter one τ_1, which strongly dominates in this region, varies from 0.3 day in glass AS22 to 0.4 day in glass AS26 and the longer one τ_2 varies from 19 days in glass AS22 to 36 days in glass AS26. The second region represents long-term fading. It can be fitted with a first-order exponential law with longer half-time values given above. Finally, in AS24 glass the total loss of defects does not exceed 40% of the initial amount whereas in AS22 it reaches about 60%. The presence of Yb in AS24 gives rise to a quicker relaxation process (Fig. 4, inset). In non-doped glass AS24_0 about 80% of initial defect's value has been conserved after 2 months. Doping even with low amount of Yb_2O_3 leads to 50% of loss of initial amount of defects.

We observe moreover an increase of the relative amount of HC defects in time. A linear anticorrelation between Al-OHC defects and

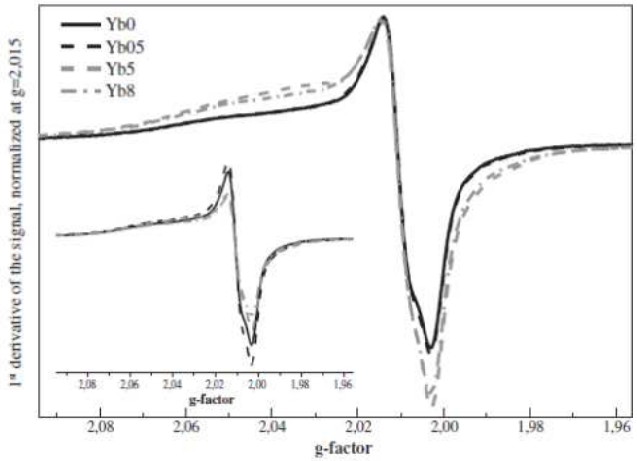


Fig. 2. EPR spectra of e^--irradiated AS24_Ybx glasses, at a dose of 10^5 Gy, and normalization at g = 2.013. EPR spectra recorded just after the irradiation and normalized only by mass and gain are in the inset.

Author's personal copy

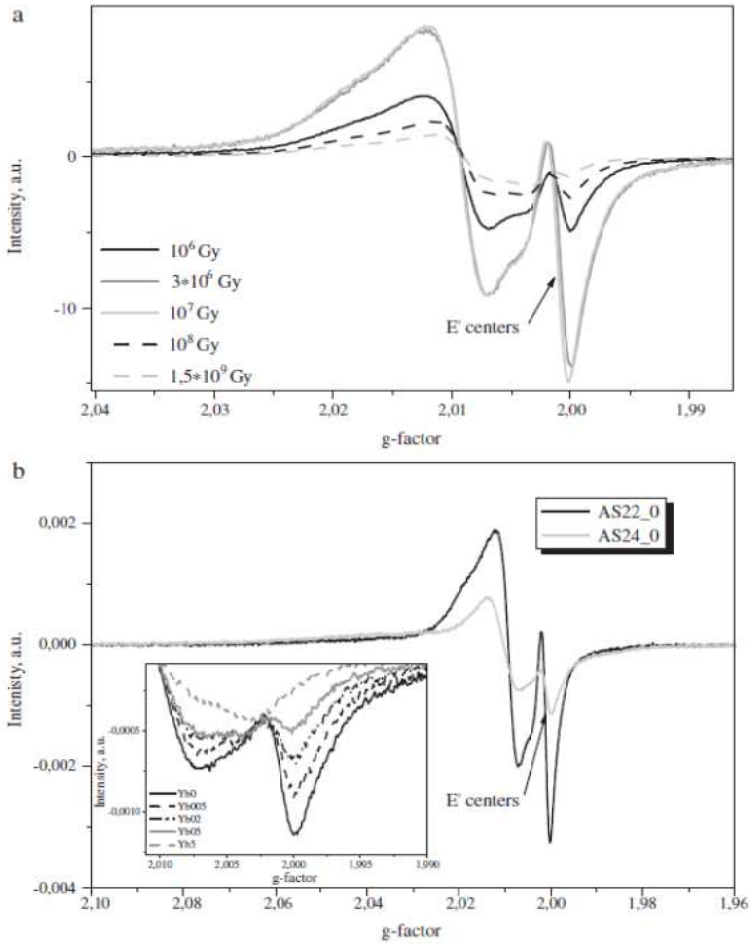


Fig. 3. EPR spectra of stabilized e^--irradiated with various doses AS22_0 glasses, (a) and AS24_0 and AS22_0 glasses, at a dose of 10^7 Gy. EPR spectra of AS24_Ybx glasses of the same dose are in the inset. (b). Intensities of spectra were normalized by sample mass and receiver gain in both figures.

HC defects (Fig. 5) can be underlined: Al-OHC defects' concentration decreases with time while the content of HC defects increases. In AS23, AS24 and AS26 samples analyzed 9 months after the irradiation one can observe significantly less relative content of Al-OHC defects than just after the irradiation (Fig. 1b).

Different relaxation times between the defects lead to a very different shape of the EPR line just after irradiation and few months later depending on the glass nature. We can notice that in 9 months after the irradiation in AS22 and AS23 glasses the quantity of paramagnetic defects is almost the same (Fig. 1b).

4. Discussion

In order to better understand the evolution of Al-OHC and HC defects as a function of the glass composition, the glass structure was investigated by Raman and MAS NMR spectroscopy. The MAS NMR spectra of ^{27}Al and are presented in Fig. 6 whereas the Raman spectra are displayed in Fig. 7. When some Na^+ ions are incorporated into SiO_2 glass network they play the role of modifiers by creating non-bridging oxygens (NBO). The Raman band at 800 cm^{-1} is ascribed to cage motion of Si–O stretching vibrations [22]. This band becomes less intensive with decreasing SiO_2 content. Similar Al–O stretching motions should be observed at a lower wave-numbers – 780–790 cm^{-1} [24]. A maximum at 780 cm^{-1} is observed due to large component of both Al and O displacements at Al–O stretching motions. It is however difficult to conclude precisely from Raman spectroscopy data on the type of Al polyhedra but ^{27}Al MAS NMR analysis brings us to conclude that aluminum is tetra-coordinated for all glass composition. As a matter of fact, the isotropic chemical shift ~60 ppm corresponds to AlO_4 species (Fig. 6a). We also detect a slight increase of the quadrupolar

Author's personal copy

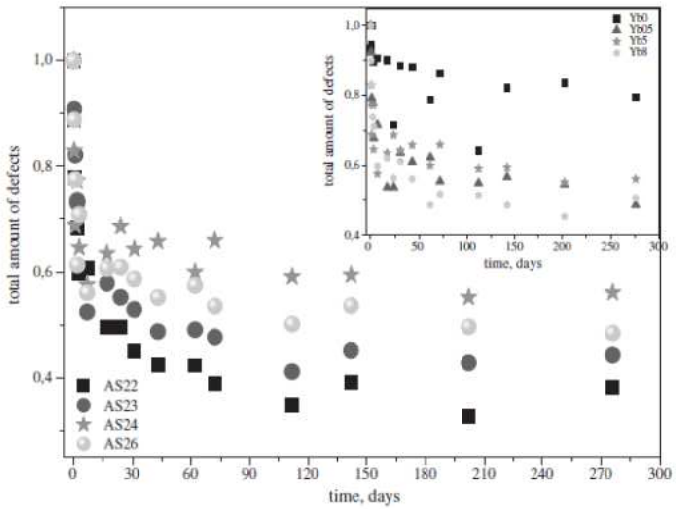


Fig. 4. Relaxation curves of Yb-doped e^--irradiated AS glasses, at a dose of 10^5 Gy, and e^--irradiated AS24_Ybx glasses, at a dose of 10^5 Gy are in the inset.

interaction from samples AS22 to AS26 (Al increasing) characterized by the broadening of the band.

Increasing of Yb content increases the width of the line (Fig. 6b), corresponding to a typical paramagnetic effect due to Yb^{3+} ions but Al remains tetra-coordinated. However no changes in ^{27}Al MAS NMR spectra of the irradiated glasses were observed, clearly indicating that Al^{3+} (in the limit of the NMR sensitivity) remained tetra-coordinated.

The broad Raman band in the 850–1200 cm^{-1} region can be attributed to SiO_4 tetrahedra connected to Si or Al and Si(Al)–O–Si(Al) linkages [23,24] (Fig. 7). The following linkages and their corresponding Raman mode can be found [23]: Si(OAl) – 1140 cm^{-1}, $Si(OAl)_2$ – 1000 cm^{-1}, $Si(OAl)_3$ – 925 cm^{-1}, and $Si(OAl)_4$ – 890 cm^{-1}. Movement of the broad band's maximum to lower wave-numbers can be assigned to appearance of more Si ions connected to Al through O-bridges. This effect was corroborated by ^{29}Si MAS-NMR measurements: the maximum of the NMR band moves from AS22 glass to AS26 towards higher values of chemical shift indicating the presence of more Al atoms linked to Q4 species [19].

When Al content increases, more Na^+ ions are used to compensate the charge of $[AlO_4]^-$ tetrahedra. In consequence, less Na^+ ions are

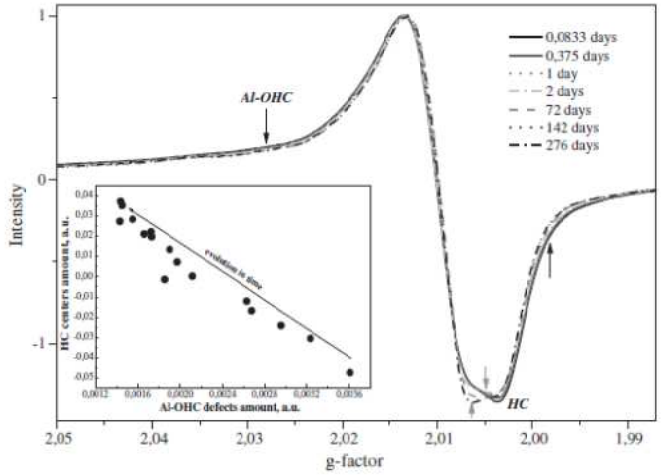


Fig. 5. Evolution in time of Al-OHC and HC defects in AS23, e^--irradiation, 10^5 Gy, and normalization at g = 2.013.

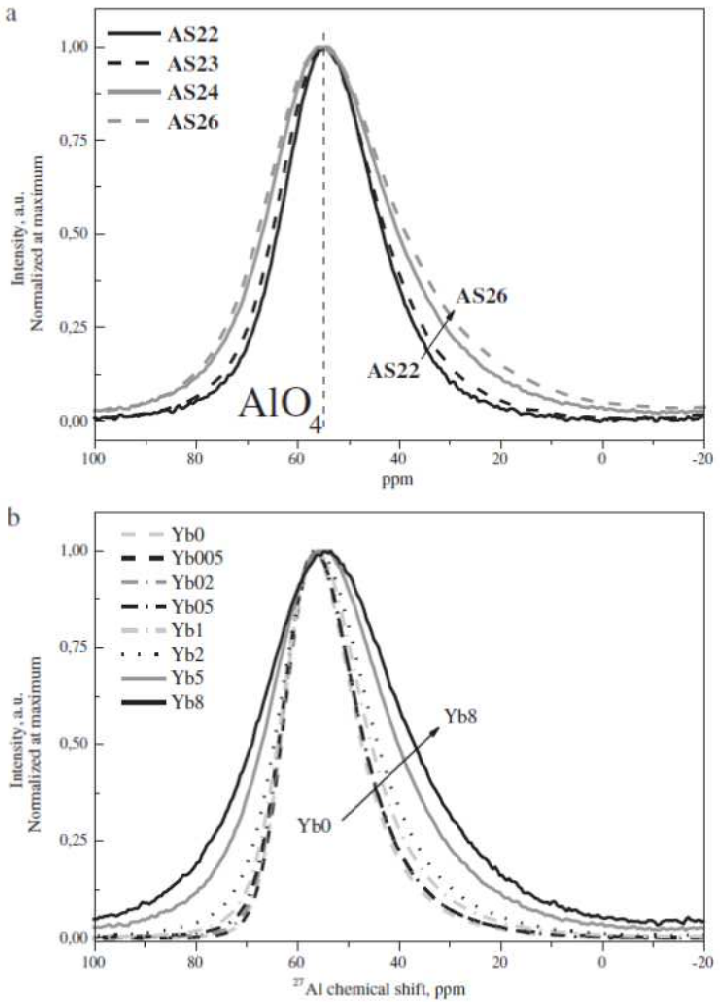


Fig. 6. ^{27}Al MAS NMR spectra of non-irradiated non-doped glasses (a) and non-irradiated glasses doped with various concentrations of Yb (b).

available in the glassy network leading to a stronger glass depolymerization. Therefore, less HC defects and E′ centers are created (Figs. 1 and 3b). Despite a lower silicon content in the AS24 glass compared to AS22, less Na^+ ions take part in HC defect formation because of the increase of Al and thus more hole centers on oxygens bonded to Al tetrahedra are trapped leading to more Al-OHC defects.

After the nature of defects, we also show that the relaxation rate of point defects depends on the glass composition (Fig. 4). The relaxation in AS24 and AS26 glasses is more rapid than in AS22 and AS23 glasses. In [13], it was shown that in AS24 and AS26 glasses Yb^{3+} ions can form some clusters more efficiently than in AS22 and AS23 due to some structural effect linked to NBO number.

The effect of Yb-doping (Figs. 2 and 3b) is in agreement with previous works [3,14–16]. RE ions can trap hole and electron charges and thus decreasing the number of point defects observed after irradiation. Even if the reduction of Yb ions into Yb^{2+} in our aluminosilicate glasses was not obviously demonstrated by EPR, we assume that an effective charge trapping of Yb^{3+} ions under cluster form is responsible for the difference observed between glasses. We propose that e^--hole recombination leading to the defect fading is less active when a high amount of cluster are present in the glass due to an effective electron trapping by Yb clusters.

The higher relaxation rate with Yb-doping can be explained by the presence of electrons trapped on Yb^{3+} ions close to the defects such as Al-OHC or E′-centers. We thus assume due to this proximity that exciton recombination is easier. The vicinity of Yb and those defects is demonstrated by the influence of Yb concentration on E′-centers and Al-OHC defect formation (Fig. 3).

Author's personal copy

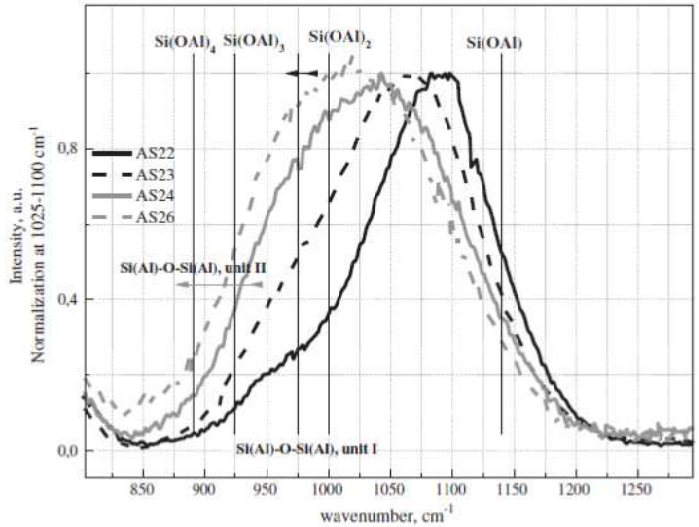


Fig. 7. Raman spectra of non-irradiated glasses. Normalization at maximum 1000–1100 cm^{-1} band.

Relaxation curve is divided into two regions (Fig. 8). Similar relaxation curve type can be found in the literature despite a calculation from optical absorption in the visible region [20,21].

The slower period can be fitted by first-order decay while in shorter period both first- and second-order kinetics dominate [20,21]. It implies a fast defect recovery in the first region and slower processes in the second one. The most rapid region is characterized with similar values of half-times in all the glass series around 0.3 day, and lasts 5–7 days indicating similar fast processes of HC defect recovery in all four glasses. Along this period the best seen change is decrease of relative HC defect intensity.

Generally the second part of the relaxation curve corresponds to electron diffusion [17] and it presents different slope in our glasses according to the AS1/Yb cluster amount Therefore it demonstrates that the Yb cluster amount is involved into e^--diffusion in irradiated glasses. More precisely, when cluster amount is high, the half time is longer implying a very efficient charge trapping by cluster.

Concerning the linear anti-correlation between Al-OHC and HC defects, it implies structural modifications of those point defects during post-irradiation processes. This could be due to hole migration from NBO linked to $[AlO_4]^-$ to a close NBO linked to $[SiO_4]$.

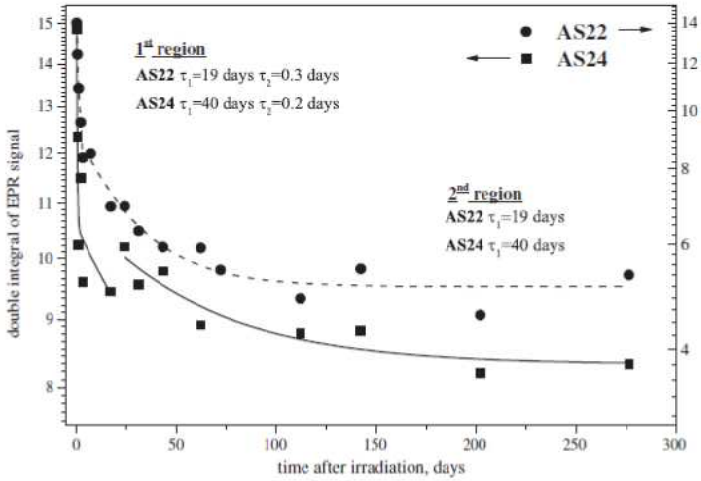


Fig. 8. Relaxation curves of Yb-doped e^--irradiated AS22 and AS24 glasses, at a dose of 10^5 Gy. The axes of abscissas are in logarithm.

Author's personal copy

. Conclusion

The amount of Al in Na-aluminosilicate glasses has an impact on de- ect formation under ionizing irradiation and their afterwards relaxa- on behavior. In glasses where Al can be regarded as network-former nder tetrahedral coordination, Al-OHC defect formation is associated ith HC defects. Doping with Yb^{3+} ions limits the paramagnetic point efect formation under irradiation and speed up the relaxation process. he presence of Yb clusters affects the relaxation of paramagnetic de- ects in irradiated aluminosilicate glasses by decreasing the electron ole recombination.

cknowledgments

We thank Vincent Métayer (LSI, Ecole Polytechnique, France) a lot r well-qualified electron-irradiation. Ludovic Bellot-Gurlet (LADIR, rance) is also thanked for his assistance during Raman experiments.

eferences

[1] Y.W. Lee, S. Shina, M.J.F. Digonnet, R.L. Byer, S. Jiang, Electron. Lett. 44 (2008) 14.
[2] T. Deschamps, N. Ollier, H. Vezin, C. Gonnet, J. Chem. Phys. 136 (2012) 01453.
[3] N. Ollier, J.-L. Doualan, V. Pukhkaya, T. Charpentier, R. Moncorgé, S. Sen, J. Non-Cryst. Solids 357 (2011) 1037.
[4] T.E. Tsai, D.L. Griscom, Phys. Rev. B 67 (1991) 2517.
[5] D.L. Griscom, J. Non-Cryst. Solids 64 (1984) 229.
[6] D.L. Griscom, E.J. Friebele, Phys. Rev. B 24 (1981) 4896.
[7] D.L. Griscom, J. Non-Cryst. Solids 357 (2011) 1945.
[8] R.H.D. Nuttall, J.A. Weil, Solid State Commun. 35 (1980) 789.
[9] R.S. Dickson, J.A. Weil, Can. J. Phys. 68 (1990) 630.
[10] D.A. Dutt, P.L. Highby, D.L. Griscom, J. Non-Cryst. Solids 130 (1991) 41.
[11] D.A. Dutt, P.L. Highby, C.I. Merzbacher, D.L. Griscom, J. Non-Cryst. Solids 135 (1991) 122.
[12] N. Ollier, V. Pukhkaya, Nucl. Instrum. Methods Phys. Res. B 277 (2012) 121.
[13] B. Schaudel, Ph.D. dissertation, l'Université Paris VI, 2000.
[14] E. Malchukova, B. Boizot, G. Petite, D. Ghaleb, J. Non-Cryst. Solids 354 (2008) 3592.
[15] N. Ollier, R. Planchais, B. Boizot, Nucl. Instrum. Methods Phys. Res. B 266 (2008) 2854.
[16] H. Ebendorff-Heidepriem, D. Ehrt, Opt. Mater. 18 (2002) 419.
[17] T.R. Waite, Phys. Rev. 107 (1957) 471.
[18] F.H. Larsen, I. Farnan, Chem. Phys. Lett. 357 (2002) 403.
[19] J. Hiet, D. Massiot, M. Deschamps, F. Fayon, J. Hiet, G. Ferru, M. Derieppe, N. Pellerin, D. Massiot, Phys. Chem. Chem. Phys. 10 (2008) 1298.
[20] J. Sheng, K. Kadono, T. Yazawa, Appl. Radiat. Isot. 57 (2002) 813.
[21] K. Farah, A. Kovács, A. Mejri, H. Ben Ouada, Radiat. Phys. Chem. 75 (2007) 1523.
[22] D.R. Neuville, L. Cormier, D. Massiot, Geochim. Cosmochim. Acta 68 (2004) 5071.
[23] P. McMillan, B. Piriou, Al. Navrotsky, Geochim. Cosmochim. Acta 46 (1982) 2021.
[24] B.O. Mysen, D. Virgo, F. Seifert, Am. Mineral. 70 (1985) 88.

Résumé

Nous avons étudié les effets de l'irradiation ionisante (e^-- et γ-) sur les propriétés luminescentes des ions Yb^{3+} et Er^{3+} dans des verres aluminosilicates (AS) et phosphates en essayant de comprendre l'impact de l'environnement initial de Yb^{3+} et surtout le rôle des clusters d'Yb. Pour cela, des verres AS et phosphates contenant les quantités différentes de clusters d'Yb ont été irradiés à des doses comprises entre 10^4 et $2 \cdot 10^9$ Gy. Nous avons montré que la relaxation des défauts ponctuels est ralentie en présence de clusters d'Yb dans le verre. La quantité de défauts ponctuels en fonction du lg(dose) est stable aux faibles doses puis décrit une courbe en cloche. La présence des clusters d'Yb limite la production de défauts aux doses élevées, quelle que soit la composition du verre (AS ou phosphate).En conséquence, la variation de la durée de vie de l'état excité $^2F_{5/2}$ en fonction du log de la dose décrit deux régions. Pour un fort contenu de cluster d'Yb, la durée de vie diminue linéairement avec le log de la dose. Ce résultat ne dépend pas du type de verre, ni de la nature de l'élément terre rare (Er^{3+}). Ceci signifie qu'il existe un mécanisme plus général n'impliquant pas un 'un type de défaut particulier. De plus, la complexité du signal RPE dû aux défauts ponctuels dans les verres phosphates a été interprétée grâce à la forte évolution de celui-ci en fonction de la composition du verre, de la dose et du temps. Au moins 8 défauts ponctuels paramagnétiques ont été identifiés ainsi qu'un défaut diamagnétique luminescent dont l'origine est discutée.

Mots clefs : verre aluminosilicate, verre phosphate, terres rares, l'irradiation, défauts ponctuels, luminescence, durée de vie

Abstract

We have investigated the effects of ionizing irradiation (e^-- and γ-) on the Yb^{3+} and Er^{3+} luminescent properties in aluminosilicate (AS) and phosphate glasses by trying to understand the impact of initial Yb^{3+} environment and mostly the role of Yb cluster. For that, AS and phosphate glasses containing different amount of Yb clusters were irradiated in 10^4-$2 \cdot 10^9$ Gy dose range. At first, we have shown that the point defect fading is slow down by a clustering effect in the glass. We have obtained a 2-step dependence of point defects quantity versus lg(dose). The cluster presence limits the defect production in the high dose range, whatever the glass composition (AS or phosphate). Consequently, we observed the same two-regions trends for the $^2F_{5/2}$ lifetime as a function of the lg(dose). But for high content of cluster, the lifetimes value decreases linearly within lg(dose). This result does not depend on the glass type nor on the rare earth element (Er^{3+}), implying a more general mechanism that implying one type of defect in particular. Secondly, we have interpreted the strong variation of the complex EPR signal in phosphate glasses within glass composition, dose and time with the formation of at least 8 point defects. In addition, the origin of the luminescent diamagnetic defect is discussed.

Keywords: aluminosilicate glasses, phosphate glasses, rare earths, irradiation, point defects, luminescence, lifetime, cluster